UNIVERSITY OF SOUTHAMPTON

FACULTY OF MEDICINE

Clinical and Experimental Sciences

Nanoparticles, Their Protein Corona and Impact on the Immune Function of Human Lung Cells

by

Harry James Whitwell

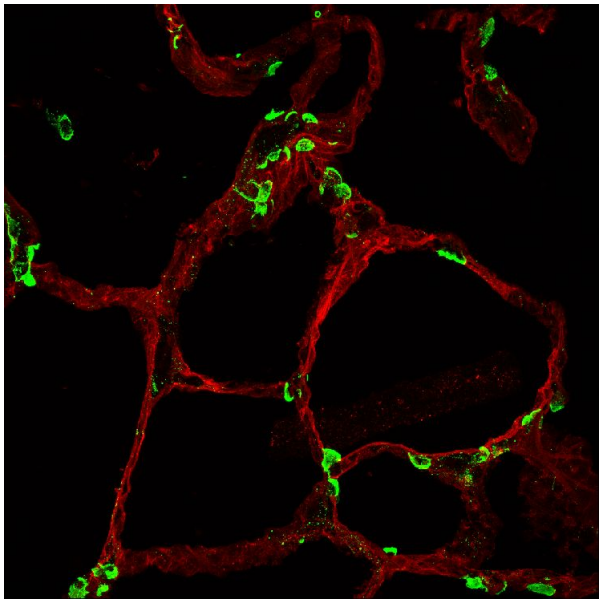

Thesis for the degree of Doctor of Philosophy

June 10, 2016

UNIVERSITY OF SOUTHAMPTON

ABSTRACT

FACULTY OF MEDICINE

Doctor of Philosophy

NANOPARTICLES, THEIR PROTEIN CORONA AND IMPACT ON THE IMMUNE FUNCTION OF HUMAN LUNG CELLS

Particles with a single dimension smaller than 100 nm are called nanoparticles (NPs). There is a large amount of epidemiology that anthropogenic particles cause increased mortality, increased risk of asthma and increased incidence of lung adenocarcinoma.

Inhaled NPs can reach the lung terminus, interacting with a lipid lining at the air-liquid interface (pulmonary surfactant (PSf)) and with an aqueous hydrophase beneath. Studies in serum have shown that upon contact with blood, proteins very rapidly adsorb to the particle surface, thus the particle accrues a biological identity. However, no such interaction studies have been performed in the pulmonary system, where there is a complex interplay of proteins and lipids. The interaction of NPs with PSf is poorly understood. Prior to reaching the lung epithelium, NPs must translocate through this layer.

The aims of this thesis are to firstly explore the interactions of NPs with proteins and lipids in the lung and secondly investigate the toxicity and effect on the immunological action of lung cells.

NPs were incubated with pulmonary lavage fluid and adsorbed proteins were analysed using state-of-the-art, high resolution, quantitative mass spectrometry. To investigate the interactions of NPs with PSf, particles were incubated with a porcine surfactant. The bound lipids were analysed by qualitative mass spectrometry. The effect of NPs and the NP-protein-corona was investigated in cell lines by a number of techniques.

Unique proteins were observed on each particle type, however the main contributors contribution was from a few key proteins. There was no biophysical property of these bound proteins that could predict their affinity to a particle. Surfactant associated protein A, B and D (SP-A, B, D) were observed to be bound to the particle surface. SP-A was bound with high abundance, suggesting it is likely these particles may interfere with PSf in vivo. All particles retained lipids on their surface through binding mediated by electrostatic interactions. Aminated-polystyrene and titanium dioxide NPs were capable of interfering with PSf *in vitro*. There was little observed effect of the particles to induce inflammation.

The key findings suggest that the protein corona does not predict particle toxicity. Any observed effect is due to the core particle chemistry, not an acquired bio-identity. The toxicity of particles observed through epidemiological surveys could be caused from the inhibition of pulmonary surfactant, not from direct toxicity of the particles themselves.

Publication List

Papers

Nanoparticle Growth and Surface Chemistry Changes in Cell-Conditioned Medium. Kendall, M., Hodges, N.J., Whitwell, H., Tyrrell, J., Cangul, H. Philosophical transcations of the Royal Society of London. Series B, Biological Sciences, 2014 370:1661

Surfactant Protein A (SP-A) Inhibits Agglomeration and Macrophage Uptake of Toxic Amine Modified Nanoparticles. McKenzie, Z., Kendall, M., Mackay, R.-M., Whitwell, H., Elgy, C., Ding, P., Mahajan, S., Morgan, C., Griffiths, M., Clark, H., Madsen, J. Nanotoxicology, 2015 5390:2008 1-11

Surfactant Protein D Is Essential for Immunity to Helminth Infection. Thawer, S., Auret, J., Schnoeller, C., Chetty, A., Smith, K., Darby, M., Roberts, L., Mackay, R.-M., Whitwell, H.J., Timms, J.F., Madsen, J., Selkirk, M.E., Brombacher, F., Clark, H., Horsnell, W.G.C. PLoS Pathogens 2016 12:2

Accepted by Nanotoxicology: Nanoparticle in the Lung and their Protein Corona: The Few Proteins that Count Whitwell, H.J., Mackay, R.-M., Elgy, C., Griffiths, M., Clark, H., Skipp, P., Madsen, J. Submitted to Nanotoxicology 2016

Immunology News

BSI Wessex Immunology Group Meeting. Whitwell, H.J., Watson, A. Immunology News, May 2013 p. 16-17

Presentations

Nanoparticles, Their Protein Corona and Impact on the Immune Function of Human Lung Cells. Facility for Environmental Nanoscience Analysis and Characterisation (FENAC) March 2014.

Nanoparticles – Interactions with Pulmonary Epithelial Lining Fluid. FENAC Academic Meeting, March 2016.

Nanoparticles – Interactions with Pulmonary Epithelial Lining Fluid. London Biological Sciences Mass Spectrometry Discussion Group Meeting, March 2016.

Conferences

British Society of Immunology Congress 2014 Nanoparticles, Their Protein Corona and Impact on the Immune Function of Lung Cells. Whitwell, H., Clark, H., Skipp, P., Warner, J., Dobbs, L., Gonzalez, R., Griffiths, M., Morgan, C., Madsen, J.

Faculty Conference 2014 Nanoparticles, Their Protein Corona and Impact on the Immune Function of Lung Cells. Whitwell, H., Clark, H., Skipp, P., Warner, J., Dobbs, L., Gonzalez, R., Griffiths, M., Morgan, C., Madsen, J.

Royal Society Bio-Nano Interactions Conference 2014 Nanoparticles, Their Protein Corona and Impact on the Immune Function of Lung Cells. Whitwell, H., Clark, H., Skipp, P., Warner, J., Dobbs, L., Gonzalez, R., Griffiths, M., Morgan, C., Madsen, J.

Faculty Conference 2015 Nanoparticles Interacting with Proteins andLipids can Disrupt Pulmonary Surfactant. Whitwell, H., Clark, H., Skipp, P., Warner, J., Dobbs, L., Gonzalez, R., Griffiths, M., Morgan, C., Madsen, J.

5th Zing Bionanomaterials Conference 2015 Nanoparticles Interacting with Proteins andLipids can Disrupt Pulmonary Surfactant. Whitwell, H., Clark, H., Skipp, P., Warner, J., Dobbs, L., Gonzalez, R., Griffiths, M., Morgan, C., Madsen, J.

British Society for Proteomics Meeting 2015 Using Mass Spectrometry to Characterise the Interaction of Airborne Nanoparticles with Pulmonary Lipids and Proteins Whitwell, H., Elgy, C., Koster, G., Postle, T., Griffiths, M., Warner, J., Clark, H., Madsen, J., Skipp, P.

Contents

List of Tables

List of Figures

List of Equations

List of Accompanying Materials

Supplementary data are supplied in the attached CD-ROM.

Supplementary1_60minuteCorona.xlsx

The first tab, 'Raw Data', contains raw data in fmol of identified proteins that were identified bound to aPS, cPS, uPC or TiO_2 nanoparticles. Subsequent tabs for each nanoparticle contain summary statistics of normalised quantification and information for the proteins determined to be attached to that particle.

Supplementary2_UniqueProteins.xlsx

The six tabs contain pair-wise comparisons of the unique proteins found on each particle.

Supplementary3_ProteinCoronaOverTime.xlsx

This file contains quanitification and identification data for proteins bound to aPS or cPS particles measured over time. The Raw Data tabs contain fmol of each protein in every run and physiochemical properties of that protein. The 'Average' tabs contain averages and summary statistics of normalised quantification.

Supplementary4_CellLysate.xlsx

The tab entitled 'top3MatchPeptideIntenSum' contains raw data (summation of the top 3 most intense peptides for each protein). Fold change tabs contain fold changes for normalised quantifications.

Supplementary5_CellLysateChangeGroups.xlsx

This is the groups of proteins having a 3-fold change or a 2-fold change with $P<0.05$ for changes in protein expression in TT1 cells exposed to BALF-coated or bare aPS particles.

Supplementary6_CoImmunoprecipitation.xlsx

This contains proteins identified from co-immunoprecipitation experiments of $HTII_{280}$ in BALF.

DECLARATION OF AUTHORSHIP

I, *Harry James Whitwell*, declare that this thesis entitled:

Nanoparticles, Their Protein Corona and Impact on the Immune Function of Human Lung Cells

and the work presented in it are my own and has been generated by me as the result of my own original research.

I confirm that:

1. This work was done wholly or mainly while in candidature for a research degree at this University;
2. Where any part of this thesis has previously been submitted for a degree or any other qualification at this University or any other institution, this has been clearly stated;
3. Where I have consulted the published work of others, this is always clearly attributed;
4. Where I have quoted from the work of others, the source is always given. With the exception of such quotations, this thesis is entirely my own work;
5. I have acknowledged all main sources of help;
6. Where the thesis is based on work done by myself jointly with others, I have made clear exactly what was done by others and what I have contributed myself;
7. None of this work has been published before submission

Signed:

Date:

Acknowledgements

A large number of people have helped, guided and supported me throughout this PhD. I would like firstly to acknowledge my supervisors, Dr Jens Madsen, Dr Paul Skill, Professor Howard Clark and Dr Jane Warner who have all contributed in supporting and guiding me throughout this research. In particular, Dr Jens Madsen has provided an enormous amount of support and guidance, his door was always open! The support of the remaining members of our research group, Alastair Watson, Dr Zofi McKenzie, Dr Rose-Marie Mackay and lab managers Dr Laurie Lau, Dr Carolann McGuire and Richard Jewell who have always been on hand for support and advice. In particular, Alastair Watson's constant coffee-fuelled, hyperactive enthusiasm has helped to maintain momentum! At my other home in Proteomics, Dr Paul Skipp, Dr Erika Parkinson, Dr Dominic Burg and Leanne Wickens were always there for support, advice, a drink and a good time.

My family have helped in many ways. The support and love of my wife, Isis Whitwell, has been unwavering through-out my PhD and without her belief that I would finish, this would have been much harder. Over the last year, my parents (Margaret and Peter Whitwell), parents-in-law (Margaret and Barry Redford) and brother, Jonathan, never ceased reminding me that I have a thesis to write, and without them, there is no doubt it would have taken much longer! Their continual support and parenting throughout the entire course of my studies has been incredible. My family has been through a lot in the last year, but Dad has always provided an unwavering service of proof reading with a super-fast turn around no matter the circumstances – which I am very grateful for!

Thank you to the biomedical imaging unit for helping with staining and imaging of nanoparticles and lung tissue. In particular thank you to Dr Anton Page and Dr David Johnson.

Many people have helped with technical advice and support. I would like to thank all the proteomics group (above) and the lipidomics groups, in particular Paul Townsend, Dr Grielof Koster, Dr Kevin Goss, Dr Tony Hunt and Prof Tony Postle have provided expertise and advice throughout this project. Also Dr Tracy Newman who conducted my transfer Viva, and transferred much advice through the process. Similarly, Dr Iseult Lynch and Dr Michaela Kendall have offered advice freely and supportively.

Thank you to Dr Mark Griffiths, Imperial College London, for providing bronchoalveolar lavage fluid and to all his patients who kindly consented to donate. Thank you to Professor Leyland Dobbs and Dr Robert Gonzalez, University of California, for donating antibodies against alveolar epithelial cells.

Dr Christine Elgy has also been a huge help, providing her expertise and an enormous amount of time at the Facility for Environmental Nanoscience Analysis and Characterisation (FENAC, University of Birmingham).

Over the past year, I have been working in Cancer Proteomics at University College London. I would like to thank Dr John Timms, for taking me on without a PhD and offering support and advice – often over a pint – whilst I wrote my thesis, he's pretty good for a Lancastrian... Also the rest of my current research group, Dr Joy Cuenco, Anna Kazarian, Stella Irungu, Richard Gunu and Dr Oleg Blyuss have been supportive and good fun!

I would like to thank those who have asked me to collaborate on their research, Dr Michaela Kendall and Professor William Horsnell.

The support of all my friends is important, in particular Simon Harding, Jack Harder, James Houghton, Hugo Tyrell, Mischa Van Kesteren, Rosanna Milner, William Day, Graeme Smith and Lotta Räty have all been sarcastic, abusive, offensive, mocking and belligerent at every opportunity and whichever pub was closest.

Thank you to all who have helped myself and this project.

Definitions and Abbreviations

1 Introduction

1.1 Nanoparticles

Particles with at least one dimension less than 100 nm are termed nanoparticles[1] (NPs) and can be found in food packaging, diesel fumes, metal shards from railways, medicines, electronics, plastics, paint and beauty products. Consequently they are an intense area of research from a number of different perspectives. Many physical and chemical properties of NPs have been shown to influence how they interact with cells and tissue; such as their size[2], shape[3] and surface chemistry.[4] From a medical perspective, there is much research in exploiting these characteristics to provide targeted drug therapy[5, 6] identify toxicological effects and discern NPs' distribution at a cellular and systemic level.[7]

One would expect to be exposed to NPs during all parts of the day. Someone living in a very rural environment may be exposed to natural particles that have co-evolved with life and geographical formation. However, in the home or in urban environments, particulate exposure to man made, 'anthropogenic' particles may have more detrimental effects on health such as lung disease and cancer.

A typical day in an urban environment would begin at home, where exposure to dust particles, carbon-based nanoparticles from ironing and cooking, radon, mould spores and zinc/titanium oxides from cosmetics (<50 nm) could occur. During a commute, particularly on foot, the pollution levels from nano-particulates increases as traffic peaks. Diesel exhausts (deisel exhaust particles (DEP)) (<60 nm), metallic particles, metallic oxides (<50 nm), nitrogen-oxides and polyneuclear aromatic hydrocarbons (<10 nm) are prevelant. A large proportion of these particles are sub 100 nm (NP or ultrafine particle (UFP)) and are capable of reaching lower airways (alveolar region) where they escape immediate expulsion via mucus and ciliary action. Particles may enter as single particles, or as clusters depending on their concentration and electrostatic attractions. In the lung, the particles have the potential to cause pathology in a number of ways. Firstly, they will encounter pulmonary surfactant, an essential component that maintains a low surface tension within the lung. Interferance here can trigger inflammation and affect lung performance. Lipids are likely much smaller than the particles, therefore interactions between chemical groups on the particle surface and phospholipids may be important. After passing through this layer, the particles enter a proteinascious, saline phase (hydrophase) where they may adsorb important inate immune molecules and signalling molecules before reaching a cell

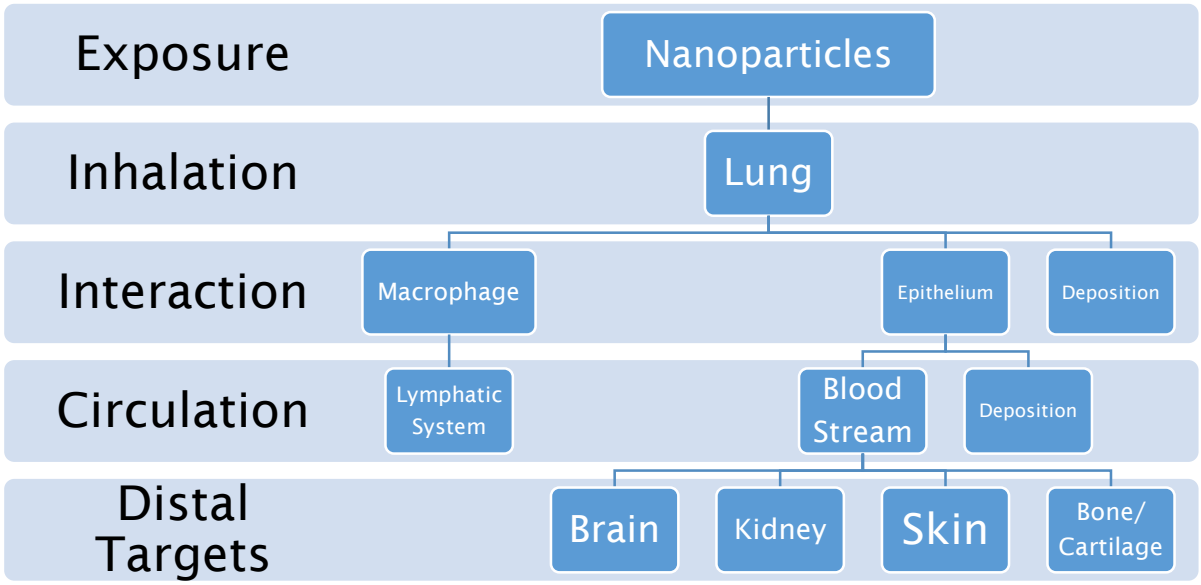

Figure 1: Potential route of deposition of inhaled nanoparticles.

membrane. Here, interactions are on a much larger scale as some proteins may be similar in size or larger than the particles and average electrostatic or hydrophilic properties may be important in mediating adsorption. In the main, particles will encounter either epithelial cells or macrophages and many particles have been shown to be taken up into these cells. Macrophages may rapidly transport particles to the lympatic system or particles translocating through the epithelium may enter the blood stream or underlying tissue. Therefore pathologocial effects of particles are not necessarily limited to the pulmonary, but more distal effects are possible via their transport in the circularity system (Figure **??**).

Following a similar evening comute, exposure continues in the home with particulates from open fires (nitrogen oxides), cooking, care products (voletile organic compounds, VOCs), candles (VOCs, carbon monoxide and carbon-based particulates), insulating material (<5 nm fibres), dust and formaldehyde being present. Furthermore, the exposure to these materials over night may be worse, particularly in children, due to the duration of exposure whilst sleeping.

The work presented here investigated the interaction of nanoparticles with pulmonary fluids and cells, to further understanding behind the potential effects of nanoparticles on health.

1.1.1 Sources of Nanoparticles

Nanoparticles can come from a wide variety of natural and anthropogenic sources. Volatile biological NPs from natural phenomenon such as volcanic explosions, forest fires, dust storms, viruses and mineral acpnps from microbial metabolism[8, 9] account for

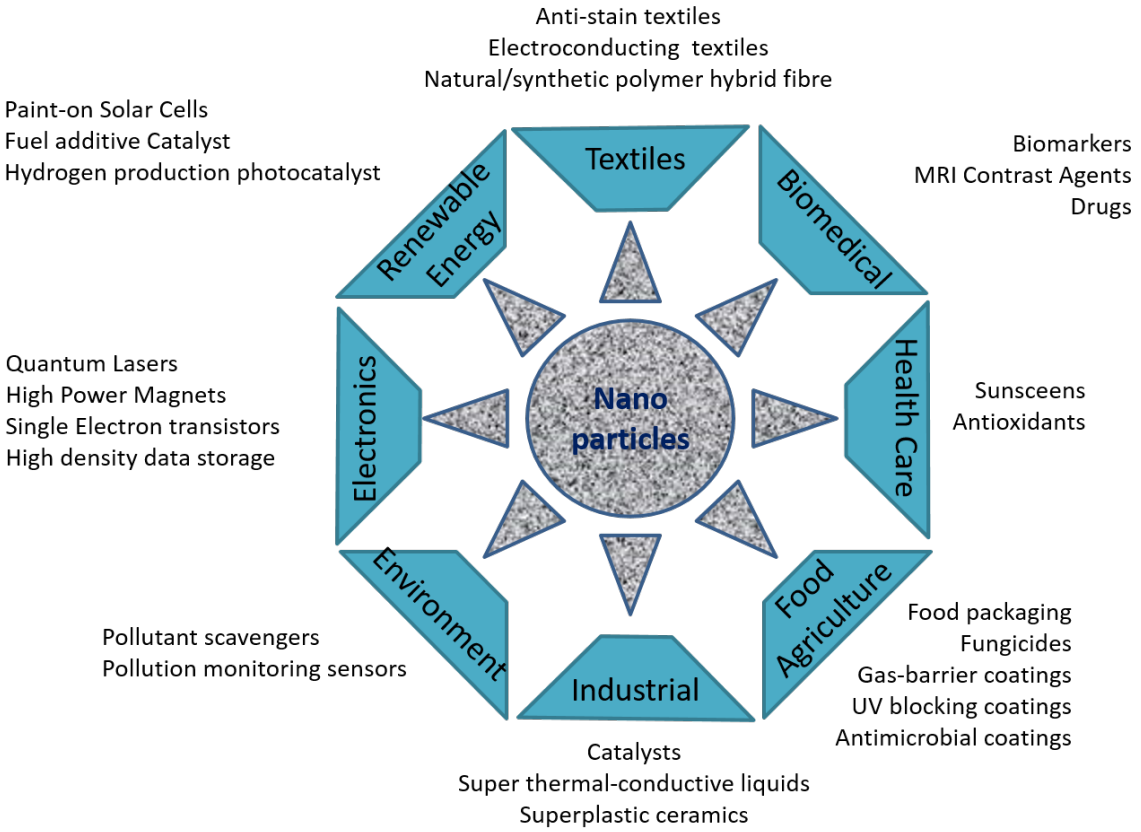

Figure 2: Uses of Nanoparticles. Figure adapted from Takuya (2009).[20]

approximately 90% of atmospheric NPs.[8] The remaining particles are derived from anthropogenic sources; combustion, industrial bi-products and deliberate manufacture.

The use of NPs is widespread; in 2011 there were 1317 products listed on the Project of Emerging Nanotechnologies' database (an increase of 512% from 2006). They are incorporated into a wide variety of areas including cosmetics, sun creams, toothpastes, car tyres (carbon black) electronics and research (Figure **??**). NPs can be fabricated in a number of ways and from a huge array of materials giving them a wide number of properties. Zinc oxide and titanium oxide absorb ultra-violet light and are very efficient in sun-cream due to the huge surface-area:volume ratio that can be achieved. Carbon NPs are being developed for military stealth vehicles due to their ability to absorb radio waves. In biological research, quantum dots can provide high resolution fluorescent imaging of specific cells, protein or DNA[10–13]. In medicine, particles are being exploited for rapid, topical application of antibiotics and chemotherapies either intravenously or ventrally.[14–19]

Anthropogenic NPs may enter the environment from a range of sources (Table **??**).[21] Aerosolised particles arise primarily from combustion which can be low scale (e.g. cooking, candles) or larger scale industrial combustion such as power plants. Particles may enter the human body from ingestion, inhalation or via skin lesions.

Natural	Anthropogenic Unintentional	Intentional
Gas-to-particle conversions		
Forest files	Internal combustion engines Power plants	Controlled size and shape, designed for functionality
Volcanoes	Incinerators	Metals, semiconductors, metal oxides, carbon polymers
Viruses	Jet engines	
Biogenic magnetite: magnetotactic bacteria, protoctists, molluscs, arthropods, fish, birds, human brain, meteorite	Metal fumes (smelting, welding etc.)	Nano -spheres, -wires, -needles, -tubes, -shells, -rings, -platelets
	Fumes: polymer, other	
	Heated surfaces	Untreated, coated (nanotechnology applied to many products: cosmetics, medical, fabrics, electronics, optics, displays, etc.)
Ferritin (12.5 nm)	Frying/broiling/grilling	
Microparticles (>nm; activated cells)	Electric motors	

Table 1: Sources of nanoparticles from natural and anthropogenic sources. Table adapted from Oberdörster et al (2005).[21]

Atmospheric NPs are primarily organic-based particles, formed as a combination of natural decay and combustion. In cities, where vehicle concentration is high, exhaust fumes may account for a large proportion of organic particles. In Los Angeles, approximately 65% of airborne UFPs ($<0.1\mu$m) are organic or elemental carbon, with smaller contributions from metal sulphates and nitrates.[22]

DEPs are formed from the combustion of diesel and nucleation within the exhaust pipe. 90% of the formed particles are in the region of 20-60 nm spheres or fibres.[23, 24] The composition of DEP includes the presence of polynuclear aromatic hydrocarbons which have been shown to be carcinogenic in rat.[8]

NPs have been used in cosmetic products for hundreds of years.[8] They may be used to provide colouring (TiO_2), wrinkle-concealment (aluminia powder) or for anti-oxidant effects and UV-scavenging (TiO_2, fullerenes).

1.1.2 Epidemiological Evidence of Harm to Health

Our immune systems have evolved with natural acpnp but studies have linked a detrimental effect of anthropogenic NPs to human health.[25–31]

Two pivotal studies, the Six Cities Studies,[28, 32] discovered a strong association between airborne particulates and mortality. The authors investigated mortality statistics from six US cities and the airborne levels of particulate matter <2.5 µm (PM2.5) with a follow up study of the same cities 10-20 years later. It was discovered that for a 10 µg/m^3 increase in airborne PM2.5, there was an increase in overall mortality with a risk ratio of 1.16. Furthermore, the inhalation of PM2.5 was associated with cardiovascular disease, lung cancer, and to a smaller extent, non-malignant respiratory disease.[32]

A different study investigating mortality in 20 US cities during 1987-1994, demonstrated an association with particulate matter <10 µm (PM10), even after adjustment for levels of ozone, NO_2 and SO_2.[25] For every increase in 10 µg/m^3, there was an increase of 0.68% in the relative rate of death from cardiovascular disease and respiratory causes.

A recent prospective analysis from the European Study of Cohorts for Air Pollution Effects (ESCAPE)[29] has shown an increased risk of acquiring lung cancer from exposure to acp10 and acp25. In this study, the effects of smoking, fresh fruit and geographical location (17 sites across Europe) were considered to discount possible confounding variables, and there was no risk associated with traffic-levels or NO_x. Furthermore, whilst adjusting for smoking

did reduce the risk of developing lung cancer, it did not eliminate the it. For every 5 µg/m^3 increase in PM2.5, the risk ratio was 1.18. In particular, the risk of developing adenocarcinoma was elevated (risk ratio of 1.55-1.65). The current recommendations from the European Commission for the Environment[33] is for PM2.5 to not exceed concentrations of 25 µg/m^3, in this study, there was an increase in risk for developing lung cancer with thresholds as low as 10 µg/m^3.

The effect of smaller particles has been difficult to assess by large scale epidemiology owing to the lac of monitering stations equipped to discriminate smaller, UFPs (<0.1 µm) and confounding factors relating to particular source and exposure route.[34] However, toxicity studies with UFP have shown that these particles may have greater toxicological effect compared to smaller particles (this is discussed in greater detail in **??**). In a study carried out on the road side in Birmingham, UK, UFP were identified from both diesel and petrol engines. At 4 m and 25 m away from the traffic, UFP accounted for 36-44% of the detected particles.[35] Similarly, a study in Atlanta has shown plooms of UFPs generated throughout the year. Anthopogenic particles were high during winter months, with increased atmospheric sulfur and nitrogen oxides suggesting a fossil-fuel source.[36]

The risk of NP pollution may extend to neonatal development. Polystyrene particles up to 240 nm were found capable of crossing the placental barrier[37] and silver NPs have been shown to impair foetal development in zebrafish.[30, 38] The effect of NPs on birth outcomes is not conclusive with a recent systematic review of epidemiological studies finding only a small association between maternal exposure to NPs and birth weight.[39] However, in a different study, a statistically significant association was observed for lung function (forced expiratory volume, FEV) in infants following prenatal PM2.5 exposure.[27]

A recent report (2016) from the Royal College of Physicians and the Royal College of Paediatrics and Child Health has stressed the impact of nanoparticulate exposure to health in neonates, young and elderly.[40]

1.1.3 *In Vivo* Deposition

Having entered an organism, particles may persist either via deposition in organs or via ingestion and accumulation in the food chain.[41] The blood load of ingested 10 and 25 nm silver NPs in rats was shown to decrease rapidly within 1 month following the end of treatment.[42] Similarly, there was a reduction of particle load in ovaries, kidney and liver over the course of 1-2 months, although systemically, particles persisted over the course of

at least 4 months (the study duration). In other essential organs, the brain and testis, particles persisted without decreasing for the time course of the study.

Nanoceria is used in an array of industrial processes and end-products as well as having therapeutic applications as an antioxidant.[43] Rats intravenously infused with 100 mg/kg nanoceria showed very little egestion of the particles over 90 days, with accumulation observed in all tissues, and in particular, the spleen, liver and bone marrow. Whilst the dosage was potentially very high, (3 nM is sufficient to reduce reactive oxygen intermediates *in vitro*),[44] there was near complete absence of any clearance of these particles.

The deposition of a particle may depend on both its size and surface chemistry. Bachler et al.[45] showed that particle size is inversely related to its ability to translocate through a monolayer of A549 cells. Nearly 100% of particles <10 nm were able to translocate through the cell culture whereas particles >20 nm showed very little translocation. Thus it may be that small inhaled particles are capable of passing through the lung epithelium. A study in which rats were ventilated with 5 nm zwitterionic particles or 27 nm anionic particles showed that both were capable of rapidly translocating to the lymph and blood stream, but only the 5 nm particles were passed into the urine.[46] In a long term-exposure model, rats inhaled 139 nm NiO particles over 4 weeks and the biological half time of the particles determined to be 62 days.[47] This demonstrates the importance of particle size. Small particles are capable of translocating rapidly and may be excreted, however larger NPs may be retained in the lung.

Studies have shown that intravenous NPs can pass through the blood brain barrier, and so it is feasible that inhaled acpnp entering the blood stream via lymph nodes could cause pathology in more distal parts of the body.[48–50]

Inhaled NPs smaller than 1 µm may reach the alveolar region of the lung, with greater deposition predicted for particles ¡100 nm.[22] The pulmonary system is the most likely entry portal for airborne NPs into the body. This region is highly evolved and the interactions of NPs in this region are discussed later (section **??**).

1.1.4 Interactions Between Nanoparticles and Biological Fluids

Proteins and lipoproteins interact with acpnp to form a dynamic structure called the protein corona which is hypothesised to be essential in establishing the 'biological identity' of the NP.[51] The protein corona is made up of proteins and lipids that form transient interactions,'soft corona' and permanent interactions, 'hard corona', with the NP itself.[51]

The corona can permit biological interactions between the NP and biological structures, organs and cells.[52] As particles translocate into different compartments within the body, the corona retains tightly bound proteins whereas others may be displaced by new proteins forming a new corona.[50] Since the corona gives the NP a biological identity, it follows that the bio-identity of the NP will change as it moves through the body. The protein corona, therefore, may move proteins into compartments where they may not normally be, causing atypical cellular responses such as altered transcription, translation, vesicle trafficking, cell death or inflammation. It has been shown that alveolar macrophage cells prior treated with acpnp and then exposed to lipopolysaccharide (LPS) have reduced tumour necrosis factor (TNF) and interleukin-8 (IL-8) secretion from inhibition of cytokine release, mRNA induction and protein production.[53] This demonstrates that acpnp may not just interact with proteins directly but also have a downstream effect on their synthesis, potentially altering susceptibility to disease.

1.1.4.1 Interactions With Proteins

1.1.4.1.1 Interactions with Single Proteins The interactions of proteins with NPs can be studied at a single protein level to reduce complexity at the particle surface. Thus techniques such as isothermal calorimetry, surface plasmon resonance and circular dichroism to determine binding enthalpy, association/dissociation constants and secondary structure effects and be used to investigate protein-particle interactions.[54]

Protein-particle interactions could be mediated through a number of protein properties. Arai et al.[55] showed, using polystyrene, polyoxymethylene and hematite that the primary effect mediating protein binding is through electrostatic interactions (charge repulsion/attraction) with secondary effects of hydrophobicity. A further influence of stability was postulated to be important following the strong absorbance of α-lactalbumin (LA) that was resistant to displacement by other proteins tested (lysozyme, ribonuclease and myoglobin). The lower stability of acala compared to other proteins results in structural rearrangements and greater free energy.

A study of protein binding kinetics showed that some proteins have a greater rate of association/dissociation than others and these rates are dependent on the particle characteristics, with hydrophobic particles having faster dissociation rates compared to more hydrophilic particles.[51] Furthermore, the binding capacity of hydrophobic particles was greater than hydrophilic ones. The curvature of the particles was further investigated

and shown to be an important consideration in the proportion of binding. For serum albumin, the optimal curvature was achieved with particles approximately 120 nm.[56] Presumably, this offers the most favourable stoichiometry for albumin binding, with the surface being either too curved or too flat for smaller and larger particles respectively.

Bound particles may interact with cell surface receptors. In a study of 20 and 50 nm gold particles with surface adsorbed fibrinogen, fibrinogen bound to 50 nm particles was able to interact with macrophage-1 antigen (Mac-1), generating a pro-inflammatory response via the activation of the transcription factor NFκB. Fibrinogen adsorbed to 20 nm was not able to elicit this response owing to alteration in surface structure.[57]

These experiments demonstrate mechanisms of protein-particle interactions, but do not represent the complexity of the in vivo environment for which it would be impossible to model the dynamics with the same degree of resolution. The interaction of proteins at the surface will be affected not only by the particle surface, but also neighbouring proteins and proteins already bound.

1.1.4.1.2 Dynamic Protein Corona The Vroman Effect[58, 59] describes how complex mixtures absorb to a flat surface in a multistep process. Proteins with a high association constant will bind rapidly to the material but will be replaced over time by proteins with a lower association constant and lower dissociation constant. Association constant is affected by the concentration of the protein and the proteins' diffusion rates, so that initially, highly abundant proteins will adhere to the material – such as human albumin in serological samples. These are replaced over time by proteins of greater affinity to form a corona more specific to the material. This is largely the prevailing theory as to how proteins interact with NPs and there are a number of reports that support this.[50, 60–63] The corona 'finger print' or 'hard corona' will be different depending on the surface chemistries/properties of the material and is the likely major contributor to the biological identity of the material. Loosely bound proteins may bind to the NP even after the hard corona has formed, forming a more transient layer – the 'soft corona'. Interactions between the proteins in the hard and soft corona may also interact with other proteins through protein-protein interactions (e.g. random forces of attraction, enzyme-substrate) to extend the corona beyond that of a single layer of proteins. Milani *et al.*[64] incubated fluorescently-labelled-transferrin-coated particles with plasma and showed that the corona was stable for at least two hours. They then incubated particles with unlabelled transferrin to form a stable hard corona first, followed with fluorescently-labelled transferrin to

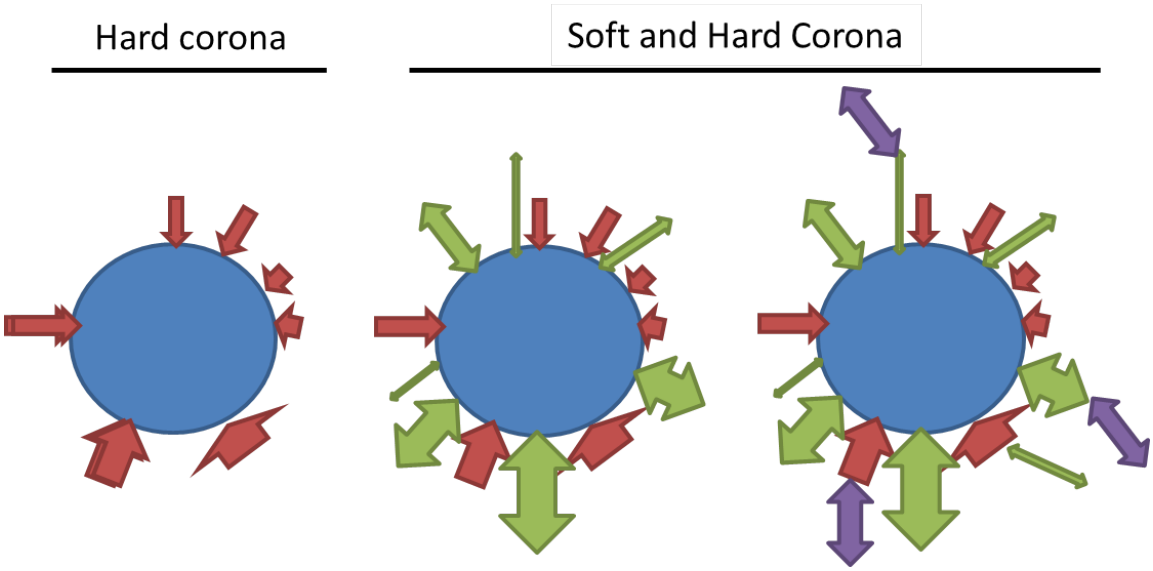

Figure 3: Hard and Soft corona. The hard corona (red arrows) is made of tightly bound proteins that form a stable shell. The soft corona (middle and right) is made up of more loosely bound proteins that dissociate and are exchanged over time. These may be bound directly to the surface of the particle (green double ended arrows) or via protein-protein interactions (purple double headed arrows). Since this is how NPs will present themselves to the cells, the protein corona is the primary site of interaction for single (not agglomerated) NPs. The proportion of proteins bound to the NP surface weakly (green arrows) will decrease over time as the hard corona matures.

generate a labelled soft corona. They showed that the soft corona was exchanged by plasma proteins through a drop in particle-associated fluorescent signal. This shows the multi-layered nature of the corona, consisting of at least a highly stable 'hard' corona and a more transient 'soft' corona (Figure **??**).

The Vroman theory stands in a lot of studies looking at the time-evolution of the corona. However, many studies do not have the time-resolution to look at very early stages of corona formation. Furthermore, quantification is difficult to achieve at the accuracy needed to monitor the kinetics of individual proteins over time in a complex sample. Through high resolution mass spectrometry, Tenzer et al.[63] have been able to generate quantitative data on individual proteins in human serum binding to various NPs. Their methods rapidly separated the NP-protein corona from unbound material by centrifugation through a sucrose cushion, meaning they could analyse protein corona formed within the first 30 seconds of its formation. Their data shows that the composition of the protein corona does not change significantly over time. Furthermore, whilst some proteins do conform to the Vroman effect, many binding patterns are not explained by this theory with some proteins (such as apolipoprotein A4) only binding between 15 and 60 minutes.

A common flaw with NP-protein studies is a failure to account for the soft corona as separation of the NPs from unbound material by centrifugation is thought to shear the soft

corona.[51] Proteins forming the soft corona are bound either directly and transiently to the NP surface or indirectly via protein-protein interactions and could account for the binding patterns seen in Tenzer *et al.*.

The Vroman Effect does go some way to describe the dynamics of the corona but does not accurately describe or predict the binding of individual proteins. This information could be vital in developing targeted drugs and predicting the movement/effect of NPs in the body. Therefore a combined approach, studying interactions of particulates with both single proteins and complex systems is required.

1.1.5 Interactions of Nanoparticles with cells

1.1.5.1 Particle Internalisation An early paper investigating the cellular interactions of colloidal gold nanoparticles showed that HeLa cells were capable of their internalisation, most likely through pinocytosis.[65] Since, there have been a large number of papers demonstrating the internalisation of particles through endocytic mechanisms.[66–68]

The possibility of particles than can enter cells via non-endocytic mechanisms has also be postulated.[68, 69] In particular, a study by Geiser *et al.*[70] showed that some internalised polystyrene and TiO_2particles were not associated to a membrane, which would be expected if uptake was through an endocytic mechanism. Cells treated with cytocholasin D, which inhibits actin polymerisation and thus prevents the membrane actin rearrangement required for endocytosis, still contained NPs. However, clathrin-mediated endocytosis is not necessarily inhibited by cytocholasin D[71, 72] and therefore their internalisation via receptor-mediated mechanisms cannot be excluded. Gold NP are not able to translocate across liposomes comprised of phosphatidylcholine, phosphatidic acid and cholesterol.[73] These liposomes are devoid of any proteins and therefore receptor-mediated transport is impossible. However, cellular membranes are a complex mixture of proteins and lipids of approximately equal mass, effecting the fluidity and surface reactivity of the membrane. Therefore this model may not be a good representation of the phospholipid bilayer and the transmission of particles into cells by passive diffusion is controversial.

If the particle is large enough, it may be possible for them to enter the cells via 'punching' a hole through the membrane. This appears particularly true for cationic particles. Holes were observed in an alveolar epithelial type I cell line, transformed type I cells (TT1s) after exposure to cationic polystyrene particles modified with a surface quaternary amine and this was associated with toxicity.[74] It is likely that is method of entry exploits transmembrane

potential, with the positively charged particles being attracted into the cytosolic space.[75]

The uptake of particles is firstly dependent upon the particle adsorbing to the cell membrane. The rate of adsorption is inhibited but not stopped by the presence of a protein corona.[76–78] As discussed, internalised particles are instantly exposed to biological molecules (proteins and lipids) and therefore uptake may be dependent on the identity of, and speed at which, this layer forms. For internalisation via endocytic mechanisms to occur, the membrane first wraps around the particle. Electrostatic forces, van der Vaals forces, hydrophobic forces and receptor-ligand reactions may all be important in driving endocytosis.[79, 80] Given that deformation of the membrane surface must occur for particle uptake, the shape, size and curvature of the particle is important in determining if the particle can be endocytosed. A spherical particle (<5 nm) may be too small for endocytosis to occur since the curvature of the particle surface is too great and the membrane surface tension required to encase the particle too high.

There is no observed effect of the cell cycle on particle uptake, although cell division may dilute particle load within dividing cells. This has important implication in tumour-targeted nanotherapeutics, as drug load may be diluted within rapidly dividing tumour cells.[81]

The endocytic uptake of particles is largely mediated by caveolae and clathrin-mediated endocytosis,[67] with the surface chemistry, size and shape being important mediators of the uptake pathway. For example, uptake of 100 nm carboxylated polystyrene (cPS) particles is inhibited by 60-70% with drugs that inhibit clathrin-mediated endocytosis (e.g. dynasore, chloropromazine) whereas similarly sized un-modified polystyrene particles are not.[82]

The shape and size of the particle similarly dictates the rate and route of uptake. In a study by Gratton *et al.* a nanofabrication technique was used to print particles of a cubic or cylindrical form. The uptake of cubic particles was greater for sizes of 2 μm^3 compared with larger. Uptake of cylindrical particles was greater than cubic with rate of internalisation depending on their aspect ratio (length/diameter). Larger aspects internalised at a much greater rate, even in the overall volume of the particle was similar.[3] Inhibition experiments showed that low aspect ratio particles were taken up by primarily by clathrin mediated endocytosis.

Caveolae-mediation pathways are favoured by larger particles. Rejman et al. showed that for ligand-free particles up to approximately 200 nm, clathrin-mediated endocytosis predominated, however uptake of 500 nm particles and greater was almost entirely by caveolae-mediated endocytosis.[83]

The uptake of particles in the lung may also be performed by immunological agents such as macrophages and dendritic cells.[84] The uptake of particles by these cells may be influenced by the presence of proteins in the corona. The interactions of inhaled particles with lung-constituents is discussed later (section **??**), however, it has been shown that proteins bound to the surface of the particles can affect their internalisation. For example, binding to pulmonary surfactant associated protein-A (SP-A) promotes the agglomeration of unmodified polystyrene (uPS) particles by acting as an opsonin, thus increasing their uptake. On the other hand SP-A stabilises aminated polystyrene (aPS) particles, maintaining their monomeric state in solution and reducing the uptake of these particles in alveolar macrophages.[85–88]

1.1.5.2 Toxicity Cellular toxicity from cationic particles has been described and explored in a number of papers.[89–92] In general, NP-induced apoptotic toxicity is thought to be mediated through the release of lysosomal contents (cathepsins) and subsequent caspase-mediated cell death. Loss of mitochondrial membrane integrity and adenosine triphosphate (ATP) production have been shown to be early events in aPS particle-mediated toxicity.[91] Amine-modified particles have been shown to induce cell death[91] in TT1 cells,[93] an immortalized human alveolar epithelial type I cell.[94] Following treatment with amine-modified NPs, cells sustained damaged membranes and their viability decreased significantly after 24 hours exposure. This shows the potential for inhaled particles to cause cellular damage *in vivo*.

Reunraroengsak *et al.* also showed the increased release of pro-inflammatory cytokine IL-6 following the same exposure.[93] The increase was more marked in TT1 cells exposed to 50 nm NPs compared to 100 nm particles matched by mass. This difference could be due to individual NPs having increased toxicity at 50 nm than at 100 nm, but when matching by mass it is important to note that both the number of particles and the surface area will be much larger for the smaller nanoparticle compared with the larger, therefore it is not clear if this is due to increased number of particles or surface area.

Particles can enter cells through energy independent[95] (through the plasma membrane) or dependent[80, 91, 96] (endocytic) pathways. Since bare NPs will never come into contact with cells *in vivo*, entrance into cells may be, at least in part, mediated via the protein corona on the surface. Indeed, it has been shown that specific proteins adsorbed on the NP surface can interact with cell surface receptors causing an activation of cytokines[57] or activation of complement.[97] Nanoparticles that have entered cells via endocytosis have

been shown to retain their corona within the lysosome.[89, 98] In this context, the corona may offer a degree of cellular protection since once it is cleaved by lysosomal proteases, damage to the lysosomal membrane is induced by the un-masked cationic particle leading to the release of pro-apoptotic signals and consequential cell death.[91] Oxidative stress has been shown to be induced by other NPs also, such as multiwalled carbon nanotubes, DEP and TiO_2.[53, 99] In TT1 cells, it has been shown that the application of polystyrene particles trigger the generation of reactive oxygen species (ROS). The surface modification on the polystyrene impacted the degree of ROS produced in the order aPS>uPS>cPS.[74] In macrophages, where uptake is likely by phagocytosis, ROS was triggered to a similar degree by all particles. But, ROS triggered in macrophages was not inhibited by N-acetyl cysteine (NAC), a strong anti-oxidant that was protective against ROS in epithelial cells, suggestive of an alternative mechanism for ROS generation and dependence on cell type and uptake mechanism. In a different study, NAC was partially capable of inhibiting ROS generated by aPS in macrophages, however, the effect was variable over time and therefore it may be that the amount of ROS generated during the oxidative burst exceeded the quenching capacity at the concentration of applied NAC.[100]

In an alveolar epithelial type II cell line, A549,[101] the application of cationic (aPS), but not anionic (cPS) particles were able to reduce the sensitivity of these cell to inflammatory signals, with reduced IL-6 and IL-8 in response to TNF-α application.[102] Both IL-6 and IL-8 are potent inflammatory cytokines; IL-8 is chemotactic for neutrophils and can interplay with IL-6, leading to further maturation of neutrophils and T-cells. Therefore it is possible that inhalation of similar particles in vivo could lead to greater susceptibility to infection.

A number of atmospheric particles have been shown to trigger inflammatory cytokines in macrophages, such as PM2.5 and DEPs, causing increases in TNF and cyclo-oxygenase-2 (COX-2).[53] In animal models, it has been shown that NPs can cause chronic inflammation, fibrosis and tumour progression. However, in human studies, the same degree of pathology is not seen.[103] This could be due to the limited number of human-based studies and that animal models may be subjected to a greater concentration of NPs. Also, as discussed later, the mechanism of chronic lung inflammation from NPs may require chronic rather than acute exposure.

It is possible that the sequestration of specific proteins onto the particle surface could induce pathology. Surfactant associated protein A and D, essential constituents of lung surfactant, have been shown to be sequestered to the NP surface, altering aggregation and

uptake.[85, 88] As important components of innate immunity,[104, 105] their sequestration may increase the chance of infection,[106] particularly in asthmatics, with reduced surfactant associated protein-D (SP-D) levels.[107]

1.1.6 Characterising the Protein Corona

The size and agglomeration of NPs may change depending on their environment. One important consideration is the media in which they are in, since particles may agglomerate differently depending on salinity, protein concentration, temperature, pH etc..[85, 108, 109] As discussed previously, the size of the particle can determine its interaction with proteins and the cell surface, as such, it is important to fully characterise the particles in all media used.[110]

There are a number of techniques for measuring the size of particles in suspension. dynamic light scattering (DLS) and NanoSight are techniques that track the Brownian motion of particles in real time. The reported size relates to how well the particle can diffuse through a solution and therefore is a combination of both the particle size and interaction with the suspension media. This is termed the hydrodynamic diameter and can be affected by particle density, shape, temperature and the viscosity and ionic strength of the suspension media. Therefore these techniques require detailed knowledge prior to derivatisation of their size.[111] However, DLS is one of the post popular techniques for this application as it is non-sample distructive, compatible with many particulates and solutes and versitile.[12, 85, 87, 88, 108, 109, 112–115]

Dynamic light scattering carries the assumption that the particles are spherical and because it measures light scattering, the technique is highly skewed towards larger particles, such that the intensity of a particle measured at 5 nm is $1x10^6$ times smaller than one for 50 nm particles. Therefore in solutions that are aggregating, the technique rapidly becomes less suitable. Some calculations can be performed to correct this, however the effectiveness of the applied formulae depends on the distribution of the acquired data.

In highly aggregated samples, other techniques, such as disk centrifugation and flow flield flow fractionation (AF4) have a much larger dynamic range and are not skewed by agglomeration. However these often require long method development and it may not be possible to recover sample post analysis.[116]

A further advantage to DLS is that zeta potential can be acquired on the same instrument. This is a measure of particles' electrostatic repulsion. As particles tend towards a 0 mV,

their stability decreases and they are more likely to form aggregates.

Through measuring the hydrodynamic diameter and zeta potential of acpnp in protein-containing media, the diameter and charge states can be seen to alter. For example, gold NPs incubated with serum have been shown to increase in diameter and have an increased zeta-potential even after washing, demonstrating that material is bound at their surface.[113, 117]

There are a number of techniques that have been applied to characterising the protein corona. size exclusion chromatography (SEC) [51, 61] and centrifugation[62, 118–121] have predominantly been used,[122] as well as AF4.[123] Cedervall *et al.* utilised SEC to analyse the hard and soft corona by comparing elution profiles when serum was incubated with and without NPs.[51] Whilst centrifugation does not allow mapping of the soft corona, one can analyse the hard corona without the expertise needed for SEC and it is more commonly available to laboratories, hence this technique is more frequently used. Flow field-flow fractionation can provide higher throughput analysis however is less-common since it requires specific expertise, equipment and method development.

The context of NP-protein-cell interactions is also very important, since the behaviour of the particles vary in different environments. *In vivo* experimentation in humans is rarely possible, and given that lung physiology, blood pressure, heart rate, metabolic rate and physiochemical environment differs between species, comparisons are not easy to make. However, the NPs are likely to be in a more similar environment in terms of pH, lipid:protein ratio and cellular make-up than in an *in vitro* model. Single cell models and multi cell models[99], cell lines and primary cells from the lung may give different results as well as including lavage or serum in media to mimic the pulmonary environment.

Proteomic analysis of bound proteins and lipids (see section **??**) has only been performed on NPs interacting with human serum. Data detailing the protein corona formed from interactions with lung tissue and fluid has not yet been collected. This could be due to a much higher degree of technical difficulty in extracting physiologically relevant samples from the lung. However, this information is of high importance in establishing, manipulating and understanding NP interactions within biological systems. By using alveolar epithelial cells from the lung and using bronchoalveolar lavage fluid (BALF), this project will collect physiologically relevant information about the protein corona formed during the early stages of NP inhalation.

1.2 Human Alveoli

During breathing, oxygenated air is drawn into the lung by low pressure generated in the chest cavity by contracting the diaphragm and intercostal muscles. The air travels down the upper airways and into the lower airways where oxygen is absorbed from oxygen rich air into oxygen-low blood by diffusion into a dense network of capillaries. Similarly carbon dioxide diffuses out of the blood stream into the air and is exhaled by relaxing the diaphragm and intercostal muscles.

The upper airways consist of the trachea which branches into two bronchi, one leading to each lung. These are lined with ciliated columnar epithelial cells and mucus-secreting Goblet cells. Mucus traps bacteria, dust and particles which is then wafted, by cilia, to the mouth or nose where it is swallowed or sneezed. Each bronchi splits into smaller bronchioles, which continue to divide into smaller branches, ending in spherical compartments called alveoli (a schematic is shown in Figure **??**). These are the primary site for gas exchange within the lung. Inhaled particles smaller than 200 nm will likely reach the alveoli region, where they interact with a highly evolved bio-mechanical surface.[21]

1.2.1 Alveoli

Air sacs (alveoli) form the airway termini in the lung. They are roughly spherical and generate a large surface area for the efficient exchange of oxygen from inhaled air and carbon dioxide from blood vessels. The surface area of the fully developed human lung alveolar-region is approximately 102.2-143 m^2.[124, 125] It is lined by epithelial cells,[124] of which there are two types, specialised for different functions (Figure **??**). AEI cells, which cover approximately 94% of total alveoli-surface area, are squamous with a large diameter (50-100 µm), ideally suited to minimise the diffusion distance for gas exchange. They also have high water permeability and could be important for controlling water distribution between the lung and underlying vasculature.[126] They are interspersed with smaller AEII cells which are cuboidal in shape and cover only 6% of the lung alveoli surface area despite outnumbering AEI cells by around 1.5 times.[124] They have two main functions: firstly, to secrete surfactant; this forms a layer on the inside of the alveolar and has a dual function of lowering the surface tension of the lung during breathing and immunological activation and regulation. Secondly, they can respond to cellular damage by re-populating AEI and AEII cells.[127–129]

Other major cell types of the alveoli include endothelial cells that form the dense network of

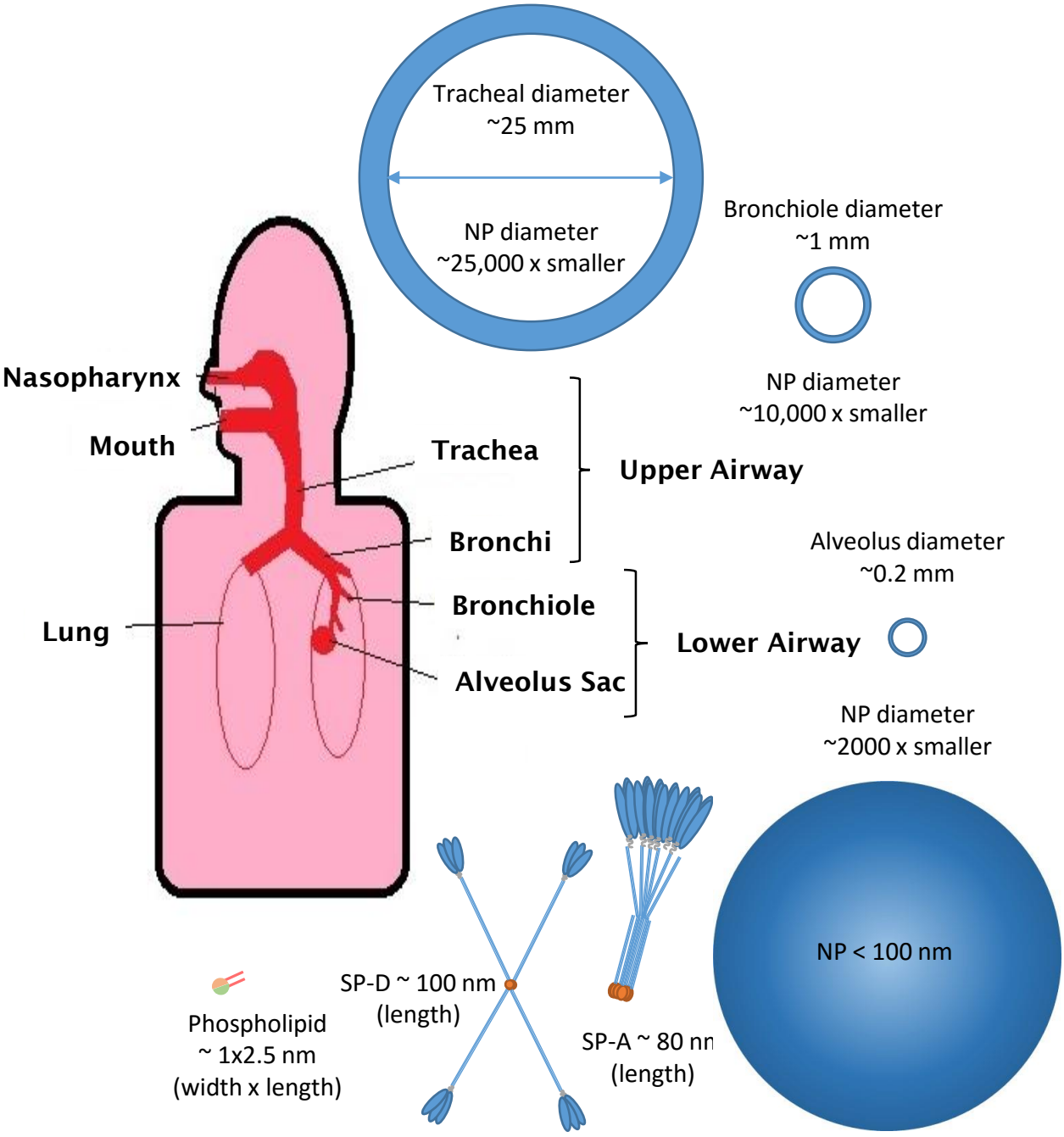

Figure 4: Schematic of Upper and Lower Airways showing relative diameters of airways, proteins, phospholipids and nanoparticles. Scales are approximate.

capillaries that surround the lung, alveolar macrophage that form part of the innate immune system and interstitial cells that maintain the surrounding structure.[124]

The immunological function of AEII cells extends beyond surfactant. AEII have been shown to express major histocompatibility complex class II and have been shown to express co-stimulatory molecules needed to activate T-cells.[130] Furthermore, AE cells have express a wide range of pro- and anti-inflammatory cytokines such as IL-1β[131, 132] TNF-α[132], IFN-β[131–133], IL-6[131–133] and RANTES[133] in response to a number of local stimuli such as Mycobacterium tuberculosis.[134] Hence they are also an important activator and regulator of the innate immune response which can be seen from excessive activation in patients suffering from chronic obstructive pulmonary disease (COPD),[135] where persistently high levels of IL-8 causes chronic over-recruitment of inflammatory leukocytes.

1.2.2 Pulmonary Surfactant

The primary role of surfactant is to reduce the surface tension at the air-liquid boundary in the alveoli space (Figure **??**), allowing the lungs to expand easily during inhalation. It is a lipo-proteinascous mixture, comprising 90% lipid and 10% protein. The predominant lipid components, phosphatidylcholines (PCs), are the primary agent for generating low surface tension and comprise approximately 80% of the total lipid, with half being the zwitterionic dipalmitoylphosphatidylcholine (DPPC). The remaining lipids are mainly charged, with a 10% contribution by negatively charged phosphatidylglycerols (PGs) and 3% from phosphatidylinositols (PIs). The protein fraction of surfactant is comprised of two hydrophobic proteins, pulmonary surfactant associated protein-B (SP-B) and C and two hydrophilic proteins SP-A and D. [136, 137]

A functional layer of surfactant is essential for lung function. Neonatal respiratory distress syndrome is a condition that afflicts premature babies, whose lungs have not yet developed sufficiently to secrete functional surfactant[138] and can be fatal if untreated with an exogenous source of surfactant.[139, 140]

The role of each lipid constituent is discussed in a review by Veldhuizen *et al.*.[136] The mechanisms by which pulmonary surfactant (PSf) reduces surface tension to near 0 mN/m[141] is not fully understood. DPPC is the only major component able to achieve the low surface tension and it is likely that during surface compression (from exhalation), the surfactant layer becomes enriched for DPPC (Figure **??**).[136, 142] The roll of negatively charged phospholipids, such as PG and PI are not clear, however surfactants comprising

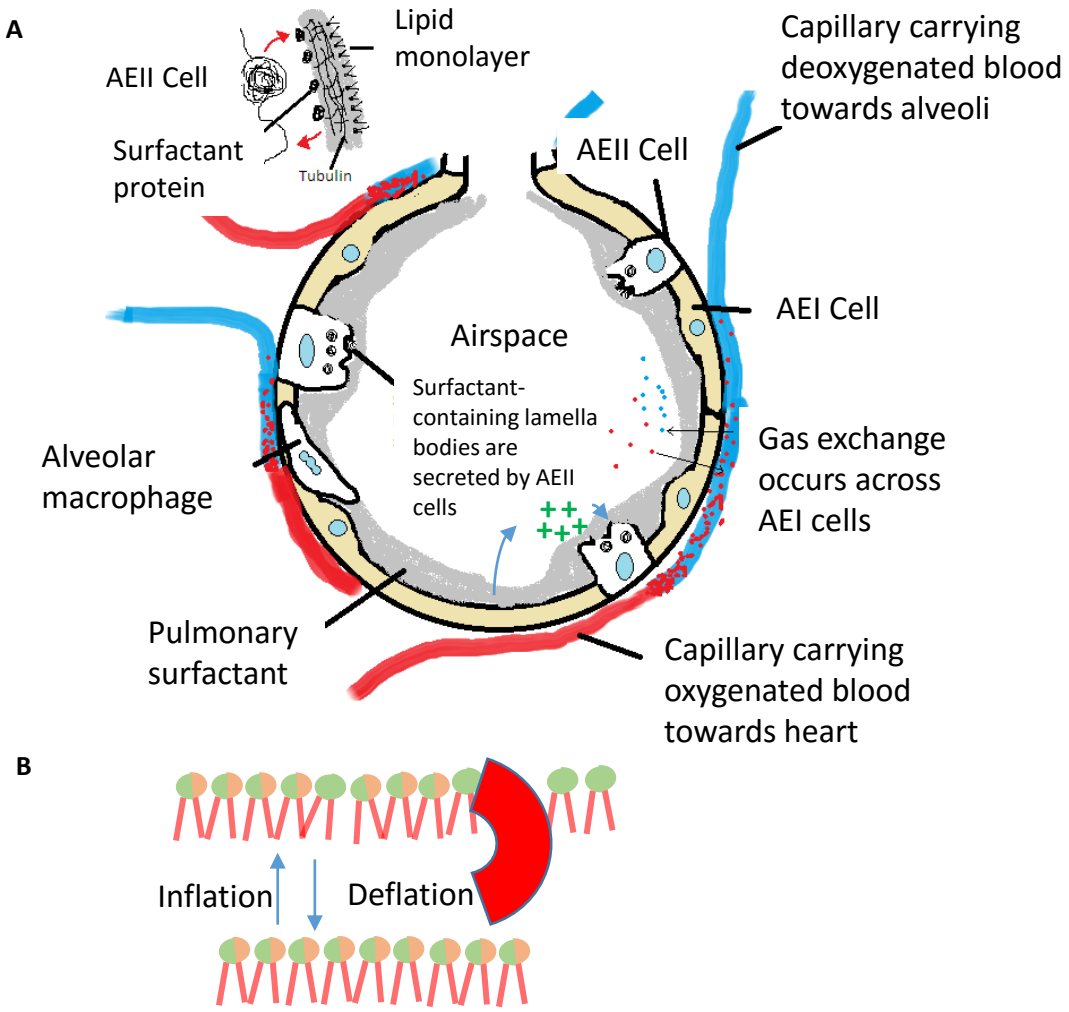

Figure 5: Lung Alveolus. (A) Alveoli are made of AEI cells, across which gas exchange occurs and AEII cells that secrete surfactant. The enlargement (top left) is of the interface between AEII cells and surfactant. Lamella bodies within AEII cells are secreted and open to release lattice-forming tubulin and other surfactant components. DPPC, the major lipid component of surfactant, forms a layer at the air-liquid interface. Surfactant is cleared and recycled by DPPC cells. Excess surfactant is also imbibed by macrophages. During expansion of the lungs, Ca^{2+} (green +) is secreted by AEI cells, triggering the release of fresh surfactant. (B) During breathing, pulmonary surfactant cylces between a mixture of lipids (ball and sticks) and proteins (red shape) during inhalation to high-enrichment for DPPC during exhalation.

DPPC-PG mixtures perform better than DPPC alone due to increased surface adsorption during compression and relaxation cycles.[143]

The hydrophobic protein SP-B can interact directly with PSf, most likely through directly binding to negatively charged species (such as PG). Its incorporation into model surfactants promotes better surface adsorption that DPPC or DPPC-acpg alone.[143] Its precise function is not fully known, but it has been implicated in having a number of roles including adsorption to the air-liquid interface, recycling of surfactant and innate immunity.[136] Knock-out for SP-B[144] in mice is lethal and deficiency can cause respiratory failure in humans.[145]

The hydrophilic proteins, SP-A and SP-D, are mannose-binding proteins, members of the collectin family, and form part of the innate immune system. Continuous recycling of the surfactant layer is essential in maintaining lung homeostasis, and SP-A may have a regulatory role in this through inhibition of surfactant secretion and enhancement of surfactant uptake by AEII cells.[146, 147] SP-A and SP-D can promote and regulate phagocytosis, T-cell polarization, hypersensitivity and inflammation as well as having specific bactericidal abilities.[104, 147–149]

SP-A and SP-D are members of the C-type collectin family. Each protein has a cysteine-containing N-terminus,[150, 151] a central collagenous region which is separated from the c-terminus by an α-helical coiled coil neck. The C-terminus is comprised of a C-type lectin domain (CRD) which binds carbohydrates in a calcium dependent manner[147] (Figure **??**). SP-A and SP-D are both large macro-molecules formed from multiple monomers that form trimers through interactions in the α-helical neck region;[152, 153] trimers further oligomerise into different macro-structures by forming disulphide bonds between N-termini.[150, 151]

SP-A is arranged by six trimers forming a tulip-like structure with all the CRD domains arranged at the same end. SP-D is comprised of four trimers (dodecamer) arranged in a cruciform shape (Figure **??**).[154] The dodecamers can further oligomerise into a spoked-wheel shape with a radius of 48 nm;[155, 156] protein superstructures with up to 8 dodecamers have been seen.[155]

1.2.2.1 Pulmonary Alveolar Proteinosis Excessive surfactant is a rare problem that leads to pulmonary alveolar proteinosis (PAP), where lipids and proteins build up in the lung interfering with gas exchange and causing shortness of breath. The disease can be

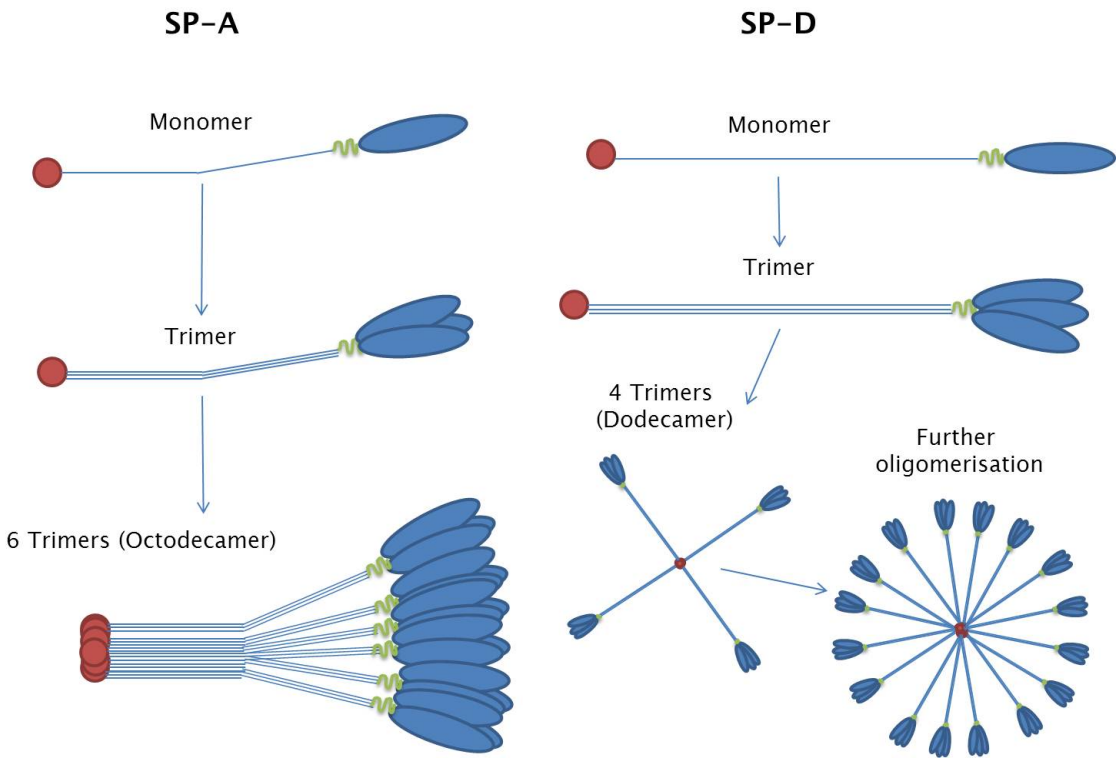

Figure 6: Structure of surfactant proteins A and D (SP-A and SP-D). Each monomer has a cysteine-containing N-terminus [red], a collagen-like domain [blue line], an α-helical coiled-coil neck region [green] and a CRD head [blue]. Monomers of SP-A [left] and SP-D [right] form trimers through interactions between hydrophobic amino acids in the neck region. SP-A monomers have a kink in the collagen-like domain which gives SP-A its tulip-bouquet-like structure when 6 trimers come together. SP-D's dodecameric macro-structure is formed from 4 trimers forming a cruciform shape. Each dodecamer may further oligomerise into a spoked-wheel structure with a radius of 48 nm.

acquired, congenital or secondary. Acquired and congenital PAP have been linked to mutations in SP-B, C and D, as well as granular monocyte-colony stimulating factor (GM-CSF).[157] Mutations in GM-CSF protein or receptor inhibit the activation of alveolar monocytes reducing the clearance of surfactant protein. Therefore, the composition of lipids are largely similar, but may be subject to time effects, such as oxidation. Treatment has evolved from lavage of individual lobes under local anaesthetic to full lavage of both lungs in the same session under general anaesthetic to remove the excess material.[157, 158] The composition of BALF is similar to non-PAP lung, however exhibits increased concentrations of proteins. In particular, SP-A and D have a 10 and 7-fold increase in concentration respectively.[159, 160] However, whilst the concentration of protein is higher, the ratio of the proteins may be similar. The disease is primarily caused by lack of surfactant clearance.

1.2.3 Nanoparticle Interactions with Pulmonary Surfactant

Measuring the effects of NPs on PSf *in vitro* is difficult. Not least because the exact ratio of protein:lipids and composition of pulmonary is unknown. As discussed earlier, the surfactant is predominantly made up of DPPC, with some PG species also present. The addition of SP-B is crucial since its absence is severely detrimental to health, however the exact ratio of DPPC:PG:SP-B is unknown. The full dynamics of surfactant spreading and recycling may depend on SP-A, which is often left out of experimental models. However, the surface tension reducing properties of these models are similar to the levels achieved in the lung and therefore can be used to assess the effect of NPs *in vitro*[161] or *in silico*.[162]

Nanoparticles can interact with PSf, and bind lipid and protein constituents to their surface.[85, 88, 163–165] They can also be pushed through the surfactant layer, passing into a hydrophobic phase underneath,[162, 166–168] and inhibit PSf.[161, 169, 170] The speed at which they may translocate through the surfactant layer is influenced by size and hydrophobicity. *In Silico* modelling of PSf with hydrophobic or hydrophilic particles shows that hydrophobic particles are more likely to be trapped within the PSf layer, whereas hydrophilic particles will rapidly translocate through to the underlying hydrophase.[162] Interestingly, both hydrophobic and hydrophilic anionic particles may have more of an effect on surfactant function as in translocating through the PSf layer, they may carry adsorbed SP-B.[171]

Dwivedi *et al.*[115] investigated the effect of different sizes of hydrophobic particles on PSf. There was no observed inhibition with particles of 12 nm, however larger, 136 nm particles,

decreased the effectiveness of the surfactant. Both particles caused some level of disruption to surfactant, however 136 nm particles caused severe morphological aberations at concentrations of 1 µg/mL, compared to 12 nm particles at 10-25 µg/mL.

The effect of particles on PSf has also been shown for TiO_2 particles. Schleh *et al.*[172] demonstrated that high concentrations (500 µg/mL) of polystyrene but much lower (100 µg/mL) concentrations of TiO_2 inhibited both the surface adsorption and minimum surface tension of a porcine surfactant (Curosurf^{TM}). The effect of particles on surfactant ultrastructure were investigated microscopically by examining Curosurf^{TM}incubated with TiO_2. Control samples had tightly packed lamella bodies, which became unfolded in the presence of particles. These lamella bodies are present in AEII cells in vivo and may act as a reservoir to deliver and replenish surfactant to the air liquid interface. The correct unfolding of these structures is essential for functioning PSf.

Nanoparticles can also bind to the hydrophilic surfactant proteins A and D. This may have implications in a number of ways. Firstly, it has been shown that the binding of SP-A to the surface of polystyrene particles alters their opsonisation of uptake by pulmonary macrophages.[85, 86] Binding to SP-D has also shown to increase uptake in A549 cells and in SP-D null mice, the uptake of NPs was reduced.[88] Secondly, the innate immune function of both SP-A and SP-D has been shown to be affected by NPs.[105, 106] The addition 0.001-0.04 cm^2/mL of unmodified, 100 nm polystyrene (uPS) coated in SP-A caused an increase in infectivity of A549 by influenza compared with the addition of SP-A alone. Similarly uPS particles inhibited the anti-viral effect of SP-D on TT1 cells infected with influenza. In an identical experiment performed with aPS particles, increases in inhibition of SP-D and SP-A were observed in A549 and TT1 cells respectively. Finally, it is possible that the sequestration of these key proteins may have detrimental effects to health. Low concentrations of SP-D in BALF is correlated with severe, treatment-unresponsive asthma[107] and mice lacking the SP-D gene have impaired lung function and structure.[173]

1.2.4 Alveolar Epithelial Cell Isolation

Since administering NPs to humans with the purpose of investigating their immunological and toxicological effect is unethical, we plan to isolate human epithelial cells from lung tissue obtained from lung wedge resection and use in monocultures to investigate the specific effect of NPs on these cell types.

There are a number of methods for extracting AEI and AEII cells from human lung tissue in the literature, such as gradient centrifugation,[174] magnetic beads[175] and fluorescent activated cell sorted (FACS).[176] AEI cells are very fragile, probably due to their large, thin structure (approximately 50-100 µm diameter) and abundance of ion channels making them susceptible to damage from non-physiological salt concentrations and physical stress. Consequently, techniques to isolate them need to be both gentle and relatively quick. AEII cells on the other hand are smaller, approximately 10 µm diameter, and more resilient to stress than AEI cells.

Fluorescence activated cell sorting interrogates individual cells for fluorescent markers and isolates them, based on a fluorescent signature, into different sample tubes. It follows that multiple cells may be isolated in a single FACS experiment, saving time and providing simultaneous analysis of live/dead status, size and number. This method has been used to isolate AEI and AEII cells from rat lung[176] using antibodies raised against rat AEI and AEII cells.

The extraction of alveolar epithelial cells is well reported in literature and reviewed by Dobbs (1990).[177] In brief, alveolar epithelial cells can be dissociated from extracellular membrane using elastase solution to specifically attack the extra cellular matrix supporting alveolar epithelial cells. Cells can be mechanically disrupted from surrounding tissue by gentle agitation and filtered through nylon meshes to individualise and remove non-cellular debris. Blocking cells with foetal calf serum and human immunoglobulin-G reduces any non-specific binding of the primary antibodies to analogous epitopes and to fragment-crystallisable (Fc) receptors present on endogenous macrophage, improving the yield of AEI and AEII cells.

1.2.4.1 Antibodies Against Human AEI and AEII Cells

Monoclonal antibodies against human AEI and AEII cells have been developed at the University of San Francisco by Dobbs and Gonzalez *et al.*. A monoclonal antibody against AEI cells was first developed in 1999 by isolating splenocytes from rats inoculated with AEI cells and culturing hybridomas.[178] Culture supernatant from 5000 hybridomas were tested against isolated AEI cells and fixed lung tissue for antibodies specific to AEI cells. Candidates were then tested against number of different tissue homogenates by western blot and shown to bind a lung-specific antigen approximately 55 kDa in size. This led to it being named HTI_{56}.

Whilst the antigen remains unknown, it is localised to the apical plasma membrane of AEI cells (shown by transmission electron microscopy (TEM) of immunolabelled lung

tissue[178]) and has been shown to have an isoelectric point between 2.5 and 3.5.

HTI_{56} has been shown to be a biomarker of acute lung injury by enzyme linked immunosorbant assay (ELISA).[178, 179] Substantially more HTI_{56} was identified in the pulmonary edema fluid of patients with acute lung injury compared with hydrostatic pulmonary edema. The biomarker was also found in serum, presumably since proteins from damaged AEI cells may be solubilised into the blood stream. HTI_{56} was 1.4-fold higher in acute lung injury patients compared with hydrostatic edema group and even greater compared with healthy controls.

A monoclonal antibody was developed by the same group against AEII cells by the same method.[180] The antibody target resolved as a dimer by western blot with two bands between 280-300 kDa. The antibody is named after the lower band; $HTII_{280}$. The antigen is specific to the apical plasma membrane and the antibody cannot be seen interacting with alveolar macrophage by immunohistochemistry. $HTII_{280}$ has not been investigated as a biomarker for lung disease as HTI_{56} has been.

1.3 Mass Spectrometry for the Detection and Quantification of Proteins in Nanoparticle Corona

1.3.1 Overview

In 1912, Joseph-John Thompson built the first mass spectrometer, which he used to show that Neon was made of two isotopes, Ne^{22} and Ne^{23}. The instrument and technique was further refined by his student, Francis Aston, who was awarded The Nobel Prize for Chemistry in 1922. Joseph Thompson had been awarded The Nobel Prize for Physics in 1902 for his discovery of the electron.

An explanation of mass spectrometry is provided in a review by Anas El-Aneed *et al.*;[181] a brief summary is provided in this section. Mass spectrometry (MS) is a method of determining the mass of individual molecules. Molecules are ionised and drawn into a mass spectrometer by an electromagnetic field. The force with which they are pushed into the MS is, therefore, a product of the magnetic field and the charge on the ion, i.e. a doubly charged ion will enter the mass spectrometer twice as quickly as the same ion singly charged. Force is also affected by mass so that heavy ions will accelerate more slowly than smaller ions; it is the ratio of mass to charge (m/z) that is detected by the mass spectrometer.

There are number of types of mass analyser frequently used in biology, exploiting either

oscillating radio-frequencies (quadrupole, Furious transform) or the time taken for the ion to pass between two points (time of flight).

Time of flight (TOF) analysers are conceptually the most simple; ions are pulsed into the MS simultaneously and fly, under vacuum, along a tube. The faster molecules (those with a low m/z) reach a detector (electron multiplier) first and the mass can be calculated since both the force applied to the ion and the speed of the ion through the TOF is known.

Quadrupole analysers are made of two sets of parallel electromagnets, positioned perpendicular to each other, across which the charge oscillates. Ions are deflected differently based on their m/z so that only ions of a specific m/z may pass through the quadrupole operating at a specific frequency. Ions that are too heavy or too light will either collide with the quadrupole or fly out of the analyser.

Prior to entering a mass spectrometer, peptides must be ionised. The most common way of achieving this for proteomics is by electrospray ionisation (ESI), where droplets of peptides in a volatile solvent are sprayed through a high voltage electric field. As the solvent evaporates, the solution becomes unstable and the peptides explode out, typically carrying a positive charge on their N-terminus. Peptides eluting from liquid chromatography (LC) can be fed directly into an electrospray ioniser and into a mass analyser (LC-MS).

After passing into the mass spectrometer, peptides (parent ions) can be fragmented further by colliding them at high speed into an inert gas - called 'collision induced dissociated' (CID) - and the m/z of both fragment ions and parent ions is detected. This generates a mass-finger print for each peptide which can be compared with a library of theoretical finger prints to identify individual proteins.

1.3.2 Tandem Mass Spectrometry and Protein Quantification

Multiple mass-selectors can be used in combination (e.g. quadrupole-time of flight, Q-TOF); this is termed tandem mass spectrometry (MS/MS).[182] This is the most common form of MS in proteomics as it allows the simultaneous identification and quantification of proteins.[183]

The mass spectrometer has a limited dynamic range of masses through which it can analyse accurately. Therefore proteins are first enzymatically digested prior to analysis. This causes a problem – because the protein mixture is now a complicated solution of unmatched peptides. To identify a protein, it is necessary to identify the peptide first, and then match

multiple peptides to a whole protein. This processes is aided by highly reproducible enzymatic digestion, using specific endopeptidases that cleave proteins in a predictable manner. Therefore the peptides expected from a protein digest can be predicted.

In MS/MS, the first analysis performed by the mass spectrometer is of the 'parent ion', this is the molecule that enters the MS – in the case of proteomics, a peptide. In the second analysis, performed immediately or soon after the first, the parent ion is fragmented and the fragment m/z values determined. The fragment masses are used to identify the peptide by searching a database of predicted fragment masses. Proteins are identified by searching the peptide masses (parent ion m/z) against a database of predicted protein digests.

Because MS/MS is very fast, multiple peptides can be isolated and fragmented before there is a need to perform a new parent ion scan. Typically, it is the top most abundant peptides identified from the parent ion scan that are fragmented. This approach is called data dependent acquisition (DDA) as the peptide selection and fragmentation depends on the intensity data acquired in the parent ion scan. Depending on the instrument speed, 6-40 peptides form the first MS analysis may be sequentially isolated, fragmented and analysed.

The disadvantage to this technique is two-fold. Firstly, only the most intense peptides are analysed and therefore lower abundance peptides/proteins may not be detected.[184] Secondly, since not all molecules entering the mass spectrometer are analysed, absolute quantification is not possible, instead, relative quantification is achieved.

An alternative approach, termed MS^E, is to fragment everything and use chromatography elution data to deconvolute the far more complex MS/MS spectrums (Figure **??**). By using this method, less bias is put on the most intense parent ions and less abundant peptides may be analysed. In order to achieve a high detection rate with accurate masses for both parent ions and fragmentation ions, the mass spectrometer switches between low collision energy and high collision energy. This pattern of data-independent acquisition provides an opportunity for simultaneous protein identification and quantification (Figure **??**).[185] A further progression in this field is the development of ion mobility incorporated into MS/MS systems (Synapt G2s, Waters). This adds a further level of separation between the parent ions, allowing more accurate deconvolution of fragment ions.

This approach to NP corona analysis has been performed by Tenzer *et al.*(2013).[63] They were able to identify and quantify a high number of proteins adhering to NPs over time with a high degree of resolution, in terms of quantification, in order to generate kinetic information on the evolution of the protein corona in serum. Whilst their approach was

largely untargeted we hope to generate similar data to answer specific questions about the effect of components of the corona on cellular immune-activity within the lung.

Absolute quantification by MS is conceptually simple although difficult in practice. A sample is spiked with a known concentration of 'standard peptide'; by comparing the intensity of the known standard peptide and the unknown samples, absolute quantification can be derived. This is analogous to Western blotting using a concentration standard against which to quantify a target peptide. As different peptides are not equally ionisable, for accurate quantification, an isotopically labelled peptide should bewhich is the same peptide as that which you are quantifying, should ideally be used. The isotope label shifting the mass of the standard peptide sufficiently to differentiate between it and sample peptide. This makes protocols for these experiments expensive since peptides for the samples need to be made either synthetically or through recombinant expression. It has been shown that the average intensity of the top 3 most abundant proteins in highly proportional (R^2=0.99) to the protein concentration.[186] This can be used alongside LC-MS^E data for absolute quantification. The 'universal signal response factor' can be calculated based on the three most intense tryptic peptides for a spiked protein standard. This value can be applied to all peptides in a sample to provide absolute quantification. There are a number of other label-free techniques for absolute quantification, such as APEX, emPAI and iBAQ.[187] Intensity-based absolute quantification (iBAQ) performs similarly well to Top3[188, 189] in terms of accurate quantification and sensitivity. However quantification by this technique is more labour and bioinfomatic intensive and therefore I have used a Top3 based quantification approach here.

Cedervall *et al.*[51] have shown than an extensive list of detected proteins can be achieved by LC-MS/MS following 1D-electrophoretic separation of proteins on a polyacrylamide gel. However we propose to digest proteins directly off the NPs as described by Zhang *et al.*[62] They made a comparison, in terms of the number of different and identical proteins detected by MS, between NP-bound proteins digested directly from the beads using trypsin and having been eluted with sodium dodecyl sulfate (SDS). They showed that there was only marginal differences between the methods. Digestion directly off the beads permitted the detection of 87 proteins (3 unique) vs 85 (4 unique) from SDS elution. Digesting with trypsin directly from the NP gave greater efficiency in terms of time, money and the number of peptides detected. This, therefore, is the strategy hoped to be adopted in this report.

It will also be important to show that washing is sufficient to remove any unbound protein from the NPs and therefore all proteins detected in the mass spectrometer are entirely from

the protein corona, although this may have implications in differentiating between the soft and hard coronas.

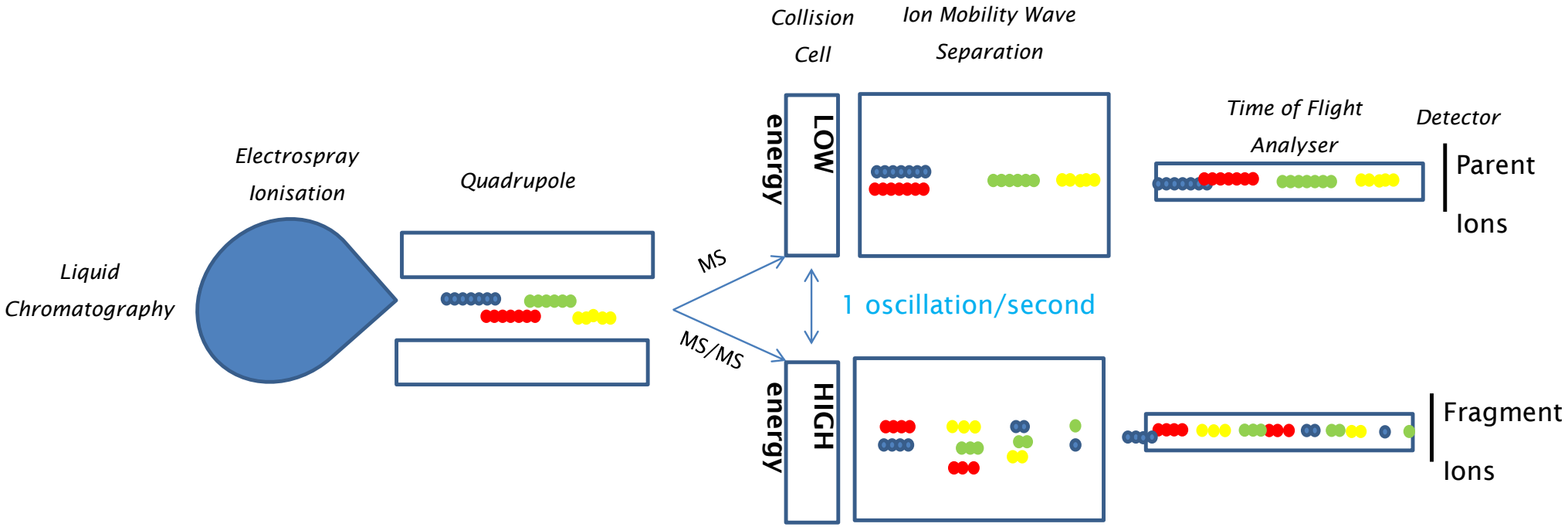

Figure 7: Schematic of MS^E. Peptides are separated, based on their hydrophobicity by HPLC and fed into electrospray ionisation. All parent ions pass through the quadrupole before moving into collision cells. The collision cell oscillates between high energy and low energy to fragment or not fragment the parent ions. Ions are separated based on their cross-sectional surface area in the ion mobility cell before entering the TOF analyser to be separated based on their mass to charge ratio (m/z). All parent ions and all fragment ions are detected without discrimination. Fragment ions are allocated to their parent ions by aligning elution times from the chromatogram and ion mobility data with mass spectra.

1.4 General Research Aims

- Isolate AEI and AEII cells from human lung tissue and develop primary cell culture.
  - Dissociate AEI and AEII cells from human lung tissue.
  - Isolate the cells by FACS using monoclonal antibodies against each cell type.
- Determine and characterise the protein corona when proteins are incubated with human lung lavage.
  - By incubating nanoparticles with bronchoalveolar lavage and detecting the proteins by mass spectrometry.
  - Quantifying individual proteins of the protein corona over time by comparing the intensity of the top three peptides for each protein with an internal standard.
- Determine the effect of the protein corona on AEI and AEII cells from the perspective of their pro-inflammatory response
  - By measuring the changes in mRNA expression of pro-inflammatory cytokines that have been exposed to nanoparticles.

2 Materials and Methods

2.1 Introduction

This chapter details general methods used throughout this thesis. Chapter-specific methods are detailed at the beginning of the relevant chapter.

2.2 Cell Culture

Unless otherwise stated, cells were cultured under humidified conditions at 37°C with an atmosphere of 5% CO_2. They were routinely passaged with 0.25% trypsin-ethyldiaminotetracetic acid (EDTA) solution (Sigma) to maintain log phase growth. For storage, cells were frozen to 80°Cat approximately 1°C/min in cell culture medium with 10% dimethyl sulfoxide (DMSO) before being transferred to liquid nitrogen. When necessary, cells were counted with a haemocytometer, using trypan blue to differentiate between living and dead cells.

2.2.1 Materials

Material	Company
RPMI 1640 with L-Glutamine	Life Technologies (52400-025)
DCCM-1	Cellseco (05-010-1A)
Fetal bovine serum	PAA (A15-144)
Heat inactivated fetal calf serum	Life Technologies (26010-074)
Penicillin/Streptomycin	Sigma (031M0787)
L-Glutamine	Life Technologies (25030-24)
G418 disulfide salt solution	Sigma
Phorbol 12-myristate 13-acetate	Sigma (P8139)
Phosphate buffered saline, pH7.4	Life Technologies (10010-015)
Trypsin/EDTA	Sigma (T3924-100ML)
Dimethyl sulphoxide	Sigma (D2650)

Table 2: Cell culture reagents.

2.2.2 A549 Cells

Human acaeii-like adenocarcinoma cells line, A549 cells[101, 190], were cultured in maintenance media of Roswell Park Memorial Institute medium 1640 (RPMI) with L-Glutamine (2 mM) supplemented with 10% fetal bovine serum (FBS) and 100 units/mL

penicillin, 100 µg/mL streptomycin (1% pen/strep) in a humidified atmosphere of 5% CO_2 at 37°C. Cells were seeded and grown in T75 flasks and routinely passaged with 0.25% trypsin-EDTA solution (Sigma) to maintain log phase growth.

2.2.3 Raw 264.7 Cells

Mouse leukaemic monocyte macrophage cell line (RAW) cells[191] were cultured in T75 flasks with a maintenance media of RPMI L-Glutamine supplemented with 10% heat inactivated FBS HIFBS (Sigma) and 1% pen/strep.

2.2.4 Transformed Type 1 (TT1) Cell

The human AEI-like cell line, transformed type 1 (TT1) cells (kindly donated by Prof. Terry Tetley, Imperial College London) are transformed primary AEII cells that have differentiated into a AEI-like phenotype.[94] They were cultured in T75 flasks in DCCM-1 media plus 2 mM L-Glutamine, 1% pen/strep, 10% achifbs and 0.5 mg/mL G418.

2.2.5 THP-1 Cells

The peripheral blood monocytic cell line, THP-1 cells[192] are a non-adherent human cell line. They were cultured in T25 or T75 flasks and maintained at a density between $4x10^5$ cells/mL to $1x10^6$ cells/mL in RPMI with L-Glutamine, 10% HIFBS and 1% pen/strep. Cells were differentiated by treating with 10 mM phorbol 12-myristate 13-acetate (PMA) for three days. Differentiated cells stop dividing and become adherent cells with extended filopodia.

2.3 Protein Concentration Determination

2.3.1 Bicinchoninic Acid Assay

Protein concentration was determined using a bicinchoninic acid (BCA) assay. The protocol is a colour-metric assay, adapted from Smith *et al.*[193] In brief, a working solution was prepared by mixing 4% (w/v) $CuSO_4$ (in distilled di-ionized H_2O (ddH_2O)) with BCA in the ratio of 1:49 and 100 μL was combined with 12.5 μL of sample in a 96 well plate. The reactions were left at 37°C for 30 minutes and absorbance read at 550 nm on a Thermomax Microplate Reader (Molecular Devices). Samples were prepared in triplicate and compared

to a standard curve of bovine serum albumin (BSA) (also prepared in triplicate) using Graphpad (Prism).

2.3.2 Infrared Spectroscopy

The concentration of proteins and peptides were determined by infrared spectroscopy (IRS) using a Direct Detect Spectrometer (Merck Millipore) as per the manufactures instructions. The technique compares the absorbance of IR by amine bonds in the region of 1600-1690 cm^{-1} with a standard curve.

2.4 Nanoparticles and their Characterisation

2.4.1 Particles

Company	Reference Number	Material	Modification	Size
Polyscience	00876-15	Polystyrene	Unmodified	100 nm
Polyscience	16586-5	Polystyrene	Amination	100 nm
Polysceince	16688-15	Polystyrene	Carboxylation	100 nm
Evonik Industries	Aerodisp W 740 X	Titanium dioxide	Unmodified	14 nm[a]

Table 3: Nanoparticles and their nominal label sizes. [a]The size of $TiO_2$was determined in house (Section **??**).

2.4.2 Surface Area Calculation

2.4.2.1 Polystyrene

$$\begin{aligned} Number\ of\ particles\ per\ mL &= \frac{6W10^{12}}{\rho\pi\varphi^3} \\ Surface\ area\ of\ a\ sphere\ (cm^2) &= 4\pi r^2 \\ Total\ surface\ area\ (\mu m^2/mL) &= \frac{6W10^{12}}{\rho\pi\varphi^3} 4\pi \left(\frac{\varphi}{2}\right)^2 \\ Total\ surface\ area\ (m^2) &= \frac{6W}{\rho\varphi} V \end{aligned} \tag{1}$$

Total surface area calculation of spherical nanoparticles in a suspension $W = grams/mL$, $\rho = density\ of\ particle\ (g/mL)$, $\varphi = diameter\ of\ particles\ (\mu m)$ and $V = volume\ (mL)$

2.4.2.2 Titanium Dioxide The above equation (Equation **??**) for the number of particles/mL (section **??**) assumes the particles are spherical. The TiO_2 NPs are irregular polygons and the equation therefore provides an estimate of their surface area. Their diameter was taken to be their median longest length as determined by TEM (Section **??**).

2.4.3 Characterisation

Nanoparticles were characterised by a number of different approaches to determine their size, hydrodynamic diameter and zeta potential in a number of different media (this is further described in Chapter **??**).

2.5 Polyacrylamide Gel Electrophoresis and Wester Blot

2.5.1 Materials

Material	Company
SDS PAGE Loading Buffer (4x)	Life Technologies (1386564)
SDS PAGE reducing agent (10x)	Life Technologies (NP0009)
4-12% Bis-tris gel	Life Technologies (NP0335BOX)
MES Running buffer	Life Technologies (NP0002)
iBlot PVDF Membrane	Life Technologies (IB4010-02)
Simply Blue Safe Stain	Life Technologies (LC6065)
TMA-6	Lumigen

Table 4: Gel electrophoresis and Western blot reagents

2.5.2 Sodium Dodecyl Sulphate Polyacrylamide Gel Electrophoresis

Sample was prepared in SDS PAGE loading buffer with ddH_2O, with or without reducing agent. Samples were heated to 80°C for 10 minutes in a heating block, briefly centrifuged and loaded onto a gel. Gel electrophoresis was performed for approximately 35 minutes at 200 V. Gels were stained with Simply Blue Safe Stain in the microwave according to the manufactures instructions and distained over-night in ddH_2O. ddH_2O was changed at least once before imaging.

2.5.3 Western Blotting

Unless stated otherwise, Western blotting was performed as follows. Polyacrylamide gels were transferred to a polyvinylidene fluoride (PVDF) membrane using an iBlot^{TM} (Invitrogen) 7 minute method as per the manufacturer's instructions. Membranes were rinsed in tris-buffered saline with tween-20 (TBST) (20 mM Tris, 150 mM NaCl, 0.1% Tween 20 (v/v) ddH_2O, pH7.4) to remove transfer buffer and blocked overnight with blocking buffer (TBST, 5% skimmed milk) at 4^{o}C. Membranes were probed with primary antibodies, washed 3x for 5 minutes in TBST and incubated with secondary antibodies. After a further three washes, protein bands on the blots were visualised by applying TMA-6 and exposing to film or camera.

Specific antibody details are given in each chapter where appropriate.

2.6 Antibodies

Antibody	Company	Purpose
Mouse Anti-HTI_{56}) (Isotype IgG^1)	Professor Leyland Dobbs and Robert Gonzalez,University of San Francisco, California	Bind AEI cells.
Mouse Anti-$HTII_{280}$ (Isotype IgM)	Professor Leyland Dobbs and Robert Gonzalez,University of San Francisco, California	Bind AEII cells.
Goat Anti-mouse IgG^1 -Alexa Fluor 633	Life Technologies (A21126)	Fluorescently label AEI cells by binding anti-HTI_{56}
Goat Anti-mouse IgM -Alexa Fluor 488	Life Technologies (21042)	Fluorescently label AEII cells by binding anti-$HTII_{280}$
Human IgG	Sigma (I4506)	Block endogenous Fc receptors for FACS and immunohistochemistry
Goat Anti-mouse IgG_1 – horse radishperoxidase	Santa Cruz Biotechnologies (sc-2967)	Chemiluminescent detection of anti-HTI_{56}
Goat Anti-mouse IgM – horse radish peroxidase	Santa Cruz Biotechnologies (sc-2973)	Chemiluminescent detection of anti-$HTII_{280}$
Mouse IgM anti-TNP -keyhole Limpet Hemocyanin	BD Biosciences (553472)	Isotype control for FACS
Mouse IgG_1 anti-MOPC-2	BD Biosciences (554121)	Isotype control for FACS
Mouse IgG_2a anti human CD45-VioBlue	Miltenyi Biotech Ltd,(130-098-136)	Discriminating against CD45+ cells by FACS
Mouse IgG_2a-VioBlue	Miltenyi Biotech Ltd,(130-098-898)	Anti-CD45 Isotype control

Table 5: Antibodies and their use in the context of this project.

2.7 Ethics

Human lung tissue was collected and supplied by Dr Jane Warner, under ethics approved by the National Research Ethics Service (NRES) Committee South Central Soton A, reference 08/H0502/32. The tissue was removed from patients undergoing bullectomy or other surgical procedures for therapeutic reasons. The tissue was donated by the patients after fully informed consent.

Bronchoalveolar lavage fluid from patients with pulmonary alveolar proteinosis undergoing the procedure for therapeutic reasons, was taken by Dr Mark Giffiths, Royal Brompton, under ethics approved by the Respiratory Biomedical Research Unit Heads of Consortia (NRES reference 10/H0504/9). All bronchoalveolar lavages were donated by patients or participants after fully informed consent.

3 Nanoparticle Characterisation and Toxicity

3.1 Introduction

Size, charge, shape and chemistry have been shown to be an important factor in determining particle uptake and cellular reactivity.[4, 66, 80] Therefore it is essential to determine the characteristics of a acnp when considering its cellular effect.

Agglomeration is mediated through weak coulombic interactions at the particle surface and therefore determination of the electrostatic charge (zeta potential) of a particle is indicative of its stability. If the zeta potential is low, (close to zero) there is little charge at the particle's surface and these particles are considered less stable and more likely to agglomerate. On the other hand, particles with a high zeta potential, either positive or negative, are more likely to be monomeric (stable) in solution due to greater repelling force between similarly charged surfaces. The charge on the particle surface can be affected by the pH of the solution or through interactions with other molecules within the media and, therefore, this measurement should be determined in all media used.[108]

The air quality standards legislated by the European Commission limit particles (<2.5 µm) to 25 µg/m^3.[33] However, studies examining particulate concentration in urban areas show that concentrations of particulates <10 µm can exceed 600 µg/m^3.[194] The application of inhaled nano-therapeutics is in its infancy and may provide benefits over conventional therapy such as increased drug absorption and carrier efficiency.[195] However, dosages would expect to exceed environmental limits and therefore assessment of particle toxicity at high concentrations is also required. To mimic likely exposure to NPs, we used a range of ˜0.02 – 200 µg/mL (0.01 – 100 cm^2/mL). Whilst the minimum dosage exceeds the maximum environmental exposure cited above (2.5 µg/m^3 = 2.5x10^6 µg/mL), in vivo airborne particles would accumulate in the lung alveolus owing to deposition of inhaled particles. A study of asthmatics in Tel-Aviv showed an association between inflammation and the accumulation of NP over 3 days.[196]

The state of particles in phosphate buffered saline (PBS) and lavage are investigated in this chapter, using a number of complementary techniques. The effect the particles have on lung epithelium was then assessed, investigating mitochondrial activity, generation of ROS, cell lysis, inflammatory response and sensitivity to inflammation.

3.1.1 Aims

To characterise the particles in the context of the pulmonary/alveolar environment, including particle-interactions with lung-lining fluids and cells by:

1. Investigating charge and size/agglomeration of particles in BALF.
2. Assessing particle toxicity to AEI and AEII cells.
3. Assessing particle-interactions with cells (uptake and membrane interactions.

3.2 Methods

3.2.1 Cell Culture

See Section **??**.

3.2.2 Preparation of BALF-Coated Nanoparticles

20 mL of lavage fluid was centrifuged briefly (˜2 minutes) at 300 x g to pellet large agglomerates before being centrifuged for 30 minutes at 14,000 x g to remove smaller lipid-complexes and debris. 500 cm^2 of NPs was combined with the centrifuged BALF and left at 37°C for 1 hour. The suspensions were centrifuged at 14,000 x g to pellet the BALF-coated particles and suspended in 0.5 mL of BALF, using the BALF to carefully rinse the particles from the side of the centrifuge tube. Particles were further centrifuged at 17,000 x g, 15 minutes at 4°C in a 1.5 mL LoBind Eppendorf. The pellet was suspended in 50 µL of lavage and vigorously pipetted and vortexed until a uniform suspension was formed (judged by eye). 10 µL of BALF-particle suspension was added to 990 µL SF-RPMI to yield a final concentration of 100 cm^2/mL with 1% (v/v) BALF. Other concentrations were prepared by serial dilution from 100 cm^2/mL.

3.2.3 Physical Characterisation

3.2.3.1 Dynamic Light Scattering and Zeta Potential Dynamic light scattering (DLS) and zeta potential (ZP) measurements were acquired using a Zetasizer Nano ZS (Malvern Instruments) in PBS pH 7.4 (Gibco by Life Technologies, UK). In both instances, 5 cm^2 of particles were mixed with 1 mL of PBS and their hydrodynamic diameter and ZP measured immediately at 37°C in a disposable polycarbonate cuvette (Malvern

Instruments). A number of size measurements were derived from the data and the average size by number-distribution was reported as this is less affected by heterogeneous particle sizes (polydispersity).

3.2.3.2 Electron and Atomic Force Microscopy This work was carried out at the Facility for Environmental Nanoscience Analysis and Characterisation (FENAC), University of Birmingham with the assistance of Dr Christine Elgy. TEM was performed using a JEOL 1200 TEM with 80 KeV electron generation. Particles (5 cm^2) were mixed with 1 mL of BALF or PBS and 15 µL deposited on a carbon-coated (approx. 15 nm) copper grid (prepared in house, Quorum Q150T ES carbon coater, Quorum Technologies) for 30 minutes before being immersed in Milli-Q water and dried overnight. Samples for atomic force microscopy (AFM) were prepared in a similar fashion except samples were deposited on freshly cleaved mica sheets. Images were acquired using an XE100 AFM (Park Systems) in non-contact mode with a Si-cantilever (PPP-NCHR, Park Systems) at 300 Hz and a force constant of 42 N/m. TEM images were analysed using ImageJ by measuring the longest length and AFM images using XEI software (Park Systems). For size quantification using TEM, approximately 100 particles were averaged.

3.2.4 MTT Assay

3-(4,5-dimethylthiazol-2-yl)-2,5-dephenyltetrazolium bromide (MTT) assay is a colorimetric based assay in which a purple substrate can be detected through absorbance at 550 nm. Water-soluble MTT is converted into insoluble formazan by live cells which can be dissolved in isopropanol and measured spectrophotometrically. 1.5 x 10^4 cells per well were seeded onto a 96 well plate and left for 24 hours to adhere with 100 µL maintenance media. Cells were washed 3 x 100 with µL PBS before being treated with NPs. BALF-incubated or uncoated NPs were applied suspended in 100 µL of serum and phenol-red free media with 1% BALF added. Following treatment, cells were washed three times with PBS and 50 µL MTT (0.5 mg/mL) (Sigma, UK) added for 4 hours at 37°C in the dark. Preliminary experiements in which NPs were incubated with MTT reagent showed no interence from NPs.

The plates were centrifuged at 300 x g and MTT carefully pipetted off. Formazan was dissolved in 100 µL isopropanol on a rotary shaker at 750 revolutions per minute (rpm) in the dark for 30 minutes at room temperature. The absorbance was read at 550 nm on ThermoMax Microplate Reader (Molecular Devices) using SOFTmax version 2.35

(Molecular Devices Corp). The percentage of viable cells was calculated after the subtraction of the absorbance from cell-free control samples.

3.2.5 Haemolytic Assay

Blood was collected in 6mL lithium-herparin vacuum tubes and either used straight away or stored for a maximum of 48 hours at 4°C. 100 mM phosphate buffer was made by making stock solutions of 200 mM mono or di basic sodium phosphate and mixing them to generate the appropriate pH. The buffer was made to a final concentration of 100 mM using ddH_2O and the pH tweaked using HCl or NaOH.

The blood was centrifuged at 800 x g for 15 minutes and the volume marked before removing the serum and buffy-coat layers. The red blood cells (RBCs) were washed three times by adding saline (150 mM NaCl in ddH_2O) to volume, mixing by inversion and centrifuging at 800 x g for 5 minutes and repeating. If more than one pH was being tested, the blood was divided into the necessary number of aliquots before the final wash. After the final washing step, phosphate buffer was added to volume and mixed with the cells by pipette. A working concentration of RBC was achieved by diluting 1 in 10 in phosphate buffer.

The assay was performed in Eppendorf tubes by adding 800 µL of NPs (in phosphate buffer, pH7.4) to 200 µL of RBC solution and incubating for 1 hour at 37°C. Unlysed cells were pelleted for 5 minutes at 800 x g and the supernatant further centrifuged at 17,000 x g for 15 minutes to remove any suspended NPs. The absorbance of the supernatant was measured in 96 well plates at 550 nm and % haemolysis was determined in GraphPad Prism 6 by normalising data between negative (buffer only) and positive (10% Tween20) controls.

3.2.6 Reactive Oxygen Species Assay

The human monocyte cell line THP-1 were cultured and differentiated as described in section **??**, and plated in 96 well plates at a density of $5x10^4$ cells/mL. Cells were washed twice with PBS prior to the addition of coated or uncoated NPs for 3 or 6 hours. Each plate also contained untreated (negative control) and 100 µM menadione bis sulphate (positive control) treated cells. CellRox Green (Invitrogen) reagent was added to each well to a final concentration of 3 µM for 30 minutes and then washed thrice with PBS.

Plates were analysed by fluorescent microscopy on a 32x objective (Zeis Axio 200) by filling

the field of view with the maximum number of cells possible and imaged by both transmitted (white) light and fluorescence.

Image analysis was performed in ImageJ 1.48v (Wayne Rasband, National Institute of Health, USA). Fluorescent images were all processed identically. Firstly the background was subtracted and the image converted to binary. Then the mean 'black' area was determined for each well (image). This value was divided by the number of cells in the image to generate a 'fluorescence per cell' value before being normalised by positive controls to exclude plate effects. Finally values were expressed as percent of negative control. Analysis was performed using R 3.2.1.

3.2.7 Quantitative Polymerase Chain Reaction (qPCR)

3.2.7.1 Phenol-Chloroform-Methanol Extraction of mRNA Cells were cultured and exposed to treatments in 24 well plates. Following exposure, cells were washed three times with 0.5 mL PBS prior to the addition of 0.5 mL TriFast solution (Peqlab). Cell lysis and dissolution was achieved by pipetting up and down multiple times and the solution either frozen (-20°C) for mRNA extraction at a later date, or mRNA extraction proceeded immediately.

Extraction was performed as per the manufacturer's directions. 0.1 mL of chloroform was added and the tube shaken for 30 seconds before standing for 3 minutes at room temperature. Samples were centrifuged for 5 minutes at 4°C at 12,000 x g and the aqueous phase transferred to a fresh tube.

Precipitation of RNA was performed by adding 0.1 mL of chilled isopropanol, leaving on ice for 15 minutes and centrifuging for 10 minutes at 4°C at 12,000 x g. The supernatant was carefully removed so not to disturb the RNA pellet. The pellet was washed twice by suspending in chilled 75% ethanol, vortexing and centrifuging for 10 minutes. The resulting pellet of RNA was suspended in RNA-free water. The purity and concentration of the RNA was checked by its absorbance at 260 and 280 nm. The RNA was further checked by running 0.5 µg into a 1% agarose (in 40 mM Tris, 20 mM acetic acid, 1 mM EDTA) gel for 30 minutes and staining with SyberSafe nucleic acid dye (Invitrogen).

3.2.7.2 Reverse-Transcription PCR (rtPCR) To generate cDNA form the extracted mRNA, rtPCR was performed on 1 µg of extracted RNA using SuperScript II (Invitrogen). All reagents were purchased from Invitrogen. To 1 µg RNA, 0.2 µL random

Product	Life Technologies Product Number
HS00985639_m1 Human IL6 TaqMan Gene Expression Assay. FAM-MGB	4331182
Hs00174103_m1 Human IL8 TaqMan Gene Expression Assay. FAM-MGB	4331182
Hs01042313_m1 Human TNFRSF1A,Taqman Gene Expression Assay. FAM-MGB	4331182
Hs02758991_g1 Human GAPDH Taqman Gene Expression Assay. FAM-MGB	4331182
TaqMan Universal Master Mix II, no UNG	4440040

Table 6: Reaction reagents and product IDs for quantitative PCR.

hexamers (50 µM stock), 1 µL of 10 mM dNTP mix were added. The total reaction volume was made up to 12 µL with RNase-free water and heated to 60°C for 5 minutes before being chilled on ice. To the reaction, 4 µL 5x first-strand buffer and 2 µL 0.1M DTT were added and the reactions incubated at 25°C for 2 minutes, after which 2 µL of Superscript II was added. The reactions were performed by heating to 25°C for 10 minutes, 42°C for 50 minutes and 70°C for 15 minutes. Reactions were chilled and held at 4°C overnight.

3.2.7.3 Quantitative PCR (qPCR) PCR was performed using Taq-Man assays (Invitrogen) with GAPDH used as an in house gene. As the assays were not 100% efficient, a pool of samples was made and used for normalisation. The same pool was used throughout. 10 µL reactions were performed using TaqMan Universal Master Mix II. Samples were made in a 384 well plate by adding the following reagents: 5 µL TaqMan Universal Master Mix II, 0.5 µL TaqMan assay reagent (Table **??**), 4.5 µL cDNA (following 100 x dilution in RNA-free water). The reaction was performed following an initial hold of 95°C for 10 minutes to activate DNA polymerase (AmpliTaq Gold). Thermal cycling between 95°C for (15 seconds) and 60°C (60 seconds) was performed for 40 cycles (7900HT Fast Real-Time PCR System, Applied Biosystems) with Sequence Detection System 2.3 software (Applied Biosystems). Analysis of the qPCR was performed using excel, normalising to GAPDH and the pooled standard.

3.3 Results

3.3.1 Nanoparticle Characterisation

Particle characterisation was performed in collaboration with the Facility for Environmental Nanoscience and Characterisation (FENAC), University of Birmingham. Particles were characterised by a number of complimentary techniques in PBS or BALF. It was not possible to acquire DLS or ZP measurements of particles suspended in BALF due to concerns of contamination from unscreened human material. Lavage is collected in a saline solution, and therefore the behaviour of particles in PBS was determined by DLS and zeta potential measurements. Measurements in PBS and lavage were obtained by TEM and AFM to measure both width and height respectively.

The diameter of polystyrene particles in H_2O was supplied by the manufacturer and this was not different from DLS measurements performed in H_2O by the author (Table **??**).

The size of TiO_2 particles was determined by TEM to be 14.09±7.26 (normally distributed, mean ± standard deviation) in PBS with some agglomerates observed (Table **??**, Figure **??**). In BALF however, they became agglomerated with a median size of 37 nm and inter-quartile range (IQR) of 13-63 nm (non-parametric distribution). However, there were a number of larger agglomerates of over 500 nm. After 60 minutes, the suspension formed larger aggregates, with the median agglomerate size increasing to 161 nm with and IQR of 49-330 nm.

Polystyrene particles did not agglomerate in PBS when measured immediately by DLS or TEM over 60 minutes and neither cPS and uPS particles agglomerated immediately when suspended in BALF (Table **??**). On the other hand, aPS particles rapidly formed agglomerates of, on average, a 1-fold increase in size (measured by TEM) in BALF (Table **??**). Atomic force microscopy of the agglomerate height did not detect an increase in particle diameter large enough to be due to agglomeration, suggesting that the agglomerates formed were held together through weak interactions (Table **??**, Figure **??**).

Aminated PS and uPS increased in height, measured by AFM, by approximately 9 and 16 nm respectively, however, cPS particles did not increase in size.

Particle	Label Size (in water, nm)	Media	Size TEM (nm)	Size AFM (nm)	Hydrodynamic Diameter (nm)	Zeta Potential (mV)
aPS	110	PBS	154.96 ± 96 (median = 101.35)	78.65 mp 8.82	115.9 ± 7.89	-11.5 ± 1.81
		BALF	293.14 ± 383.59	88.08 ± 11.33	-	-
cPS	85	PBS	69.5 ± 4.6	55.31 ± 8.06	89.26 ± 4.43	-19.73 ± 1.25
		BALF	75.7 ± 6.9	56.1 ± 5.4	-	-
uPS	82	PBS	77.7 ± 11.7	65.27 ± 6.95	90.53 ± 8.06	-17.07 ± 0.9
		BALF	78 ± 24.7	81.14 ± 6.88	-	-
TiO_2	-	PBS	14.09 ± 7.26	-	183 (n=1)	-22.7 (n=1)
		BALF	76 ± 134.9 (median = 37)	-	-	-

Table 7: Table of nanoparticle properties. Size of the particles was determined in either PBS or BALF by three different methods. Size determined from TEM and AFM was averaged from 100 particles. Hydrodynamic diameter was taken in triplicate (unless otherwise stated) in PBS only and the 'Number' value is reported. All values are mean ± standard deviation. – sample measurement not performed. Particles were suspended in the relevant media and immediately measured.

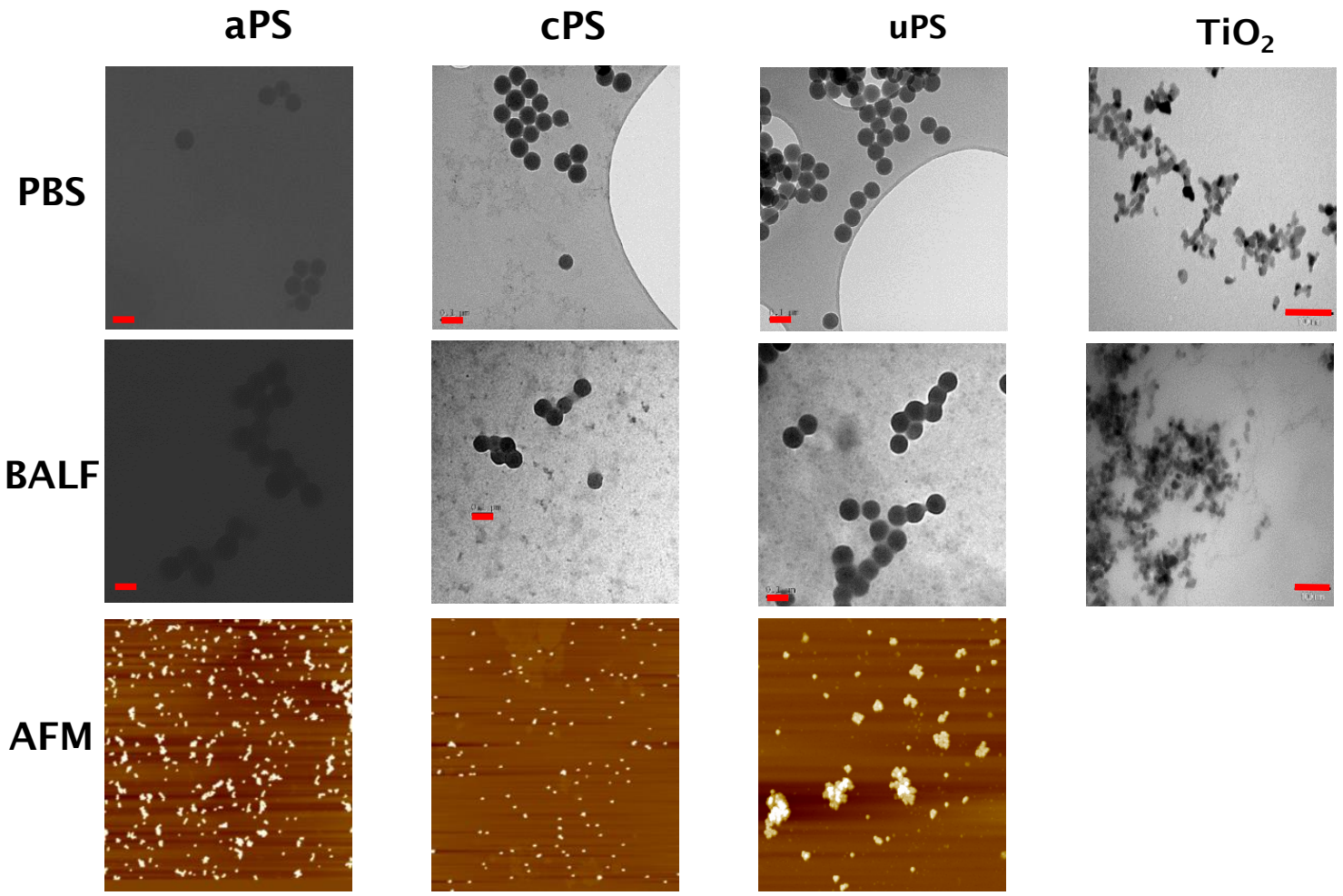

Figure 8: Microscopy images of NPs. Top two rows are example TEM micrographs of particles in PBS or BALF. The bottom row contains example AFM images of PS particles. In TEM images, the thick red line represents 100 nm. AFM images are 8x8 µm.

Imaging of polystyrene showed that these particles were spherical and TiO_2 was anatase[197] with angular, polygonal form (Figure **??**). Particles imaged in PBS has sharp, defined endges, these became less sharp and more blurred following incubation in BALF, indicating the presence of a corona. In all cases, there was a mixture of individual particles and agglomerates, following incubation in BALF, agglomerate size appeared to increase.

Further analysis of particle stability over 24 hours in solution was measured for PS NPs by DLS. Conversely to microscopic analysis of deposited particles, measurements showed that cPS and uPS (Figure **??**B and C) were stable in PBS, but formed agglomerates immediately and increasingly over time, when incubated in lavage (approximately 8 fold increase after 2 hours). Conversely aPS particles were not stable in PBS, but were stabilised by lavage fluid (Figure **??**A).

In summary, all particles increased in size upon incubation in lavage, with uPS and cPS particles becoming highly agglomerated over time, such that their size was approximately 800 nm after 2 hours. aPS particles initially increased in size, but stabilised over 24 hours, not exceeding approximately 300 nm in size. When in PBS, both uPS and cPS particles were stable, whereas aPS particles became highly agglomerated.

3.3.2 Particle Toxicity

3.3.2.1 MTT Assay Cells were exposed to a range of nanoparticle concentrations for 24 hours; the amount of reduced MTT was measured spectrophometrically and normalised to untreated control. Since the reduction of MTT to formazan is dependent on mitochondrial enzymes, this is a measure of the level of mitochondrial activity within the cells.

Particles were applied in a background of 1% lavage as this was determined to pose no detectable difference in MTT reduction on cells compared with 0% (Figure **??**).

3.3.2.1.1 A549 Cells In A549 cells, a human AEII-like cell line, aPS NPs caused a reduction in mitochondrial activity above a concentration of 0.1 cm^2/mL, becoming significant ($P<0.05$) by 100 cm^2/mL over 24 hours of exposure (Figure **??**). To both cPS and uPS particles, there was a significant ($P<0.05$ or $P<0.01$) increase in absorbed formazan relative to control from as little as 0.01 cm^2/mL. In both cases, the increase remained constant up to a concentration of 10 cm^2/mL, followed by an increase at 100 cm^2/mL. Exposure to TiO_2 particles caused no effect on the cells (Figure **??**D).

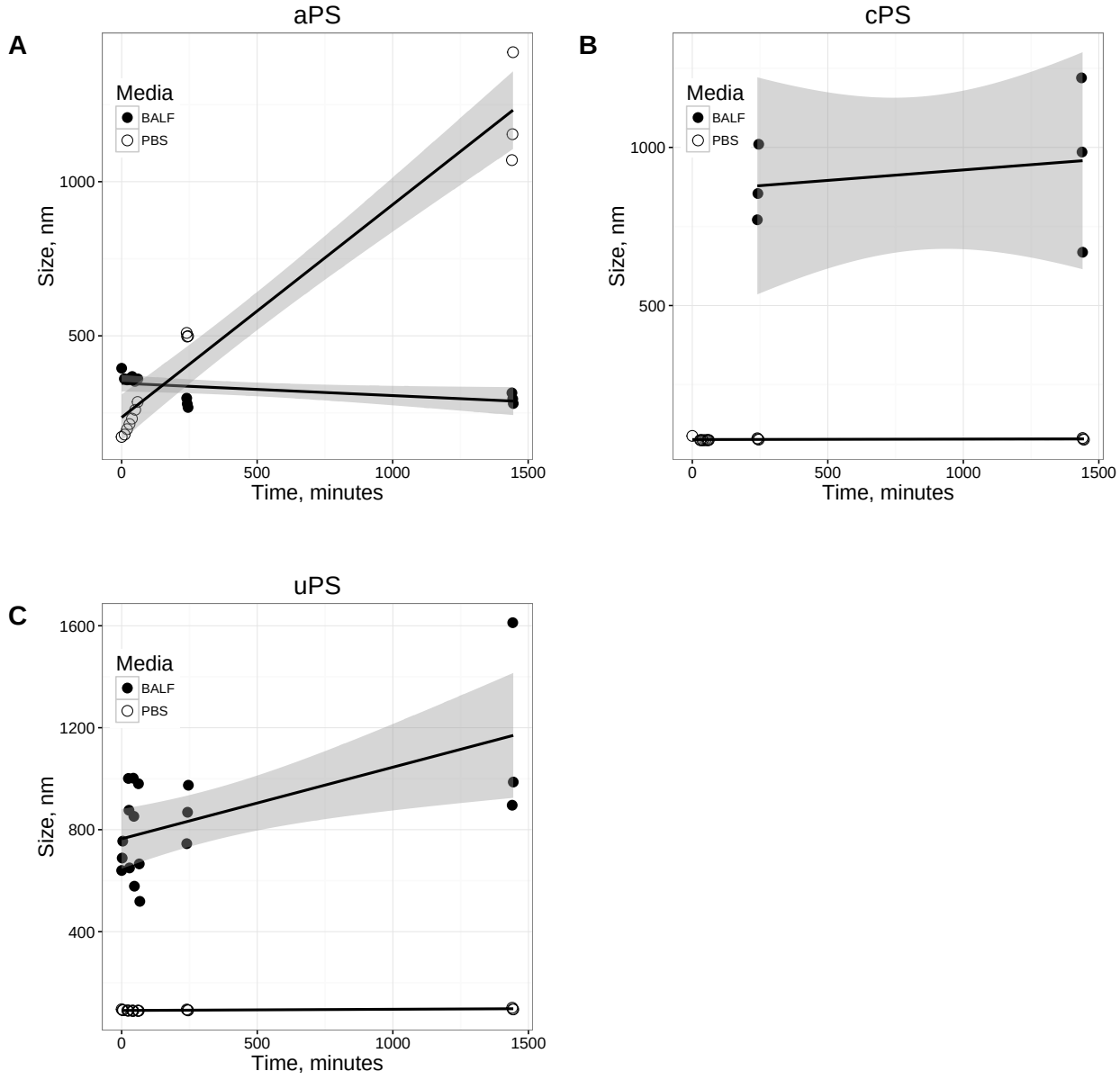

Figure 9: Increase in size of polystyrene particles in PBS or BALF over time, as measured by DLS. Lines are fitted from a linear model, with 95% confidence intervals indicated by shaded region.

Since *in vivo*, cells will not encounter bare particles, rather particles with a corona, the cells were also exposed to NPs prior incubated in BALF (Figure **??**). Preliminary experiments showed that cell culture media fortified with 1% BALF had no effect on mitochondrial activity and therefore these experiments were performed in the presence of 1% BALF (Figure **??**).

With aPS particles, there was still a reduction in the levels of formazan, however the particles did not become toxic until higher concentrations (1 cm^2/mL) and at no point was the reduction significant compared to control.

Coated uPS particles caused an increase in mitochondrial activity at concentrations up to 1

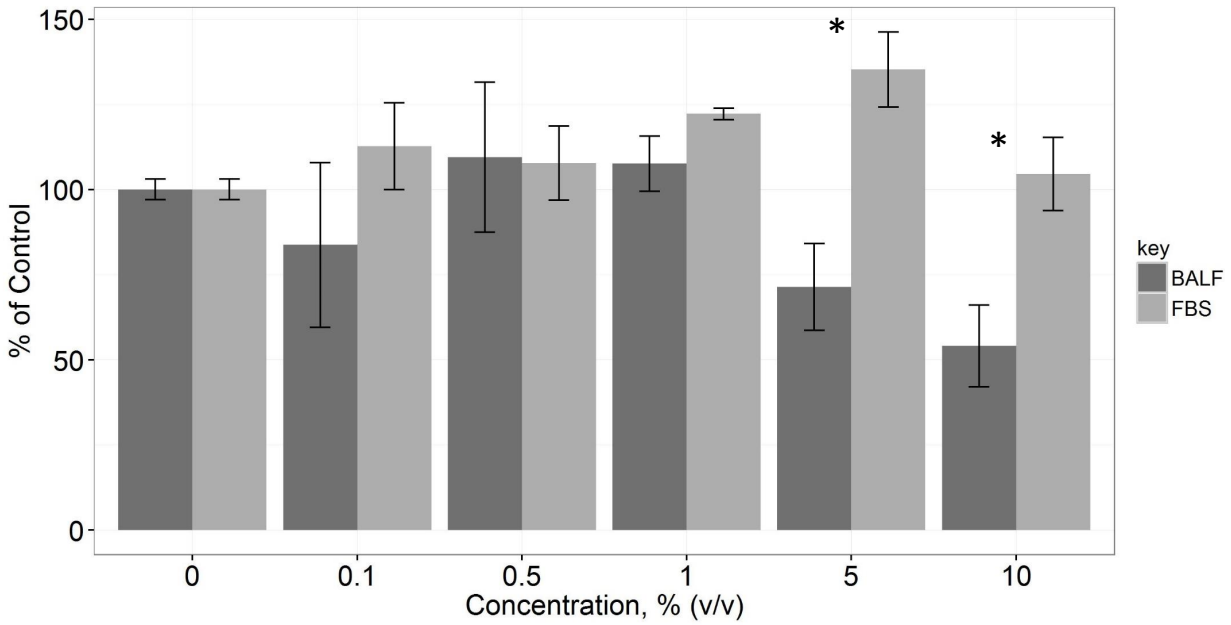

Figure 10: Effect of BALF on cell growth. Cells treated with increasing concentrations of either FBS or lavage for 24 hours were assayed for mitochondrial activity by MTT assay. Shown are mean ± standard deviation. ∗ a significant difference between lavage-treated cells and untreated ($P<0.05$), n=3, each performed in triplicate.

cm^2/mL, although not to the same degree as uncoated. At higher concentrations, the mitochondrial activity returned to baseline.

The increased mitochondrial activity observed from exposure to cPS particles was negated after pre-incubation in BALF, with no change observed at any concentration tested.

Coated TiO_2 NPs caused an increase in mitochondrial activity when cells were exposed to concentrations between 0.01 cm^2/mL and 1 cm^2/mL (Figure **??**D). At higher concentrations, the amount of formazan decreased, returning to baseline by 100 cm^2/mL (Figure **??**D).

3.3.2.1.2 TT1 Cells TT1 cells are a human AEI-like cell line. There was a similar, dose-dependent response by TT1 cells to exposure to uPS, cPS and TiO_2 particles whereby the amount of reduced formazan increased with increasing concentration of particles (Figure **??**). The trend was the same for both coated and uncoated particles and become significant in all cases ($P<0.05$).

In response to aPS particles, there was an increase in formazan peaking at 0.5 cm^2/mL and 5 cm^2/mL for uncoated and coated particles respectively (Figure **??**). Followed by a reduction in mitochondrial activity at higher concentrations. At 100 cm^2/mL of bare

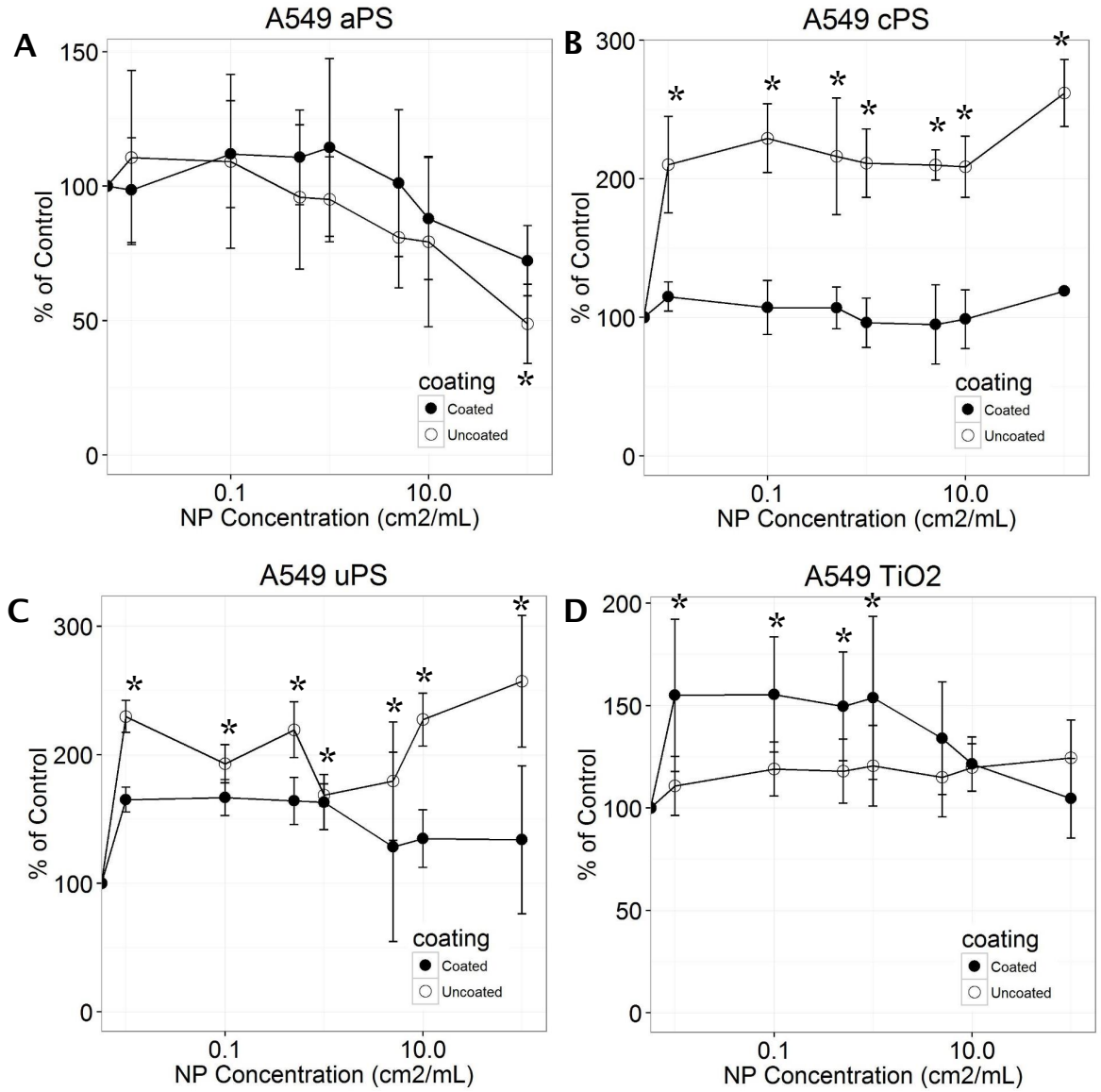

Figure 11: MTT assay of A549 cells exposed to coated (black points) or uncoated (white points) (A) aPS, (B) cPS, (C) uPS or (D) TiO_2 particles. Error bars represent mean ± standard deviation and statistical deviation from untreated ($P<0.05$, T-test) is indicated by *.

particles, the amount of reduced formazan was below that of the negative control.

3.3.2.2 Reactive Oxygen Species Nanoparticles may induce toxicity by triggering ROS. Alveolar macrophages are known to secrete ROS and therefore their reactivity to NPs was assayed. Reactive oxygen was measured with a fluorescent ROS-activated reporter. The fluorescent intensity from macrophage (THP-1 cells) exposed to particles was not sufficient to be picked up using a plate reader and therefore each well was imaged with a fluorescent microscope. The fluorescent values were normalised by dividing by the number of cells in the field of view. Analysis of the positive controls showed that there was significant differences between plates (ANOVA, $P=0.001$). Therefore values were further normalised by dividing each treatment value by the mean positive control for the plate

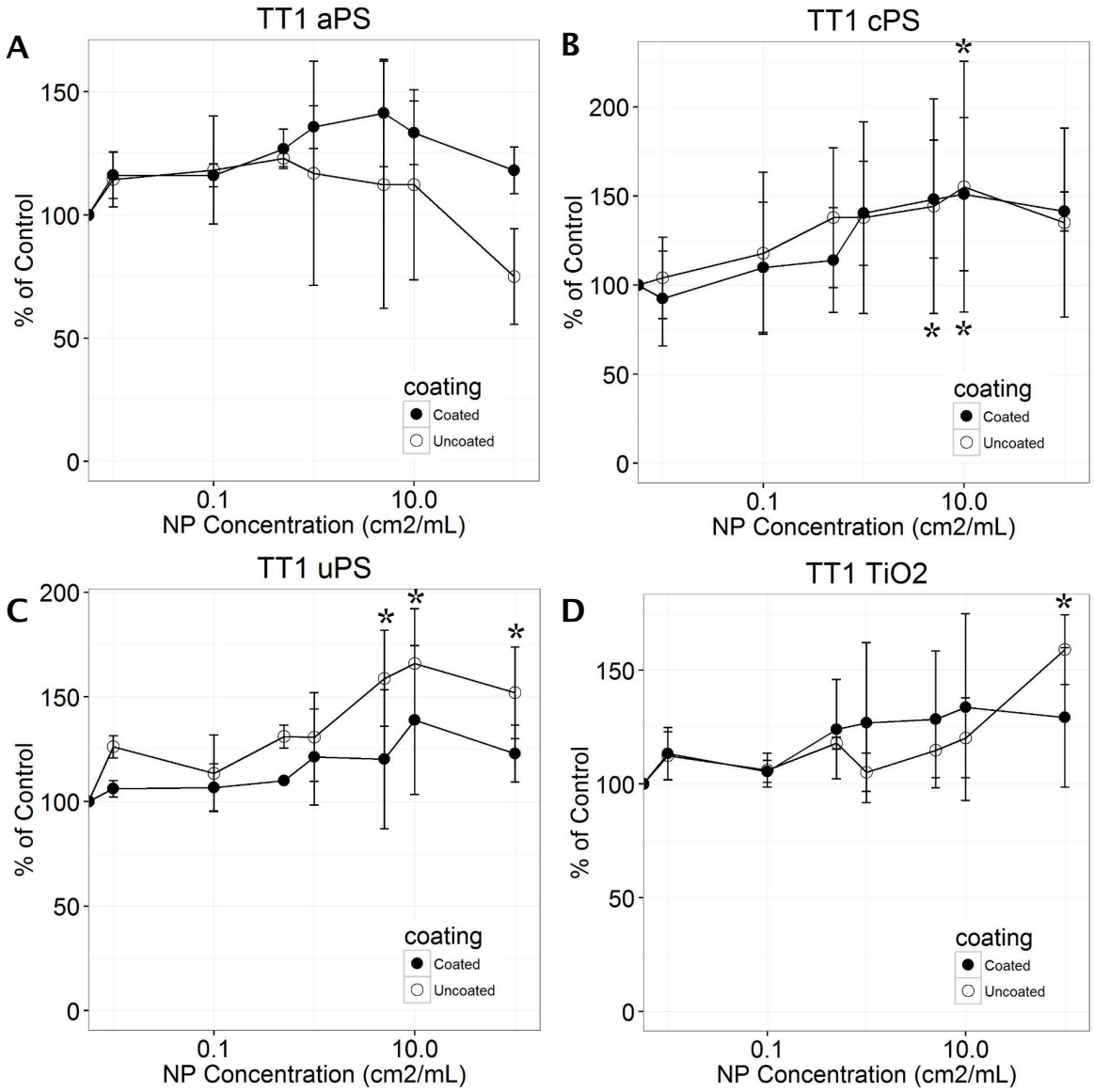

Figure 12: MTT assay of TT1 cells exposed to coated (black points) or uncoated (white points) (A) aPS, (B) cPS, (C) uPS or (D) TiO_2 particles. Error bars represent mean ± standard deviation and statistical deviation from untreated ($P<0.05$, T-test) is indicated by *.

before converting to % of negative control. There was no statistical difference between the positive controls at 3 hours or 6 hours. Experiments were performed with 3 technical repeats. It has previously been shown by McKenzie[148] that these PS NPs are not toxic to the THP-1 cell line following exposure up to 5 cm^2 of particles for 1 hour.

Negative controls (0 cm^2/mL) were significantly lower than positive controls ($P<0.001$) however, they were frequently greater than NP-treated samples and were in general highly variable with a coefficient of variance of 192%.

When treated with aPS particles for 3 or 6 hours, either uncoated or coated in BALF, there was no statistical change in ROS between concentrations of 0.1 and 100 cm^2/mL (Figure **??**A). There was a slight increase in ROS between 0.1 and 100 cm2/mL, but this only

exceeded the negative controls after 6 hours at the maximum concentration with coated particles.

Exposure to cPS particles caused an increasing trend in ROS between 0.1 and 100 cm^2/mL and in all cases except 6 hour uncoated, there was greater ROS at 0.1 cm^2/mL compared to untreated (Figure **??**B). Exposure to coated particles for 3 hours caused a statistically significant increase in ROS (T-test, P=0.015). However, the standard deviations were too high for statistical significance to be reached between any other treatments.

The results from treatment with uPS particles were highly variable with no significant differences (Figure **??**C). Titanium dioxide NPs did not trigger significantly greater ROS than untreated at either 0.1 or 100 cm^2/mL. However, there was significantly greater ROS after 6 hours of exposure to uncoated particles at 0.1 cm^2/mL compared to 100 cm^2/mL (P=0.047) and also between 0.1 cm^2/mL of uncoated particles at 3 and 6 hours (P=0.049) (Figure **??**D).

3.3.3 Inflammatory Response

Epithelial cells may regulate inflammation within the lung through the secretion of cytokines. The transcript levels of proinflammatory cytokines IL-6 and IL-8 were measured by qPCR in A549 cells. Tumour necrosis factor (TNF) alpha was also assayed in preliminary experiments (not shown), but found not to be expressed. Therefore TNF receptor-1 (TNFR1) was included to determine if the cells showed increased sensitivity to this inflammatory cytokine.

Since the efficiency of the PCR reactions was not 100% with the primers used, each experiment was normalised to a pooled sample that was used throughout and the fold change to untreated was determined.

At low concentration, uncoated aPS particles caused an approximately 5 fold increase in IL-6 and IL-8 (Figure **??**A, B) and this was negatively correlated with concentration. Uncoated aPS NPs caused a greater fold change in IL-8 and IL-6 compared with coated particles, particularly at low concentration. However, the difference decreased with increasing concentration of particles. The transcript of TNFR1 was increased following exposure to uncoated aPS particles versus coated at all concentrations, peaking at 10 cm^2/mL (Figure **??**C). Due to large variation between samples, no statistical significance was recorded.

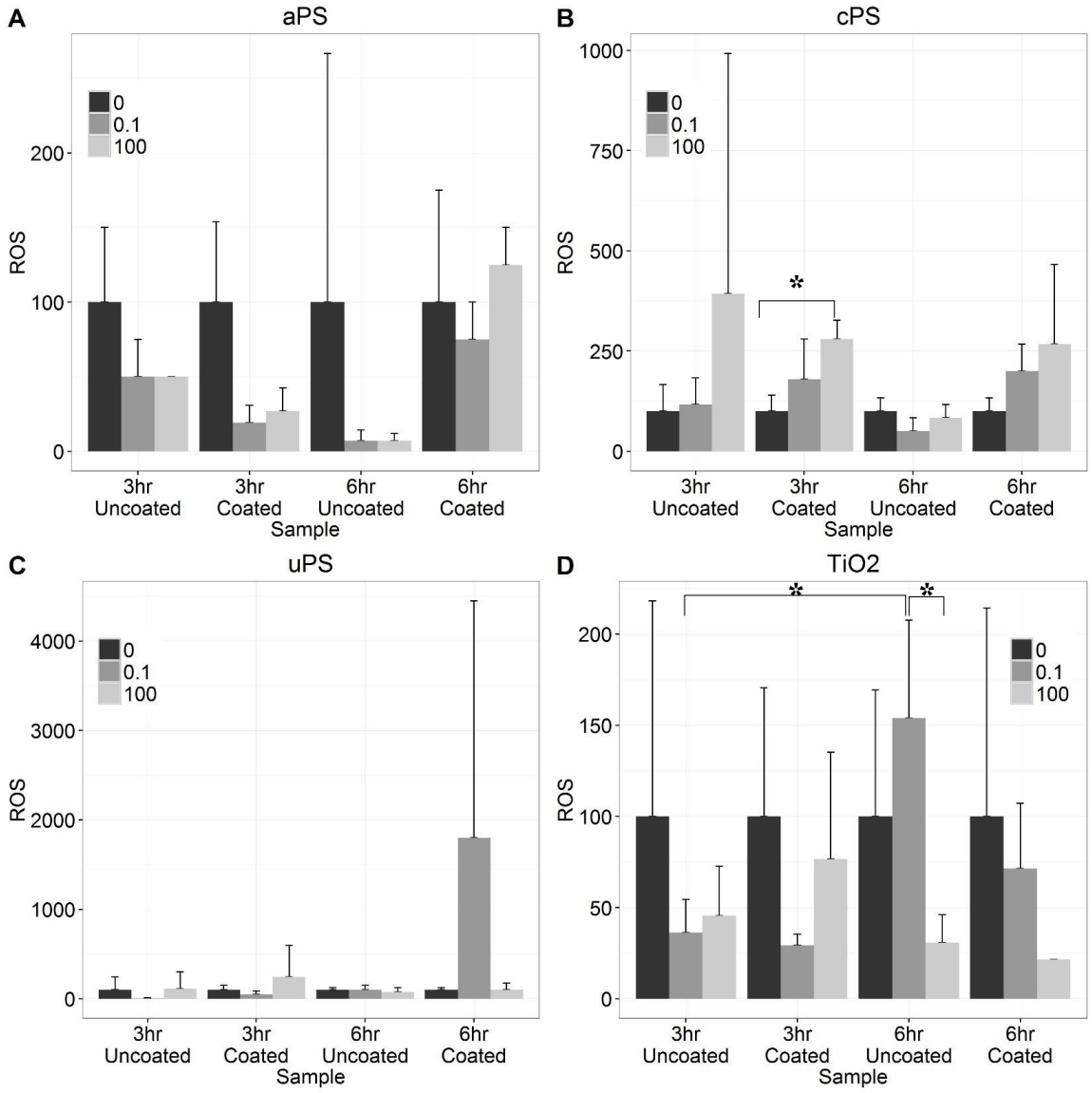

Figure 13: Nanoparticle induced ROS. Reactive oxygen species in differenciated-Thp-1 cells as a result of NP exposure for 3 or 6 hours at 0.1 cm^2/mL or 100 cm^2/mL. Error bars are mean + standard deviation and $*$ indicates P<0.05 (T-test, n=3).

Both IL-8 and IL-6 were maximally increased in A549 cells following exposure to 10 cm^2/mL of uncoated particles (∼4 fold and 15 fold respectively), however there was no difference at other concentrations with either uncoated or coated particles, with <2 fold increase (Figure **??**A, B). There were very minimal increases in TNFR1 for cPS particles, but there was a slight increase in expression levels (∼7 fold increase) in response to uncoated cPS particles at a concentration of 10 cm^2/mL (Figure **??**C). There was no change expression of any transcripts tested to uPS particles with a <1 fold difference at all concentrations (Figure **??**).

To summarise, there were increases in proinflammatory cytokines IL-6 and IL-8 in response to low-medium (0.1 - 10 cm^2/mL) concentrations of uncoated aPS and cPS particles. An increase was observed in TNFR1 mRNA when cells were exposed to uncoated aPS particles

and coated cPS particles at concentrations of 10 cm^2/mL. Therefore, both concentration and particle type may have an effect on the cellular response to particles.

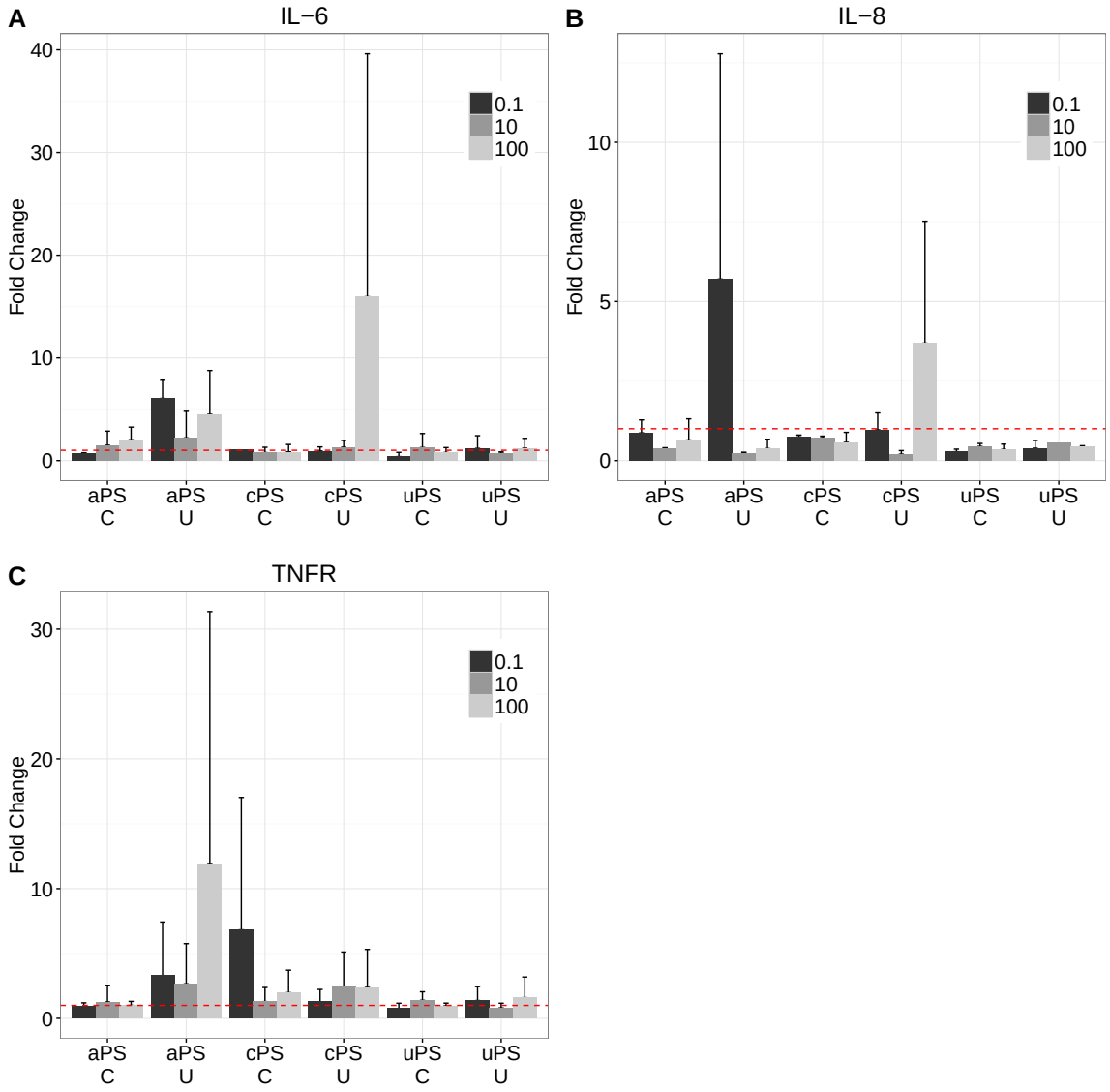

Figure 14: Expression of cytokines. Expression of (A) IL-6, (B) IL-8 and (C) TNFR1 transcript following exposure to uncoated (U) or coated (C) aPS, cPS, uPS or TiO_2 particles at a concentration of 0.1 cm^2/mL (dark grey), 10 cm^2/mL (light grey) or 100 cm^2/mL (white). Error bars are mean + standard deviation, n=3 with each performed in triplicate. Red line is at 1-fold change (i.e. no change).

3.3.4 Interactions with Membranes and Cellular Uptake

3.3.4.1 Haemolysis Cell permeation by NPs can be measured directly by assessing cell lysis in erythrocytes.

Cell lysis due to NP exposure was investigated by haemolysis assay, where the lysis of RBC is measured by the absorbance at 550 nm by haemoglobin. Samples were normalised by fitting the values between the absorbance for the negative (0%) and positive (100%) controls in Graphpad Prism and are expressed as percentage. At concentrations below 100

cm^2/mL, haemolysis was not detectable above the negative control for any particle. To show that residual NPs are not responsible for any absorbance observed, a preliminary experiment with aPS and uPS particles was performed. After incubating RBCs with particles, the solutions were gently centrifuged to remove RBCs, and half of the supernatant was further centrifuged at 17,000 x g for 10 minutes to pellet any NPs. Results showed a small reduction in absorbance for uPS particles and absorbance in aPS samples was no different to controls following centrifugation (Figure ??A). Since aPS particles returned to control, it is clear that a second centrifugation was necessary and sufficient. Absorbance observed for uPS particles was due to haemolysis as was apparent from a red solution forming due to extracellular haemoglobin (Figure ??B).

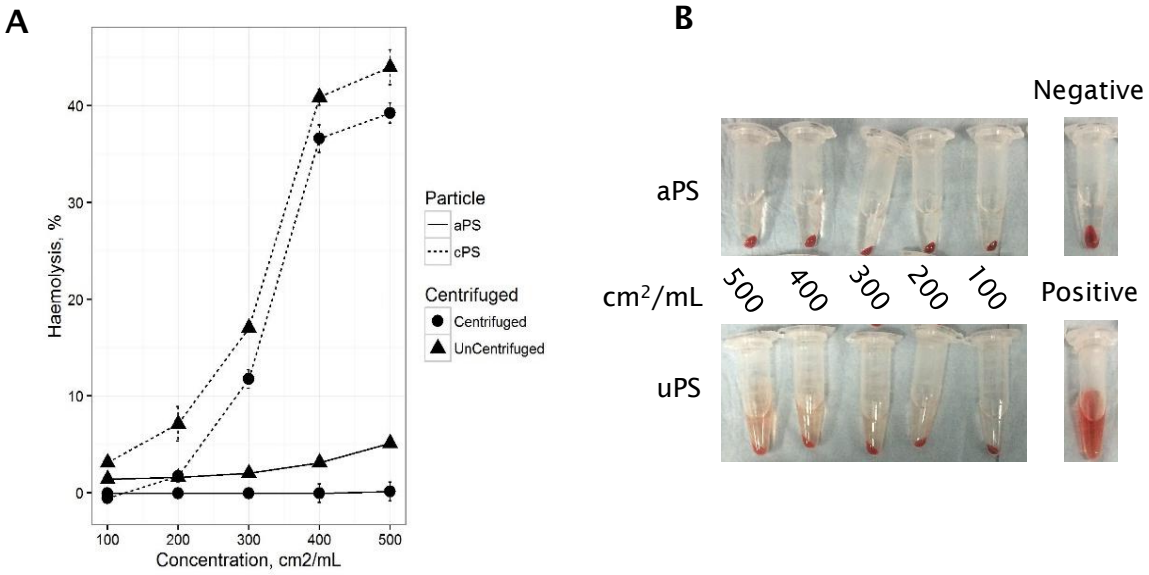

Figure 15: Haemolysis preparatory experiment. Red blood cells were exposed to aPS (dotted line) or uPS (solid line) particles and the supernatants either centrifuged for 15 minutes at 17,000 x g (circles) or not (triangles). (A) Graph showing % lysis normalised to positive and negative controls. (B) Photograph of test samples, positive (10% Tween) and negative (phosphate buffer) controls. Error bars represent mean ± standard deviation of 3 technical replicates, n=1.

The level of detectable haemoglobin was below the negative control for RBC exposed to either aPS (Figure ??A) or TiO_2 (Figure ??D) particles at concentrations up to 400 cm^2/mL, suggesting that haemoglobin is binding to the particles. At 400 cm^2/mL, the absorbance from samples exposed to TiO_2 particles had increased slightly, however only to approximately 1%.

Exposure to cPS particles (Figure ??B) caused a significant (P=0.007) increase in absorbance by 200 cm^2/mL and increased linearly to 500 cm^2/mL (R^2 = 0.979). By 400 cm^2/mL, uPS particles (Figure ??D) had also caused a significant (P = 0.014) increase in

haemolysis and this trend increased at 500 cm^2/mL. Whilst the % haemolysis increased linearly with concentration for cPS particles, with uPS particles it appeared to increase exponentially.

Coating cPS or uPS particles in BALF prevented any lytic effect at 500 cm^2/mL (data not shown).

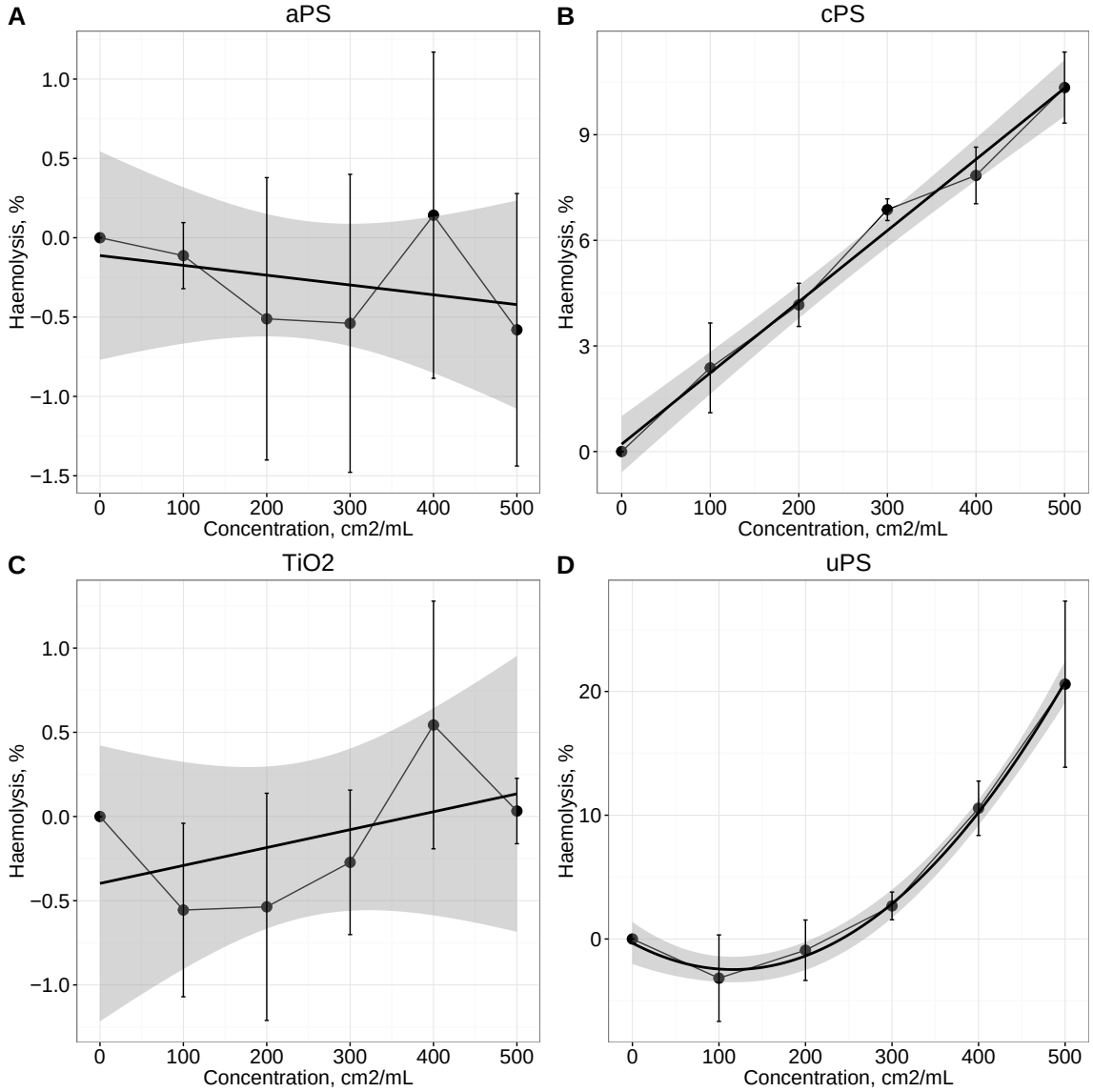

Figure 16: Nanoparticle induced haemolysis. Lysis of red blood cells following exposure to uncoated (A) aPS, (B) cPS, (C) TiO_2 and (D) uPS particles. Shown are mean ± standard deviation. $*$ indicates significant deviation from control ($P<0.05$, T-test, n=3). The grey shading indicates 95% confidence limits. Circles are data values, black line is linear regression.

3.3.4.2 Particle Uptake The uptake of NPs into TT1, A549 and THP-1 cells was to be investigated using coherent anti-Stokes Raman scattering (CARS) microscopy. However, this could not be performed due to unforeseen circumstances. The experiment is discussed in section **??**.

3.4 Discussion

3.4.1 Particle Agglomeration

A comprehensive characterisation of the nanoparticles has been performed, using a combination of complimentary techniques. Analysis of nanoparticles in suspension was performed by DLS in both PBS and human lavage fluid. When measured immediately in PBS, cPS and uPS particles did not agglomerate (Table **??**), and in a separate experiment performed over 24 hours, this held true (Figure **??**). However, when measured immediately in lavage, the particles remained stable, whereas over time they formed large agglomerates. In this circumstance, DLS becomes inaccurate as the technique assumes that particles are both monodispersed and spherical. Measurements taken of polydisrpersed substances are dominated by larger aggregates that skew the z-average disproportionately (scattering is proportional to the 6^{th} power of particle diameter).

Incubation in lavage stabilised aPS particles (Figure **??**), which otherwise became highly agglomerated in PSB over 24 hours, similarly to findings by McKenzie *et al.*[85] of aPS and uPS particles in protein-solution or PBS. The ZP of aPS particles was closer to zero than both uPS and cPS particles and this may reflect its greater tendancy to agglomerate in PBS.

Agglomeration assays were performed at very high concentrations ($100\text{cm}^2/\text{mL}$) to mimic the maximum concentrations used throughout the cellular assays performed here. To avoid agglomeration during lavage-incubation, which would result in non-uniform coating, we diluted the particles during incubation to 25 cm^2/mL to reduce agglomeration of uPS and cPS particles. However, upon contact with the cells, some particles were observably agglomerated, as reflected in the DLS assay.

Electron microscopy of the particles showed the PS particles were a uniform spherical shape ($\sim$100nm) whereas TiO_2 particles were non-uniform polygonal in shape ranging between 3-47 nm with a median of 14 nm. The mineral type of crystalline TiO_2 was confirmed by TEM to be anatase. Unlike other forms of TiO_2 (rutile), anatase has been shown to generate ROS, particularly in the presence of UV light[197]. Therefore the TiO_2 was stored in a darkened bottle and experiments were shielded from light. When incubated in lavage, a thin coating was observable over the particles and, for aPS particles, an increase in size due to agglomeration was observed. For other particles, only a small increase was observed with no difference in agglomeration. Interestingly, by AFM there was no increase in height between particles in PBS or lavage and this suggests that any agglomeration was weak, and

collapsed during drying. Therefore the agglomerate sizes in solution are likely to be continually changing and may not be predictable at the cell surface, although a general trend was clear from DLS.

The ZP of 100 nm aPS particles was surprising since despite having cationic modifications its ZP was still negative (Table **??**). The experimental sample met the criteria to perform zeta measurments, that is, they were spherical, monodispersed and in a suitable concentration to allow detection of particle-scattered light. Due to the salinity of the measurement media, there was some corrosion on the zeta-cell electrodes, however disposable zeta-cells were changed before this affected the measurement. The negative surface detected therefore suggests that the density of aminated functionalisation is relatively low, such that the positive charge of the amination does not exceed the unfunctionalised surface. Similar zeta potentials were observed by Lundqvist *et al.* and McGuinnes *et al.* for 100 nm aminated particles.[2, 198] However, the advantage of this, is that it allows us to investigate the effect of surface modifications without a confounding variable of surface charge. Despite the overall negative surface charge, aPS particles were toxic to both A549 and TT1 cells (see Section **??**), in contrast to un-functionalised particles.

3.4.2 Particle Toxicity

Nanoparticle toxicity was measured by MTT in two epithelial cells types, A549 cells and TT1 cells (modelling AEII and AEI cells respectively). The cells were exposed to NPs at a range of concentrations for 24 hours.

At concentrations above 0.5 cm^2/mL in TT1 cells, and 0.1 cm^2/mL in A549 cells, uncoated aPS particles caused a decrease in the reduction of MTT (Figure **??** & Figure **??**). For A549 cells, 50% death (LD50) was reached at approximately 100 cm^2/mL but not at any concentration tested in TT1 cells. A loss of mitochondrial membrane potential and reduction in ATP production is indicative of apoptosis[199] and has been shown to be a factor of aPS particle mediated toxicity.[200]

To determine if the particle toxicity may be due to disruption of the plasma membrane, a haemolytic assay was performed (Figure **??**), in which red blood cells are exposed to NPs, and the proportion of haemoglobin released compared to controlsis measured spectrophometrically. Titanium dioxide and aPS particles caused no cells lysis, demonstrating that the toxicity of aPS particles is not through mechanical disruption of the plasma membrane. Interestingly, both cPS and uPS particles caused haemoglobin to be

released from the RBCs, at concentrations above 100 cm^2/mL. Cell lysis was only observed at very high concentrations of uncoated particulates which may be due to saturation of haemoglobin to bare particles.[201] This shows that coated cells are unlikely to damage the cell membrane directly. It does suggest that negatively charges particles are capable of interacting with lipids – this is discussed later (Chapter **??**).

Carboxylated particles caused a linear increase in cell lysis which was shown in preliminary experiments not to be due to residual NP's scattering/absorbing light (Figure **??**). Whereas, lysis following exposure to uPS particles increased in an exponential fashion. This may reflect different interactions between the NPs and extracellular haemoglobin.[201, 202] The addition of lavage-coated particles caused no detectable increase in cell lysis, and there was no toxicity observed by uPS or cPS in either A549 cells or TT1 cells. Therefore, any lytic ability of the particles was likely prevented owing to the rapid formation of a corona.

In PBS, cPS and uPS had an approximate diameter of 90 nm and caused an increase in mitochondrial activity at all concentrations tested in A549 cells. In PBS, TiO_2 was approximately 14 nm and prompted no change in mitochondrial activity. In lavage, however, TiO_2 triggering cellular-reactivity between the particles. In TT1 cells, there was a similar response to particles in PBS or BALF for cPS, uPS and TiO_2. Particle toxicity and uptake has been demonstrated to be particle size[80] and cell-type dependent. For example Xia *et al.*[203] demonstrated particle uptake was mainly through endosome-lysosome pathways in a macrophage cell line, but caveolae mediated in bronchial epithelia.

The MTT assay measures the mitochondrial activity and therefore is a measure of live cells. However, this will include early stage apoptotic cells, whose mitochondrial activity is not yet compromised. In the future, it would be useful to include and early stage apoptotic marker.

3.4.3 Cytokines

The increase in metabolic activity was further assessed to investigate if the A549 cells were producing pro-inflammatory factors in response to particulate exposure. Transcript of the potent pro-inflammatory cytokine TNF-α was not detected in A549 cells, as is reported elsewhere for these cells[99] and primary AEII cells[131], however, IL-6 and IL-8 were. IL-8 is a potent chemokine, attractive towards neutrophils and its increased expression would be highly suggestive towards triggering inflammation. Interleukin 6 was increased in uncoated aPS particles (at 0.1 cm^2/mL) and uncoated cPS particles (at 10 cm^2/mL) and this matched increased expression of IL-8 (Figure **??**). Expression of both IL-6 and IL-8

decreased as concentration of uncoated aPS particles increased, which correlated with decreased mitochondrial activity measured by MTT assays (Figure ??).

The PCR data was not further corroborated by quantification at the protein level, e.g. Western blotting or ELISA, and so it cannot be certain if the increased mRNA of IL-6 and IL-8 is translated into increased protein. However, further to this, it would be useful to investigate the effect of the cell culture media on neutrophils. Activated neutrophils can be discriminated by FACS through their forward scatter (size), and could be used to assess the biological relevancy of the increased transcript levels.

Mitochondrial activity was higher following exposure to uncoated uPS particles compared with coated particles (Figure ??C), and this was also observed with levels of IL-6 and IL-8. However, this association did not hold true for cPS particles, where no change in expression of IL-6 or 8 was observed despite mitochondrial activity being much higher in response to uncoated cPS particles compared to coated (Figure ??B).

A549 cells can secrete proinflamatory cytokines in response to TNF-α[102] and therefore we also measured TNFR1 as an indication of the cells' potential reactivity to TNF-α. In response to NP exposure, TNFR1 was not significantly increased compared to an untreated control however a small fold change was observed in most cases and this was greatest in coated uPS particles and uncoated aPS particles (Figure ??C). These changes did not correlate with the observed increases in IL-8, IL-6 (Figure ??A, B) or with MTT assays (Figure ??).

Thach *et al.*[102] showed that upon stimulation with TNF-α, PS NP-incubated A549 cells secreted less IL-8 and IL-6. This finding was reversed followed the depletion of cholesterol from the cell membrane, suggesting a cholesterol-dependent mechanism. The authors suggest that TNFR1 may be found in cholesterol-rich sections of the plasma membrane and therefore signalling is interrupted during cholesterol-dependent endocytosis of the nanoparticles. Therefore, observed increases in TNFR1 may be in response increased endocytosis, and not an inflammatory response.

It would be useful to investigate this further by measuring the uptake of nanoparticles and the cell surface expression of TNFR1. Uptake experiments in A549, TT1 and RAW cells were prepared by the author for analysis by CARS. However, owing to unforeseen circumstances these could not be assayed.

3.4.4 Reaction Oxygen Species

Macrophages can rapidly generate ROS in response to infection or exposure to air particulates.[53, 204] Once generated, ROS may trigger inflammation through downstream reactions and impair surfactant function.[205–207] Alveolar surfactant may be inactivated by the presence of ROS through lipid peroxidation and reaction with surfactant proteins.[206, 208] Therefore we measured the induction of ROS in a macrophage model derived from the activation of a monocytic cell line (THP-1) with PMA. Mckenzie[148] has previously shown that THP-1 cells are not susceptible to toxicity from the particles used.

CellROX green, which following oxidisation by hydroxyl radicals, nitric oxide and superoxides binds to DNA and becomes fluorescent, was used to detect cellular ROS. A high throughput approach was employed using a 96 well format and fluorescent plate reader with the ROS-reactive dye CellROX green which was optimised in preliminary experiments. However, this approach lacked sensitivity and therefore the plates were manually imaged by fluorescent microscopy and analysed with ImageJ. There was a large amount of error within the experiment design that was apparent from positive controls across all plates, even when normalised for cell count. Despite this, error remained high, as is evident from the standard deviation (see error bars, Figure **??**). It was likely due to background noise from fluorescence microscopy as the fluorescence intensity was generally low, exposure times were relatively high.

Some nanoparticles, such as metallic oxides (TiO_2) have been shown to induce ROS,[99, 209] however no such relationship is expected here directly from polystyrene, since they lack the surface chemistry required for the direct induction of ROS.

In general, there was a decrease or no change in ROS generated compared to controls for cells treated with TiO_2 particles at any time point. However, there was an increase after a 6 hour treatment of uncoated particles at 0.1 cm^2/mL compared with 3 hours of treatment with the same particles and an approximately 50% increase compared with controls, although this was reversed at 100 cm^2/mL (Figure **??**). Reactive oxygen generated by TiO_2 exposure is exacerbated by exposure to ultra-violet (UV) light and without UV may only trigger significant ROS at very high concentrations – Sayes *et al.* only observed ROS generated at concentrations exceeding 100 µg/mL.[197, 209] The cells in the experiments reported here, were incubated in the dark and experiments carried out under ambient ceiling lighting which will contribute little to no UV as the laboratory has no windows. Some UV exposure will have occurred during imaging although on a small time scale (<30

seconds) and therefore unlikely to cause an effect on detected cellular ROS.

Exposure to uncoated aPS particles for 3 hours caused a decrease in ROS compared to control that decreased further over 6 hours. Interestingly, whilst coated particles caused a decrease in ROS after 3 hours (by approx. 50%), over 6 hours ROS was restored to control levels for both concentrations tested (Figure **??**). Whilst aPS particles are toxic, their mechanism of toxicity is through lysosomal-bursting triggering apoptosis,[89, 90] ROS observed is likely a hallmark of apoptosis and not directly generated by the particles themselves93. It has previously been demonstrated within the lab that aPS particles are not toxic towards THP-1 cells over 1 hour[148], although toxicity has been observed over 24 hours in primary macrophages elsewhere.[74]

A reduction in ROS observed following exposure to both aPS and TiO_2 was not dose-dependent and therefore is unlikely to be due to sequestration of ROS-generating enzymes to the particle surface. The reversal of the apparent anti-oxidant function aPS particles between 3 hours and 6 hours exposure to coated particles may be due to the delayed induction of apoptosis that could be dependent on the removal of the protein corona from the particle surface in the lysosomal compartment.[89] Oxidative burst generated by macrophages may be inhibited by the detection of apoptotic cells, which could explain the time-dependent reduction of ROS observed for uncoated aPS-exposed cells.[210] However it is not clear if this effect would decrease ROS below baseline levels. Since CellROX green does not detect hydrogen peroxide or peroxide radicals, it is possible that ROS was generated via alternative mechanisms. Ruenraroengsak *et al.* have shown that PS induced ROS was observed in macrophage following the application of dihydroethidium (DHE) that detects superoxide radicals, but could not detect ROS with peroxide or singlet oxygen-reactive dyes.[74]

There was a dose dependent increase in ROS following exposure to cPS particles that reached statistical significance following exposure to 100 cm^2/mL coated particles after 3 hours (P=0.015, T-test) (Figure **??**). The ROS generated was greater than either aPS, TiO_2 or uPS particles. Contra to the findings here, in other studies aPS has been shown to trigger a greater production of ROS in primary macrophages than cPS.[74] The reason for this is not clear. However, particle uptake may lead to ROS induction via the NADPH oxidase pathway.[211] Furthermore, carboxylated particles caused a large increase in mitochondrial activity in A549 and TT1 cells (Figure **??** and Figure **??**), particularly without prior incubation in BALF and this may explain the increase in ROS generation if true for THP-1 cells.

TiO_2 particles were not detected to induce ROS in this experimental system. Whilst TiO_2 have been shown to induce cellular ROS,[209, 212] the production of large amounts is dependent on UV exposure. Since UV would not be present in the lung, the exposure to UV of these cells was kept to a minimum. Toxicity of TiO_2 is comparatively low in the literature with reports of toxicity varying depending on cell type and UV-exposure. Xia *et al.* report that whilst TiO_2 are capable of spontaneously generating ROS in abiotic conditions (also see Sayes *et al.*[197]) they are incapable of generating ROS in RAW (macrophage-like) cells.[100] On the other hand, Jin et al demonstrate that anatasie-TiO_2 particles are capable of triggering ROS production in HaCaT (human skin keratinocyte) cells, although at much higher concentrations (200 µg/mL vs 50 pM in Xia *et al.*).[213] We did not observe ROS production at either low (0.1 cm^2/mL) or high (100 cm^2/mL) concentrations of TiO_2 (for comparison, ∼0.3 – 30 ug/mL).

3.4.5 Interaction with Cell Membranes

Both cPS and uPS particles were able to lyse RBC, releasing haemoglobin into the surrounding media. These particles represent the middle two particles in terms of surface charge (Table **??**) and since aPS and TiO_2 (most positively and negatively charged respectively) did not cause lysis, this effect is unlikely due to surface charge.

The interaction with particles and cell membranes may be dependent on their surface curvature, as this mediates the force required for the membrane to wrap onto their surface through adsorption. The steeper the curve (smaller the particle), the greater the force required to adsorb to an equivalent surface area of a larger particle and therefore this interaction may less likely to occure.[79] Thus it is not suprising that TiO_2 did not cause cell lysis as it is by far the smallest particle.

Red blood cell lysis from negatively charged silica particles was observed by Tenzer *et al.*[63] Haemolysis due to silica particles is thought to occur through mechanisms dependent on surface silanol groups.[214, 215] The mechanism for cell lysis by cPS particles observed here is unknown. In vivo the particles would rapidly for a corona; no cell lysis was observed following incubation of NPs in BALF and therefore it is unlikely that the particles would cause RBC lysis *in vivo*.

The experiment shows that there may be a capacity for the particles to interact with cell membranes, which could result in deposition on the cell surface or uptake. As mentioned previsouly, and discussed in more detail in section **??**, particle uptake was to be investigated

by CARS, however due to unforeseen circumstances could not be. Interactions with cell membranes could be investigated further by scanning electron microscopy (SEM). This could be performed at 4°C to inhibit internalisation of the particles and thus yield information regarding the particles' relative affinity to the cell surface.

3.4.6 Toxicity of BALF

It was interesting to observe that at concentrations above 1% (v/v) BALF became toxic (Figure **??**), and the reasons for this are not clear. The BALF is acquired form PAP patients, however is not in itself known to be toxic. Pathology in PAP patients in due to a build up of material that interferes with lung-function, not from expressed factors within the BALF fluid. BALF is collected in a warm, saline solution and it is possible that at high concentrations, it interferes with the osmotic balance of the media. However, this is unlikely as the osmotic levels of the media is probably not affected significantly by the low concentrations of BALF. Lungs are constantly exposed to pathogens and therefore, the BALF is highly unlikely to be sterile. It is possible that infectious agents within the BALF is responsible for toxicity at concentrations above 1%, although no growth was seen during routine cell culture observations. The toxicity towards the cells is not clear, but it would be interesting to investigate this further as it suggests potential new pathology of PAP.

3.4.7 Summary

All particles agglomerated to some degree but in a manner dependent on suspension-media and particle type. Aminated particles were stabilised in BALF over time whereas cPS and uPS formed large, but weak, agglomerates. TiO_2 particles became highly agglomerated in BALF but not in PBS.

A decrease in mitochondrial activity, presumably due to toxicity was observed in TT1 and A549 cells following exposure to aPS particles. However, increases were observed in other particles, the degree of which is dependent on surface chemistry and corona formation. Increases in mitochondrial activity were greater following exposure to uncoated uPS and cPS compared with coated, but this trend was reversed for TiO_2 . This suggests that agglomeration may play an important role as uPS and cPS particles become highly agglomeration in BALF. However TiO_2 particles also become highly agglomerated and therefore the corona itself could be a mediating factor. Further investigation into the identity of the corona is necessary for a full evaluation of the particles.

Both cPS and uPS, but particularly uPS particles caused cell lysis in RBCs and this was prevented by incubating in BALF, suggesting a mechanism dependent on surface modification and size (agglomeration).

Cytokine studies were inconclusive. Interleukin 6 and 8 were increased in some cases in A549 cells. As TNFR1 was increased, It would be interesting to see the effect of stimulating the cells with TNF-α to see if this observation translated into the generation of an inflammatory environment.

Alveolar macrophages are capable of generating large amounts of ROS through the respiratory burst and thus creating a potentially harmful microenvironment within the alveolus. We did not observe the generation of ROS in differentiated THP-1 cells following exposure to aPS, uPS or TiO_2 particles. However cPS particles caused a dose dependent increase. Alveolar epithelial cells are both important in modulating inflammation in the lung through the production of cytokines and surfactant proteins (by AEII cells). It would be interesting to find out if cPS particles are capable of inducing inflammatory cytokines, in particular IL-8, via ROS generation in macrophage. This would be indicative that these particles are capable of triggering inflammation in vivo.

Caboxylated and unmodified particles behaved similarly in terms of agglomeration and effect on mitochondrial activity, yet induced differed by ROS and cytokine profiles. The causes of these differences may lie in their corona. Therefore further investigation into the particles' corona is undertaken in the following chapters.

The aims of this chapter to assess the particle-cell interactions by looking at particle uptake and interactions with membranes were only partially met. Whilst interaction with membranes was investigated by haemolytic assay, uptake studies to investigate the effect of particle-adsorbed lipids and protein on particle internalisation were planned by CARS (Section **??**) however owing to unforeseen circumstances could not be performed.

4 Protein Corona

4.1 Introduction

Nanoparticles in biological media become engulfed by a protein shell, 'corona' and may gain a biological identity (Section **??**). To date this phenomenon has been investigated almost exclusively in serum. Comprehensive lists of seurm-proteins that adsorb to the NP corona have been published[63, 117, 121] and it may be possible to predict the cellular fate of NPs from this data.[216] However, there remains no analysis or identification of proteins bound to NPs in the context of the lung. This is likely due to the abundant and convenient availability of serum compared to a lung-related bio-fluid.

Despite having similar surface characteristics (curvature and ZP, Table **??**), the particles had different toxicity towards A549 and TT1 cells (Section **??**) and displayed different reactivity to cell membranes (Figure **??**). The particle surface functionalisation will become masked by a protein corona, and therefore differences in MTT could be due to the proteins present on the particle surface. If proteins interact with the surface functionalisation, it may be possible to observe differences in terms of the protein corona and would suggest a charge/electrostatic mediated interaction between proteins and small groups on the particle surface. aPS, cPS and uPS all have different surface groups, TiO_2 has a different core (although similar ZP) and these will be use to investigate interactions between particles and functional groups.

I have used BALF to analyse the protein corona formed around NPs in the lung. Patients with pulmonary alveolar proteinosis (PAP)[157] have reduced recycling and consequent build-up of pulmonary surfactant within their alveolus. The increased amount of lipo-proteinaceous material may be removed through whole lung lavage that is typically performed during a single procedure and can result in approximately 12-15 L of material per patient.[158, 217] This material differs from 'healthy' lung through increased levels of lipids and SP-A[160] and D[159] with a 10-fold and 7-fold increase respectively. The proportion of SP-A to the total protein is similar between PAP and healthy control, suggesting that whilst the fluid may be more concentrated for lipid and proteins, the proportions of these proteins may be similar.[160] Therefore, we consider this media is be a useful source of pulmonary material for investigating NP-protein interactions within the context of the pulmonary system.

Using high resolution, quantitative mass spectrometry MS^E with Hi-3 quantitation[186,

218]), the proteins from BALF binding to 4 different NPs, and a time study of the corona formed around 2 of the particles are described. The research has demonstrated that a few proteins bind to the NPs with high fidelity but many bind in a transient manner, with low copy numbers on the surface of the particles. Furthermore, we have observed the adherence of surfactant associated proteins (SP-A, SP-B and SP-D) binding to the surface of the particles, suggesting mechanisms through which inhaled NPs may affect health.

4.2 Methods

4.2.1 Corona Formation

BALF was acquired by therapeutic lung lavage of a patient suffering PAP by Dr Mark Griffiths (Imperial College London) and donated with informed consent under approved ethics (NRES reference 10/H0504/9). Approximately 13 L were acquired from a single patient, and the first 4 L were pooled and aliquoted prior to freezing at -20°C. Before incubating the particles the BALF was defrosted and briefly centrifuged at low speed (300 x g) to pellet large agglomerates and cellular debris before being centrifuged for 30 minutes at 10,000 x g to remove smaller agglomerates.

For LC-MS analysis of the proteins corona, 50 cm^2 of particles were incubated in 20 mL (approximately 5 mg total protein) of BALF for 15, 30, 60 or 120 minutes. For cellular assays, 500 cm^2 of particles were suspended in 30 mL of BALF for 60 minutes. Particle-BALF mixtures were centrifuged at 10,000 x g for 30 minutes to pellet the NPs, which were either washed 5 times with 1 mL phosphate buffered saline, centrifuging for 15 minutes at 17,000 x g (for corona analysis) or diluted to relevant concentrations by serial dilution in serum-free media for cellular assays.

4.2.2 Elution and In-gel Digestion

Nanoparticle pellets were suspended in 30 µL SDS loading buffer (NuPAGE) for 10 minutes and heated to 80°C before running into the top of a 4-12% bis-tris polyacrylamide gel (NuPAGE) for 10 minutes at 200 V with MES buffer. The gels were washed twice for 5 minutes in ddH_2O and stained with Simply Blue Safe Stain (Life Technologies) for 20 minutes before being detained in ddH_2O overnight. The gels were imaged and each lane was cut out, and further destained in 10% methanol. Each lane was cut into approximately 1 mm^3 pieces and in-gel digestion was performed based on Shevchenko (1996).[219] Gel pieces

were dehydrated with 150 µL acetonitrile (ACN, Fisher Scientific) for 10 minutes which was aspirated before the addition of 50 µL 10 mM dithiothreitol in 0.1 M ammonium bicarbonate buffer (AmBic) for 30 minutes at 56°C. Excess reagent was removed and the pieces dehydrated before the addition of 40 µL 55 mM iodoacetamide in 0.1 M AmBic for 20 minutes at room temperature in the dark. The gel pieces were subsequently washed with 150 µL 0.1 M AmBic for 15 minutes before the addition of 40 µL of modified porcine trypsin (Promega) (12.5 ng/µL) for 45 minutes at 37°C. A further 10 µL of 0.1 M AmBic was added to each reaction which was then left over night at 3°C.

During peptide extraction, all solutions were retained and pooled. Trypsin was removed the following morning and 20 µL 25 mM AmBic was added for 15 minutes at 37°Cto wash before dehydrating with 20 µL of acetonitrile for 15 minutes at 37°C. The supernatants for each sample were removed and pooled before adding 20 µL extraction buffer (1% formic acid, 2% ACN, ddH_2O) for 15 minutes at 37°C. The supernatants were collected and pooled for each sample and the extraction repeated once more. Samples were then dried at 45-60°Cin a vacuum centrifuge and stored at -80°C until ready for analysis by LC-MS^E.

4.2.3 nanoLC-MS^E

Samples were suspended in 20 µL of buffer A (0.1% formic acid, ddH_2O) and the concentration of peptides determined by direct detect. Sample concentration was adjusted to 0.5 µg/µL and enolase internal mass standard (Waters, UK) was added to 100 fmol/µg. Approximately 1 µg (2 µL) was loaded on to the liquid chromatography (LC) column (Waters, Acuity UPLC M-Class HSS T3 1.8 µm, 75 µm x 250 mm column). LC was run with a 37 minute gradient increasing from 3% buffer B (ACN, 0.1% formic acid) to 40% over 30 minutes before being increased to 85% in the 31st minute, after which the column was flushed with 97% buffer B. Nano-LC (Nano Acquity UPLC, Waters, UK) was fed directly into the mass spectrometer (Synapt G2s, Waters, UK) by nano-spray and analysed by MS^E in resolution mode. The collision energy oscillated between 15 and 40 kV with scan times of 1 second and m/z recorded between 50 and 2000.

4.2.4 Data Analysis

Data was analysed on Protein Lynx Global Server version 3.0 (PLGS, Waters) searching against UniProt human database including yeast enolase (internal standard), and assuming carbaminomethyl cysteine (fixed modification), deamination of asparagine and glutamine

Protein Characteristic	Description
Isoelectric Point (pI)	The pH at which the protein carries no charge. This is predicted from the amino acid sequence.
Molecular Weight	Calculated from the full amino acid sequence, excluding any post translational modifications.
Grand Average of Hydropathy (GRAVY)	The average hydropathy values for all the amino acids in the protein sequence. Isoleucine, has the greatest hydrophobicity (4.5), whilst argenine has the greatest hydrophilicity (-4.5).[224]
Aliphatic Index	This is the relative volume occupied by aliphatic side chaines (alanine, valine, isoleucine and leucine). This is an indicator of thermostability for globular proteins.[225]
Predicted % α-Helix	Proportion of amino acids thought to contribute to a α-helical secondary structure.
Predicted % β-Sheet	Proportion of amino acids thought to contribute to a β-sheet secondary structure.

Table 8: Protein properties extracted from ProtParam and used for corona characterisation.

(variable modification), and oxidised methionine (variable modifications). Proteins identified from single peptides were excluded from further analysis. Quantification was performed using Hi3 method against yeast enolase.[186]

Samples for each experiment were merged using an in-house script and normalised by dividing each individual repeat by the sum (fmol) of proteins present in 90% of all samples. Physiochemical information for each protein was extracted from Protparam[220] (ExPAsy) (Table **??**). Statistical analysis were performed in Prism 6 (Graphpad Software Inc.). Clustering analysis and heat maps were generated using Graphical Proteomics Data Explorer[221] (GProX 1.1.16, University of Southern Denmark, Denmark). principle component analysis (PCA) analysis was performed using the Bioconductor packaging pRoloc.[222, 223] Correlation plots were performed using InfernoRDN (http://omics.pnl.gov/software/infernordn).

4.2.5 BCA

See Section **??**

4.2.6 Western Blot

See Section **??**

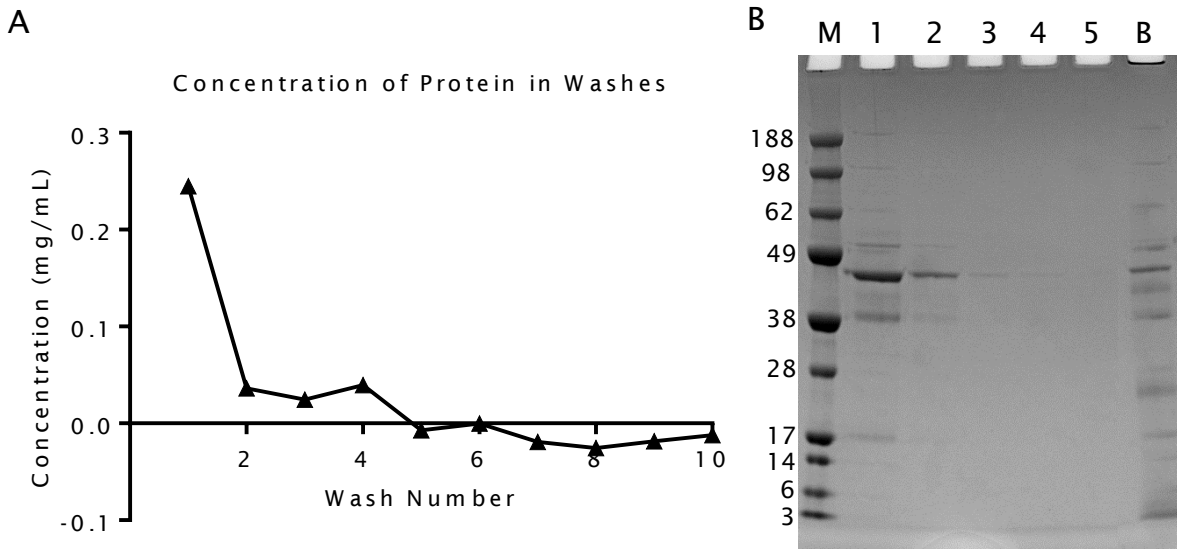

Figure 17: Analysis of particles washes. (A) Washes 1-10 were analysed by BCA assay to determine protein concentration. (B) The first 5 washes were further analysed by SDS PAGE (1-5), and an aliquot of BALF was also included for comparison 'B'. 'M' = molecular marker (kDa).

4.3 Results

4.3.1 Method Validation

4.3.1.1 NP Washing and Saturation After incubating the particles with BALF, the wash supernatants were analysed by BCA assay and SDS PAGE gel to show that all non-bound material was removed (Figure **??**). After 5 washes, the amount of protein in the supernatants had reduced below detectable limits for BCA assay and simply blue safe stain (<10 ng). Therefore particles were washed at least 5x, transferring the pellet to a clean Eppendorf tube between each wash.

To determine the amount of protein required to saturate the particles, BALF was spiked with BSA to a concentration of approximately 5.2 mg/mL and 500 cm^2 of aPS or cPS were incubated with increasing volumes for 2 hours and the bound proteins analysed by SDS PAGE (Figure **??**). The aPS particles required at least 15 mg of protein to reach saturation, whereas cPS were saturated after 10 mg. Therefore, during all experiments, the ratio of particle surface area to proteins was adjusted to at least 0.3 g/m^2.†

† $15mg/500cm^2 = 0.03mg/cm^2$
$= 0.00003g/cm^2$
$= 0.3g/m^2$

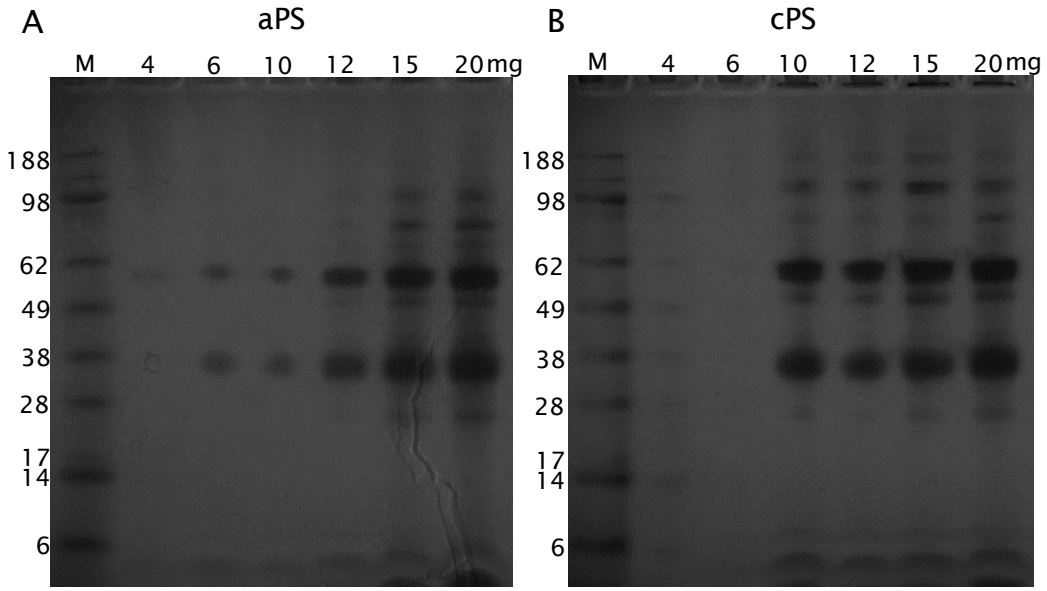

Figure 18: Saturation of NPs. Particles (500 cm^2) were incubated in increasing volumes of BALF-BSA mixture and analysed by SDS PAGE. Saturation of aPS particles was reached after 15 mg of protein (A) or 10 mg for cPS particles (B). Molecular weights of the molecular marker (M) are given in kDa

4.3.1.2 PEG Contamination The elution of proteins from particles by different methods were considered; directly digesting with trypsin, eluting with denaturing buffers (8M urea or SDS loading buffer) or SDS PAGE.

Denaturing buffers yielded more protein compared with direct digestion off the particles, with a combination of SDS PAGE loading buffer and urea eluting the most proteins (data not shown) as assessed by SDS PAGE.

However, following digestion with trypsin or with denaturing buffers, the samples were heavily contaminated with polyethylene glycol (PEG), which was evident by the presence of peaks 44 m/z apart (Figure **??**), and can cause strong suppression of peptide peaks during MS.

The most successful way to remove this was by eluting the proteins off the particles with SDS PAGE loading buffer and running into the stacking gel of a pre-formed 4-12% polyacrylamide gel. The increase in yield achieved by including 8M urea was minimal and, given incompatibilities of urea with tryptic digestion, it was decided to exclude this from subsequent elutions.

4.3.1.3 Reproducibility The number of proteins detected in each replicate are given in a Venn diagram (Figure **??**). We detected the greatest number of proteins bound to uPS, (221) with over 85% of proteins present in at least two replicates. Similarly, over 85% of

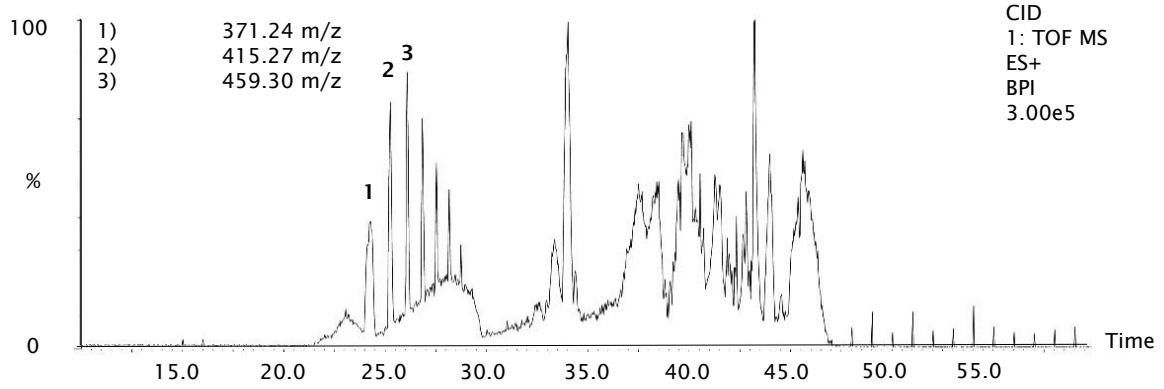

Figure 19: LC-MS of polyethylene glycol. Base peak intensity chromatogram of nano-LC. The m/z for peaks 1-3 are given in the top left corner. A series of singly charged peaks eluted, separated by 44Da, typical of PEG.

Sample	1 v 2	1 v 3	2 v 3	Mean (R^2)	Mean CV
aPS	0.71	0.98	0.66	0.78	26.5%
uPS	0.99	0.92	0.82	0.91	22.8%
cPS	0.99	0.99	0.95	0.98	23.2%
TiO_2	0.99	0.9	0.94	0.96	20.0%
aPS_15	0.93	0.92	0.97	0.94	20.9%
aPS_30	0.96	0.97	0.95	0.96	21.1%
aPS_60	0.73	0.97	0.67	0.79	26.0%
aPS_120	0.9	0.94	0.99	0.94	27.3%
cPS_15	0.93	0.99	0.98	0.97	28.6%
cPS_30	0.97	0.97	0.98	0.97	21.6%
cPS_60	0.98	0.99	0.95	0.97	20.7%
cPS_120	0.91	0.99	0.9	0.93	26.0%

Table 9: Values from correlation plots for 60 minute samples (aPS, uPS, cPS and TiO_2) and over time (aPS_x, cPS_x). The mean CV for all proteins present across all repeats for each particle are given.

proteins were detected in a least two replicates of aPS and 76% in TiO_2. Considerably fewer proteins were detected bound to cPS (38), compared to uPS, aPS and TiO_2 (221, 198, 123 respectively) with 52.6% being present in at least 2 samples.

We considered the reproducibility of each replicate as a system using correlation plots (an example is given in Figure **??**) which are summarised using R^2 values (Table **??**). These plots only take into account proteins that were detected in both replicates being compared. The average R^2 value for all samples and repeats was 0.93 with a standard deviation of 0.09, indicating that there was good reproducibility between samples.

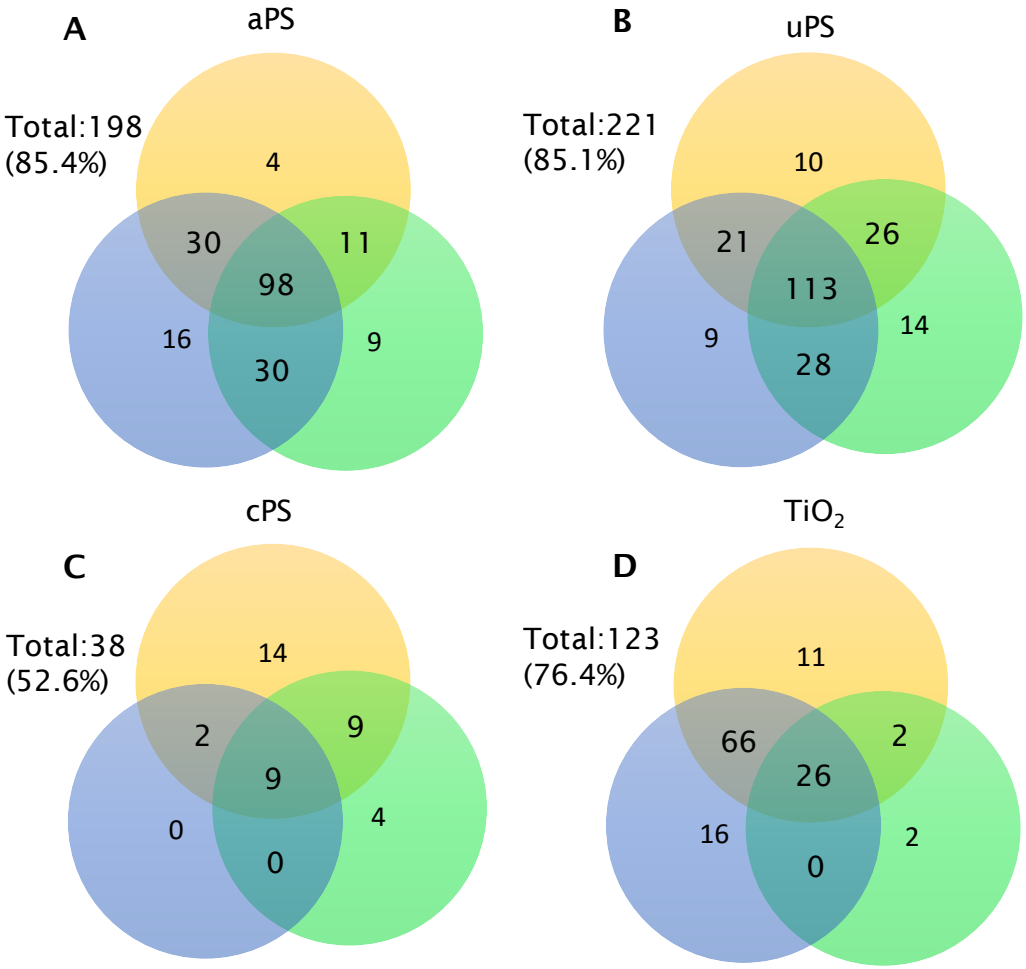

Figure 20: Venn diagram of triplicate repeats for (A) aPS, (B) uPS, (C) cPS and (D) TiO_2. Values are the number of proteins, the total number of unique proteins detected are also given as well as the % of proteins present in at least 2 experiments.

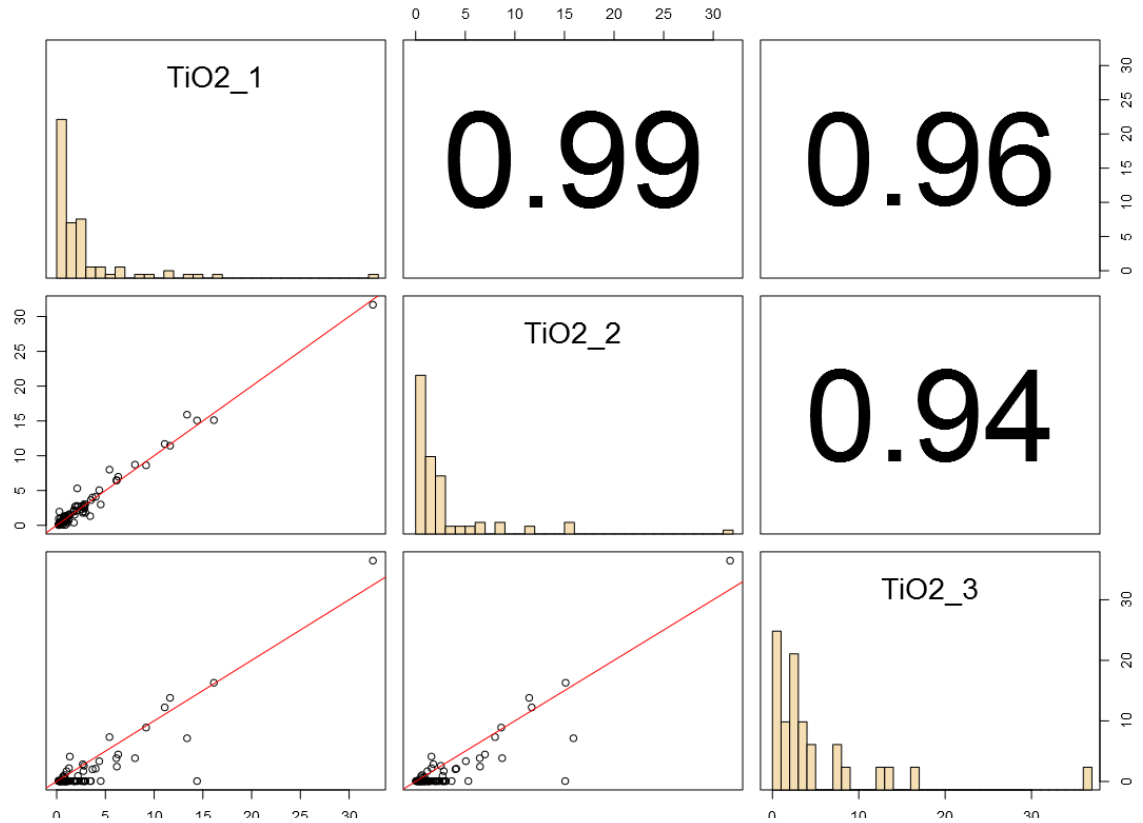

Figure 21: Example of a correlation plot. The expression value for each protein is plotted against a replicate value and an overall R^2 is determined. This is repeated for each replicate.

4.3.1.4 Composition of BALF

To determine the presence of phospholipids, an assay was performed with ferric thiocyanate. This showed the concentration of phospholipid to be below 10 µg/mL. Protein concentration was determined by BCA assay to be approximately 0.6 mg/mL. The pH was approximetly 6.4.

4.3.2 A Comparison between Different Particles

Nanoparticles, aPS, cPS, uPS and TiO_2, were incubated in BALF for 1 hour. SDS PAGE of PS particles showed that in all cases protein was eluted from the particle surfaces and that the composition of proteins was different to BALF. We also confirmed that the wash supernatants were devoid of any proteins (Figure **??**). The pattern of bands between aPS and uPS particles is very similar. Carboxylated PS may enrich for low molecular weight (Mw) proteins but this was not seen during mass spectrometric analysis of the proteins (see below).

In separate experiments, LC-MS^E was used to analyse the proteins eluted from the nanoparticles. The number of molecules per particle was calculated by multiplying the number of molecules (mols), as determined by LC-MS/MS, with Avogadro's number and

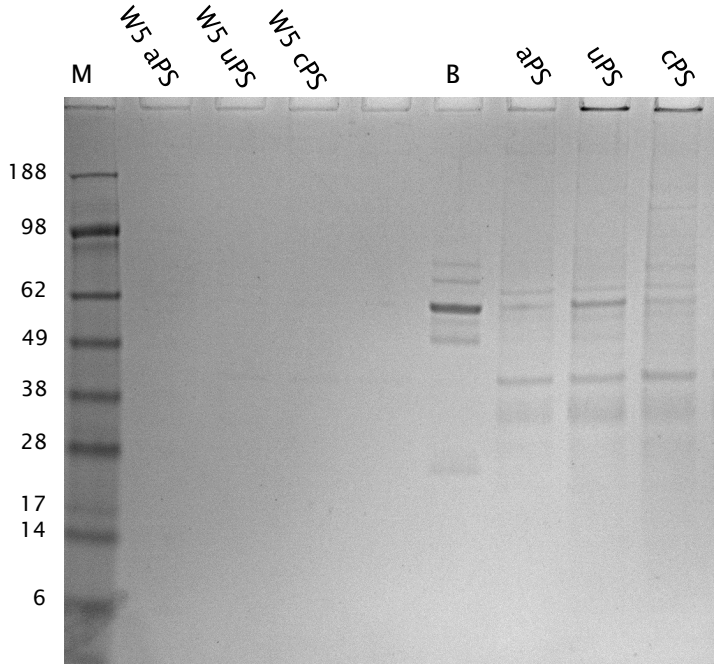

Figure 22: SDS PAGE of proteins eluted from PS particles. The eluted proteins (aPS, uPS and cPS) show different intensities to BALF (B). All three particles have a similar band pattern in the medium-low Mw proteins. cPS appears to bind to more higher Mw proteins. The particle elutes contain more low abundance proteins that were not visible in the BALF alone and are not dominated by the most abundant proteins present in BALF. The 5^{th} wash was also run (W5) for each particle to show all unbound material had been removed. Molecular weights of the molecular marker (M) are given in kDa.

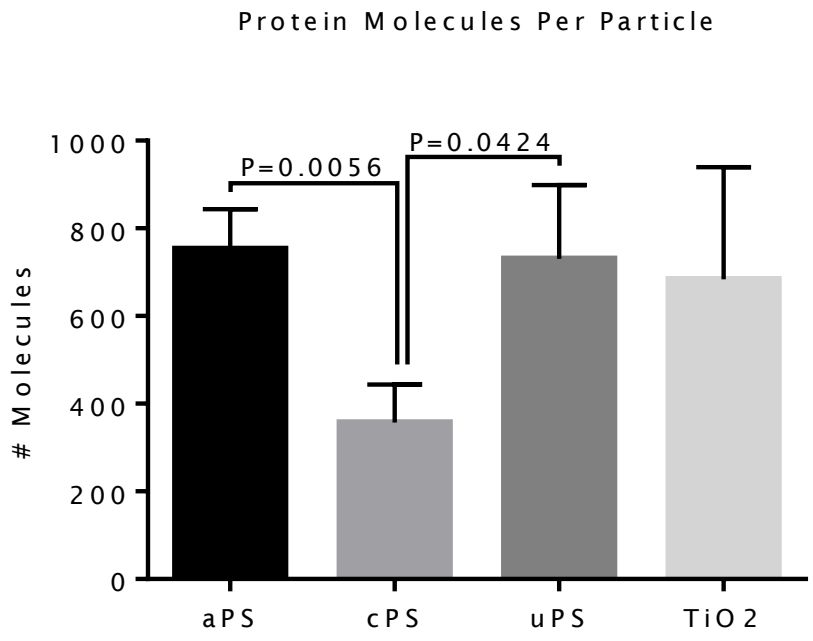

Figure 23: Number of adsorbed molecules per particle. A similar number of molecules was detected per particle on aPS and uPS and TiO_2. cPS particles had statistically fewer molecules per particle compared to aPS and uPS (T-Test). (mean ± SD, n=3).

dividing by the number of particles. The results show that aPS, uPS and TiO_2 had approximately 650-757 molecules per particle whereas cPS had 357 particles on average, which was statistically significantly fewer than aPS and uPS particles (Figure **??**).

29 proteins (11%) were common to all particles, but these proteins were not present in the same concentration in each corona elute (Figure **??**). Some of these were highly abundant lavage proteins, such as serum albumin, IgG and annexin. However, the proteins that bound were not necessarily dependant on the concentration. Proteins such as SP-A (Q8IWL1) and alpha-enolase (P06733) were low-abundance in BALF, and high abundance on the particles' corona (Figure **??**). Table **??** lists the top 20 proteins present in all coronas. For a complete list of identified proteins, see Supplementary 1.

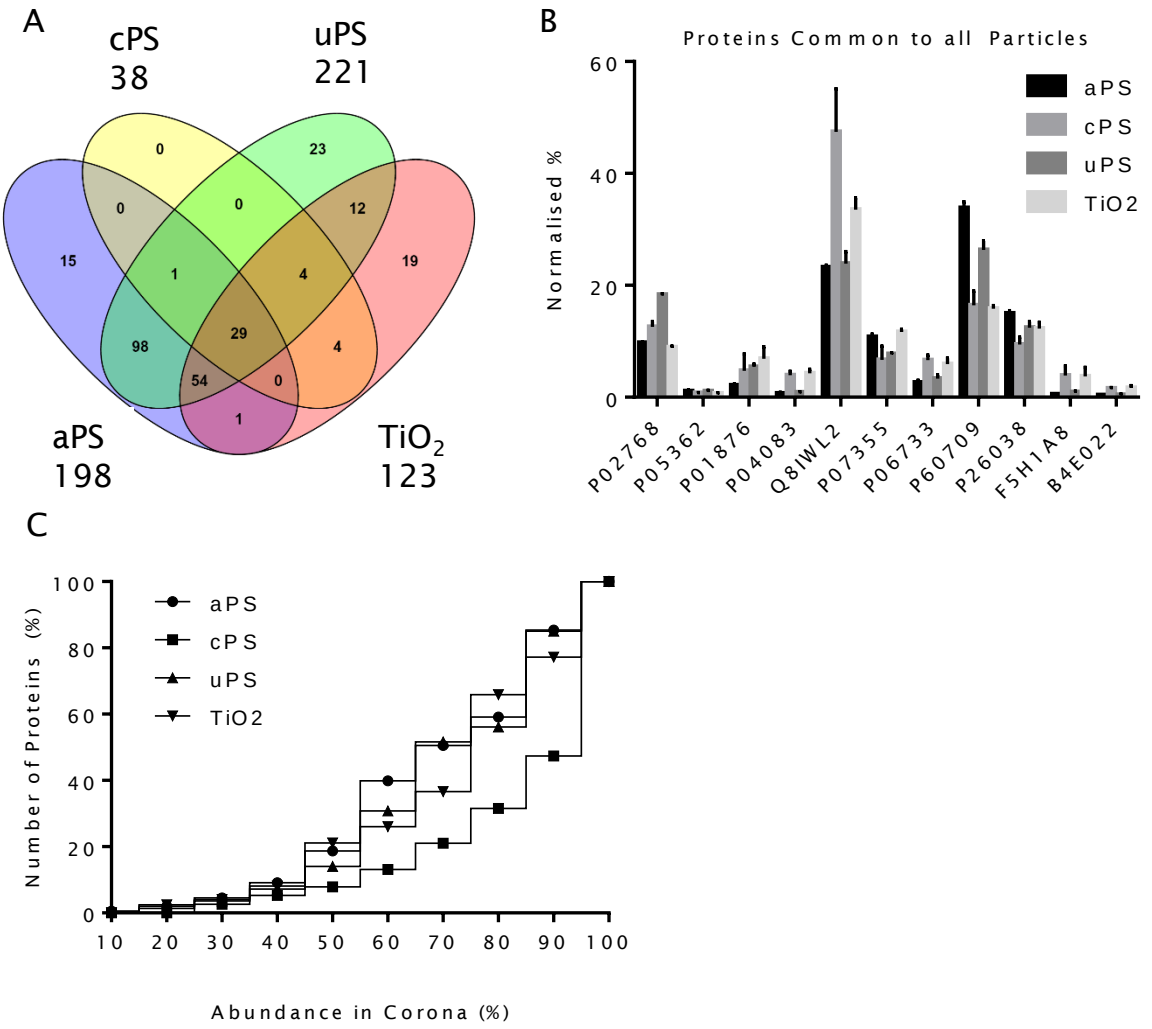

Figure 24: Comparison of PS coronas. (A) Venn diagram showing number of quantified proteins bound to each particle; 11% of proteins were common to all particles. (B) Proteins detected in all NP coronas, in at least 90% of samples, after 60 minute incubation in BALF. For each protein, there were statistical differences (Students T-Test) between each particle. The bar chart shows mean normalised abundance ± SD, n=3. (C) A cumulative count of the number of proteins present in the corona. Approximately 10% of the total number of proteins occupied 40% of the corona.

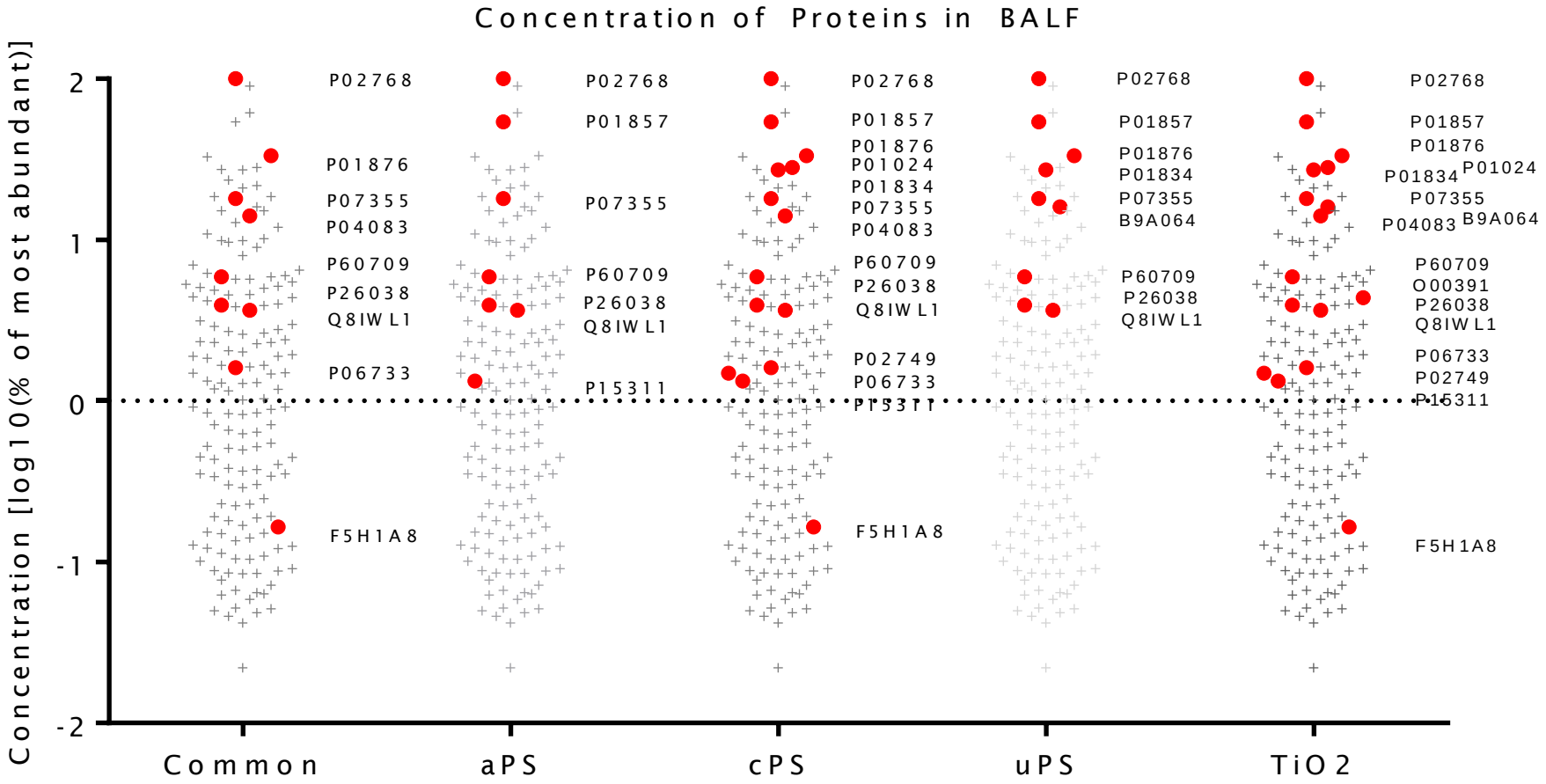

Figure 25: The distribution of proteins in BALF, ordered by abundance (normalised to the most abundant protein - serum albumin, P02768 and log transformed). Red points represent proteins that are amongst the top 20 proteins eluted from the particle after incubation in BALF for 1 hour. Since not all proteins that were detected on the particles were identified in BALF, not all top 20 proteins are depicted. Uniprot accession numbers for each red point are given.

The average physio-chemical properties of the corona were assessed using quantifiable properties of the detected proteins (Figure **??**). The quantities were adjusted to reflect the concentration of the identified protein and therefore represents the overall characteristic of the corona (Figure **??**). There was little difference between the corona surrounding aPS, uPS, TiO_2 or cPS particles. uPS and aPS particles had very similar coronas, the % of predicted α-helices or β-sheet and grand average of hydropathy (GRAVY) was slightly skewed towards higher content prepared with TiO_2 and cPS particles.

The pI of bound proteins was similar for all PS particles, with over 50% having a pI <6. The pI of bound proteins was evenly distributed (50/50) around a pI of 6.

In general, approximately 2/3 of the proteins that bound to the particles were smaller than 60 kDa and had a pI of less than 7, indicating the majority of bound proteins were acidic. Slightly more than half of the proteins had negative hydropathy values, suggesting a tendancy towards more hydrophobic proteins binding (Figure **??**).

Table **??** shows there are differences between the most abundant proteins bound to the particles. We compared the unique proteins between every pair of particles to determine if there was any common feature of the particles that may explain specific binding (Figure **??** - Figure **??**). For lists of unique proteins see Supplementary 2. A functional comparison for the proteins is also presented. This was performed using Panther gene ontology (GO)-term analysis, in which enrichment for GO-terms within the supplied protein list is determined. A single protein is described by many GO terms and therefore there may contribute to enrichment of different properties.

4.3.2.1 aPS Particles *versus* uPS Particles There were differences in the molecular function of the unique proteins bound to either corona. A greater portion of the proteins had receptor or translation regulator activity on aPS particles compared to uPS particles (Figure **??**B). There is little difference in the physical properties of the proteins bound to the particles with the proteins showing a similar distribution, median and interquartile range across all the characteristics tested (Figure **??**C-F).

4.3.2.2 aPS Particles *versus* cPS Particles A greater proportion of the proteins bound to cPS particles had receptor binding activity compared with aPS particle-bound protein, whereas conversely, only aPS particles had proteins with structural activity (Figure **??**B). The unique proteins are similar in terms of their isoelectric point (pI), GRAVY, aromatic index and α-helix (Figure **??**C, D, F and G). There were statistical differences

No.	aPS	cPS	uPS	TiO2
1	Actin, cytoplasmic 1	Pulmonary surfactant-associated protein A1	Actin, cytoplasmic 1	Pulmonary surfactant-associated protein A1
2	L-lactate dehydrogenase A-like 6A	Actin, cytoplasmic 1	Pulmonary surfactant-associated protein A1	Actin, cytoplasmic 1
3	Pulmonary surfactant-associated protein A1	L-lactate dehydrogenase A-like 6A	Serum albumin	L-lactate dehydrogenase A-like 6A
4	Heat shock cognate 71 kDa protein	Serum albumin	Heat shock cognate 71 kDa protein	Alpha-actinin-4
5	Ezrin	Moesin	Moesin	Moesin
6	Moesin	Annexin A2	L-lactate dehydrogenase A-like 6A	POTE ankyrin domain family member E
7	Annexin A2	Alpha-enolase	Alpha-actinin-4	Annexin A2
8	Serum albumin	14-3-3 protein zeta/delta	POTE ankyrin domain family member E	Ras-related protein Rab-8A
9	Alpha-actinin-2	Alpha-actinin-4	Annexin A2	Serum albumin
10	Dihydropyrimidinase-related protein 2	Ig alpha-1 chain C region	Dihydropyrimidinase-related protein 2	Keratin, type II cytoskeletal 8
11	Chloride intracellular channel protein 3	POTE ankyrin domain family member E	Ig gamma-1 chain C region	Ig alpha-1 chain C region
12	Ig gamma-1 chain C region	Annexin A1	Ezrin	Keratin, type I cytoskeletal 19
13	Heat shock protein HSP 90-beta	Gelsolin	Ig alpha-1 chain C region	Alpha-enolase
14	Pyruvate kinase PKM	Pyruvate kinase PKM	Keratin, type I cytoskeletal 19	14-3-3 protein zeta/delta
15	Peptidyl-prolyl cis-trans isomerase	Putative beta-actin-like protein 3	Pyruvate kinase PKM	Ig kappa chain C region
16	HLA class II histocompatibility antigen	Ig kappa chain C region	HLA class II histocompatibility antigen	Annexin A1
17	Alpha-actinin-1	Keratin, type II cytoskeletal 8	Ras-related protein Rab-8A	Gelsolin
18	Annexin A5	HLA class II histocompatibility antigen	Alpha-actinin-1	Cell cycle control protein 50A; Plastin-3
19	Alpha-actinin-4	Keratin, type I cytoskeletal 19	Chloride intracellular channel protein 3	14-3-3 protein gamma
20	Chloride intracellular channel protein 4	cDNA FLJ56274, highly similar to Transketolase	Alpha-actinin-2	HLA class II histocompatibility antigen

Table 10: Top 20 proteins present eluted from NPs. The proteins in darker blue were present in all particles.

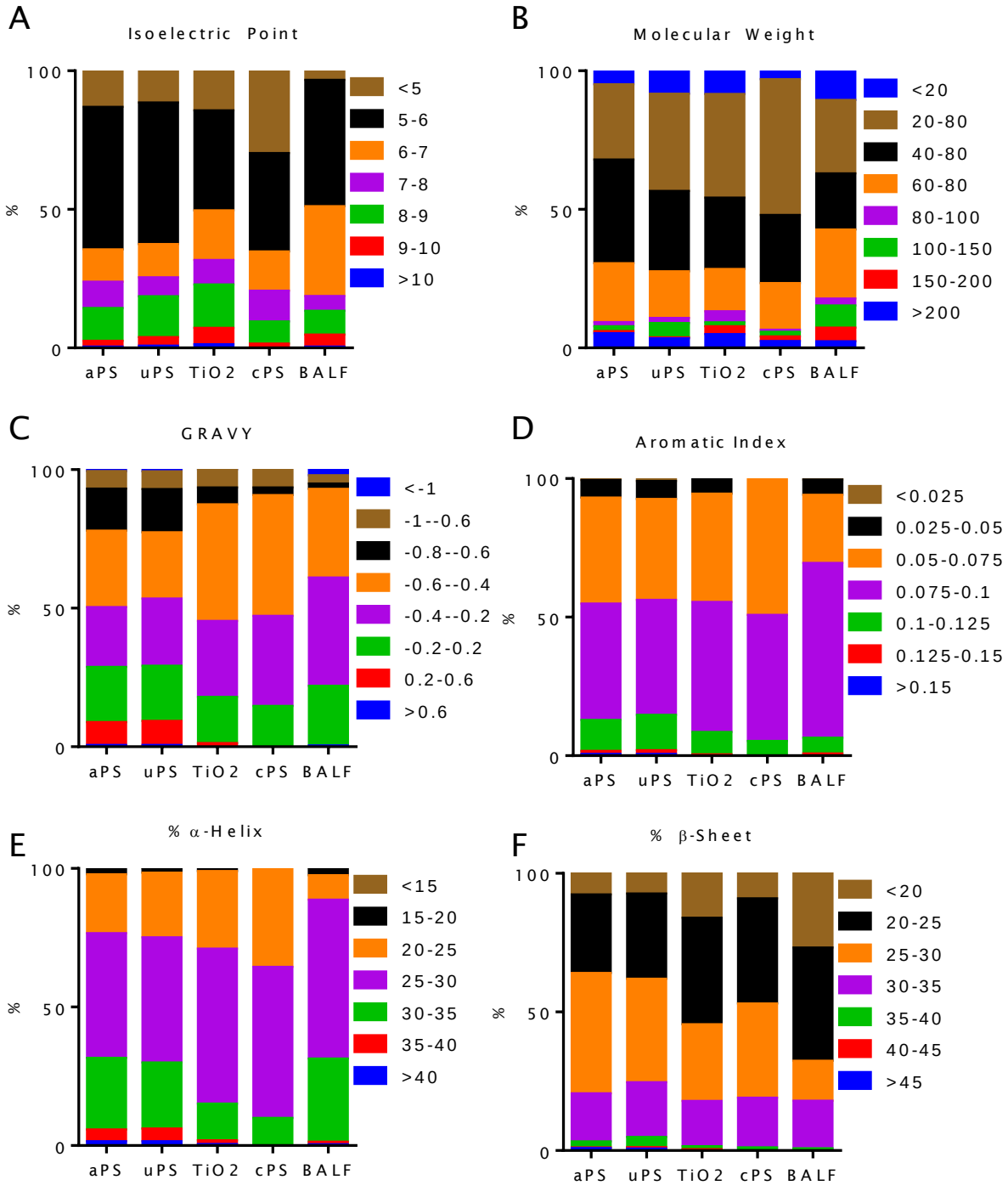

Figure 26: Physical characteristics of the proteins identified in the corona of each particle; values are weighted by abundance and expressed as a % of total concentration. There is little difference between the coronas of any of the particles in terms of pI (A), Mw (B), GRAVY (C), aromatic index (D), % α-helix (E) or % β-sheet (F). Proteins from whole BALF is added for comparison.

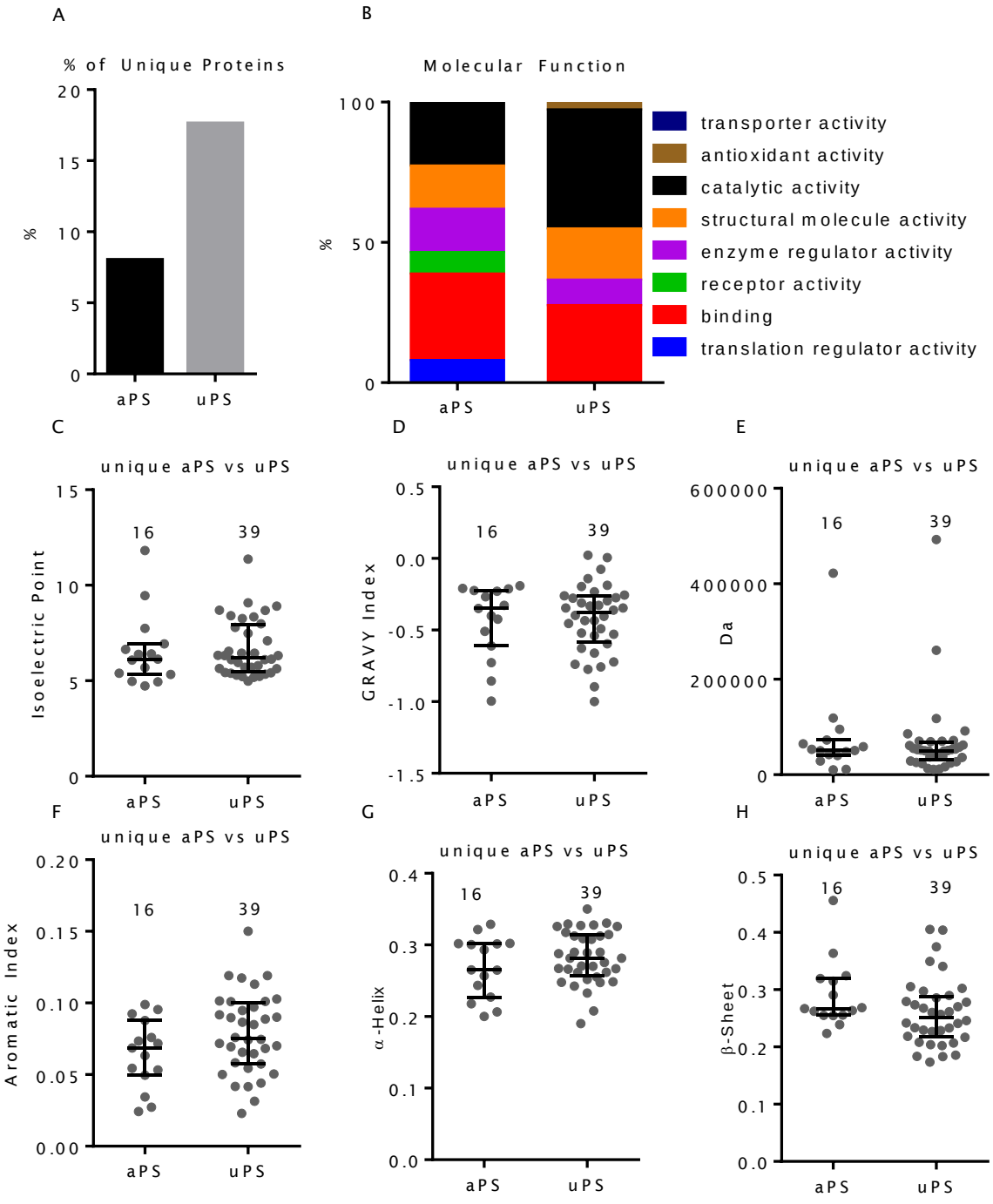

Figure 27: Comparison of unique proteins bound to aPS particles compared to uPS particles. (A) The number of unique proteins as a % of the total number of proteins on each particle. A larger proportion of uPS are unique compared to aPS. (B) GO term analysis of unique proteins, shown as % of total number of terms, shows differences between the molecular functions of the unique proteins. (C-H) The distribution of physio-chemical characteristics of the proteins unique to each corona show no differences between the proteins. Error bars show median with inter-quartile range, and numbers above each scatter plot represents the number of proteins.

between the mean Mw (Figure **??**E) and % β-sheet (Figure **??**H) (P=0.0192, P=0.006 respectively), although these are not very confident given the low number of proteins unique to cPS (Figure **??**A).

4.3.2.3 aPS Particles *versus* TiO_2 Particles There were more unique proteins bound present in the aPS particle corona compared to the TiO_2 particle corona although both unique coronas contained proteins with similar molecular functions, including binding (Figure **??**B). The median value and distribution of GRAVY, pI, aliphatic index and % α-helix were similar between both particles (Figure **??**C, D, F, G), although again, significant differences in Mw (Figure **??**E) and % of β-sheet (Figure **??**H) were observed (P=0.0274 and P=0.0001 respectively).

4.3.2.4 cPS Particles *versus* uPS Particles There were very few common proteins between cPS and uPS particles, reflecting the large difference in numbers of proteins detected on each corona (4 and 186 respectively) (Figure **??**A). The unique proteins bound to cPS did not have any structural function unlike uPS (Figure **??**B) but were functionally similar in other respects. There was no statistical difference between any of the physical parameters tested (Figure **??**C-H), The unique proteins bound to uPS are typically diverse in all of the physical properties where the unique proteins bound to cPS particles clustered around a small % α-helix composition (Figure **??**G).

4.3.2.5 cPS Particles *versus* TiO_2 Parrticles Only 1 protein was unique to the cPS corona when compared with TiO_2 (Figure **??**). There was a broad distribution of the proteins bound to TiO_2 in terms of their physical/chemical (Figure **??**C-H) and molecular function (Figure **??**B).

4.3.2.6 uPS Particles *versus* TiO_2 Particles The unique proteins bound to TiO_2 particles, when compared with uPS particles, are lacking in structural molecular activity (Figure **??**B). As with other pairs, statistical differences were observed between the mean Mw and mean predicted % β-helix (P=0.0065 and P=0.0024 respectively) (Figure **??**E, H). However the distribution of proteins is similar for both properties, and statistical significance is probably due to a small number of larger proteins, or proteins with higher % β-helix bound to uPS particles, and may not be of biological significance.

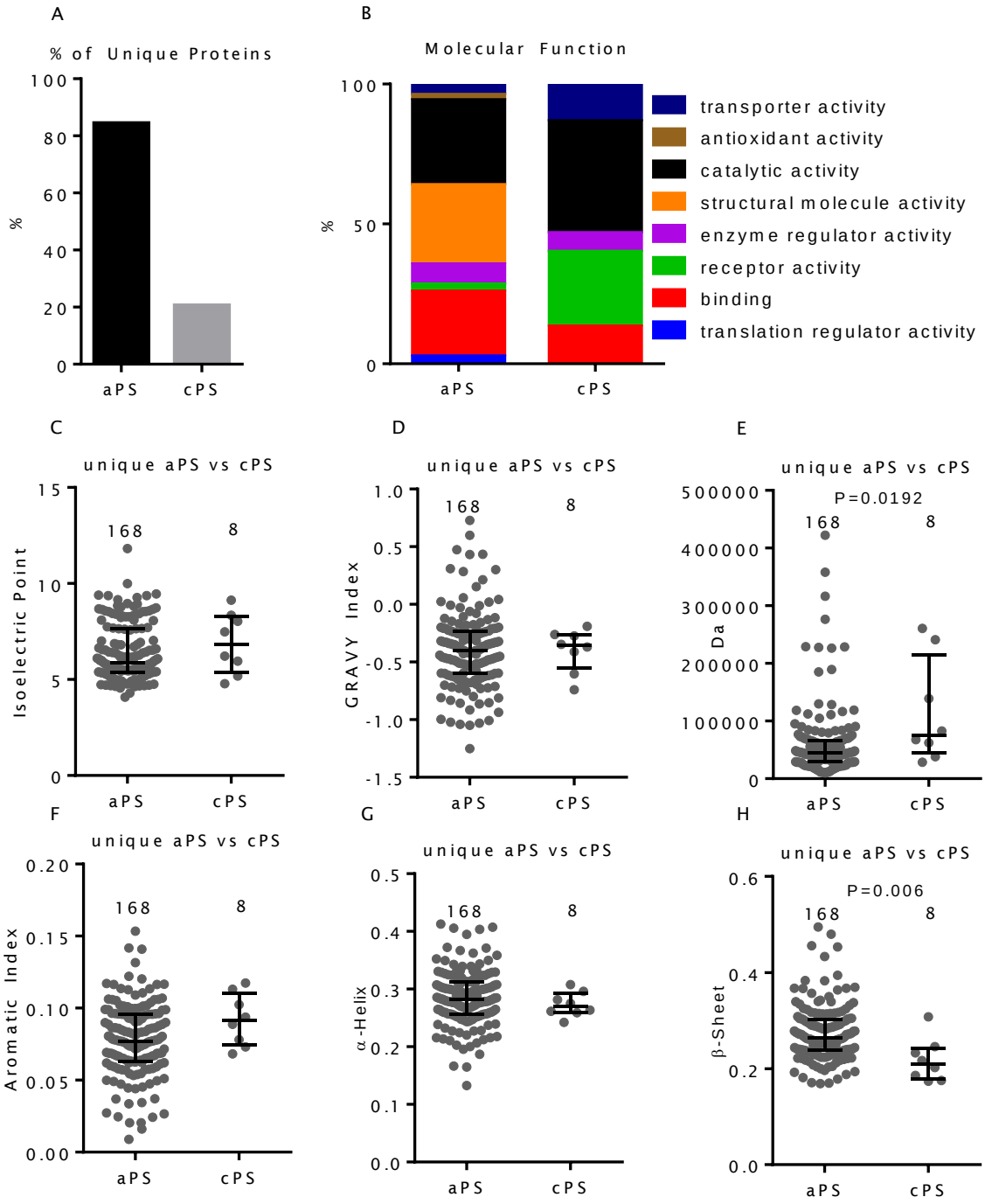

Figure 28: Comparison of unique proteins bound to aPS particles compared to cPS particles. (A) The number of unique proteins as a % of the total number of proteins on each particle. A larger proportion of aPS are unique compared to cPS. (B) GO term analysis of unique proteins, shown as % of total number of terms, shows differences between the molecular functions of the unique proteins. (C-H) The distribution of physio-chemical characteristics of the proteins unique to each corona show statistical differences between the Mw and % β-sheet of the bound proteins. Error bars show median with inter-quartile range, P-values were determined from Students' T-Test and numbers above each scatter plot represents the number of proteins.

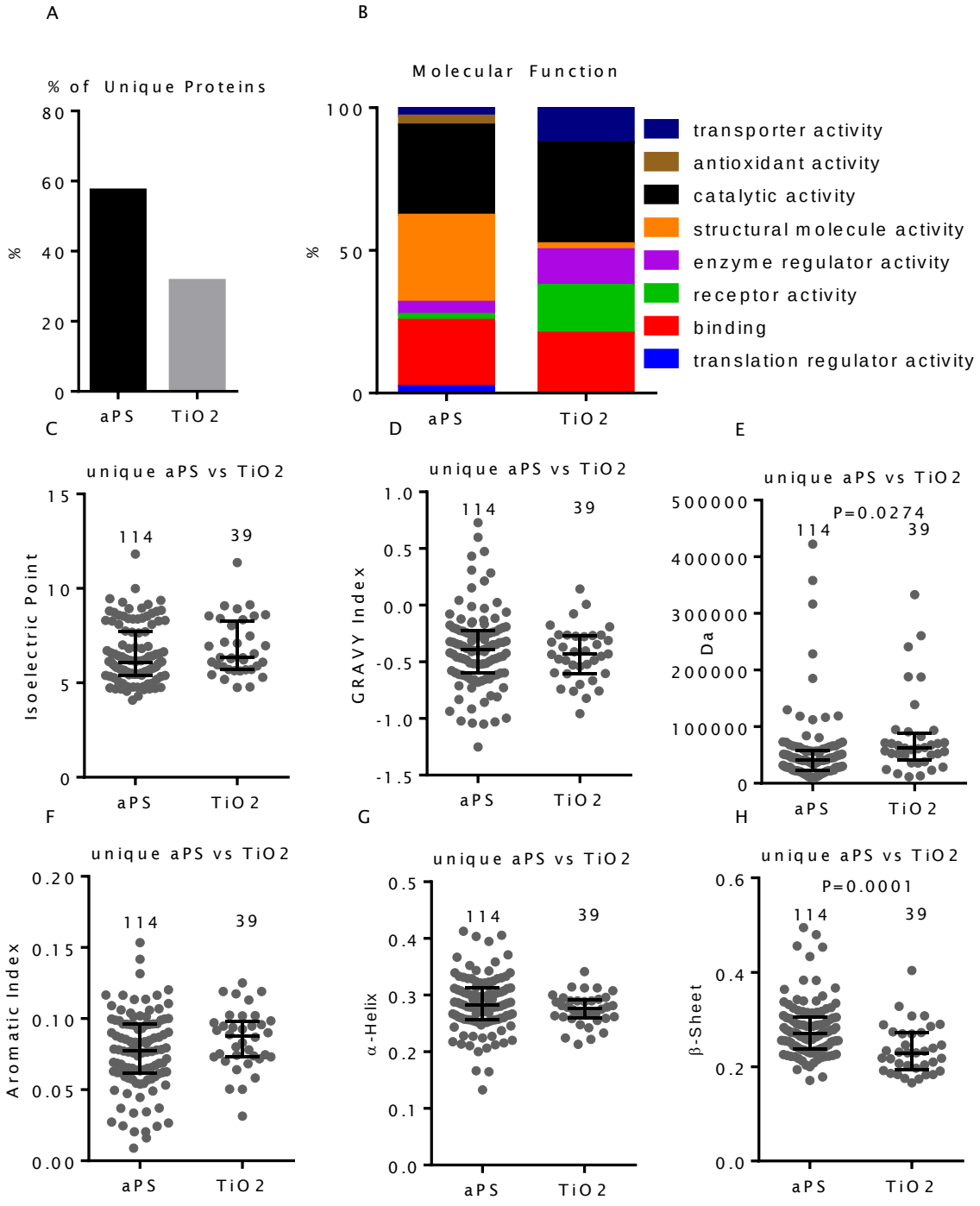

Figure 29: Comparison of unique proteins bound to aPS particles compared to TiO_2 particles. (A) The number of unique proteins as a % of the total number of proteins on each particle. A larger proportion of aPS are unique compared to TiO_2. (B) GO term analysis of unique proteins, shown as % of total number of terms. (C-H) The distribution of physio-chemical characteristics of the proteins unique to each corona show statistical differences between the Mw and % β-sheet of the bound proteins. Error bars show median with inter-quartile range, P-values were determined from Students' T-Test and numbers above each scatter plot represents the number of proteins.

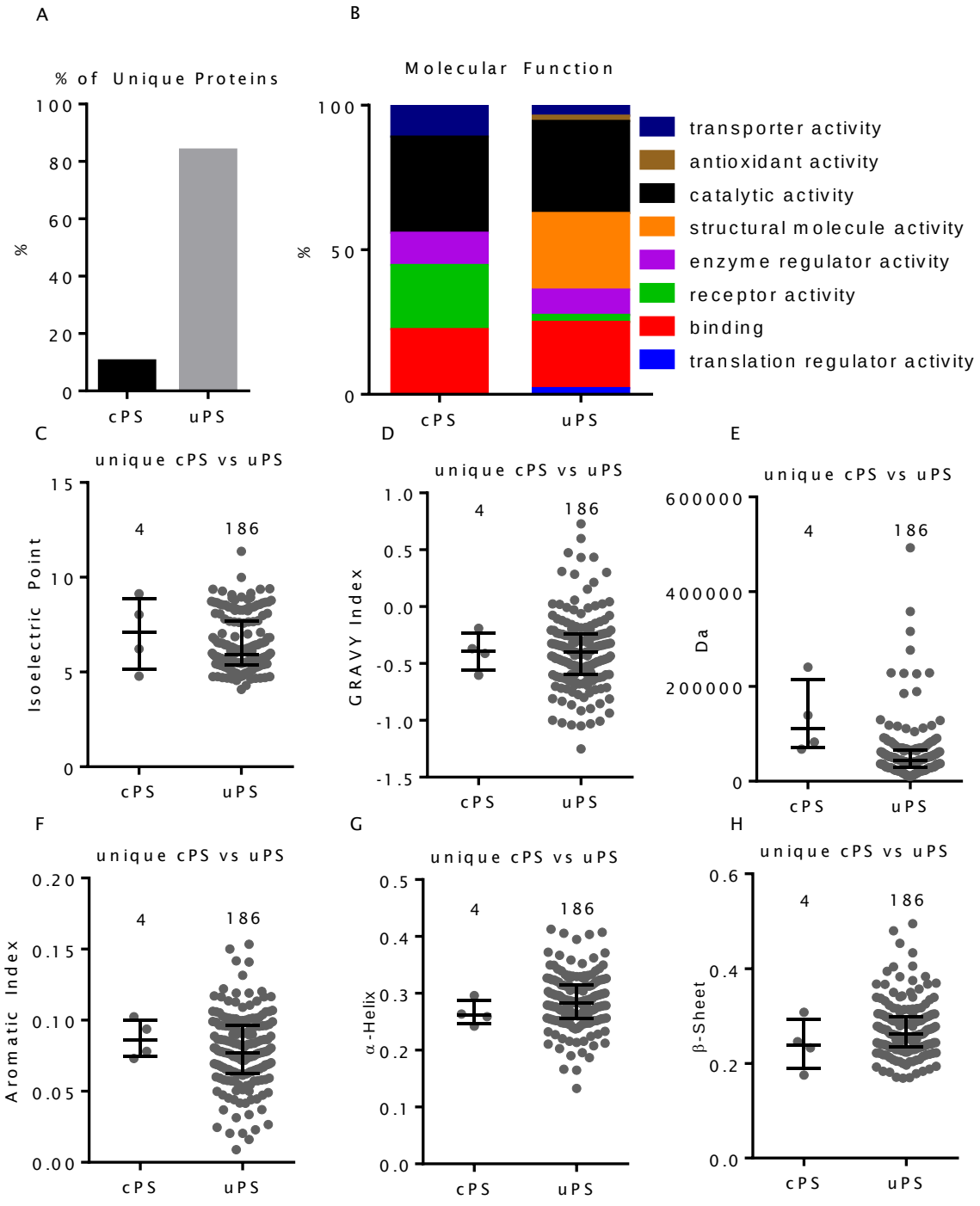

Figure 30: Comparison of unique proteins bound to cPS particles compared to uPS particles. (A) The number of unique proteins as a % of the total number of proteins on each particle. A larger proportion of uPS is unique compared to cPS. (B) GO term analysis of unique proteins, shown as % of total number of terms, shows differences between the molecular functions of the unique proteins. (C-H) The distribution of physio-chemical characteristics of the proteins unique to each corona. There are no statistical differences observed between the particles for any of the properties tested. Error bars show median with inter-quartile range and the number above each scatter plot represents the number of proteins.

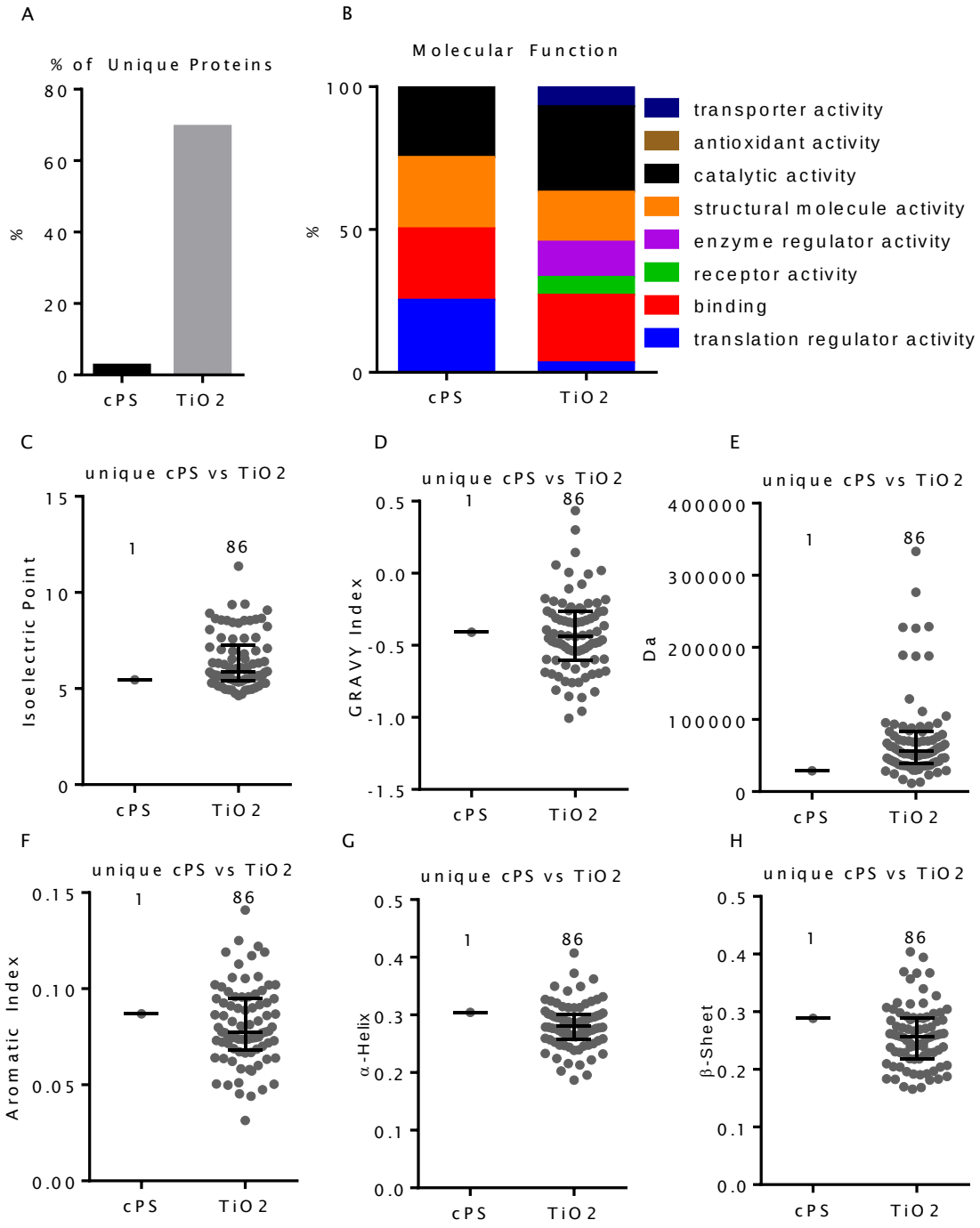

Figure 31: Comparison of unique proteins bound to cPS particles compared to TiO_2 particles. (A) The number of unique proteins as a % of the total number of proteins on each particle. A larger proportion of uPS is unique compared to cPS. (B) GO term analysis of unique proteins, shown as % of total number of terms, shows differences between the molecular functions of the unique proteins. (C-H) The distribution of physio-chemical characteristics of the proteins unique to each corona. There was only 1 unique protein detected bound to cPS compared to TiO_2. Error bars show median with inter-quartile range and the number above each scatter plot represents the number of proteins.

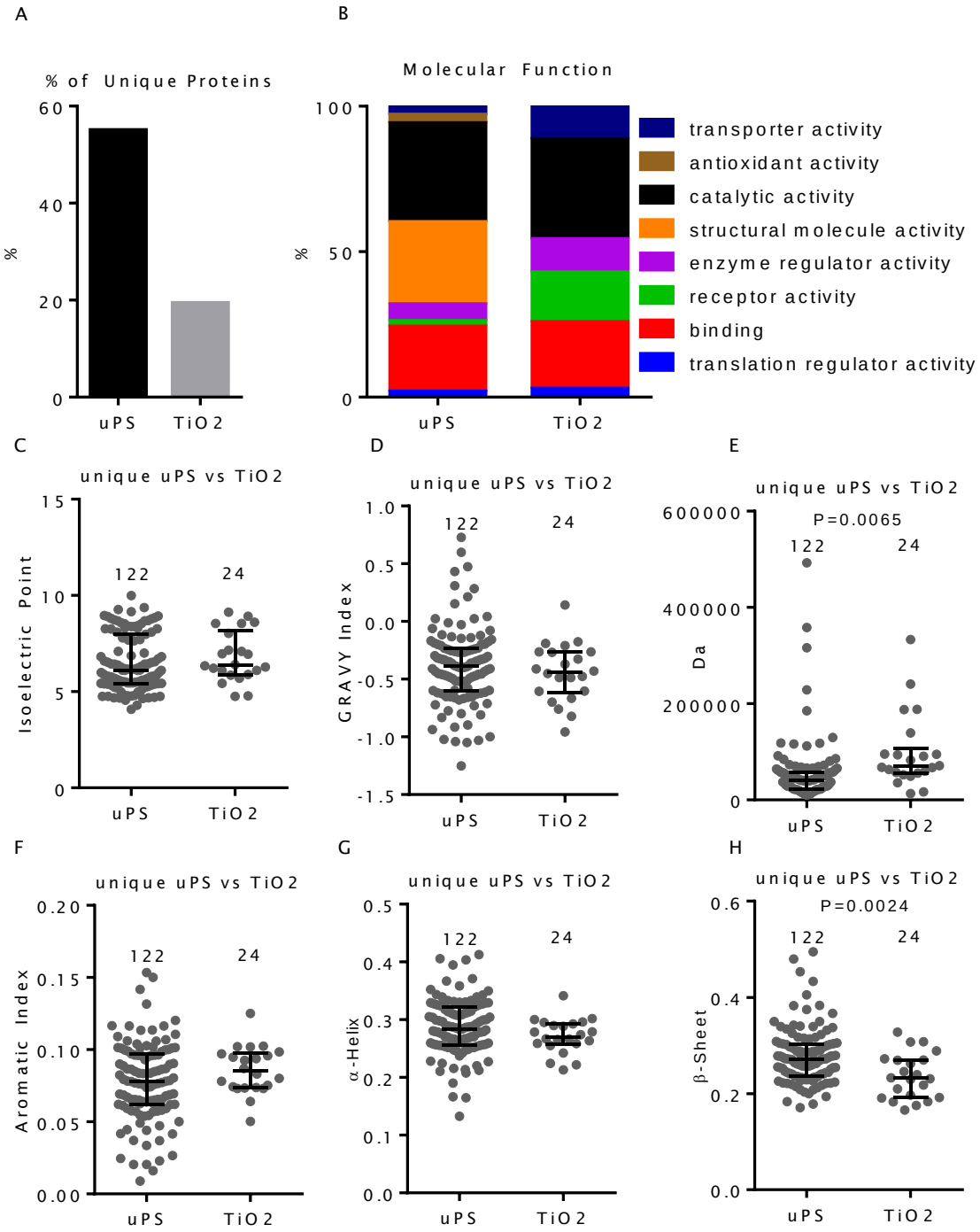

Figure 32: Comparison of unique proteins bound to uPS particles compared to TiO_2 particles. (A) The number of unique proteins as a % of the total number of proteins on each particle. A larger proportion of uPS is unique compared to TiO_2. (B) GO term analysis of unique proteins, shown as % of total number of terms, shows differences between the molecular functions of the unique proteins. (C-H) The distribution of physio-chemical characteristics of the proteins unique to each corona. There are statistical differences observed between the particles for Mw and β-sheet. Error bars show median with inter-quartile range and the number above each scatter plot represents the number of proteins. P-values were calculated from Student's T-test.

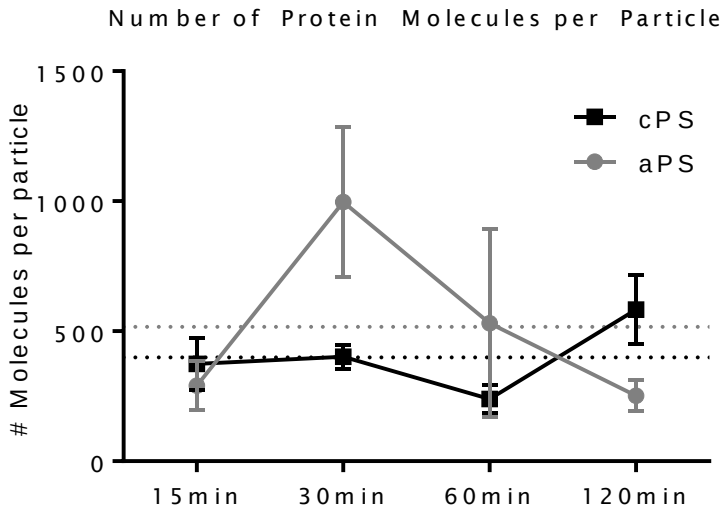

Figure 33: Average number of protein molecules per particle over time for cPS particles (black line) and aPS particles (grey line). Error bars represent standard deviation from n=3. Dotted line - mean number of particles across all time points.

4.3.3 Changes to the Protein Corona over Time

4.3.3.1 General Properties of the Coronas Nanoparticles may be present in the hydrophase for a number of hours before being endo- or phagocytosed by pulmonary cells. Therefore we investigated changes to the protein corona over time, at four time points, (15, 30, 60 and 120 minutes) for particles - aPS and cPS. These particles were selected as they have the greatest difference in surface charge but opposite charges in terms of surface functional groups. Therefore the effect of surface funcationalisation can be further investigated here.

The calculated average number of protein molecules per particle fluctuated over the four time points for each particle (Figure **??**). There was less variation in the number of molecules per particle from the cPS compared to aPS, which increased over 30 minutes before decreasing over the following 1.5 hours.

Of the proteins bound to cPS particles over time, 20% were present at all time points and 16% were present at all time points bound to aPS particles (Figure **??**). Proteins that were quantified in at least two replicates and were common to all time points are shown in Figure **??** C and D. Many of these proteins were present at similar concentrations at every time point. Whilst the concentrations of some of the proteins differ significantly over time on the same particle, this contrasts with particles of different types incubated in BALF for the same time, where all proteins differed significantly between different particles (Figure **??**).

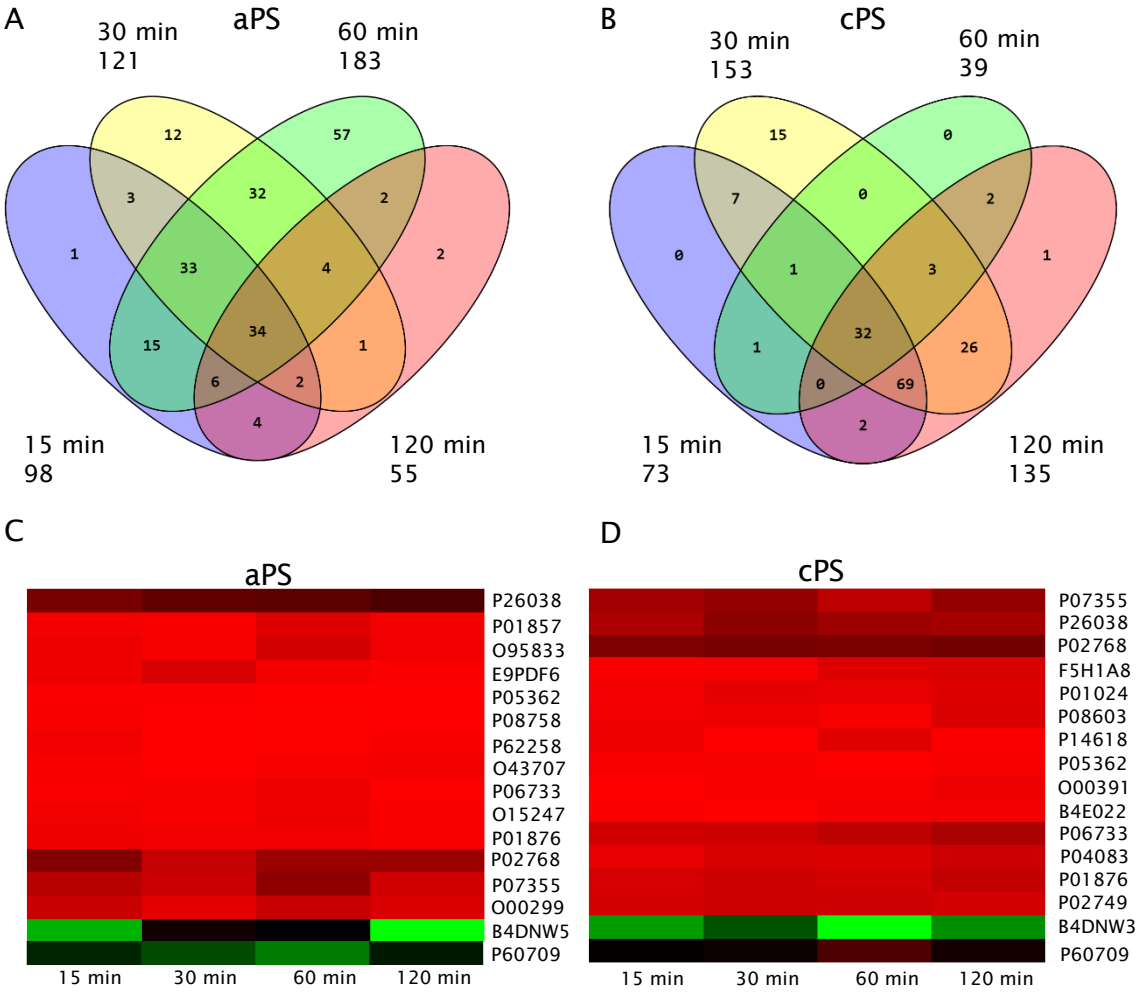

Figure 34: Proteins present on aPS and cPS particles incubated in BALF for different periods of time. Venn diagram show proteins quantified in aPS (A) and uPS (B) particles; 16% of proteins were present at all time points in aPS particles and 20% for cPS particles (total number of unique proteins detected at each time point is indicated). Heat maps for the proteins present in at least 90% samples, and repeats for aPS (C) and uPS (D), show that the abundance of these proteins does not change much over time and that they are not necessarily the most abundant proteins present in the corona. Heatmap colours; red = low, black = middle, green = high. $*P<0.05$ differences between any two time points (Students' T-Test).

This is further shown by the observation that there was very little change in the physico-chemical properties of the corona proteins (Figure **??**). There was a slight increase in high-Mw proteins bound to aPS particles over time (Figure **??**B) and a general increase in proteins with low aromatic indices (Figure **??**D), however these changes were only slight. BALF has a pH of 6.4, approximatly 50% of proteins had a pI higher or lower than this pH, and similar distrubutions in both BALF and on the particles, indicating no effect on protein charge.

4.3.3.2 Cluster Analysis of Dynamic Changes Since some proteins changed significantly over time, we performed a cluster analysis on the changes of protein concentration over the four time points, on proteins that changed at least 2 fold. Since the number of proteins present at all time points was not enough to perform reasonable clustering, we included proteins that were present in at least 2 time points, and set the concentration to 0 for the times where the protein was not quantified. We found the trends did not conform to 'simple' increase or decreases, rather some proteins peaked at different times. Four different clusters were idetendified where proteins peaked at either 15, 30, 60 or 120 minutes. The clusters were examined further using a principle component analysis (PCA) of the physical properties of the proteins (pI, instability index, Mw, aromatic index, GRAVY, % α-Helix, % Turn, % β-Sheet) and coloured by cluster. This would show if there was any feature of the proteins that would contribute to them belonging to a particular cluster (Figure **??** and Figure **??**).

No group could be seen on the PCA plot for aPS (Figure **??**) or cPS particles (Figure **??**). There were 9 proteins (out of 207) that could not be placed into any cluster for aPS particles – this is because they did not change concentration greater than 2 fold between any adjacent time points. The remaining proteins were fitted to 4 clusters with the majority of the proteins fitting to cluster 2, that described an increase in concentration up to 60 minutes followed by a decrease over the next hour (Figure **??**A). Proteins in cluster 3 tended to increase in concentration over 120 minutes whereas they decrease in clusters 1 and 4. However we could not find any defining factors for proteins within these groups.

There were 159 proteins taken into the analysis for cPS particles and of these only 9 were not incorporated into any cluster (Figure **??**A). The majority of proteins were in cluster 1, where there was a dip in concentration at 60 minutes. This could be due to the small number of proteins detected at 60 minutes which would lead to lots of '0' values for these proteins at 60 minutes. Proteins in the other groups do not all conform well; cluster 3

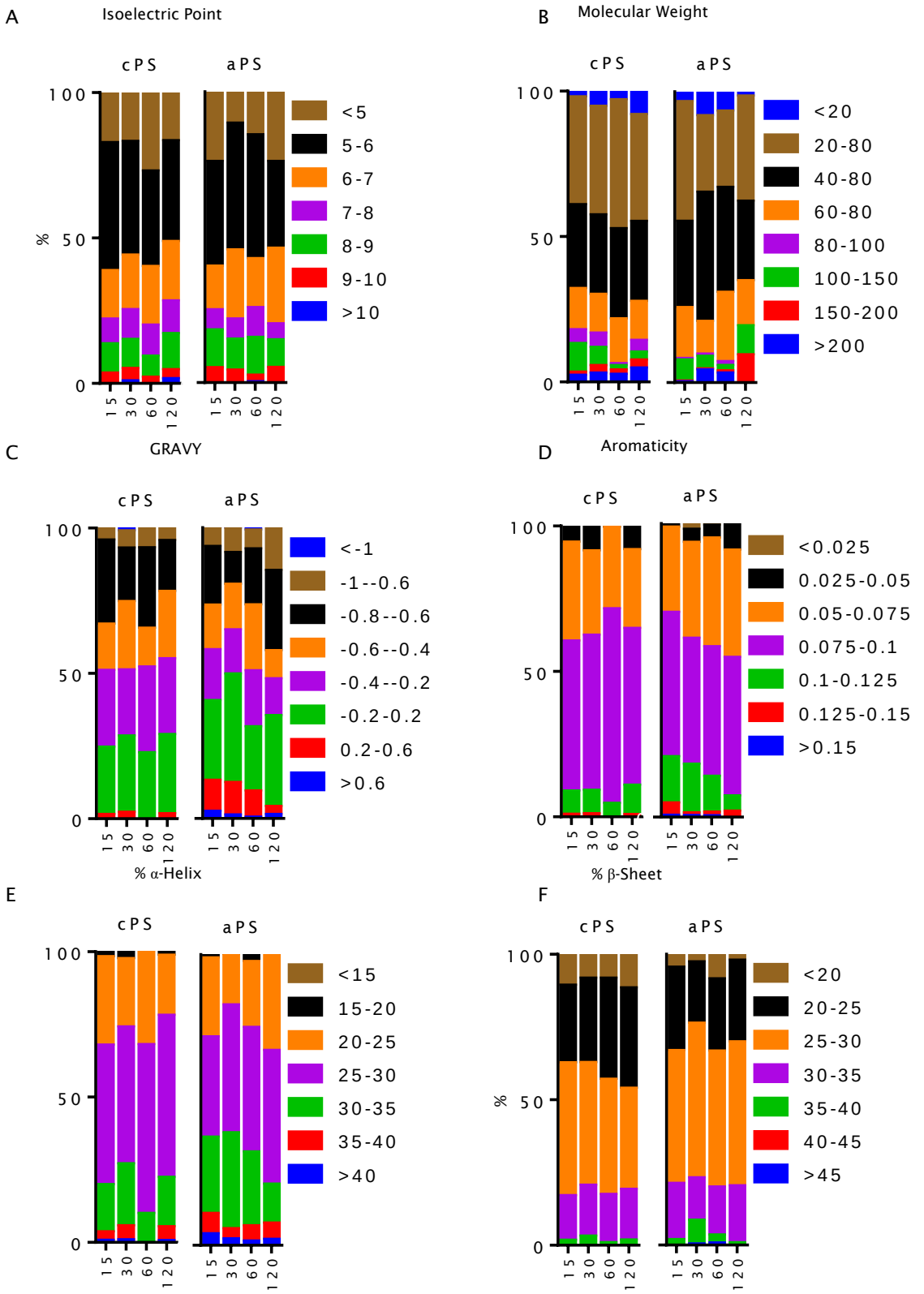

Figure 35: Physical characteristics of the proteins identified in the corona of aPS or cPS particles over time. Values are weighted by abundance and expressed as a % of total concentration. There is little difference between the coronas over time in terms of pI (A), Mw (B), GRAVY (C), aromatic index (D), % α-helix (E) or % β-sheet (F).

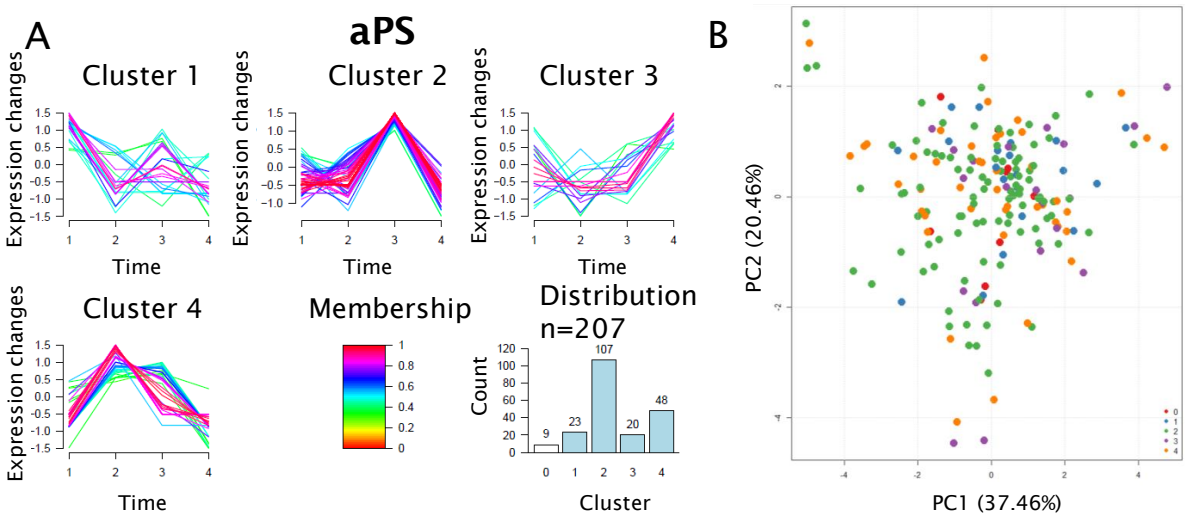

Figure 36: Longitudinal analysis of aPS protein corona. (A) Proteins from aPS particles that changed with a minimum of 2-fold difference were analysed by cluster analysis with 4 groups. The ratio of each protein was determined and normalised by z-score. The ratio for each protein is plotted (Cluster 1-4) as well as a key to how well they conform to each cluster ('Membership'). Time on the x-axis is labelled 1-4 and corresponds to 15, 30, 60 and 120 minutes respectively. (B) A PCA analysis was performed against a number of physical characteristics and the proteins colours based on their cluster – blue (cluster 1), green (cluster 2), purple (cluster 3), orange (cluster 4).

describes a general trend of increasing over time whereas cluster 2 describes the inverse. However the some of the proteins only obey these trends weakly. Again, there was no feature of the proteins that we could detect that could explain their binding profiles (Figure **??**B). We also tried to increase the number of variables in the PCA plots by including the % of each amino acid. However, again, no grouping was seen (data not shown). For a full list of the proteins and the cluster which they were assigned, see Supplementary 3.

In an independent experiment, a single protein from each of clusters 1, 2 and 3 of cPS particles was selected, and its change in concentration on the particle investigated by Western blot. SP-B from cluster 1, SP-A from cluster 2 and deleted in malignant brain tumour-1 (DMBT1) from cluster 3 were (Figure **??**). The normalised ratio of each protein over time as detected by LC-MS^{E} (Figure **??**A) with the corresponding Western blots from independent experiments (Figure Figure **??**B). The intensities of the Western blots change similarly to the quantification performed by LC-MS^{E}. There are some differences, for example SP-A was found to be most abundant after 60 minutes by mass spectrometry, but after 120 minutes by Western blot. However, SP-B maps very similarly, with a dip at 60 minutes and a peak after 120 minutes. DMBT1 showed a slight initial decrease followed by an increase in concentration between 60 and 120 minutes by Western blot and MS.

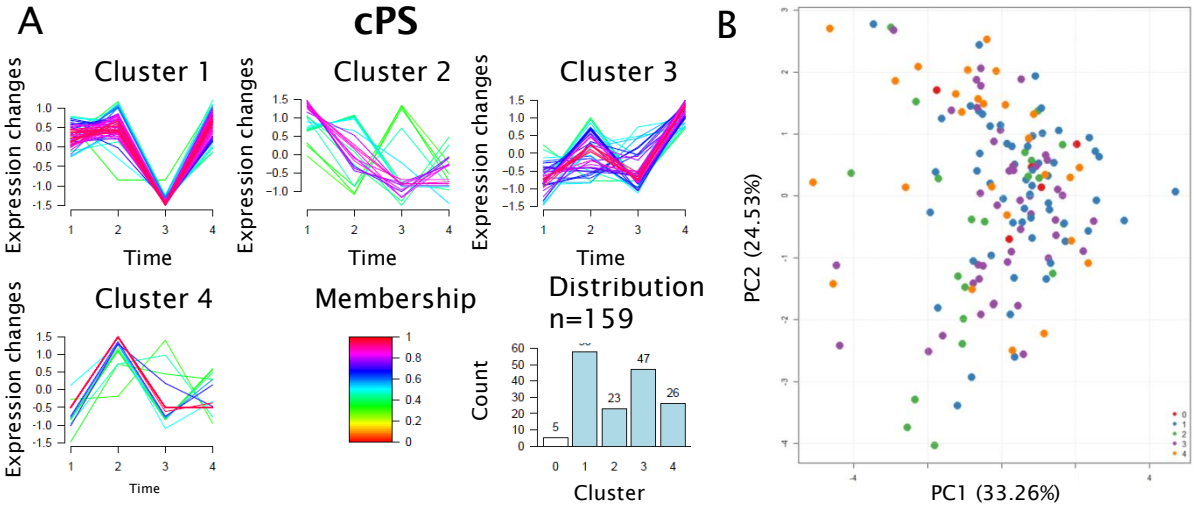

Figure 37: Longitudinal analysis of cPS protein corona. (A) Proteins from cPS particles that changed with a minimum of 2-fold difference were analysed by cluster analysis with 4 groups. The ratio of each protein is determined and normalised by subtracting the mean ratio and dividing by standard deviation. The ratios for each protein are plotted (Cluster 1-4) as well as a key to how well they conform to each cluster. Time on the x-axis is labelled 1-4 and corresponds to 15, 30, 60 and 120 minutes respectively. (B) a PCA analysis was performed against a number of physical characteristics and the proteins' colours based on their cluster – blue (cluster 1), green (cluster 2), purple (cluster 3), orange (cluster 4).

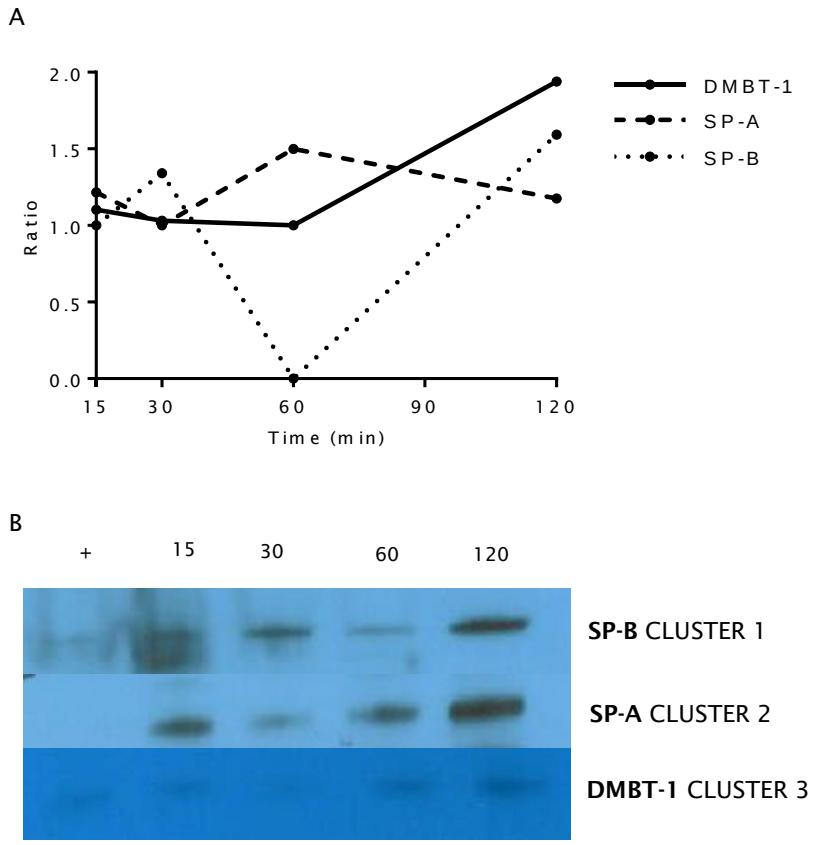

Figure 38: Validation of quantification. The ratios of the amount of DMBT1 (solid line), SP-A (dashed line) and SP-B (dotted line) bound to cPS particles as determined by LC-MS^E Hi-3 quantification were normalised and plotted (A). In an independent experiment, a Western blot was performed on the eluted proteins (B) over the same time points (15 minutes, 30 minutes, 60 minutes and 120 minutes). The cluster to which the proteins were assigned is also indicated (see Figure ??). A positive control of BALF was run in lane 1.

4.4 Discussion

4.4.1 Method Validation

When analysing the protein corona, it is important to verify that only the bound proteins are identified. Five washes were required to remove any unbound material from the NPs (Figure **??**), as is common throughout the literature.[2, 50, 226] This was further supported by saturation assays, as the particles would appear saturated at all concentrations if unbound material was not removed (Figure **??**). The size of the particles, as measured by AFM (Table **??**), differed depending on functionalisation. The increase in size for cPS particles was lower compared to aPS particles which were saturated at a lower concentration. Therefore saturisation is likely a description of particle thickness – with proteins saturating both the surface and protein-protein interactions. We also observed by MS that proteins were sticking to the Eppendorf during washes and, therefore, used low-binding tubes and transferred the pellet to a fresh tube between washes to eliminate this source of contamination.

Zhang *et al.*[62] have compared eluting the proteins by direct tryptic digestion from the particle surface and by eluting with SDS from particles in serum. They found that both methods gave similar results in terms of the number of and identity of the proteins detected. There is an advantage in digesting the proteins from the surface of the particles in that they are prepared for mass spectrometry in a single step. Therefore we initially tried this method in our sample preparation. Unfortunately, our samples were contaminated with PEG – which may have been present as a lubricant or within the plastic packaging of the sterile equipment used during lung washing – and adversely affects peptide detection (Figure **??**).[227] SDS PAGE and in-gel digestion have been used in many studies of NP coronas.[2, 51, 63] We have simplified these methods by only running the proteins into the stacking part of the gel, since the proteins move into the gel electrophoreticly, non-charged molecules, such as PEG, remain at the top. Furthermore, the proteins remain concentrated in the top of the gel, meaning that the total protein can be extracted by processing a small area, reducing time and volume of reagents required.

MS^E has been used to analyse the proteins from serum-incubated particles[63], identifying between 250-300 proteins in the hard corona. We were able to detect between 100-200 unique proteins per sample in the hard-corona of lavage-incubated particles, which may reflect decreased proteomic-diversity of lavage compared to serum. It is interesting that in our studies and in Tenzer *et al.*, the bound proteins were not necessarily the most abundant

proteins present in the incubation media.

To check the variability, proteins common to at least 2 repeats of each particle/time point were plotted in pairs on a scatter diagram and R^2 calculated (Figure **??**, Table **??**). There was strong consistency (positive correlation) between the abundance of these proteins in all samples, with scores exceeding 0.9 in most cases. After 60 minutes of incubation, aPS particles were noticeably more variable in samples used for the time point study (Table **??**, aPS_60) as well as the 60 minute comparison (Table **??**, aPS), although their scores were still strongly correlated and therefore the variation was deemed acceptable. We have reported the mean CV for each analysis (Table **??**), including only the proteins present in all 3 repeats for each particle. The CV's were less than 30% in all cases which is within the limits determined by Silva *et al.*.[186] However, with a small sample size (3 repeats) these values should be taken tentatively and correlation plots (Figure **??**), which account for more many proteins simultaneously, may be better representative in this case.

The bioinformatics presented here carry a number of assumptions. GO-term analysis of the proteins' molecular function was performed by Panther[228] and supposes that all the proteins have been annotated. The Panther GO database is updated biweekly as protein annotations are updated based on the current literature. Therefore, it is possible for results of the analysis to change over time. The physical characteristics of the proteins were reported using the ProtParam[220] tool on the ExPASy portal using the full protein sequence. Therefore, these values may vary from mature forms of the proteins (e.g. with targeting or pre-regions cleaved).

To help minimise agglutination of particles in BALF, a large volume of BALF was used to dilute the NPs in suspension and encourage mono dispersion. This also ensures an excess of protein in relation to NP-binding capacity (Figure **??**).

Mass spectrometry normalisation and protein clustering was validated for three proteins (SP-A, SP-B and DMBT1) by Western blot in an independent experiment (Figure **??**). The BALF used was from the same patient, however from a different pool and was therefore adjusted to match the concentration of the BALF used throughout the MS corona analysis. As it is from the same patient, the ratio of proteins was assumed to be the same. SP-B and DMBT1 were detected in positive controls (BALF) but SP-A was not. However SP-A was detected in the NP elutes, demonstrating an enrichment on the surface of the particle. The intensity of the bands corresponds to the fluctuation of bound protein to the particle surface as determined by mass spectrometry, however SP-B, which was not detected by

LC-MS^E at 60 minute time point, was detected by Western blot although the band is fainter than at any other time point.

4.4.2 Protein Corona

With the exception of cPS particles, there was a small subset of proteins bound uniquely to each particle after 60 minutes incubation (Figure **??**). Relatively few proteins (11%) were detected in all particles and these were present in different abundances. Therefore, each particle could be described in terms of a unique 'finger print'. However, it may be more useful to determine the factors driving the differences between the bound proteins.

Some of the proteins bound were highly abundant in BALF (for example, serum albumin) suggestive of a concentration-dependant mechanism. However, by comparing the most abundant proteins present in each corona with the abundance of proteins in BALF (Figure **??**), it is apparent that this is not the case. Protein low in abundance in BALF (e.g. gelsolin, F5H1A8, Figure **??**) Therefore, there is likely a property of the proteins, related either to its function, physiochemical properties or post translational modification (PTM) that is driving the adhesion to the particle surfaces.

The top twenty proteins bound to each particle are listed in Table **??**. The coronas are made up primarily of 5 proteins – Actin, L-lactate dehydrogenase, SP-A, serum albumin and moesin, accounting for 20-50% of the bound proteins on the different particles – with other proteins present in much lower abundances (Figure **??**). Therefore *in vivo* there may not be any difference in what the cell 'sees', in terms of the corona of particles. This is further reflected by analysing the physiochemical properties of the bound proteins, weighting for abundance, where there is almost no difference between the distributions of hydropathy, pI, aromaticity, Mw and secondary structures between the coronas of the particles (Figure **??**). In comparison to the average properties of protein identified in BALF, there is also little difference for chemical properties (GRAVY, aromatic context Mw), but there are potential differences in predicted secondary structure. In particular, there is a greater proportion of predicted β-sheets in the corona compared to BALF.

There was a slightly greater proportion of proteins with a pI <6 (∼60%) bound to PS particles than of proteins >6 (Figure **??**) in contrast to TiO_2 and BALF where the distribution was approximately 50/50. The pH of BALF was determined to be 6.4 (Section **??**) and therefore proteins with a pI lower than 6 would be expected to become protonated and may carry a net positive charge. As the ZP of all PS particles was negative, this

supports the notion that electrostatic interaction between the proteins and the surface of the particle may be driving their adsorption. Indeed, cPS particles that had the lowest surface charge of the PS particles (Table **??**) had the greatest proportion of proteins with a pI in the range of <5. However, proteins binding to TiO_2 particles, which had the most negative ZP, had a similar pI to proteins in BALF and no such enrichment was obvious for low pI proteins. Furthermore, there was still a high proportion of proteins present on the corona of PS particles that had a pI greater than 6.4. This suggests two things. Firstly, that proteins do not interact significantly with functional groups (as no different was seen betweel aPS and uPS particles). Secondly, that electrostatic interactions only explain a small proportion of protein binding. In an investigation by Arai *et al.*[55], in which proteins were sequentially added to PS NPs and their displacement measured, it was shown that as well as electrostatic interactions, hydrophobicity and stability also contributed. Binding of proteins may also be via protein-protein interactions, thereby circumventing electrostatic interactions with the particle surface. A combination of many factors in a complex proteinascious environment akin to *in vivo* likely leads to highly chaotic interactions at the surface. The protein coronas here were highly similar, suggesting that surface functionality (that doesn't impact sterically) does not affect the overall protein corona.

On the other hand, there are differences in the identification of the proteins adsorbed at lower abundances to the particle surfaces. A pair wise analysis of particles was performed to maximise the identification of factors that may direct protein-particle binding. In some cases, there were not enough proteins uniquely bound to both particles to make a fair comparison. This is particularly evident when comparing TiO_2 and cPS (Figure **??**), where only a single protein was unique to cPS particles. However, there were enough proteins unique to each particle in comparisons between aPS-uPS (Figure **??**), aPS-TiO_2 (Figure **??**) and uPS-TiO_2 (Figure **??**) to be confident in any observed differences. The physiochemical properties of the unique proteins in these corona have very similar distributions and mean values. There was statistically significant differences between TiO_2 and both aPS and uPS in terms of molecular weight and the % of predicted β-sheet structures (Figure **??** and Figure **??**). In both cases, the mean molecular weights of the bound proteins was slightly higher for TiO_2 and there was a slightly lower % of predicted β-sheet. However, the overall distribution of the molecular weights was similar, and the mean values of aPS and uPS may be affected by a single large outlier (cytoplasmic dynein, approx. 500 kDa) that is not present in TiO_2. Therefore this observation may not reflect a biologically significant finding.

The percentage of predicted β-sheet was lower in TiO_2 in comparison with the unique

proteins bound to aPS and uPS. Again, this could be due to skewing in the aPS and uPS unique pool. However, the unique proteins from the TiO_2 corona were distributed around a smaller standard deviation in both comparisons, with much less skewing towards proteins with high % β-sheet content. Fleischer and Payne (2014)[229] investigated the secondary structure of BSA binding to anionic and cationic particles by circular dichroism and reported a decrease in % α-helix structure when binding to cationic particles, which they hypothesised was due to the protein spreading out upon adsorption to the particle surface. Therefore effects of secondary structure may represent a biologically significant result, and warrants further investigation. A relatively large number of proteins were detected bound to the surface of TiO_2 particles (Figure **??**) in comparison to the other particles, which are approximately 7x larger in diameter. The conformation of the adsorbed protein may go some way to explaining this – whereby proteins could be more closely packed on the particle surface due to the exclusion of less dense β-sheet configurations.

To date, many studies have investigated NP-protein interactions in serum, for which comprehensive lists of proteins that adsorb to the NP corona have been published[63, 108, 121, 216, 230] and it may be possible to predict the cellular fate of NPs from this data.[216] However, there remains no analysis or identification of proteins bound to NPs in the context of the lung. This is likely due to the abundant and convenient availability of serum compared to a lung-related bio-fluid, for nanoparticle-protein kinetic studies. Tenzer *et al.*[63] show that there are hundreds of different proteins binding to NPs in serum, in contrast to previous suggestions that the corona is made up of relatively few proteins[62] that stabilise over time due to the exchange of low affinity with high affinity proteins.[113]

Few papers describe, in detail, the corona formed from particles in lung lavage fluid. Kendall *et al.*[163] describe the adherence of amino acids and phospholipid species from lung lavage to airborne particles but do not comment on the quantity or identity of specific proteins.

The identification of relatively few proteins in previous studies (for example Zhang *et al.*[62]) is likely due to serum being a highly complex mixture of proteins and as such, MS identification of proteins is difficult owing to ion suppression from the most abundant proteins (98% of the serum proteome consists of 20 proteins). Recent technological advances in mass spectrometry (such as ion mobility) allow greater coverage of the serum proteome, which means that not just the most abundant proteins are identified, as in the paper by Tenzer *et al.*.

This study has shown that up to 200 proteins bind reproducibly from lavage, which support

the findings by Tenzer *et al.* that the protein corona may be more complex and stable than suggested in the literature. However, quantification of the detected proteins has shown that whilst there is a large number of different proteins bound to the surface, in fact these are of very low abundance and the corona is comprised of a few, but relatively high abundance proteins.

No mediating factor behind the adsorption of protein to the NP surface was established. In all cases the particles were coated in highly similar coronas, suggesting that the interaction of protein was independent of the particle functionalisation. The scale of interaction between proteins and nanoparticles is such that the protein may not necessarily interact with particles' functional groupds directly, but the particle surface as a whole (Figure **??**). The ZP for bare particles is negative in all cases (Table **??**) and therefore the effect of surface charge was probably not assessed in these experiments. Two particle cores were used – TiO_2 and PS – these have very difference chemical properties (although similar surface ZP) which demonstrates the type of particle may not be a mediating factor in the adsorbing corona, rather the surface of the particle very rapidly becomes the same for every particle owing to the adsorbed corona.

4.4.3 Corona Changes over Time

The stability of the corona over time was further investigated. It was observed that after 60 minutes the majority of the corona was comprised of relatively few but highly abundant proteins. The low abundance proteins show greater variability and whether these proteins bind consistently or if their association is random was considered.

The proteins bound at all time points were consistent in their concentration, in contrast to proteins bound to all particles at 60 minutes, which were of variable concentration (Figure **??**). In particular, cPS particles had only five proteins that showed any significant differences between any time points. Clustering analysis identified 4 modalities of protein interaction whereby some proteins generally increased over time, some decreased and some peaked at intermediate time points. This shows that the dynamics of protein interaction is not a 'simple' reflection of the Vroman effect and there is more complex interchange of molecules at the particle surface.

PCA analysis of the physio-chemical properties of the bound proteins did not identify groups of proteins that clustered by their binding modality (Figure **??** and Figure **??**), and again we could observe no effect of protein average chemistry in predicting binding to the

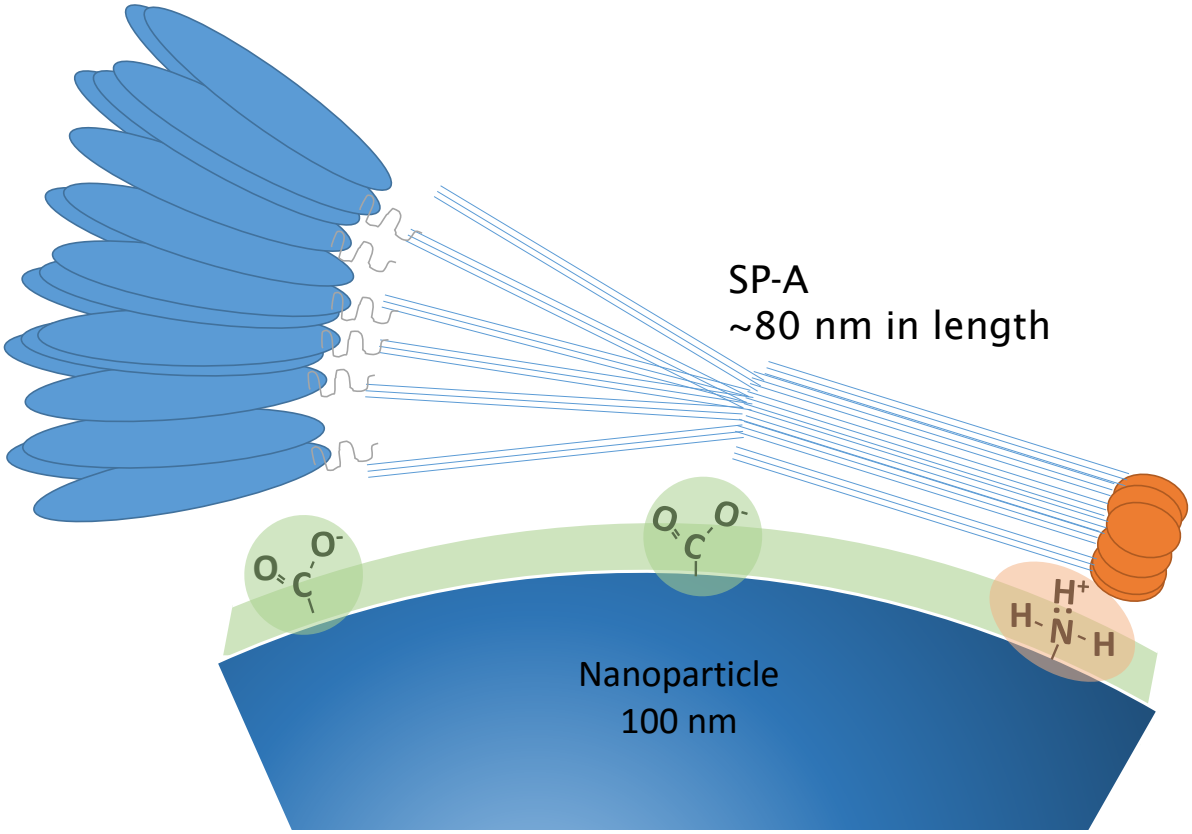

Figure 39: Approximate scale of SP-A in relation to size of the nanoparticle and surface functionalisation.Green shading indicates an area of negative zeta (particle surface), COO- and NH3+ are identified by green or red shaded circles. Scale is approximate. SP-A is depicted here to indicate scale and does not signify binding orientation.

particle. This could be because the properties we have tested are an average across the entire protein and may not reflect the direct characteristics at the point of contact between the protein and the particle. It has been shown that surface hydrophobicity[51], and ZP[231], can effect of the binding of BSA in studies with only a single protein. However this does probably not reflect in vivo interactions where protein-protein, protein-lipid interactions and competition for the particle surface may have a substantial effect.

Given that the corona is predominantly made up of a small number of high abundance-conserved proteins, the surface of the coronas may be come equalised, and the adherence of low abundance proteins may not be dependent on the particle modifications but on the abundant proteins. C. Ruge *et al.*[87] have demonstrated a similar effect. They showed that in solutions containing only SP-A and D, their adherence was dependent on the hydrophobicity of bare particles. However, if the particles were incubated in pulmonary surfactant (lipids), their interactions with SP-D or SP-A was the same – i.e. independent of the particle's intrinsic properties. This is because the surface of the particle becomes the same due to coating by pulmonary surfactant. In our investigation of lipid-binding, we have observed that pulmonary surfactant lipids can bind to all four NPs used throughout this investigation (Chapter **??**). Therefore, binding of proteins may not be strongly influenced by the surface chemistry owing to 1) Lipid binding and 2) Saturation of binding by a small number of proteins (or lipids).

Lundqvist *et al.*[2] show that there is dissimilarity between the corona formed in plasma of 50 nm and 100 nm polystyrene particles, suggesting that size may influence the formation of the corona. Furthermore, they show there were fewer differences between the particles of the same size but with different surface modifications. Whilst we have not investigated the size of the particles in this study, we did observe a large difference in the identity of the bound [low abundance] proteins. I only included quantified proteins within the data set. If it is expanded to include all identified proteins, we can observe more disimilarities between the coronas (data not shown). However, these proteins are probably very low in abundance and therefore will not contribute significantly to the biological identity or fingerprint of the corona.

Physiochemical analysis of the bound proteins showed very little change over time. The proportional composition of each protein corona (Figure **??**) was determined using weighted averages, to account for the abundance of each protein within the corona. Therefore, the most abundant proteins will contribute to the biophysical property the greatest. Given that the most abundant proteins are fairly stable on the corona over time, they will dominate

the physical characteristics of the particles and act to 'average' the surface properties. This is similar to the results presented by Tenzer *et al.*[63], who also observed very little change to the properties of the particles over time and whilst they saw some variation between polystyrene and silica particles, in the main there was very little difference between the properties of each particle.

Over time, the proportion of proteins with a pI <6 was roughly even. This supports that electrostatic interaction may not be a definitive or major contributor to protein adsoption as discussed earlier.

It was observed that in unique proteins bound to TiO_2 compared to aPS, there was a greater enrichment for proteins with receptor activity (Figure **??**). The unique proteins bound the particles were low abundance on the corona and therefore are unlikely to have a physciological effect. However, it would be interesting to determin if this observation correlates with particle uptake.

This data would suggest that the surface modifications of the particle have very little effect on the proteins that bind. However, this may also be due to an enrichment of proteins that have similar physiochemical properties during the lavage collection and preparation. The fluid is collected using saline and therefore may favourably enrich for hydrophilic proteins. Centrifugation may further deplete very hydrophobic proteins since they may form part of lipid complexes and precipitates that are removed during this process. However, as discussed, it is a small pool of proteins that are binding to a high degree and this suggests that there is a high affinity for these proteins and the particles that may also exist *in vivo*.

Clustering analysis identified a number of patterns of binding. There was no cluster of proteins that increased through all time points or *vice-versa* for either aPS or cPS particles. A PCA analysis was performed on the proteins using their biophysical properties which were then coloured depending on which binding modality they conformed to. The analysis did not group the proteins, suggesting that the interaction of the proteins at the surface may not be predicable based only on their biophysical properties, including hydrophobicity. Therefore, the interactions of the proteins at the surface are not explainable simply by the Vroman effect, but there are more complex interactions determining the protein adhesion at the surface, such as competition and protein shape.

The interactions described are a snap shot in time and we can only describe the average properties of each corona. It is not possible, by these methods, to investigate the direct interaction between a protein and the surface of the particle. This may be difficult to

investigate, but a thorough understanding of protein-particle adsorption may be necessary to predict the effect of particles on the level of single proteins – with direct application towards drug design. One possible approach may be to analyse the binding kinetics of single amino acids and short, logically designed peptides by time of flight-secondary-ion mass spectrometry (TOF-SIMS)[163].

4.4.4 Possible Physiological Effects

Bronchoalveolar lavage fluid is a complex mixture of lipids and proteins. Phospholipids are the predominant species of lipid within pulmonary surfactant[137] – the lipid lining at the air-liquid interface that reduces surface tension. The BALF may contain trace amounts of lipids. Whilst this was determined to be below 10 µg/mL by ammonium ferothiocyanate, trace amounts could be detected by MS following lipid extraction (data not shown). Therefore, it is possible that some lipids may bind to the surface of the particles, introducing further competition for the particle surface. However, since the concentration of the lipids in BALF was very low in comparison to the protein (at least 25x), the contribution is likely to be very minor here but could be different *in vivo*. That said, proteins known to interact with pulmonary lipids, such as SP-A, (Table **??**), SP-B and SP-D (Supplementary 1) were found on the particle surface. SP-A and SP-D have been shown to bind to NP in non-complex media[85–88, 106] and that furthermore, their adherence can affect the uptake of NPs by pulmonary macrophage.

The BALF used was taken from patients with PAP, a disease characterised by a reduction in clearance of PSf and consequently is rich in surfactant associated proteins.[157, 158] The presence of SP-A as a dominant protein on the particle surfaces may be as a consequence of its exaggerated abundance in PAP-BALF, in which it is known to be high. However, in the analysis of BALF only, it was only the 50^{th} most concentrated protein detected (Figure **??**, Q8IWL1). Therefore, there may also be significant binding of SP-A in non-PAP BALF, particularly as it is profuse in PSf.

Here we show that the particles may bind surfactant proteins *in vivo*. In particular, SP-A (being the most abundant of the surfactant proteins) was present in high abundance on all particles. SP-A has multiple functions in innate immunity, pulmonary surfactant recycling, and pulmonary surfactant spreading.[147, 232] SP-B, which was also observed to bind to NPs, is a hydrophobic protein that interacts and assists spreading of pulmonary surfactant to maintain low surface tension.[233, 234] Hence, sequestering of these surfactant proteins

could influence the surface lowering properties of surfactant. Furthermore, as discussed in the introduction (Section **??**), airborne NPs have been shown to have a detrimental effect on mortality, particularly amongst people with respiratory diseases[235]. Mice null for SP-A or SP-D have impaired surfactant metabolism and substructures[173, 236] and an impaired innate immune defence against bacterial and viral infections[104, 237]. We have shown previously that that NPs can modulate the ability of SP-A and D to bind influenza virus, and hence sequestering of these proteins could leave individuals more susceptible to infections by micro-organisms.[106] As both SP-A and SP-D have been suggested to have a protective role in asthma[238], sequestration of SP-A or SP-D could compromise the innate immune role of these proteins in the airways and one might hypothesise that this could trigger more severe exacerbations in patients with chronic respiratory diseases, such as asthma or COPD.

The air-liquid interface of the lung is lined by a single molecule-thick layer of PSf. This is predominantly lipid in composition (90%, 10% protein), of which the prevailing species is DPPC[137]. Nanoparticles can, and must, pass through this before reaching the hydrophase beneath.[162, 239] Particles have been shown to bind to lipids from this layer[87, 163, 165] and in doing so, may become saturated in pulmonary surfactant prior to encountering any proteins. The interplay of lipids may change or even mask the surface modification, resulting in a uniform surface for protein binding (as discussed previously; **??**, Ruge *et al.*). Inclusion of this layer is essential for a full description of nanoparticle-interactions with pulmonary fluids.[240] The BALF used throughout these experiments contained trace lipids species that could be identified by mass spectrometry (data not shown), and we observed the binding of proteins known to interact with pulmonary surfactant lipids. Nanoparticles have been shown to affect the functioning of pulmonary surfactant monolayers *in vitro*[115, 241] and *in silico*[162, 242], therefore future work would benefit from including a full description of the lipids binding to NPs.

The toxicity of the NPs on cells is discussed in Chapter **??**. Aminated NPs were toxic to the cells at fairly high levels (compared with atmospheric values) and the presence of a protein corona only slightly abated this. With other particle types an increase in mitochondrial activity was observed and in some cases, particularly cPS and TiO_2, this was dependent on the protein corona. The results described here suggest that the proteins act to average the surface of the particles, tending to make them more similar in terms of their surface characteristics. Therefore the effects observed in the MTT assays may not be due to the proteins on the surface directly, but due to particle agglomeration/aggregation states

and intrinsic surface properties, which may affect particle uptake.[3, 78, 243] The overall charge state on nanoparticle surfaces will be an average of both the protein corona and the intrinsic charge-properties of the particle. Since the protein component is similar between particles, it is the functionalisation of the particle that may be important, not the proteins in determining toxicity and cellular uptake and therefore effects on cellular activity. For example, clathrin-mediated endocytosis has been shown to favour 100 nm cationic particles whereas caveolae-mediated endocytosis favours anionic particles.[243] However, for smaller particles, such as quantum dots, the protein corona may play a larger role in the uptake, perhaps because they account for a greater proportion of the protein-particle characteristic compared to larger particles.[77]

4.4.5 Conclusions and Further Work

The NP corona of two types of particle (TiO_2 and PS) incubated in BALF consist of approximately 100-200 different proteins. Of these, only a small subset bind with high copy number and these proteins are not necessarily the most abundant proteins in BALF. Therefore, there is likely to be a mechanism driving the specific adherence of some proteins over others. This analysis could not identify any physiochemical properties that may drive this adhesion. Protein binding is not affected by surface functionalisation (and may not be affected by particle core – although another type of particle should be included to support this).

SP-A is present in high abundance on the protein coronas of all NPs used in this investigation. SP-B was also detected on all particles, whereas SP-D was bound to aPS and uPS NPs only. These proteins are important anti-inflammatory mediators and SP-A and SP-B are components of functional pulmonary-surfactant. Therefore there is potential for NPs to have a detrimental effect on pulmonary surfactant through sequestration of these proteins to their surface.

The averaging effects of the protein corona discussed implies that the cellular effects observed in Chapter **??** are not due to the proteins bound, but are a consequence of the intrinsic properties of the particle. Therefore it is unlikely that the increase in cellular activity is due to individual proteins on the particle surface, but a response to the NPs. To investigate this, the effects of NPs on protein expression was investigated using a transformed, human type 1 epithelial cell line (Chapter **??**).

The interaction between proteins and the particle surface is such that the protein likely

interacts with a large proportion of the particle surface. Therefore, the protein is interacting with the nanoparticles' average surface. As such, the particle functionalision is probably not an important factor in driving differences in protein adsorbance (Figure **??**). However, upon inhalation, the particles encounter pulmonary surfactant prior to entering a proteinascious environment. The lipids contained within this layer are much smaller, and therefore may interact with surface functionalisations. Therefore it would be interesting to investigate lipid-particle interactions with the same particles (Figure **??**).

5 Lipid Corona

5.1 Introduction

Nanoparticles reaching the lung alveoli will first come into contact with pulmonary surfactant. This is a predominantly lipid monolayer that reduces surface tension to near 0 mN/m when compressed during breathing and is essential for lung function.

Pulmonary surfactant is composed of 90% lipids, predominantly the zwitterionic PC with some anionic PG.[244] Of the PC species, DPPC predominates and this molecule is responsible for achieving the low surface tension.[245] The mechanisms through which pulmonary surfactant can produce stable monolayers at very low surface tension are not well understood, as discussed in Zuo and Possmayer.[142] It is thought that compression of the surfactant during exhalation squeezes out non-DPPC species, leaving a DPPC rich layer that is stable at low surface tensions. PG is required to improve fluidity of pulmonary surfactant and some surfactant-associated proteins, particularly SP-B are required for re-spreading during inhalation.[234]

It has been shown that DPPC can bind to NPs[163] and furthermore, alter the uptake of NPs by macrophages *in vivo*.[86] It has also been shown that PS particles and TiO_2 can affect the ability of surfactant to lower surface tension.[161, 172] Gonzalez *et al.*[165] have shown that anionic surfactant can bind to nanoparticles and that this is via a two-step mechanism whereby the head group mediates initial attraction followed by hydrophobic interaction of the fatty acid tail. However, this was determined by measuring the depletion of PG from solution following incubation and pelleting of NPs and may have overestimated the proportion due to co-pelleting of surfactant with agglomerated particles. Furthermore, the experiments were carried out in a solution of only PG that does not reflect competition with more abundant species *in vivo*.

To date, nobody has identified the proportion of PC or PG that is bound to NP surface. We wish to investigate the interaction between particles and surfactant, in particular the interplay of the two most abundant species, PC and PG with PS particles of different surface chemistry.

We observed no difference in protein-binding to PS particles with different modifications. However, we have observed that bare NPs interact with cell membranes in a haemolysis experiment and that the interaction was different for the particles tested (Figure 15). The interactions between proteins and particles are such that whilst proteins may not interact

with individual surface-functionalisation, lipids might. Therefore, it could be expect to see a greater degree of variation in lipid-particle binding owing to charge-based interactions between lipid head groups and charged surface groups on the particle.

Phospholipids can be identified by MS/MS and quantified against an internal standard. PC and PG are identified through precursor ion scanning of 184 and 153 m/z respectively. Quantification is determined through internally spiking PC and PG species that are not found endogenously.[246]

5.1.1 Aims

1. Isolate human pulmonary surfactant from BALF acquired therapeutically from PAP patients and characterise the lipid composition and surface tension reducing abilities compared to Curosurf^{TM}.
2. Investigate the interaction of aPS, uPS and cPS with pulmonary surfactant, determining the proportion of PC and PG bound to their surface.
3. Assess the effects of the nanoparticles on the function of pulmonary surfactant.

5.2 Methods

5.2.1 Overview

An overview of the experimental procedure is provided in Figure ??.

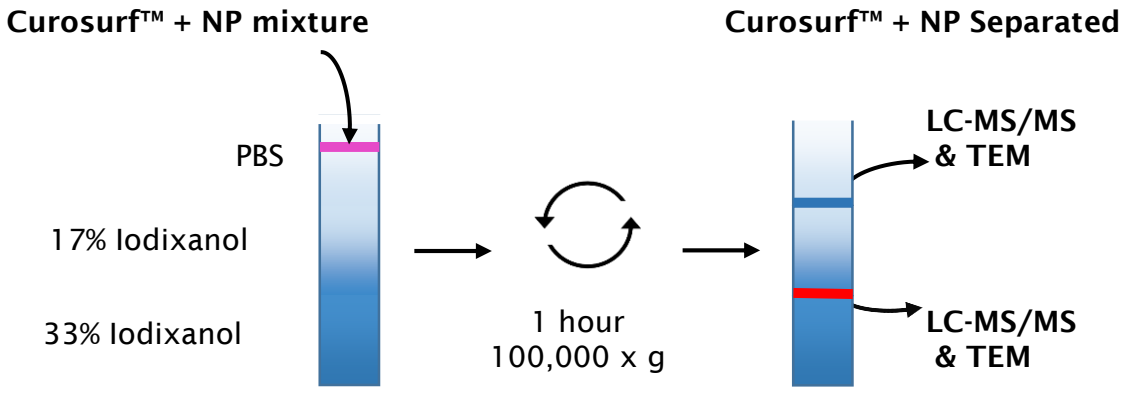

Figure 40: Gradient centrifugation of NP-Curosurf^{TM} mixtures. Curosurf^{TM} is mixed (purple band) with NPs in an equal volume and separated by gradient centrifugation into upper (blue) and lower (red) bands. Bands were then assessed by TEM to observe the localisation of NPs and the lipids determined by MS/MS.

5.2.2 Isolation of Human Pulmonary Surfactant

Pulmonary surfactant was isolated from human BALF acquired therapeutically from PAP patients, by methods adapted from Shelley *et al.*.[247] 285 mL of BALF fluid was centrifuged at 100,000 x g for 1 hour at 4°C in a SW-28 rotor. The pellet was kept and weighed. The pellet was suspended in 0.9% (w/v) NaCl at approximately 44 mg/mL and vortexed for approximately 5 minutes, it was also necessary to incubate in a sonicating water bath for 2 minutes to remove clumps and form an even emulsion. The surfactant was separated by NaBr gradient centrifugation. The gradient was formed by pipetting 1mL of 0.9% NaCl into the bottom of an ultracentrifuge tube. 1 mL of BALF pellet emulsion was carefully pipetted underneath by placing the tip of a narrow glass pipette on the bottom of the tube. 13% NaBr (w/v) solution was prepared in 0.9% NaCl and 3.5 mL was pipetted into the bottom of the centrifuge tube. The gradient was centrifuged at 100,000 x g at 4°C for 1 hour in a SW50.1 rotor with no brake; surfactant forms a band at the interface between NaBr and NaCl. 1 mL was carefully removed at the interface, being careful to remove as little NaBr as possible. The surfactant was washed by mixing with 4.5 mL 0.9% NaCl and centrifuging for 30 minutes at 100,000 x g. The surfactant formed a white pellet at the bottom of the tube. It was necessary to perform multiple runs to isolate all the surfactant from the BALF pellet. The isolated surfactant was pooled, dried at 45°C in a speedyvac (Eppendorf) and weighed.

5.2.3 Gradient Centrifugation of PS Particles and Surfactant

PS-Curosurf^{TM} mixtures were separated by gradient centrifugation. 10 cm^2 of particles was made up to 10 µL with PBS and combined with 10 µL of Curosurf (40 µg/µL final concentration). After mixing by pipette, the solutions were applied to the top of a gradient and centrifuged for 1 hour at 100,000 x g. The gradient was formed using iodixanol (OptiPrep, Sigma) by carefully layering densities in a 5.5 mL Beckman ultracentrifuge tube (Figure **??**), and lying horizontal for 2 hours at 4°C. See (Table **??**). After centrifugation, layers were carefully removed using a syringe. As much of the layer was removed as possible in a volume not exceeding 400 µL. 20 µL was kept for TEM (Section **??**) and the remainder analysed by MS/MS (Section **??**).

Layer	Volume (mL)	Ratio	Density
Upper	2	PBS Only	0.995 g/mL (0%)
Middle	2	Iodixanol:PBS 1:2	1.049 g/mL (17.5%)
Lower	1.5	Iodixanol:PBS 1.2	1.103 g/mL (33%)

Table 11: Iodixanol density gradient.

5.2.4 Gradient Centrifugation of TiO_2 and Surfactant

TiO_2-Curosurf^{TM} mixtures were diluted with 100 µL of 0.9% NaCl (w/v) and transferred to 500 µL Eppendorf tube. 50 µL of 13% NaBr (w/v) in 0.9% NaCl (w/v) was pipetted gently underneath and the sample centrifuged for 15 minutes at 17,000 x g. Unbound Curosurf^{TM} was removed from the top of the tube and the remaining supernatant aspirated. The TiO_2 was pelleted to the bottom and was suspended in 100 µL 0.9% NaCl, transferred to a clean tube and washed by repeating the centrifugation with 13% NaBr. After one wash, 300 µL of butanol-methanol (BUME) mixture (see Section **??**) was added for 5 minutes on ice to dissolve the adsorbed lipids. TiO_2 was removed from the extracted lipids by centrifugation for 15 minutes at 17,000 x g and the sample processed as per section **??**.

5.2.5 Transmission Electron Microscopy

5 µL of particle/Curosurf^{TM} was pipetted onto the surface of a carbon coated copper TEM grid for 30 seconds. Excess liquid was wicked off using filter paper and the grids allowed to dry. Grids were imaged on an FEI Tecnai T12 TEM microscope. Grids are coated to approximately 15 nm of carbon using a Quorum Q150T ES carbon coater (Quorum tehcnologies, Lewes).

5.2.6 Lipid Extraction

Owing to solvent incompatibilities, lipids from samples containing PS particles were extracted using BUME extraction.[248] Bands obtained from gradient centrifugation were adjusted to 375 µL with PBS and added to 1125 µL of BUME (3:1 butanol:methanol), vortexted for 15 seconds and left on ice for 5 minutes. Samples were centrifuged at 17,000 x g for 15 minutes at 4^{o}C and the supernatants transferred to a glass vial. 1125 µL of hexane/ethyl acetate (3:1) was added along with 10 nmol dimyrisitoylphosphatidylcholine (DMPC), 1 nmol 1-heptadecanoly-2-hydroxy-3-phosphocholine (LPC17:0) and 2 nmol

dimyrisitoylphosphatidylglycol (DMPG) and the samples briefly vortexed to mix. Phase separation was performed by adding 1125 µL acidified ddH_2O (1% (v/v) acetic acid) and briefly centrifuging. The upper, organic phase was transferred to a glass vial and dried under N_2(g) at 37^{o}C.

Dried samples were stored at -20^{o}C before analysing by electro-spray ionisation-tandem mass spectrometry (ESI-MS/MS).

5.2.7 Lipidomics

Samples were suspended in 350 µL MS buffer (66% (v/v) methanol, 30% (v/v) dichloromethanol (DCM), 4% (v/v) 300 mM NH_4OH) and 300 µL applied to the mass spectrometer at a flow rate of 8 µL/min for ESI-MS/MS. Mass spectrometry was performed as described[246] using a Xevo Tq (Waters). Briefly, after collision induced dissociation (CID) with argon gas, precursor scans for m/z +184 were used to identify PC and LPC species. PG species were detected from precursor scans of a negative ion of m/z -153, corresponding to PG head group. Data was processed using Masslynx software (Waters) and species quantification and identification performed using an in house algorithm that adjusts for the proportions of ^{13}C. Phospholipid species were expressed as a % of total and quantified based on the internal standards described above.

5.2.8 Total Phospholipid Detection

Lipids were BUME extracted (Section **??**) from samples and dried down to completion under a constant stream of N_2(g) at 37^{o}C . 10 µL of Curosurf^{TM} was also dried to completion in duplicate for a standard curve. The dried extract was suspended in 2 mL DCM and vortexed for approximately 30 seconds. Following this, 0.5 mL of ferric thiocyante solution (0.1M $FeCl_2$, 0.4M NH_4SCN, ddH_2O) was added to each sample and they were vortexed for approximately 1 minute. To separate the organic and inorganic phases, the mixture was centrifuged at 300 x g for 1 minute. The lower band, DCM-phase, will have a red-hue if phospholipids are present. The intensity was measured by absorbance at 488 nm in a glass cuvette. A standard curve was made by diluting Curosurf^{TM} in DCM between 10-100 µg/mL.

5.2.9 Tensiometry

Surface tension was determined using a Dynamic Surface Tensiometer (Biegler Electronic). An 11.5 x 1.17 x 1.2 cm Teflon-coated trough was washed by immersing sequentially in 70% industrial methylated spirits (IMS) and 100% DCM and drying using a clean disposable microscope-lens cleaning cloth. 10 mL of 0.9% NaCl was pipetted into the trough and a flame passed across its surface to remove potential contaminants form the surface. The paddle was cleaned using 70% IMS and the float was heated until it glowed. The machine was assembled (Figure **??**) and the surface tension of saline measured over a single compression/expansion (20%-100%), with the temperature set to 24°C. If the minimum surface tension was approximately 72 mN/m and there was no hysteresis, sample was applied to the surface during the next compression cycle. If saline did not meet this criteria, the trough was dissembled, re-cleaned and the machine re calibrated.

Samples were prepared by combining 2 µL of NPs (approximately 25 cm^2 PS and 2 cm^2 TiO_2) to 2 µL of Curosurf^{TM} and the minimum surface tension recorded over 6 cycles. 2 µL Curosurf^{TM} in 2 µL saline was run as a control.

Between each run, the components were cleaned as described and the machine re-calibrated. Samples were run in triplicate.

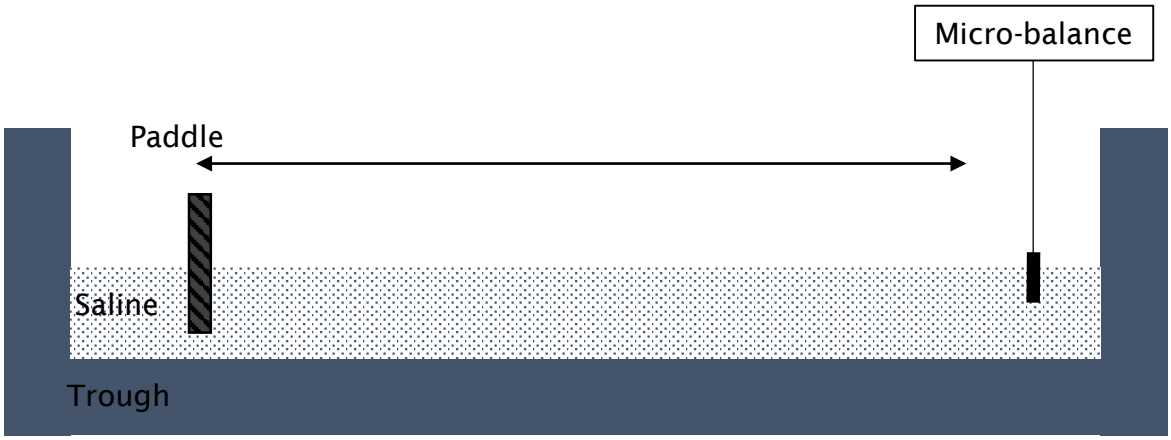

Figure 41: Dynamic surface tensiometer. Saline is pipetted into the bottom of a heated (24°C) trough and a platinum float is dipped approximately 2 mm into the surface. The paddle moved across the surface, completing a single compression and expansion every 3 minutes.

5.3 Results

5.3.1 Human Pulmonary Surfactant

Isolation of PSf was performed based on the methods developed by Shelley *et al.*[247] (Section **??**). From 1.108 g pellet from BALF, 0.74 mg was purified by dry weight. The surfactant was lipid-extracted and the composition of the lipid species was investigated by MS/MS. The percentage composition of PC, LPC and PG was determined using spiked standards and compared with Curosurf^{TM} lipid extracted in the same manner (Blight Dyer, see **??**). There were striking differences in the composition of the two (Figure **??**); notably hPSf had approximately 4 fold less PC compared with Curosurf^{TM} and 8-fold more PG. The relative amount of LPC in each was similar. A further comparison of the composition of PC, normally the most abundant species in PSf, is also given in Figure **??**. DPPC is the most abundant PC present in Curosurf^{TM}, comprising approximately 40% of the total PC, where as in purified hPSf, this was reduced by approximately half (Figure **??**).

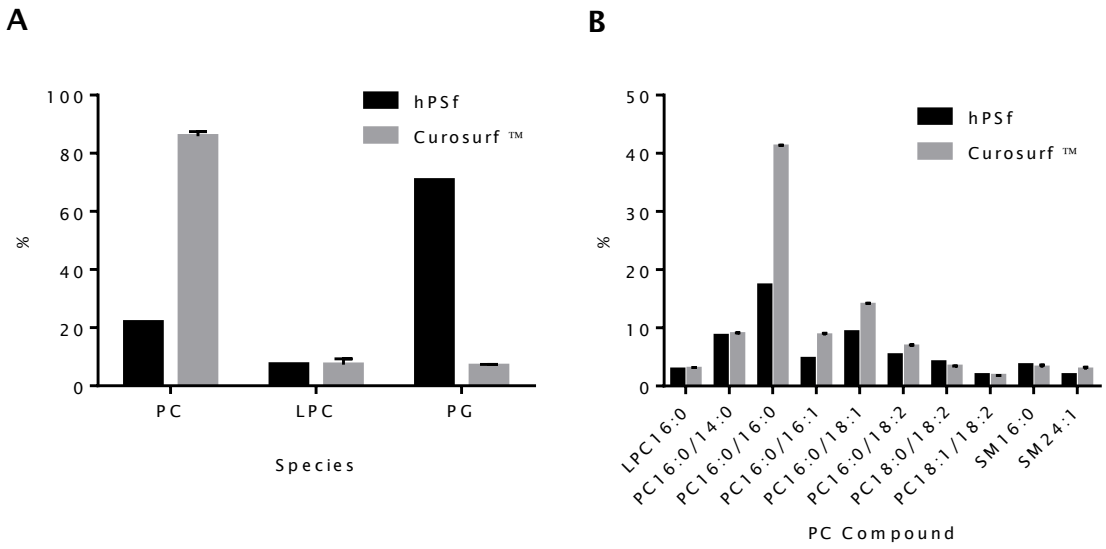

Figure 42: Percentage composition of Curosurf^{TM} and hPSf purified from BALF. Phosphatidylcholine (PC), lysophosphatidylecholine (LCP) and phosphatidylglycerol (PG) were compared (A), showing a reduced amount of PC present in hPSf compared with Curosurf^{TM} and the inverse for PG. The composition of PC were also compared (B). The most abundant compound in both was DPPC (PC 16:0/16:0), however, there was twice as much in Curosurf^{TM} compared with hPSf.

Given the differences in composition, the functional properties of hPSf was assessed by a Langmuir-Wilhelmy balance and compared with Curosurf^{TM}. The hPSf was suspended in saline to the same concentration as Curosurf^{TM} (80 mg/mL) and by eye had a similar consistency (white-cream suspension).

1 µL of Curosurf^{TM} was able to reduce the surface tension from 73 mN/m to almost 0 mN/m, as expected of functioning surfactant. However, the same volume and concentration of isolated hPSf reduced surface tension only to 44 mN/m after 10 cycles (Figure **??**). Since the amount of material recovered from BALF was low combined with its poor functionality and composition, it was decided to use Curosurf^{TM} for the NP interaction experiments.

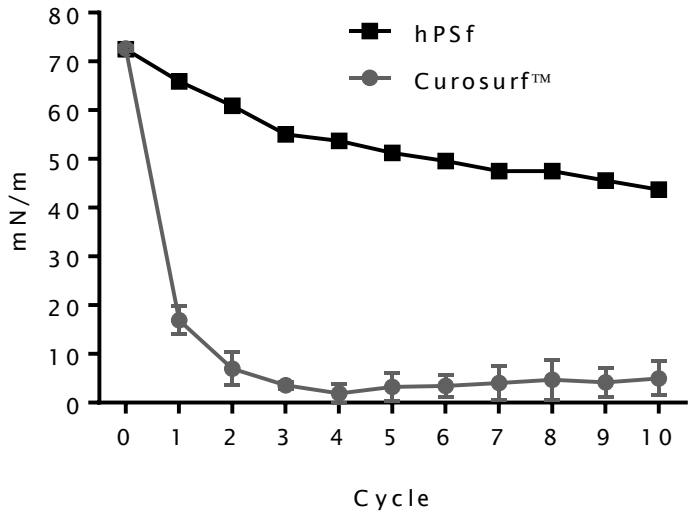

Figure 43: Minimum surface tension of hPSf and Curosurf^{TM}. Purified human pulmonary surfactant (hPSf) and Curosurf^{TM} were compared by their ability to reduce surface tension. Surfactant was applied after an initial baseline reading (cycle 0) before being applied during cycle 1. Curosurf^{TM} reduced surface tension to less than 10 mN/m after 1 complete cycle. After 10 cycles, hPSf had reduced surface tension to appoximatly 45 mN/m. hPSf is n=1, Curosurf^{TM} is mean value of n=3, error bars represent standard deviation.

5.3.2 Interaction of PS with Curosurf^{TM}

Polystyrene particles were mixed with Curosurf^{TM}, and nanoparticle-surfactant complex separated by gradient centrifugation (Figure **??**). After a trial and error approach to establish suitable gradient composition, a non-linear, continuous gradient of iodixanol in saline was found to be provide the greatest separation (Figure **??**).

Interestingly, aPS, cPS and uPS particles have different densities (Figure **??**), such that when mixed together, they can be separated through the gradient. Aminated and unmodified particles had similar densities where as carboxylated had a lower density by comparison. Curosurf^{TM} on its own formed a single white band at a point higher up the tube (lower density) than the particles which formed a blue-white band. When combined with Curosurf^{TM} and applied to the gradient, two bands were observed. Transmission electron microscopy (TEM) (Figure **??**) showed that the white upper band (UB) was depleted of NPs whereas the lower, blue-white band (LB) was particle rich. All particles

changed density after being mixed with Curosurf^{TM}, for aPS and uPS, this was indicated by a shift up the centrifuge tube compared with particles on their own. The density of cPS did not appear to change very much, although the appearance of the band changed from a tight blue-white band to a fuzzier band lacking an obvious blue tint. The density of cPS and Curosurf^{TM} were fairly similar, so one would expect a less dramatic shift in density caused by the interaction of CCurosurf^{TM} with the particles.

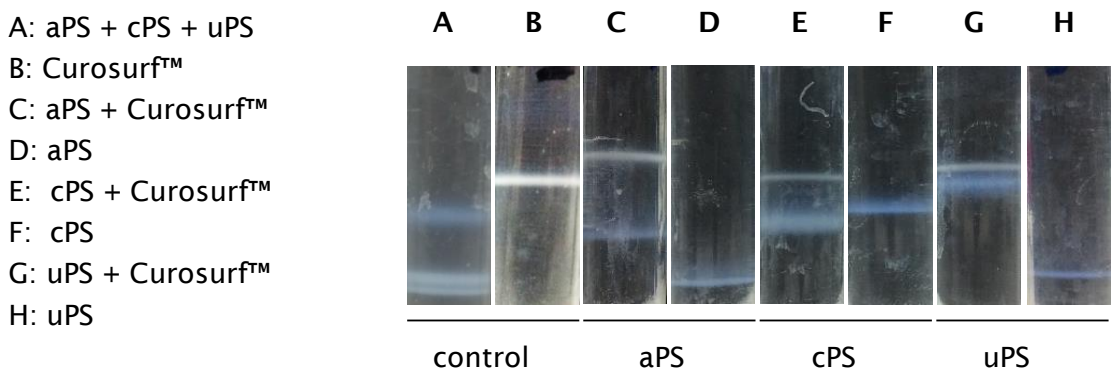

Figure 44: Gradient centrifugation of PS NPs and Curosurf^{TM}. The aPS, cPS and uPS NPs were combined with Curosurf^{TM} (C, E, G) or without (D, F, H) and applied to a non-linear gradient of iodixanol. NPs focused at different densities depending on their modification (A) and all are of a greater density than Curosurf^{TM} (B). After being mixed with Curosurf^{TM}, the particles changed density, suggesting an interaction with the surfactant. Images are representative of n=3, the content of each sample is given in the figure (left).

To investigate what was interacting with the particles, a syringe was used to extract each band and a small aliquot of the recovered material used for TEM (Figure **??**). The remaining material was kept for MS/MS analysis.

After centrifugation, Curosurf^{TM} formed a single band, containing a mixture of vesicle and dense-polygonal structures that were frequently seen agglomerated together (Figure **??**). Within the vesicles, small, round structures could be seen associated with the interior vesicle wall. These could be distinguished from PS NPs as they were smaller and often not very spherical.

The aPS and cPS particles that were passed through the gradient were a mixture of single particles (approximately 100 nm in diameter) and agglomerates (Figure **??**G and H). After mixing, the UB was NP-depleted in comparison with the LB and contained similar structures as seen in Curosurf^{TM} only. The aPS and uPS particles did not appear to be retained within the upper band (Figure **??**A and C) but agglomerations of cPS particles were seen (Figure **??**B). When aPS NPs were mixed with Curosurf^{TM}, the LB contained mainly particles with very few Curosurf^{TM}-like structures (Figure **??**D). The particles were

agglomerated or seen individually with or without a corona. When mixed with either cPS or uPS particles, dense-polymeric structures were present in the LB (Figure ??E and F). These had formed long shell-on-a-string like structures looked to be spatially-distinct from NPs. The uPS particles were seen within vesicles with extensions connecting them to the interior wall (Figure ??F). On the other hand, cPS particles were seen as single particles and not associated with any particular structure (Figure ??E). Images in Figure ?? are representative of 3 independent experiments.

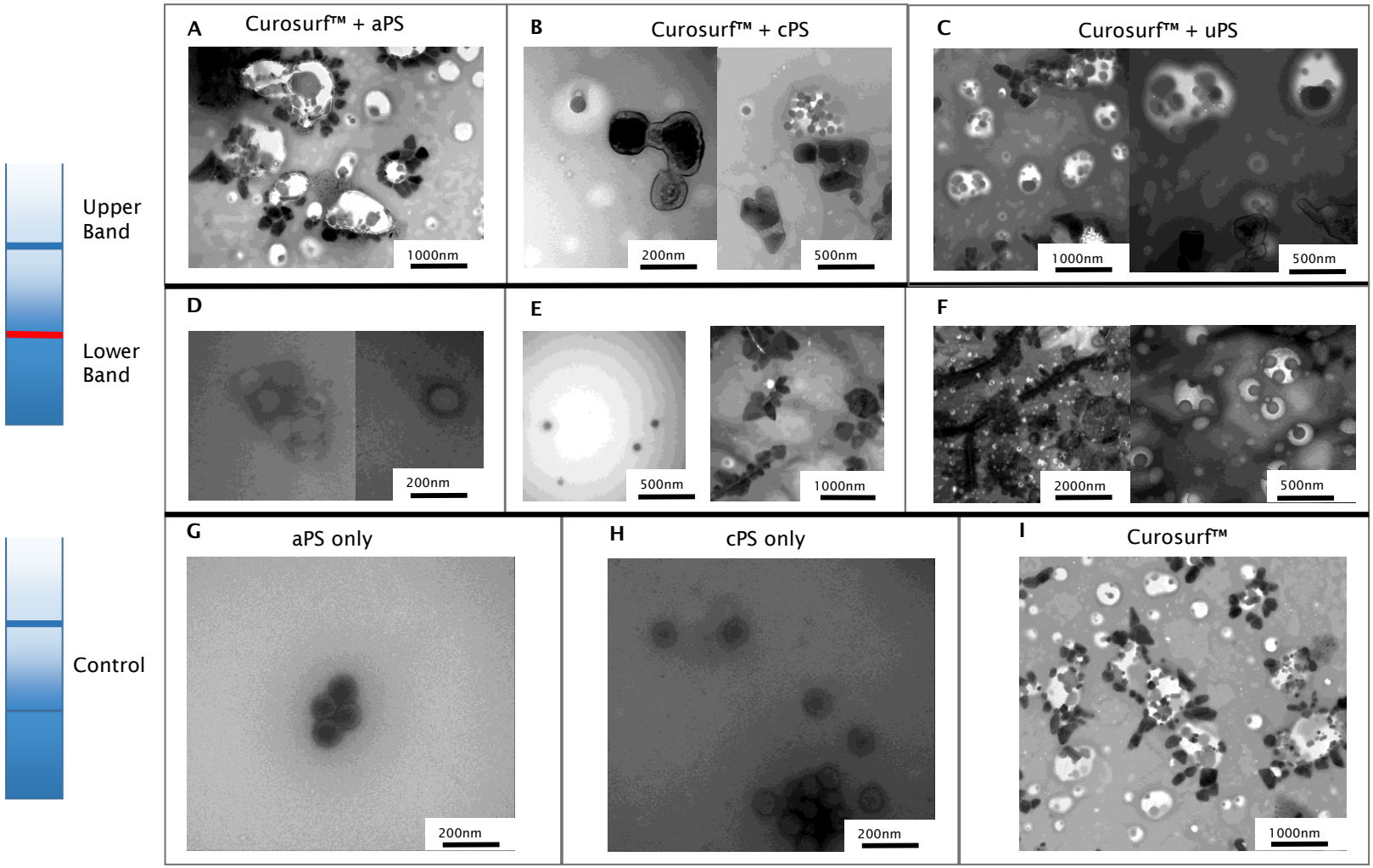
Upper Band
Lower Band
Control
A
Curosurf™ + aPS
1000nm
B
Curosurf™ + cPS
200nm
500nm
C
Curosurf™ + uPS
1000nm
500nm
D
200nm
E
500nm
1000nm
F
2000nm
500nm
G
aPS only
200nm
H
cPS only
200nm
I
Curosurf™
1000nm

Figure 45:

Figure 45: TEM of upper (UB) and lower (LB) bands (A-F) and controls (G-I) from gradient centrifugation of Curosurf^{TM} and PS NPs. The aPS and uPS paticles were only seen in the LB (D and F), whereas cPS were seen in both the upper (B) and lower (E) bands. The upper bands (UB) consisted largely of dense-polygonal structures that tended to agglomerate either to each other or around vesicles. In the LB of Curosurf^{TM} + aPS (D), particles were separated completely away from any Curosurf^{TM}-associated structures and some had a fuzzy coating, possibly a corona, around their surface. In the LB of Curosurf^{TM} + cPS (E), some dense-polygonal structures had co-focused with NPs and were agglomerated along a straight line, like a necklace of shells. These did not appear to be contact-associated with NPs but were only seen in LB of separated Curosurf^{TM}-NP (F) mixtures. Similar structures were seen in the LB of Curosurf^{TM} + uPS (F). uPS NPs had been incorporated into vesicle looked to form connection to vesicle walls. In samples where only NPs were passed through the gradient (G and H), particles were seen as spherical agglomerates with sharp edges. Curosurf^{TM} without particles was a mixture of vesicles and dense-polygonal structures (I). Images are representative of n=3.

5.3.3 MS/MS of Lipid-Nanoparticles

5.3.3.1 Data Overview and Normalization As interactions of NPs with Curosurf^{TM} resulted in structural effects, MS/MS was performed on the isolated UB and LB to identify if any differences in lipid classes. The UB and LBs from three separate experiments and Curosurf^{TM}-only from two independent experiments were analysed by MS/MS. Standards (PC, PG and LPC) were spiked in for quantification and LPG quantification was derived from the PG standard. A quantile-quantile (Q-Q) plot was performed with the residuals from all experiments to assess the normality between groups. The plots conformed well to predicted data, assuming normal distribution (Figure **??**) and therefore parametric tests were used for statistical analysis. The total concentration of PC, PG lyso-PC (LPC) and lyso-PG (LPG) is reported in Figure **??**. As standard deviations were different between groups, statistical analysis was performed using Student's T-Test assuming non-equal variance. There were significant differences between the amount of lipids found in the UB and LB band of the cPS sample (P=0.036) (Table **??**). The amount of lipids detected in the UB and LB of aPS samples were close to, but not significantly different (P=0.064). The amount of lipid isolated from the UB and LBs of uPS samples were not significantly different, however, in all cases, the UB had a higher mean concentration than the lower band.

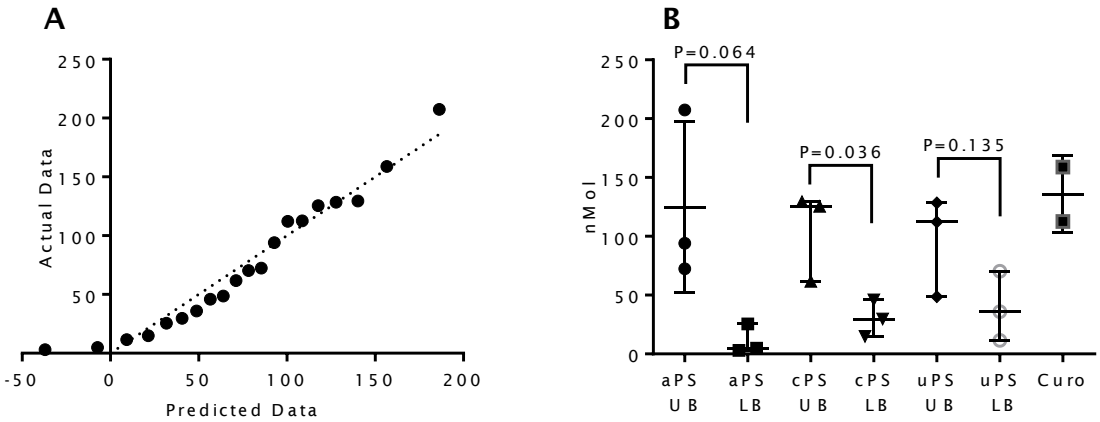

Figure 46: A Q-Q plot was performed with residuals from all experiments to assess normality of data across all groups (A). The data conforms to the line of identity indicating good agreement with Gaussian distribution. Total concentration of PC, PG, LPC and LPG for each group were plotted and differences between UB and LB's compared for each particles type using Student's T-test and not assuming equal variation (B). In all cases, UB contained more lipids, however, there was only statistical difference between cPS UB and LB. Median and IQR are shown by whiskers. All data fell within 1.5xIQR and therefore are not defined as outliers by Tukey's criteria.

Trace amounts of phospholipids were detected (<2% of total lipids) in negative controls (NPs only) which is most likely contamination from lab-ware and therefore constant

NP	UB (nMol)	LB (nMol)	P-Value
aPS	124.6 ± 76.21	11.17 ± 12.66	0.064
cPS	105.6 ± 39.08	30.19 ± 15.47	∗0.036
uPS	96.45 ± 43.54	39.33 ± 30.04	0.135
	aPS LB *vs* cPS LB		0.720
	aPS LB *vs* uPS LB		0.608
	cPS LB *vs* uPS LB		0.800

Table 12: Mean total lipid ± standard deviation for the upper band (UB) and lower band (LB) of each NP. P-values were determined by unpaired Student's T-test without assuming equal variance. ∗ depicts significant value.

between all samples (Figure **??**). Samples were normalised by multiplying the quantification by a scaling factor. The scaling factor for each NP was determined by summing the average total lipid in LB and UB and dividing by the total lipid in Curosurf^{TM} (Equation **??**). Hence the total lipid in each band was determined by multiplying the UB or LB by the scaling factor.

$$Scaling\ Factor = \frac{Mean\ Total\ Lipid\ in\ UB + Mean\ Total\ Lipid\ in\ LB}{Mean\ Total\ Lipid\ in\ Curosurf^{TM}} \quad (2)$$

5.3.3.2 Absolute and Relative Abundance of Phospholipids There was a greater amount of lipid detected in the UB compared with the LB in all cases. In aPS samples, 92% of the lipids were retained in the UB. This proportion was less in cPS and uPS, with 78% and 71% respectively, which is concurrent with the TEM images of the bands (Figure reffig:lipidtem).

The amount of PC, PG, LPC or LPG present in either UB or LB was determined (Figure **??**). There was a large difference between the amount of PC, LPC (P=0.034) and PG (P=0.006) in UB of the aPS samples compared with the LB. LPG was also higher in the UB, however, the difference was reduced compared to the other species. More PC and LPC species were seen in the UB of both cPS and uPS samples compared to the LB. The difference was significant for PC species in both cPS and LPC for cPS (Figure **??**). The difference was reduced for LPG, which was found in the UB of cPS samples, only marginally higher compared with the LB and in the case of uPS, the reverse was seen (Figure **??**).

As different amounts of total lipid was present in each band, the species were analysed by %

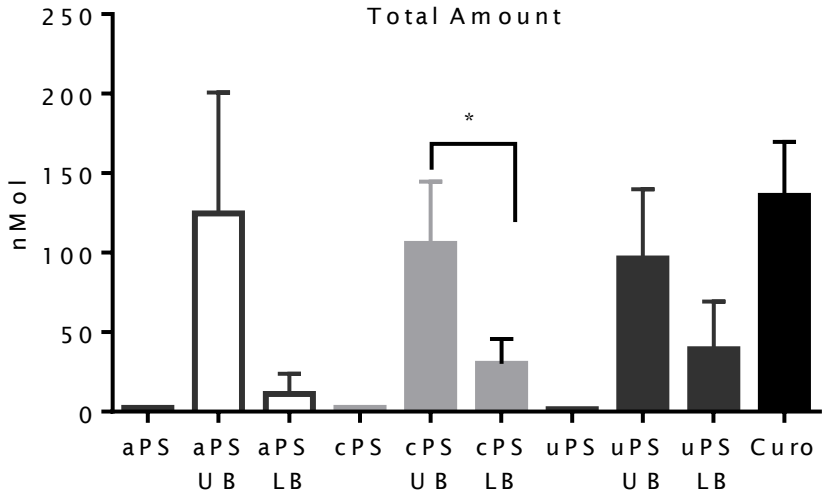

Figure 47: Total quantified lipids present in each sample. There was negligible amounts detected in NPs only (aPS/cPS/uPS). In all cases, there was an increased amount of lipids present in the UB compared with the LB; this was significant in the case of cPS (P=0.036). Curosurf^{TM} (Curo) is displayed for comparison. Values are mean of n=3, error bars represent standard deviation.

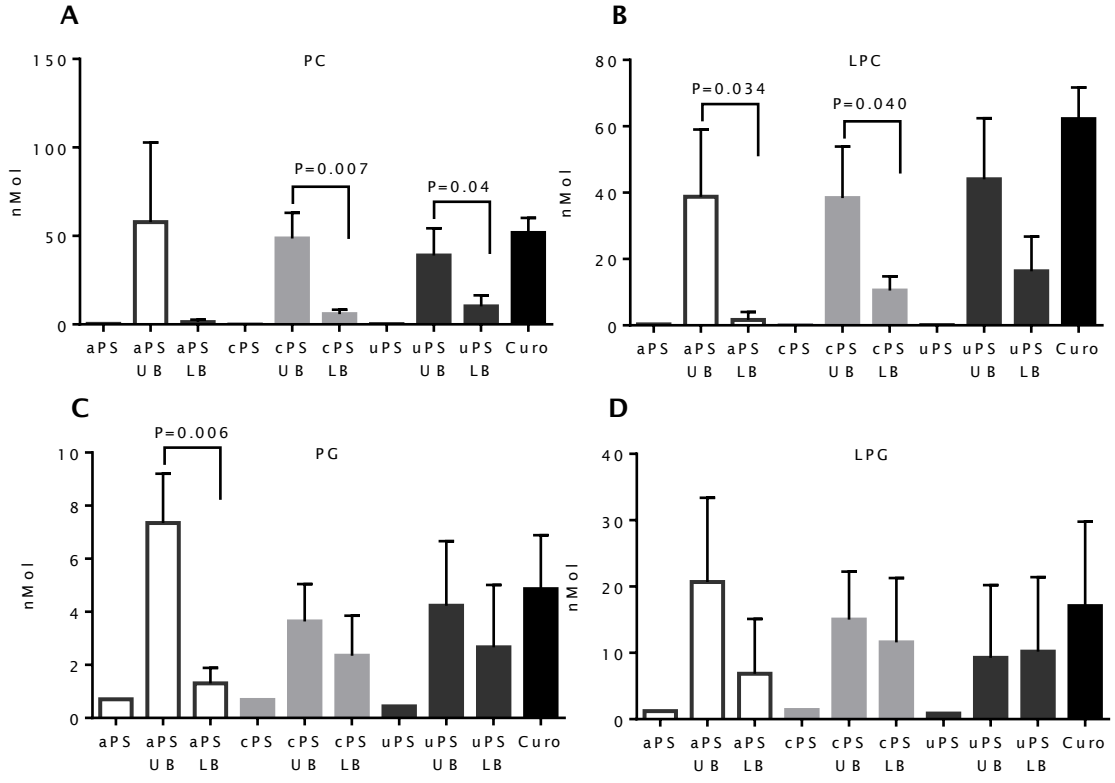

Figure 48: Total amount of PC (A), LPC (B), PG (C) and LPG (D) found in each sample. P-values are given where was P<0.05 and was calculated from Student's T-test assuming non-equal variation. Values are mean of n=3, error bars represent standard deviation.

of total lipid in each sample to investigate if there is enrichment for a specific species or if the differences are simply concentration-dependant (Figure **??**). The proportion of PC

(zwitterion/neutral species) present in the UB was greater than in the lower band in all cases, however this was only significant (P=0.006) for cPS samples (Table **??**). The proportion of PC or LPC in the UB was similar to the proportion determined for Curosurf^{TM} whereas PC was must lower in the LB. The proportion of LPC in the LB and UB was similar in cPS and uPS samples however, there was a difference between UB and LB in aPS although this was not significant. The proportion of PG and LPG (negatively charged species) in the LB was greater than the UB and Curosurf^{TM} in all cases, however, the differences were not significant. Overall, the proportions of each species were LPC>PC>LPG>PG for uPS and Curosurf^{TM}, however, the proportion of LPG was elevated in cPS and more so in aPS such that this was highest by proportion (Figure **??**A).

The ratio of PC:PG (Figure **??**) was significantly greater in Curosurf^{TM} alone compared with the lower band of any of the NP-Curosurf^{TM} samples. Furthermore, cPS and uPS both had a ratio greater than aPS (P=0.031 and P=0.005 respectively).

The proportion of positively charged species in the LB was greater than the UB and this was reversed for neutrally charged species suggesting charge may play a role in lipid-binding. To investigate hydrophobic interactions, the effect of fatty acid chain length was determined. The total number of carbons present in the hydrophobic tails of PC (Figure **??**) and PG (Figure **??**) were summed and the proportion of each compared to Curosurf^{TM}. For example, PC16:0/16:0 (DPPC) would have a total of 36 carbons (Table **??**).

5.3.3.3 Hydorphobic Interactions Adsorption to the particles may be mediated between hydrophobic binding of the fatty acid tails. A paired T-test showed there was no significant difference between the proportions of PC or PG, grouped by chain length, in LB and Curosurf^{TM} for aPS, cPS or uPS (data not shown).The proportions of PC in the LB and Curosurf^{TM} follows a bimodal distribution (Figure **??**), with peaks at 16 and 32 carbons. There are very little phospholipids with 24-28 carbons in their fatty acid (FA) chains bound, except in aPS, where there was significantly more 26-carbon containing species bound (P=0.002, Student's T-Test). In all cases, the group of 16 carbons contributed the largest proportion of species. This group contained LPC with a single FA chain (Table **??**).

There were no statistical differences between any PG species in the LB of any NP samples and Curosurf^{TM} (Figure **??**). In all cases, the largest contributing group was 20 carbons, and this contained only LPG20:3a (Table **??**). There was only 1 PG detected PG12:0/18:2, with the remaining phospholipids being LPG species.

Species	UB (%)	LB (%)	P-Value	
aPS	PC	46.41 ± 36.05	12.14 ± 12.44	0.195
	LPC	31.11 ± 16.25	14.78 ± 21.09	0.348
	PG	5.90 ± 1.50	11.68 ± 5.25	0.14
	LPG	16.59 ± 10.22	61.41 ± 74.03	0.358
cPS	PC	46.00 ± 13.72	19.18 ± 8.16	∗0.044
	LPC	36.34 ± 14.71	34.72 ± 14.19	0.897
	PG	3.45 ± 1.33	7.77 ± 5.00	0.221
	LPG	14.21 ± 6.87	38.33 ± 32.17	0.273
uPS	PC	40.37 ± 15.82	25.91 ± 15.90	0.328
	LPC	45.64 ± 19.09	41.41 ± 26.66	0.834
	PG	4.38 ± 2.53	6.77 ± 5.98	0.559
	LPG	9.60 ± 11.36	25.91 ± 28.58	0.410
Curosurf^{TM}	PC		38.04 ± 6.26	
	LPC		45.81 ± 7.00	
	PG		3.58 ± 1.50	
	LPG		12.57 ± 9.38	

Test	PC (P-Value)	LPC (P-Value)	PG (P-Value)	LPG (P-Value)
aPS LB vs cPS LB	0.459	0.246	0.404	0.646
aPS LB vs uPS LB	0.303	0.246	0.346	0.482
uPS LB vs cPS LB	0.550	0.721	0.834	0.643
aPS UB vs Curosurf^{TM}	0.777	0.333	0.188	0.688
cPS UB vs Curosurf^{TM}	0.512	0.473	0.924	0.833
uPS UB vs Curosurf^{TM}	0.862	0.992	0.719	0.781
aPS LB vs Curosurf^{TM}	0.078	0.15	0.136	0.443
cPS LB vs Curosurf^{TM}	0.072	0.395	0.351	0.37
uPS LB vs Curosurf^{TM}	0.397	0.842	0.532	0.585

Table 13: Mean percentage of lipid species ± standard deviation for the upper band (UB) and lower band (LB) of each NP and Curosurf^{TM}. P-Values for statistical test between LB for each particle and between fractions with Curosurf^{TM}. P-values were determined by unpaired Student's T-test without assuming equal variance. ∗ depicts significant value.

	Sum of Carbons in Fatty Acid Chains	Species
PC	14	LPC14:0
	16	LPC16:1 LPC16:0
	18	LPC18:2 LPC18:1 LPC18:0
	24	PC10:0/14:0
	26	PC14:0/12:0
	28	PC14:0a/16:0
	30	PC10:1a/20:5 PC14:0a/16:0 PC16:0/14:0
	32	PC16:0/6:1 PC16:0/16:0
	34	PC16:0a/18:1 PC16:0/18:2 PC16:0/18:1
	36	PC16:0/20:4 PC18:1/18:2 PC18:0/18:2 PC18:0/18:1
PG	14	LPG14:1a
	16	LPG16:3 LPG16:2 LPG16:0
	18	LPG18:3a LPG18:1
	20	LPG20:3a
	30	PG12:0/18:2

Table 14: Total carbons in fatty acid chains. PC and PG phospholipids, present at >1% of that species, were grouped by total carbons present in their fatty acid chains. LPC and LPG equivalents were also included.

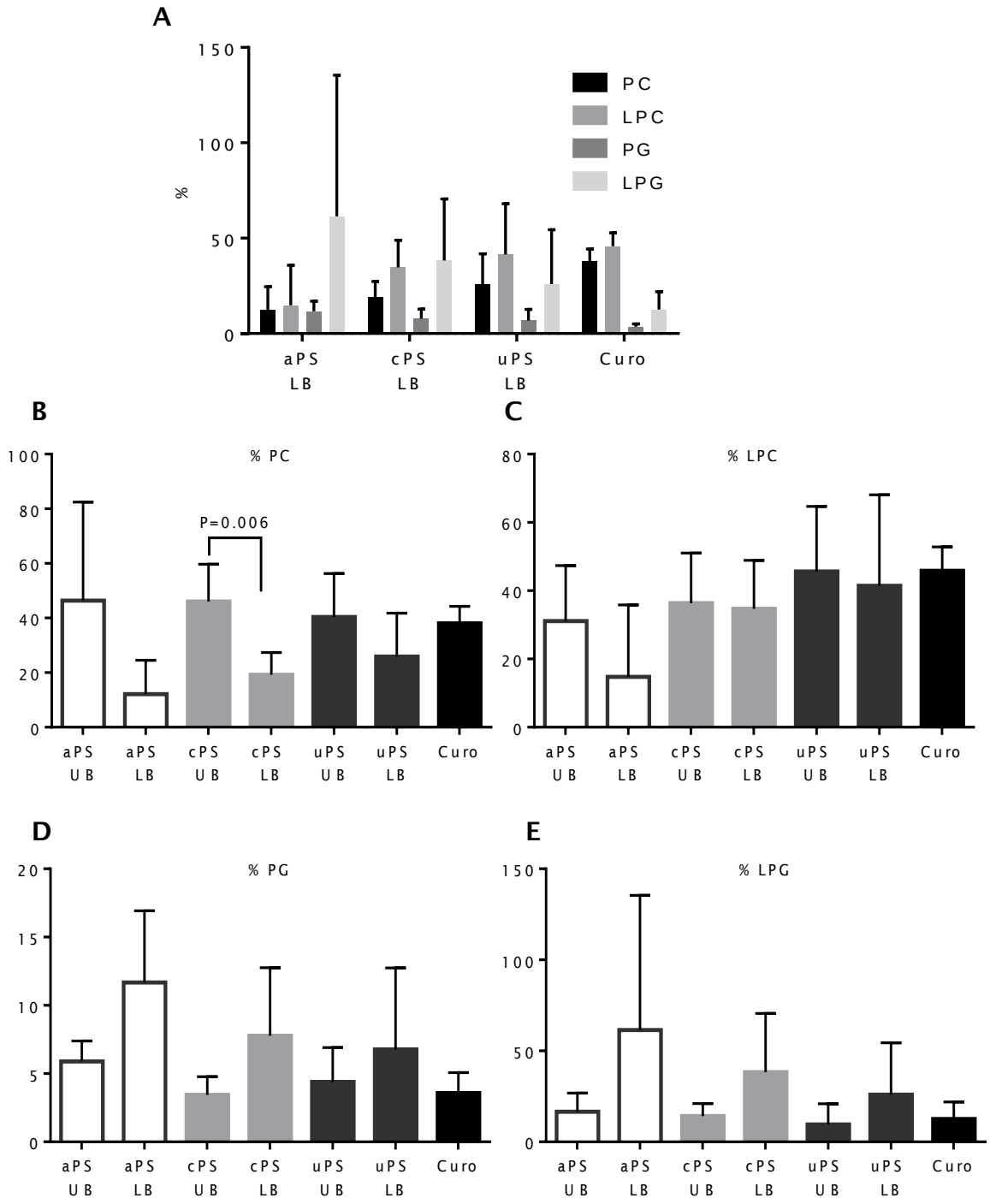

Figure 49: Relative composition of lipids in each sample as a percentage of total quantified lipids. The mean overall pattern of PC, PG, LPC and LPG for the LB fraction of each NP sample (A) and for each lipid species for all samples (B-E) are shown with error bars depicting standard deviation

Grouping the species by saturated or unsaturated fatty acid chains showed that there was no statistical difference between what was in Curosurf^{TM} or bound to the particles. However, whilst the difference is not statistically significant, there was proportionally less saturated PG/LPG bound to the particles compared to Curosurf^{TM} (Figure **??**).

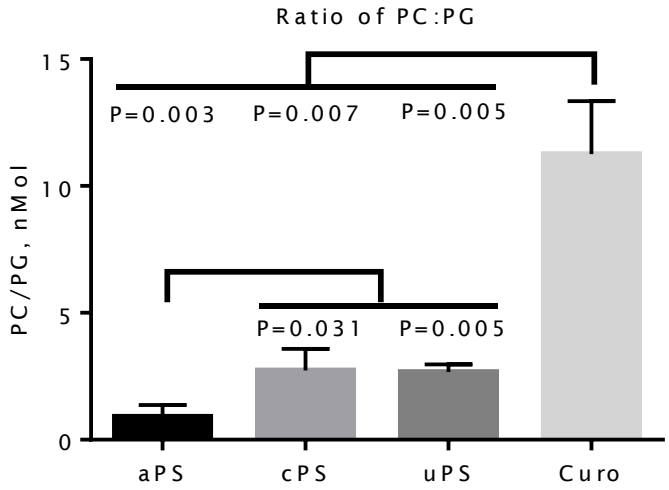

Figure 50: Ratio of PC:PG in the LB of aPS, cPS and uPS. The sum of LPC and PC was divided by the sum of PG and LPG. The smaller the value, the more PG there is in relation to PC. Mean with standard deviation of n=3. Probability was calculated from Student's T-Test.

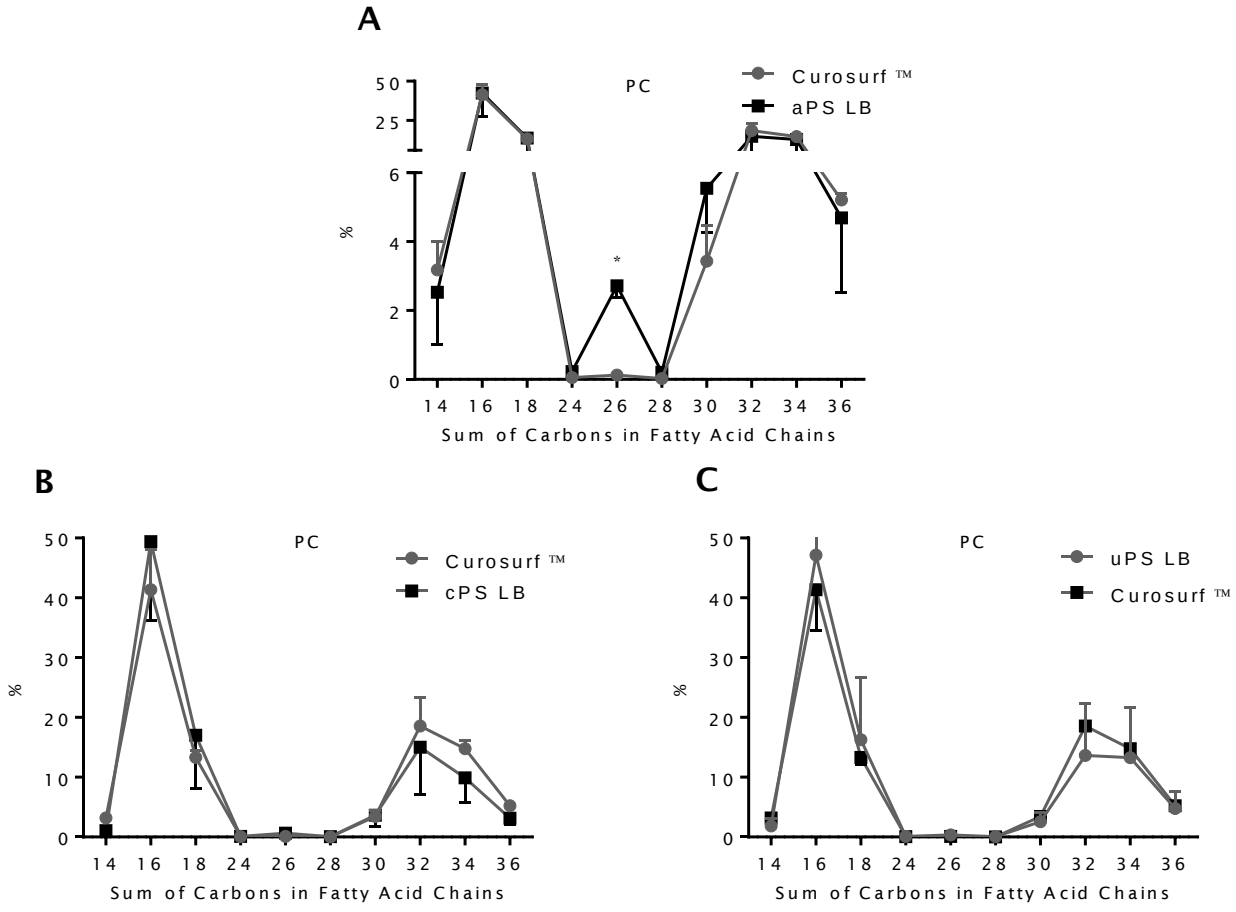

Figure 51: Proportion of PC and LPC, grouped by total number of carbons in their fatty acid chains, present in the LB of aPS (A), cPS (B), uPS (C) and Curosurf^{TM} only samples. The pattern follows a bimodal distribution centering on 26 carbons and peaking at 16 and 32 in all cases. aPS had more 26-carbon species compared to Curosurf^{TM} (P=0.002), which is PC14:0/12:0. The largest group in all cases was 16, which contains LPC16:1 and LPC16:0. Error bars represent standard deviation.

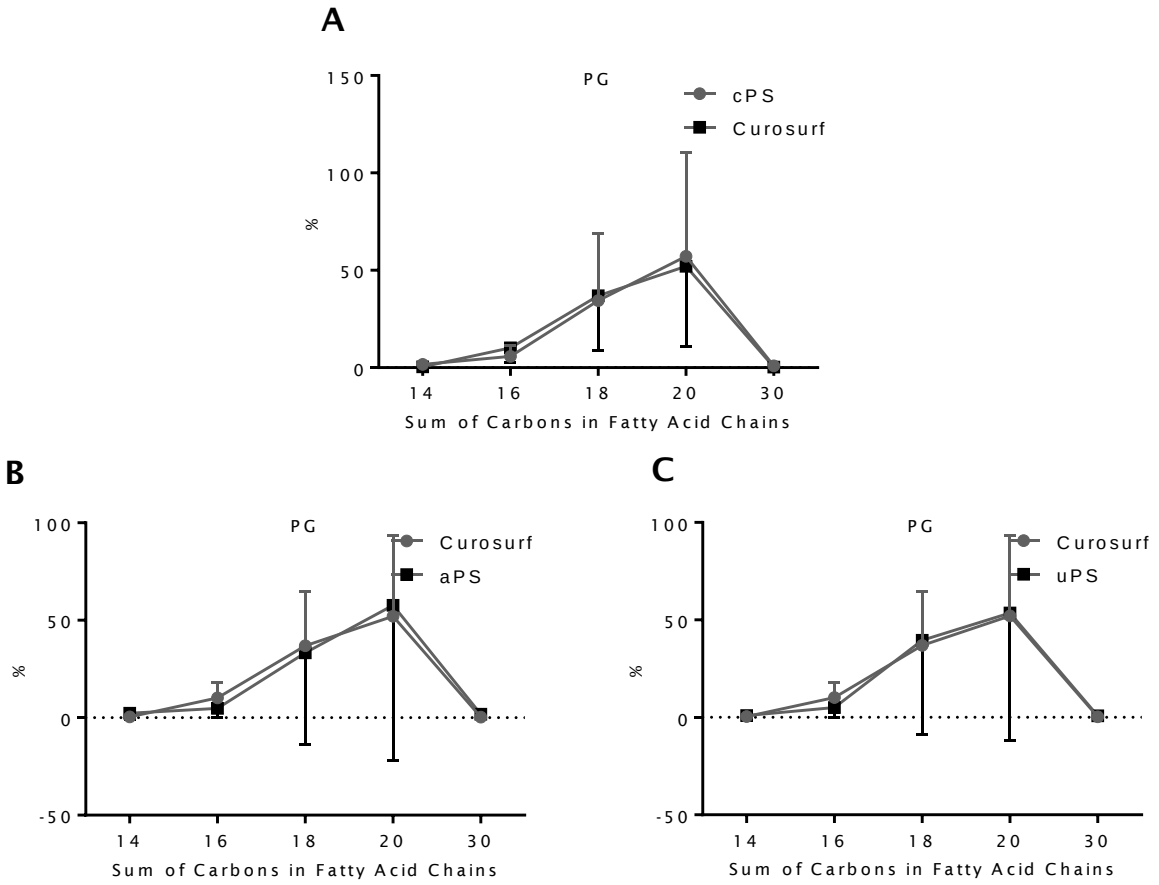

Figure 52: PG and LPG grouped by total number of carbons present in fatty acid chains compaired to Curosurf^{TM} There was no significant differences between aPS (A), cPS (B) or uPS (C) and Curosurf^{TM}. Error bars represent standard deviation.

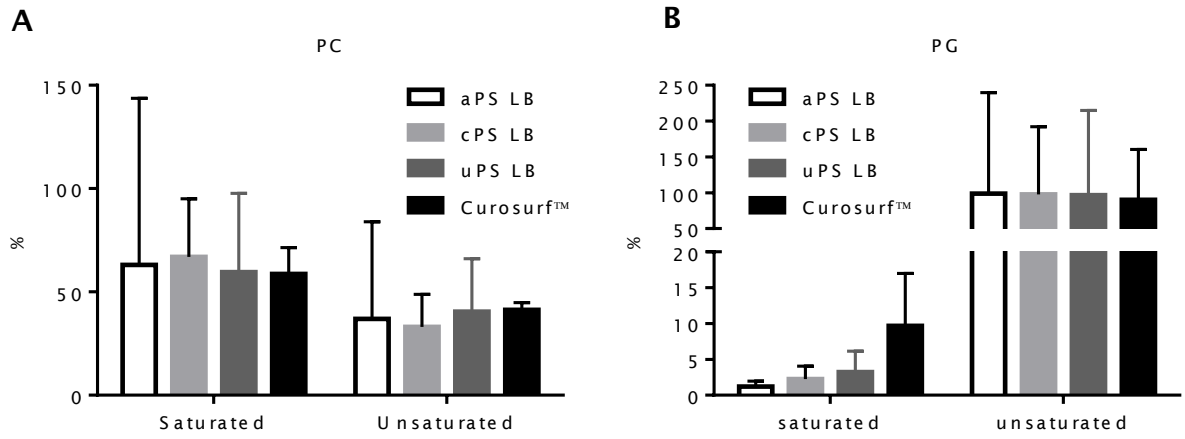

Figure 53: Proportion of saturated and unsaturated phospholipids in the LB. In comparison to Curosurf^{TM}, there was no difference between saturated and unsaturated PC (A). There was less saturated species of PG bound to aPS, cPS and uPS compared with Curosurf^{TM}, however, this was not significant (Student's T-Test) (B).

5.3.4 Nanoparticle Effect on Surfactant Function

Pulmonary surfactant reduces surface tension to near zero. 2 µL of Curosurf^{TM} reduced surface tension to below 10mN/m (3.4 mN/m at cycle 6, (Table **??**) when added to a 13.5 cm^2 saline surface in a Langmuir trough over 6 cycles of 100-20% compression. To test the

Sample	Volume (µL)	Surface Area (cm^2)	Mass (µg)	Surface Tension at cycle 6 (mN/m)	P-Value
Curosurf^{TM}	2	-	160	3.4 ± 2.3	-
aPS	2	27	50	13.4 ± 1.3	∗0.0001
cPS	2	34	50	4.4 ± 3.8	0.069
uPS	2	34	50	5.0 ± 4.3	0.234
TiO_2	2	20	6	11.1 ± 3.0	∗0.007

Table 15: Surface area and mass of particles added to Curosurf^{TM} for surface tension experiments. The minimum surface tension at cycle 6 is given ± standard deviation. P-values are determined by paired T-test of cycles 1-6, ∗ depicts $P<0.05$.

effect of NPs on the function of surfactant, the particles were mixed with equal volumes Curosurf^{TM} (Table **??**) and the mixture added to saline in a Langmuir trough. 6 cycles of compression were measured and the minimum surface tension recorded (Figure **??**).

The minimum surface tension of saline solution was first measured (cycle 0) and was between 72-74 mN/m in all samples. Curosurf^{TM}-NP mixtures were added during cycle 1 and an immediate drop in surface tension was observed that continued for 3 cycles. Paired T-tests were performed using data from cycle 1-6; cPS and uPS did not statistically significantly difference ($P=0.069$, $P=0.234$ respectively).

The aPS particles significantly affected the function of Curosurf^{TM} (Paired T-test, $P<0.0001$). The surface tension was statistically different between cycles 2-6 (Student's T-Test, Figure **??**A), increasing the surface tension from 3.4 to 13.4 mN/m (Table **??**). TiO_2 was also included as it is a common particle found in many household products. TiO_2 reduced the function of Curosurf^{TM} ($P=0.007$) with the surface tension statistically greater at 4 and 6 cycles compared to Curosurf^{TM} only (Figure **??**), increasing to 11.6 mN/m at cycle 6 (Table **??**).

TiO_2 had a significant effect on the function of Curosurf^{TM}. Therefore the proportion of PC and PG was also assessed for TiO_2 (Figure **??**). TiO_2 had significantly more PC and less PG bound to its surface compared with Curosurf^{TM}, $P=0.035$ and 0.002 respectively. The total amount of phospholipid bound to TiO_2 was determined by ferric thiocyante assay to be 9.6 µg.

5.3.5 Lipid Binding at High or Low pH

To investigate further the possible charge-mediated interactions between particles and lipids, MS was performed on lipids bound to TiO_2 from Curosurf^{TM} at a high (pH7.4) or low (1N HCl) pH. There was no significant difference in the proportion of PG bound at

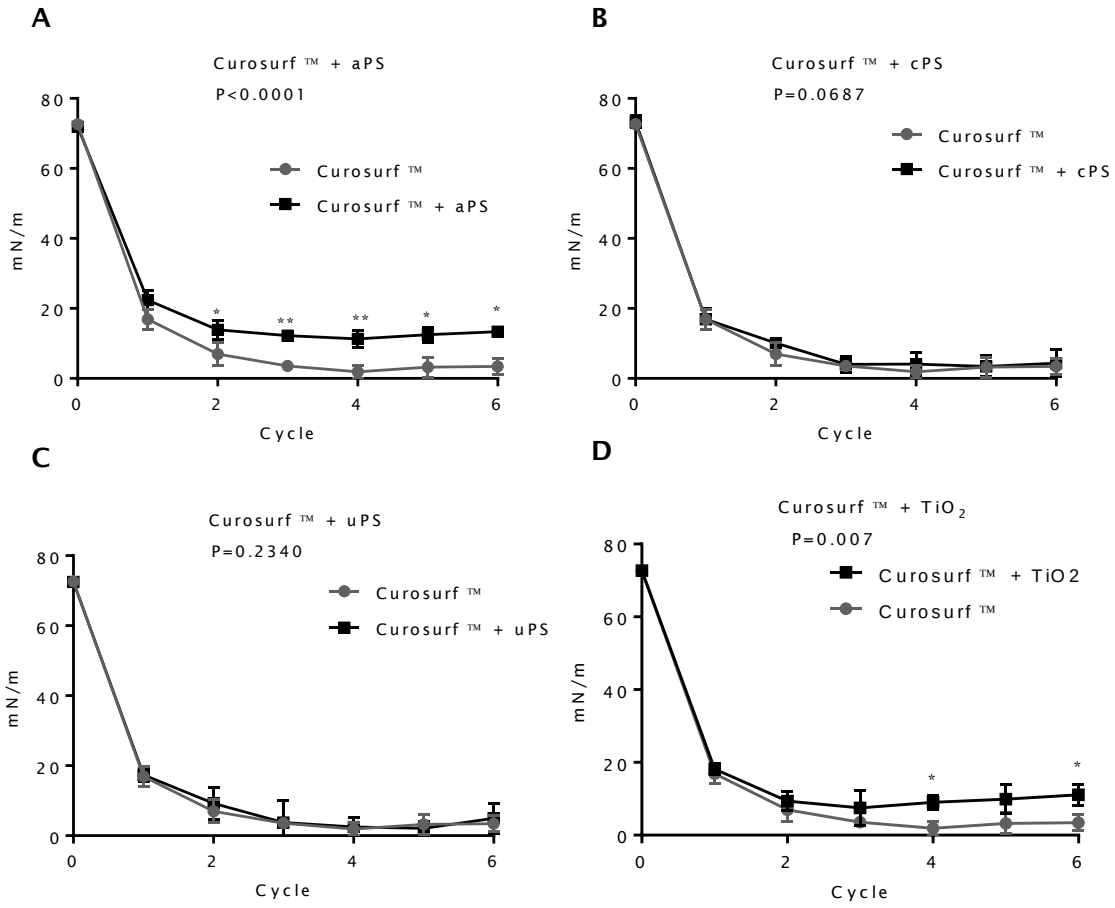

Figure 54: Effects of nanoparticles on surface tension. Surface tension was measured in saline after the addition of Curosurf^{TM} (grey line) or Curosurf^{TM} combined with NPs (black line). Cycle 0 is a baseline measurement, the test solutions were added during cycle 1. There was no effect of cPS NPs (B) or uPS NPs (C) on the function of Curosurf^{TM}. The aPS particles (A) and TiO_2 particles (D) impaired the function of Curosurf^{TM}, with aPS NPs being statistically different after 2 cycles and TiO_2 NPs after 4 cycles. Values are mean of n=3 with error bars representing standard deviation. P-values are calculated from a paired T-test of cycles 1-6. ∗Student's T-test P<0.05, ∗∗Student's T-test P<0.01.

either pH, but there was a significantly more PC detected at high pH compared to low pH. However, a similar pattern was observed in Curosurf^{TM} alone (Figure **??**).

5.4 Discussion

5.4.1 Isolation of Pulmonary Surfactant from PAP BAL

The isolation of surfactant from lung lavage was reported in Shelley (1977).[247] Rabbit lungs were washed with saline and the surfactant extracted by gradient centrifugation. We wished to adapt this methodology to isolate surfactant from BALF taken from human PAP patients. The lavage fluid was too dilute to isolate surfactant directly from the fluid and so the solid-phase (pellet), which contains lipids and lipid-associated proteins[217, 249, 250], was recovered by centrifugation and used.

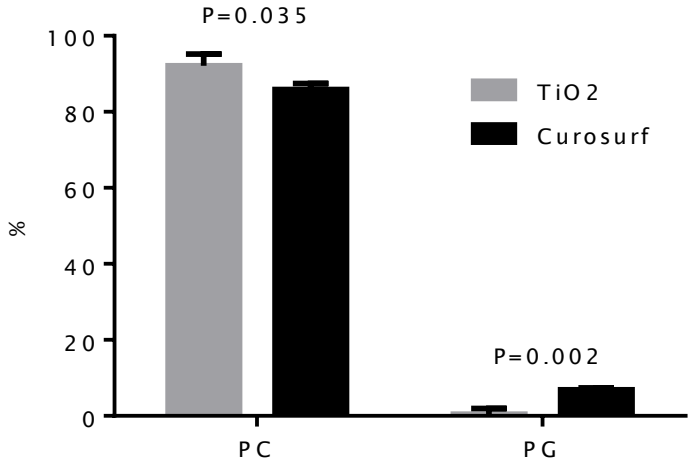

Figure 55: The proportion of PC or PG species bound to TiO_2 following incubation with Curosurf^{TM}. There was proportionally more PC and less PG in TiO_2 compared with Curosurf^{TM}. Bars represent the mean from three independent experiments, error bars show standard deviation. P-values were determined by Student's T-Test.

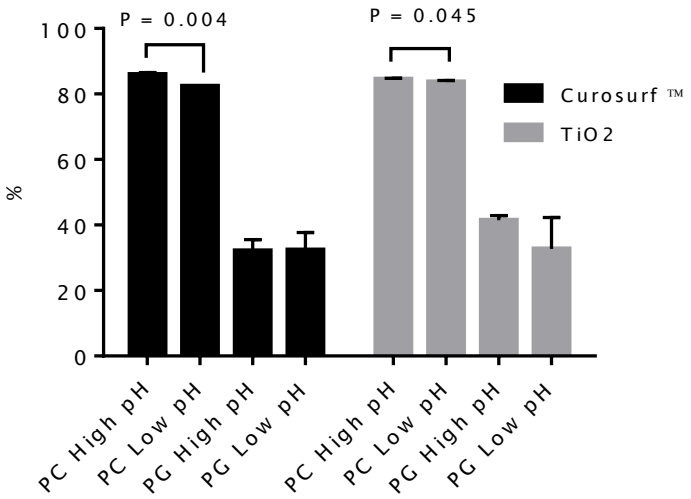

Figure 56: The amount of PC and PG detected as a proportion of total lipid at high (pH7.4) or low (1N HCl) pH inCurosurf^{TM} only (black), or bound to TiO_2 (grey). Mean ± standard deviation, n=3, significant P-Values are shown (T-test).

Typically, the proportions of PC and PG found in hPSf are 8:1 respectively.[244] Analysis of the lipid content of hPSf from PAP-BALF by MS/MS showed that there was approximately 1(PC):3.5(PG). The major PC component within pulmonary surfactant is DPPC (PC16:0/16:0), which normally accounts for approximately 50% of the total PC. Whilst DPPC was the major component of the PC in the PAP-isolated hPSf (Figure **??**), the proportion was reduced to 20%. In native functioning pulmonary surfactant, PC is uniquely able to lower the surface tension to near zero, as required for appropriate lung function.[142, 251] The lack of PC species in the PAP-isolation hPSf therefore may explain its poor functionality (Figure **??**).

It has been documented than acidic phospholipids (PG and phosphatidylinositol) are reduced in PAP patients[252] and tend to contain oleic and stearic acids (18 carbon chain) rather than palmitic acid (16 carbon chain),[253] however PG was more abundant component compared with PC in these samples (Figure **??**). Depletion of PC could have occurred if it remained in the soluble phase during centrifugation, however, this is unlikely given the insolubility of non-polar phospholipids.

5.4.2 Nanoparticle-Curosurf^{TM} Interaction

In developing methods to separate Curosurf^{TM} from NP-Curosurf^{TM}, a number of size exclusion chromatography preparations and gradients were tried (data not shown). It was observed that Iodixanol, which can spontaneously form continuous gradients,[254] was the only substrate able to separate the particles and Curosurf^{TM} completely (Figure **??**). Iodixanol does not react with proteins[255] and did not appear to effect the masses of lipids in any way.

It was interesting to observe that when all three PS particles types were mixed, they positioned differently in the iodixanol gradient with cPS having a lower density than aPS and uPS. There was no agglomeration of the particles observed by DLS that could account for this. Whilst cPS was marginally smaller than the other two particles (Table **??**), the size should not affect the particle density. Iodixanol is used clinically under the trade name 'Visipaque' as a contrast agent for MRI scanning. In few cases, adverse events have been recorded with patients presenting with allergic symptoms and elevated IL-2 and IFNy261–263. It is possible, therefore that there are interaction between iodixanol and organic molecules' surface modifications that could lead to changes in density. However, this seems unlikely as pharmacokinetic studies have shown it to be cleared from the body without modification after intravenous injection.[256] Furthermore as there was no interaction observed with proteins,[255] it is unlikely iodixanol would bind to either carboxyl or amide groups present on the polystyrene particles.

Curosurf^{TM} is a suspension of lipid vesicles and when centrifuged, it did not contain lattice-structures of tubular myelin, nor did we observe concentric rings of packaged myelin. However, it is possible that the dense polymeric bodies (Figure **??**) are densely packaged myelin.138 Another study have observed similar structures in reconstituted surfactant containing predominantly DPPC, PG and two low molecular weight proteins (SP-B-like), which were isolated from pig surfactant, similarly to Curosurf^{TM}.[234] Vesicles observed

may be made of uni-lamella myelin and these tended to be surrounded by dense polymeric bodies.

The density of the particles changed after mixing with Curosurf^{TM}. This suggests that there were interactions between the particles and lipids strong enough to overcome the centrifugal forces. Even in aPS-Curosurf^{TM} samples, where no Curosurf^{TM} structures were visible in the lower NP-rich band (Figure **??**), the density of the particles decreased – approaching the density of Curosurf^{TM}. Some of the aPS particles that were seen appeared to have a coating, suggesting a corona formation (Figure **??**D, right).

There were structural changes present in the Curosurf^{TM} samples that had been incubated with cPS or uPS. The dense particles that were surrounding vesicles were arranged in long strands, which may be vesicles that have 'opened' to arrange themselves into long strands, as myelin may in its functional conformation.138 These long strands of dense-polymeric particles resembled shells on a string and were only present in the particle-rich LB, with the UB unchanged in comparison to Curosurf^{TM}. This supports that the particles are interacting with lipids in Curosurf^{TM}. Schleh *et al.*[172] showed that there is disruption to lamella bodies after the addition of TiO_2 and this also affected the structure of unpackaged lamella bodies after 8 hours of alternating compression/expansion. In the experiments performed here, the particles were mixed with the Curosurf^{TM} for only a few seconds prior to centrifugation, rather than after prolonged compression/expansion cycles as data suggests that the particles very rapidly get pushed through the surfactant monolayer.[162, 166, 167]

It is important to consider SP-B and SP-C, that are essential for the unpacking and correct formation of functional surfactant *in vivo*[233] and are present in small amounts (<1%) in Curosurf^{TM}. Structural changes seen could be due to the binding of the protein to the particle surface as well as direct interactions between the particles and lipids, particularly as SP-B from BALF was observed binding to particles (see Chapter **??** and Supplementary 1). The binding of SP-B and lipids has been investigated in computer models.[162, 242, 257] Guoqing *et al.*,[162] showed there was direct adsorption of SP-B to anionic PS surfaces and indirect – i.e. via lipid interactions - to neutral or cationic particles. We have shown that uPS and cPS, but not aPS affected the structure of Curosurf^{TM}. Since SP-B was only observed binding to aPS and uPS, the adherence of SP-B may not be a critical factor in altering the structure of Curosurf^{TM}.

5.4.3 MS/MS Analysis

The data was assessed for normality with a Q-Q plot by plotting the residuals form all experiments (Figure **??**). The data was normally distributed across all samples. The same MS instrument and acquisition methods were used by Bernhard *et al.*[258] who used parametric test for data analysis. There was no data outside 1.5 x inter-quartile range and we therefore assumed that our data was normally distributed within groups as well. The standard deviation varied between groups (Figure **??**) and therefore T-test were performed without assuming equal variance.

There is an assumption in the normalisation that all of the Curosurf^{TM} is present in the UB and LB and not focused anywhere else. The centrifugation was performed in transparent tubes and there was no other bands or a pellet visible in any of the samples other than those described. Summation of the upper and lower bands was frequently lower than the total amount of lipid included (approximatly 80% of total lipid), which is probably due to lipid-interactions with the size of the centrifugation tubes, variation in extraction of bands following centrifugation and variation in BUME extracted lipids. Therefore normalisation was performed to correct for these variations.

Lyso products were higher in the Curosurf^{TM} used in the NP-Curosurf^{TM} experiments compared with the batch used to compare with isolated hPSf (Figure **??** *versus* Figure **??**). Therefore the same batch of Curosurf^{TM} was used throughout the experiments.

There were less phospholipids detected in the LB of aPS samples compared with uPS and cPS samples. The experiments were carried out at pH 7.4, at which the amine group present on the PS particles are likely uncharged. On the other hand, the carboxyl group present on cPS is most likely to be negatively charged owing to the dissociation of a proton. Unmodified polystyrene particles contain small amounts of sulfyl-esters on their surface, as a bi-product of the manufacturing process, which will confer a slight negative charge. The differences therefore may be explained by charge-interactions between the head groups and the surface of the PS particle. This was supported by the proportion of PG present in each of the LBs in each sample (Figure **??**, Figure **??**). The PG head group has a negative charge compared with PC that is a zwitterion. There was an opposite trend in the proportion of PC present in each band, suggesting competition for PC and PG, which are the two major species present in Curosurf^{TM}.

However, this trend does not hold true when looking at the absolute amounts in each band (Figure **??**). That said, the LB of uPS and cPS both contained large amounts of complexes

that were not observed directly bound to the particles, unlike aPS, where there were no observed Curosurf^{TM} complexes. It was therefore assumed that the lipids present in the LB were in the same proportion as those bound to uPS and cPS particles. The ratio of PC:PG was determined with very little variation between repeats (error bars Figure **??**) suggesting that the proportion of the PC:PG was well preserved between the individual samples and therefore added confidence to this assumption.

Aside from electrostatic attraction between oppositely charged NP and phospholipid head groups, hydrophobic interactions between fatty acid tails and the particle surface could be important. To investigate this, PC/LPC and PG/LPG were grouped by chain length or by having saturated/unsaturated fatty acids, and plotted by % composition alongside Curosurf^{TM}.

There was no difference in chain length compared with Curosurf^{TM} or statistical difference in saturation compared with Curosurf^{TM}. It was interesting that the percentage of saturated PG species found in the LB was less than in Curosurf^{TM} for all particles, such that the LBs for aPS particles had proportionally the least and uPS particles the most. This may reflect differing hydrophobicity of the functional groups.

This suggests that the primary factor mediating the absorption of phospholipids to the particle surface may be head group with a secondary effect determined by the saturation of the fatty acid tail. Conversly, we observed no effect of surface modification with the interactions of NPs and proteins, however, the scale of interaction between lipids and particles surface is such that they may interact with the functional group on the surface of the particle (Figure **??**). As discussed earlier, proteins interact with the surface of the particle as a whole, rather than local moieties on the surface. This explains why the surface chemistry of the particle my affect binding of charged phospholipids via coulombic affinity between the phospho-head group of the lipid and surface modifications on the particle surface.

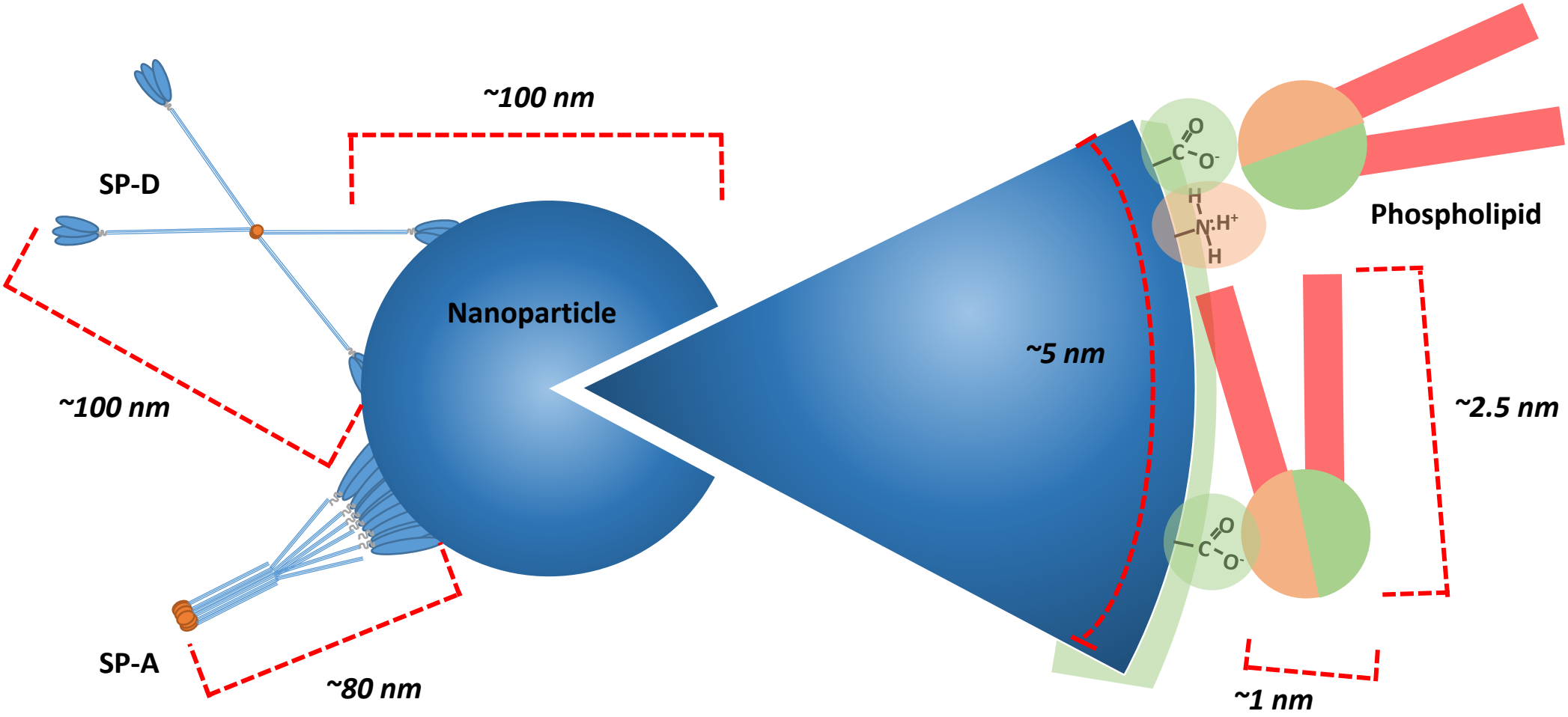

Figure 57: Interactions between proteins and lipid at the paticle surface. Surface charges are indicated on the blown-up segment; green indicates the negative zeta of unmodified surface, orange and green shaded circles represent COO- and NH_3+ respectively. Scale is approximate. SP-A and SP-D are present for scale and are not indicative of binding orientation. However,evidence from agglomeration of particles by SP-A and D suggests interactions may be via their C-type lectin domain as shown.[106]

5.4.4 Tensiometry

Pathogenic effects of NPs binding to surfactant could materialise from reduced function. Surfactant is essential for reducing the surface tension of the wet surface of the lungs during contraction, enabling subsequent expansion during inhalation. Surfactant irregularities have been indicated in a number of lung diseases266 including asthma.[259]

We have shown that aPS particles but not uPS or cPS particles can cause a reduction in the function of Curosurf^{TM} (Figure **??**). The surface tension of rat lung during contraction has been shown to be $\leq$ 9mN/m *in situ.*[260] In our experiments, the surface tension was lowered to less than 5 mN/m at maximum compression with Curosurf^{TM} alone and this was increased to above 10 mN/m following with aPS particles showing a failure of the Curosurf^{TM} to maintain physiological surface tensions.

Harishchandra *et al.*[168] have recently suggested that hydrophobic NPs are pushed out of the surfactant lining, and this is supported by older papers as mentioned earlier (Section **??**). aPS particles may bind to PG, and rapidly be pushed out of the surfactant layer, reducing the ability of surfactant to re-spread and causing a collapse of its structure at high compressions. uPS and cPS particles on the other hand appeared to remain associated with the surfactant (Figure **??**) and may not deplete the surfactant of key components.

Finally, we looked at the effect of TiO_2 particles, which is known to interfere with the structure and function of pulmonary surfactant.[172] We showed that after 6 cycles, the function of pulmonary surfactant was significantly reduced. Analysis of the bound components compared to Curosurf^{TM} showed the reversal of what was seen with aPS particles. There was more PC and less PG bound to its surface in comparison with Curosurf^{TM} and therefore may interfere through a different mechanism.

To investigate charge-mediated binding effects further, an experiment as performing with TiO_2, using high or low pH, to cause the zwitterionic DPPC to form either neutral or positive charges respectively and to cancel out the charge on PG through the addition of a proton. Binding of lipids to TiO_2 at different pH was inconclusive as a similar increase in detected PC at higher pH was observed in controls (Figure **??**). This may be due to charge effects of the lipid species upon entering the mass spectrometer.

The surface area of TiO_2 used in surface tension experiments was approximately 20 cm^2 ($\sim$6 µg) and is likely to be higher than the levels of atmospheric TiO_2 (0.08-0.16 µg/m^3).[261] However, the total particle load within the lung is an accumulation from many

breaths. In a study of asthmatic children in Tel Aviv, the proportion PM2.5s deposited in their lungs was 80% of the total deposited particulates and was a risk factor for eosinophilic inflammation.[196]

5.4.5 Conclusions and Further Work

Particles with different surface modifications bind different proportions of PG suggesting interactions between the particle surface and the phospholipid head group through interactions between opposing charges. The effect of different particle is dependant of surface chemistry with animated particles interacting differently to unmodified or carboxylated polystyrene. Different interactions with Curosurf^{TM} may have physiological effects through the disruption of pulmonary surfactant (Figure **??**).

Further investigation of the effect of lipid charge, using high or low pH was inconclusive. If the effect observed was due to enhanced efficiency of charged species within the mass spec in high-pH samples, then this may be negated through pH'ing prior to BUME extraction.

The effects of particles on surface tension *in vivo* are difficult to assess. Monitoring the surface tension of lung explant tissue, by methods described by Schürch *et al.*[260] in the presence of NP may demonstrate the effect of inhaled particles with greater *in vivo* power.

There is evidence that shows a correlation between increased airborne particulate matter and increased incidences and mortality from respiratory diseases and furthermore, that pulmonary surfactant is altered in severe asthmatics.[259] This data shows that NPs have the capacity to interfere with pulmonary surfactant that may contribute to detrimental effects *in vivo*.

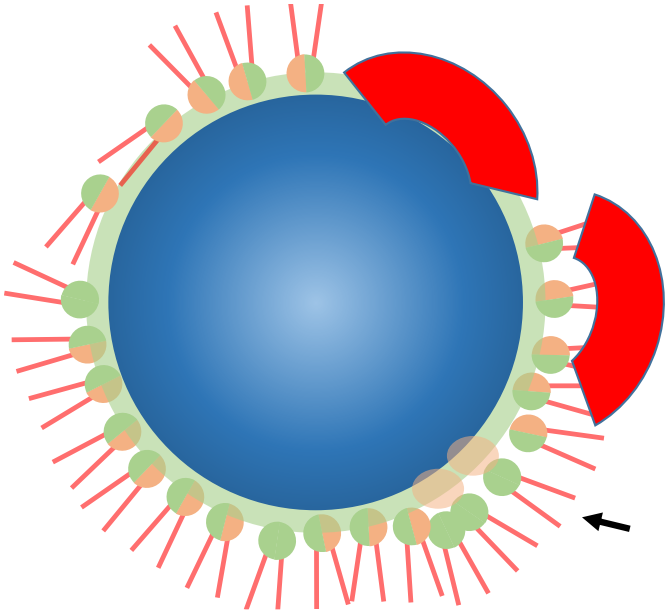

Figure 58: Schematic of surfactant-nanopaticle interaction. Charged lipids bind to the surface of the particle. PG (green-heads, arrow) may be enriched to areas of positive charge on the surface of the particle. PC (green/red heads) also bind in a non-specific manner. Proteins/SP-B (red shape) may bind directly to the particle surface or via lipids. Schematic not to scale.

6 Changes in the Proteome of TT1 Cells in Response to aPS Nanoparticle Exposure

6.1 Introduction

The toxicity of aPS was observed in both A549 and TT1 cells (Section **??**). Mechanisms for toxicity of these particles has been discussed elsewhere, and is likely to involve the induction of apoptosis following lysosomal bursting. At sub toxic levels of aPS and low concentrations of other particles, they still have an effect on the cells, as can be seen by increased mitochondrial activity. No increase of ROS was observed in THP-1 cells or increases in IL-8, IL-6 or TNFR1 mRNA in A549 cells; therefore the driver behind increased mitochondrial mechanisms are unknown.

The epithelial surface area within the alveolus is predominantly AEI cells, which have a morphology adapted to gas exchange. Therefore, these cells are most likely to come into contact with inhaled particles that are not phagocytosed by resident macrophages. Using a transformed type I (TT1) cell line, resembling *in vivo* AEI cells, it has been shown that particles were internalised by these cells,[93, 94] either through endocytic mechanisms or by 'punching holes' into the cellular membrane. The effect of particle internalisation on the level of the whole-cell proteome has not been analysed and may yield information regarding the cellular effects of particle exposure.

With high resolution mass spectrometry it is possible to measure thousands of cellular proteins in a quantitative manner.[262, 263] Through bioinformatic analysis it is possible to identify putative pathways that have altered activity in treatments versus control samples.[264] In this chapter, the proteome of the TT1 cells are analysed following exposure to sub-toxic concentrations of BALF-coated or uncoated aPS particles.

6.2 Methods

6.2.1 Cell Culture and Treatment with Nanoparticles

TT1 cells were cultured as described in Section **??** in T75 flasks and maintained at sub-confluence. Cells were treated with trypsin to dissociate them from the surface of the flask, and a small aliquot was used quantify cell number and viability. Only cultures with at least 95% viability were used, and 6.35 x 10^5 cells were seeded into T25 flasks and allowed to adhere for 24 hours.

BALF-coated aPS particles were prepared as described in **??**, by incubating in BALF for 1 hour. After washing the cells once with 5 mL of PBS, 5 mL of BALF coated, or uncoated aPS particles was applied at a concentration of 1 cm^2/mL for 24 hours in serum free (SF) DCCM1 and 1% BALF. Cells were left at 37°C, 5% CO_2.

After 24 hours excess media was removed from the cells, and they were washed with 5 mL PBS. 1 mL of trypsin was applied to dissociate the cells which was neutralised with 5mL of 10% fetal calf serum (FCS). The cells were transferred to a 5 mL centrifuge tube and washed three times with 1mL PBS, centrifuging for 5 minutes at 300 x g between washes and transferring the pellets to fresh LoBind Eppendorf tubes between each wash. Pellets were frozen at -80°C for a maximum of 2 weeks.

6.2.2 Cell Lysis, Protein Extraction, Reduction, Alklyation and Digestion

Pellets were lysed by suspending in 300 µL of lysis buffer (0.1 % SDS (w/v), 0.1 M triethyl amminum bicarbonate (TEAB), ddH_2O) and sonicating on ice for 6 x 25 second busts with 1 minute cool-down in between. Following centrifugation for 20 minutes at 13,250 x g on a bench top microcentrifuge (4°C), protein concentration was determined using Direct Detect (Merk Millipore), blanked against lysis buffer.

100 µg protein was transferred to a fresh Eppendorf tube and extracted by chloroform/methanol precipitation.[265] The volume of each sample was adjusted to 100 µL with ddH_2O, after which the following solutions were added sequentially vortexing for 2 seconds between each addition: 400 µL methanol, 100 µL chloroform and 300 µL ddH_2O. Proteins were focused at the aqueous/organic interface by centrifuging for 1 minute at 13,250 x g. The top phase was partially removed, being careful not to disturb the focussed protein, and 400 µL of methanol added. Proteins were pelleted by centrifuging for 2 minutes at 13,250 x g and as much methanol was removed as possible before being air dried in a laminar flow cabinet.

The protein was dissolved in 100 µL 6M urea 100 mM AmBic and reduced by incubating with 1mM dithiothreitol (DTT) for 20 minutes at 40°C. Free cysteine-thiols were alkylated with 5.5 mM iodoacetic acid for 20 minutes in the dark at room temperature. Prior to digestion, the samples were diluted with 4 x volume of 100 mM AmBic to dilute the urea to 1.5M. Porcine sequencing-grade modified trypsin was added at a ratio of 1:50 trypsin:protein and left over night at 37°C.

6.2.3 Off-Gel Fractionation of Peptides

Each sample was spiked with 150 fmol of enolase for quantification and the volume adjusted to 360 µL. Off-gel isoelectric focusing (IEF) was performed according to the manufacture's instructions (3100 OFFGEL Fractionator, Agilent) with 13 cm 12 well Immobiline Dry Strips pH 3-10 until there was not further movement of ions. The resulting 12 fractions were transferred to a 96 well plate and desalted (Empore C18 High Performance Extraction Disk Plate, 3M). The C18 cartridges were wetted with 100 µL methanol followed by 50 µL of methanol and then hydrated by passing through 200 µL 80% acetonitrile + 0.5% acetic acid at 100 x g for 2 minutes. After equilibrating with 200 µL 0.5% acetic acid and centrifuging, acidified samples were added (acidified with trifluroacetic acid until pH ¡ 3) and centrifuged through the plate at 250 x g for 1 minutes. Two washes were performed with 250 µL 0.5% acetic acid and peptides were eluted with 150 µL of 80% acetonitrile + 0.5% acetic acid by centrifuging at 100 x g for 2 minutes. If all the elution buffer had not passed through, the speed was increased to 250 x g and repeated as necessary.

De-salted samples were transferred to a v-well 96 plate, dried to completion at 35°Cand stored in the fridge until ready for LC-MS^{E}.

6.2.4 LC-MS^{E}

Samples were reconstituted in 4 µL buffer A (ddH_2O + 0.1% trifluoroacetic acid) by vortexing for 10 minutes and centrifuging at full speed (13,250 x g) for 10 minutes. Samples were transferred to glass vials and fractions 2 & 3 and 9 & 10 were pooled, resulting in 10 fractions per sample. LC-MS^{E} was performed as described previously (Section **??**) using 90 minute gradients and injecting all the sample. A blank sample was run between every 3 fractions or 2 blanks and a standard (Enolase) was run between every 10 fractions (1 sample).

6.2.5 Bioinformatics

Merging of files, database searching and Hi3 quantification was performed using PLGS 3.0. Since enolase was not detected in most samples, protein abundance was not normalised to an internal standard. Proteins were normalised using the total Top3Sum for proteins present in 88% of the samples.

Normalised data was imported into R 3.2.1 for further data manipulation and determination

of fold-changes. Only proteins that were identified in at least two samples were carried forward for further analysis. Prior to performing T-tests, the data was log10 transformed to produce a normal distribution. Volcano plots were generated with the ggplot2 package.

Network analysis was performed using the $STRING_{10}$[266] with protein-protein interactions only displayed with a STRING-score greater than 0.4. Protein-protein interactions were exported to Cytoscape and analysed with the Biological Networks Gene Ontology (BiNGO) tool [267] by hypergeometric testing, false discovery rate (FDR) correction and a 0.05 significance cut-off to generate maps of GO-terms related to the data.

GO-Slim over representation analysis was performed using Panther.[268]

6.3 Results

6.3.1 Cell Culture

Preliminary experiments showed that 6.35 x 10^5 cells were sufficient to procure enough protein for analysis, yielding 0.48 mg of protein. Cell viability was determined to be above 95% in all culture prior to exposure to NPs. The amount of protein yielded from each culture used for LC-MS^E analysis is given in Figure **??**. There was significantly more protein yielded from cells incubated with 1% lavage only compared with exposure to 1% lavage and either uncoated aPS or coated aPS particles (P=0.046, P=0.017 respectively) (Figure **??**), or pooled control samples (control + lavage) and NP-treated samples (uncoated + coated) (P=0.019) (data not shown). There was no statistical difference between the number of cells or cell viability after treatment.

6.3.2 LC-MS^E

Samples were fractionated by IEF into 12 fractions along a gradient of pH 3-10. It has been observed within the lab that fractions 2-3 and 9-10 typically contain fewer peptides and therefore these samples were pooled.

During LC-MS^E, an internal mass-standard is required throughout the run to maximise mass accuracy. In some cases, signal from the lock-mass (Glu-1-fibrinopeptide (Glu-fib)) dropped out during the middle of the run. In these cases, mass correction factors were determined using the mass of Glu-fib at the beginning and end of the runs and added into the raw data file manually. Furthermore, due to a technical fault with the instrument, samples from cells treated in serum free media were not possible to analyse. This control

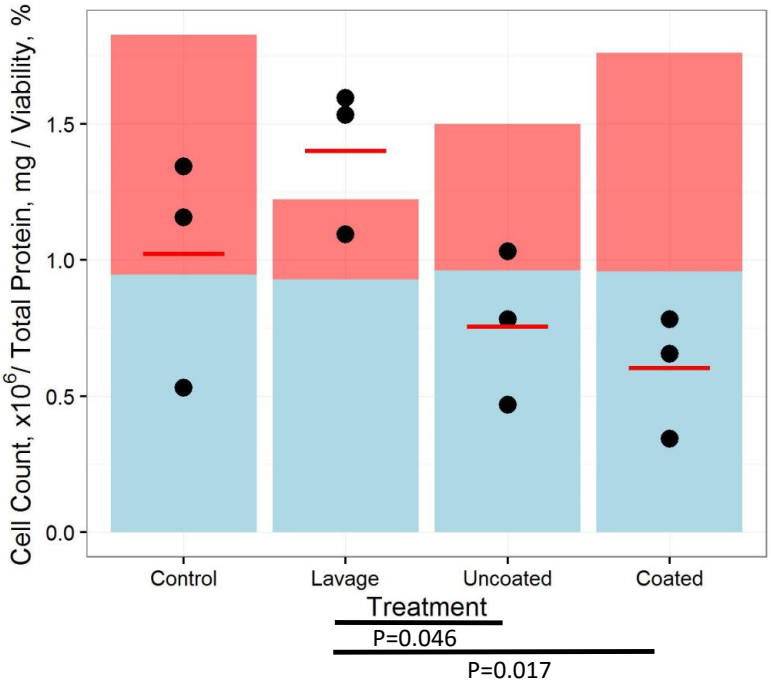

Figure 59: Protein yield from whole cell lysates of NP-treated cells (black dots, mean=red bar), mean cell viability (blue) and mean cell count after treatment (red). Control = serum free media only, Lavage = 1% lavage added to cells (no NPs), Uncoated = NPs added with 1% BALF and Coated = NP incubated in BALF prior to adding to cells with 1% BALF. P-values indicated below the graph are from a T-test for differences in total protein, n=3.

was there to observe the effect of 1% BALF on the cells. However, particle treatments can be compared to cell treated with 1% BALF only and therefore the effect of the particles can still be observed. We have already shown that adding 1% BALF to cells has no effect on viability (Figure **??**).

Enolase was added into the samples at 150 fmol per injection for Hi3 quantification. However, in some cases the intensity of enolase was too low to be detected. Therefore quantification was performed by relative, rather than absolute quantification, using the average intensity of the top 3 most abundant peptides.

In total, 4736 proteins were identified with 2353 proteins quantified in at least 2 repeats of any treatment (approx. 50% for each treatment group) (Figure **??**). The mean normalised protein abundance, standard deviation and coefficient of variance are summarised in Table **??**.

An initial analysis of GO-Slim terms for biological function and molecular function of all protein detected at least twice in control, BALF-Coated aPS treated and uncoated aPS treated cells was performed. There were no observed differences between each treatment group. The main biological activities observed were for catalytic activity, binding and nucleic acid binding (Figure **??** A-C). The largest molecular function classifications for the

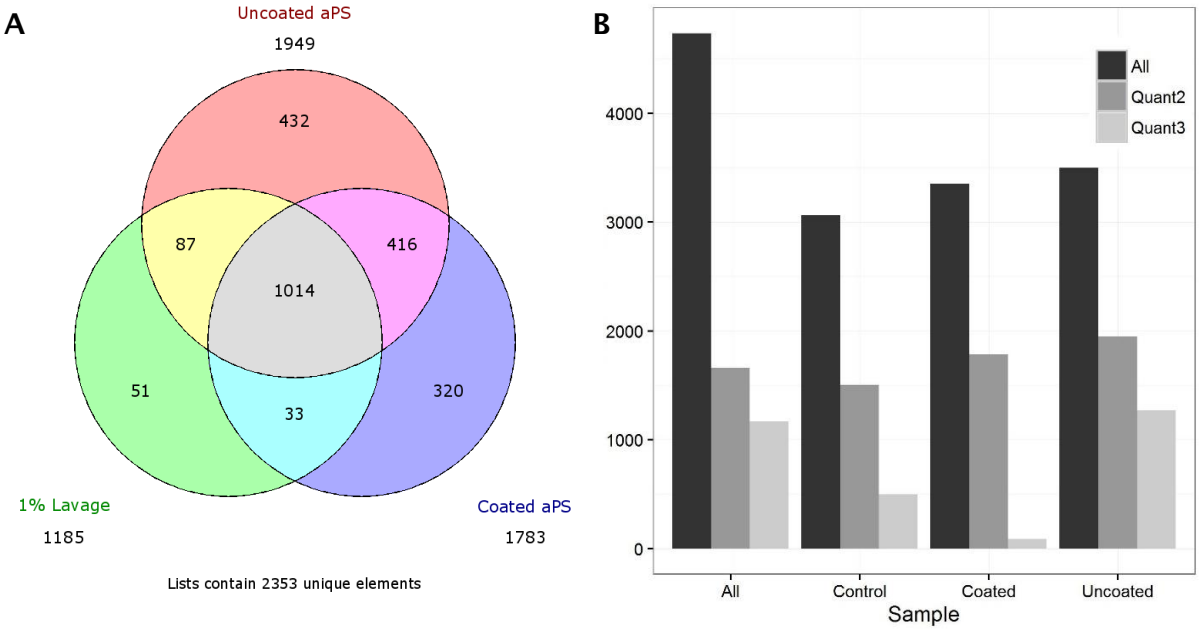

Figure 60: Numbers of detected proteins. (A) Venn diagram of proteins detected at least twice in each sample. (B) Summary of all detected proteins and in each sample. All (black) = all proteins identified in that sample, Quant2 (dark grey) = all proteins quantified at least twice in that sample, Quan3 (light grey) = all proteins identified in all repeats.

Sample	Number of Proteins Identified at Least Twice	Normalised Abundance Range	Normalised Abundance Mean	Mean Standard Deviation	Mean Coefficient of Variation
1% Lavage	1185	0.0008-5.03	0.517	0.141	29.560
Uncoated aPS	1949	0.003-4.35	0.445	0.113	31.42
Coated aPS	1783	0.003-3.64	0.477	0.102	24.76

Table 16: Statistical summary for cell lysate proteins. Number of proteins, range (min-max), mean abundance, mean standard deviation and mean coefficient of variation for each treatment. Proteins were only counted if they were identified in at least 2 repeats. During normalisation, the units cancer and therefore values are arbitrary.

detected proteins were metabolic process, and cellular process (Figure ?? D-F). Apoptotic processes were also a major classification, but the proportion was not different between control and treated groups.

For each protein detected at least twice, a fold change was determined compared to lavage-only treated cells. A 2-fold change was used as a cut-off to discriminate between proteins with altered abundance compared with untreated – this corresponds to approximately 2.3 standard deviations. The fold-change was log-transformed to generate normalised data and a P-value generated by performing T-tests between each protein pair (control vs particle-treated). For each treatment, there is a subset of proteins that are up or down regulated at least 2-fold and have a P-value <0.05 with respect to control (Figure ?? and Figure ??). The subset of proteins that had both 2-fold change and a P¡0.05 was relatively small, therefore proteins with a 3-fold difference, regardless of their P-value were analysed separately.

6.3.3 Bioinformatic Analysis

In both sample sets, there were more proteins that were significantly up regulated by at least 2-fold than down regulated (Table ?? and Table ??). The proteins were submitted to $STRING_{10}$ and analysed for enrichment of protein-protein interactions; interactions with a score greater than 0.4 were permitted (Table ??). In $STRING_{10}$ diagrams, protein are represented by coloured circles, the size of which carry no significance. The colour of the proteins represents clustering (see below) and protein-protein interaction are depicted by joining lines. Proteins that were significantly 2-fold up or down regulated in response to uncoated aPS particles were significantly enriched for interactions, unlike in response to coated particles, where enrichment was only observed for all proteins together. However, when the data sets were expanded to consider proteins with a 3-fold difference, regardless of P-value, there was no enrichment for protein-protein interactions observed with uncoated aPS treated cells. However, proteins with a 3-fold change from cells exposed to coated aPS particles showed significant enrichment for protein-protein interactions.

K-means clustering of proteins was performed in $STRING_{10}$, using string scores, proteins with similar interactions and scores will cluster together. Proteins that are interacting and have a higher score are more likely to group. Clustering showed a number of groups of proteins from cells that were exposed to uncoated or coated particles (Figure ??-??), particularly in the 3-fold change subset of proteins. In both cases there was a cluster of

Key	Name	Description	Fold-Change	P-Value
434	K1C16_HUMAN	Keratin_ type I cytoskeletal 16	0.062	0.006
43	RA1L2_HUMAN	Heterogeneous nuclear ribonucleoprotein A1-like 2	7.122	0.037
1550	NUP54_HUMAN	Nucleoporin p54	4.925	0.039
1443	LRC40_HUMAN	Leucine-rich repeat-containing protein 40	0.215	0.015
1453	UBF1_HUMAN	Nucleolar transcription factor 1	3.898	0.021
392	NB5R3_HUMAN	NADH-cytochrome b5 reductase 3	3.738	0.014
180	RLA1_HUMAN	60S acidic ribosomal protein P1	0.287	0.041
1350	RAVR1_HUMAN	Ribonucleoprotein PTB-binding 1	3.405	0.047
1460	RAD50_HUMAN	DNA repair protein RAD50	3.335	0.036
1340	GPI8_HUMAN	GPI-anchor transamidase	0.310	0.048
1712	TEX10_HUMAN	Testis-expressed sequence 10 protein	0.329	0.048
1011	LEG3_HUMAN	Galectin-3	0.351	0.006
741	PLSL_HUMAN	Plastin-2 OS=Homo sapiens	2.675	0.011
1043	CC124_HUMAN	Coiled-coil domain-containing protein 124	2.537	0.034
1549	NUP85_HUMAN	Nuclear pore complex protein Nup85	2.526	0.035
1132	MGN_HUMAN	Protein mago nashi homolog	0.396	0.009
770	AP1M1_HUMAN	AP-1 complex subunit mu-1	0.401	0.033
1000	PSME1_HUMAN	Proteasome activator complex subunit 1	0.409	0.014
1533	MYO1B_HUMAN	Unconventional myosin-Ib	2.442	0.024
331	NHRF1_HUMAN	Na(+)/H(+) exchange regulatory cofactor NHE-RF1	2.412	0.036
173	TCTP_HUMAN	Translationally-controlled tumor protein	2.398	0.039
1165	PSB3_HUMAN	Proteasome subunit beta type-3	0.418	0.024
1042	CMC2_HUMAN	Calcium-binding mitochondrial carrier protein Aralar2	0.430	0.020
947	LSM4_HUMAN	U6 snRNA-associated Sm-like protein LSm4	2.320	0.008
1002	DYN2_HUMAN	Dynamin-2	0.446	0.025
497	RD23B_HUMAN	UV excision repair protein RAD23 homolog B	2.056	0.040

Table 17: Protein expression changes in TT1 cells. Proteins with expression changed of at least 2-fold and P-value <0.05 following exposure to uncoated aPS NPs.

Key	Name	Description	Fold-Change	P-Value
1278	SUV3_HUMAN	ATP-dependent RNA helicase SUPV3L1_ mitochondrial	4.834	0.049
1014	KLC2_HUMAN	Kinesin light chain 2	4.530	0.019
1121	ERP44_HUMAN	Endoplasmic reticulum resident protein 44	3.970	0.030
392	NB5R3_HUMAN	NADH-cytochrome b5 reductase 3	3.491	0.031
885	ADRM1_HUMAN	Proteasomal ubiquitin receptor ADRM1	3.475	0.024
309	TBAL3_HUMAN	Tubulin alpha chain-like 3	0.322	0.013
947	LSM4_HUMAN	U6 snRNA-associated Sm-like protein LSm4	2.848	0.010
1105	SBDS_HUMAN	Ribosome maturation protein SBDS	2.821	0.036
933	SMD2_HUMAN	Small nuclear ribonucleoprotein Sm D2	2.623	0.021
173	TCTP_HUMAN	Translationally-controlled tumor protein	2.405	0.039
555	SH3L3_HUMAN	SH3 domain-binding glutamic acid-rich-like protein 3	2.302	0.037
1066	CNN2_HUMAN	Calponin-2	2.255	0.023
1250	TGON2_HUMAN	Trans-Golgi network integral membrane protein 2	2.253	0.050
408	PTN1_HUMAN	Tyrosine-protein phosphatase non-receptor type 1	2.218	0.025
751	CSK22_HUMAN	Casein kinase II subunit alpha'	2.177	0.005
604	PLOD3_HUMAN	Procollagen-lysine_2-oxoglutarate 5-dioxygenase 3	2.142	0.010
134	RS5_HUMAN	40S ribosomal protein S5	2.099	0.040
1218	PCY1A_HUMAN	Choline-phosphate cytidylyltransferase A	2.096	0.019
770	AP1M1_HUMAN	AP-1 complex subunit mu-1	0.485	0.019
480	RBMX_HUMAN	RNA-binding motif protein_ X chromosome	2.012	0.024
536	FERM2_HUMAN	Fermitin family homolog 2	2.008	0.001
1173	DHE3_HUMAN	Glutamate dehydrogenase 1_mitochondrial	2.000	0.014

Table 18: Protein expression changes in TT1 cells. Proteins with expression changed of at least 2-fold and P-value <0.05 following exposure to BALF-coated aPS NPs.

	Uncoated at least 2-fold & P<0.05	Coated at least 2-fold & P<0.05	Uncoated at least 3-fold	Coated at least 3-fold
Up Regulated	0.012	0.067	<0.001	0.0211
Down Regulated	0.036	N.D	0.055	0.033
All	0.002	0.0114	0.056	<0.001

Table 19: P-values for the probability that there are interactions between proteins. Proteins that were upregulated, down regulated and both together were submitted to $STRING_{10}$-db. All proteins submitted had a change of at least 3-fold, and those with a P <0.05 were submitted again separately. There were not enough proteins with a P <0.05 from Uncoated or Coated aPS treated cells to generate the statistic. N.D Not Determined.

proteins involved in vesicle trafficking (Figure **??** light brown, Figure **??** red). Pathway analysis of differentially-regulated proteins from cells exposed to BALF-coated particles in theKyoto Encyclopedia of Genes and Genomes (KEGG) database identified enrichment of synaptic vesicle cycle (Table **??**) but was not able to detect any enrichment for proteins from other samples.

Dataset	KEGG-Pathway	P-Value
BALF-Coated aPS 3-fold change in protein expression	Synaptic vesicle cycle	0.006
	Endocrine and other factor-regulated calcium reabsorption	0.035
	Splicesome	0.035

Table 20: Enrichment for KEGG pathways performed in $STRING_{10}$. Only those with a P-Value <0.05 were reported.

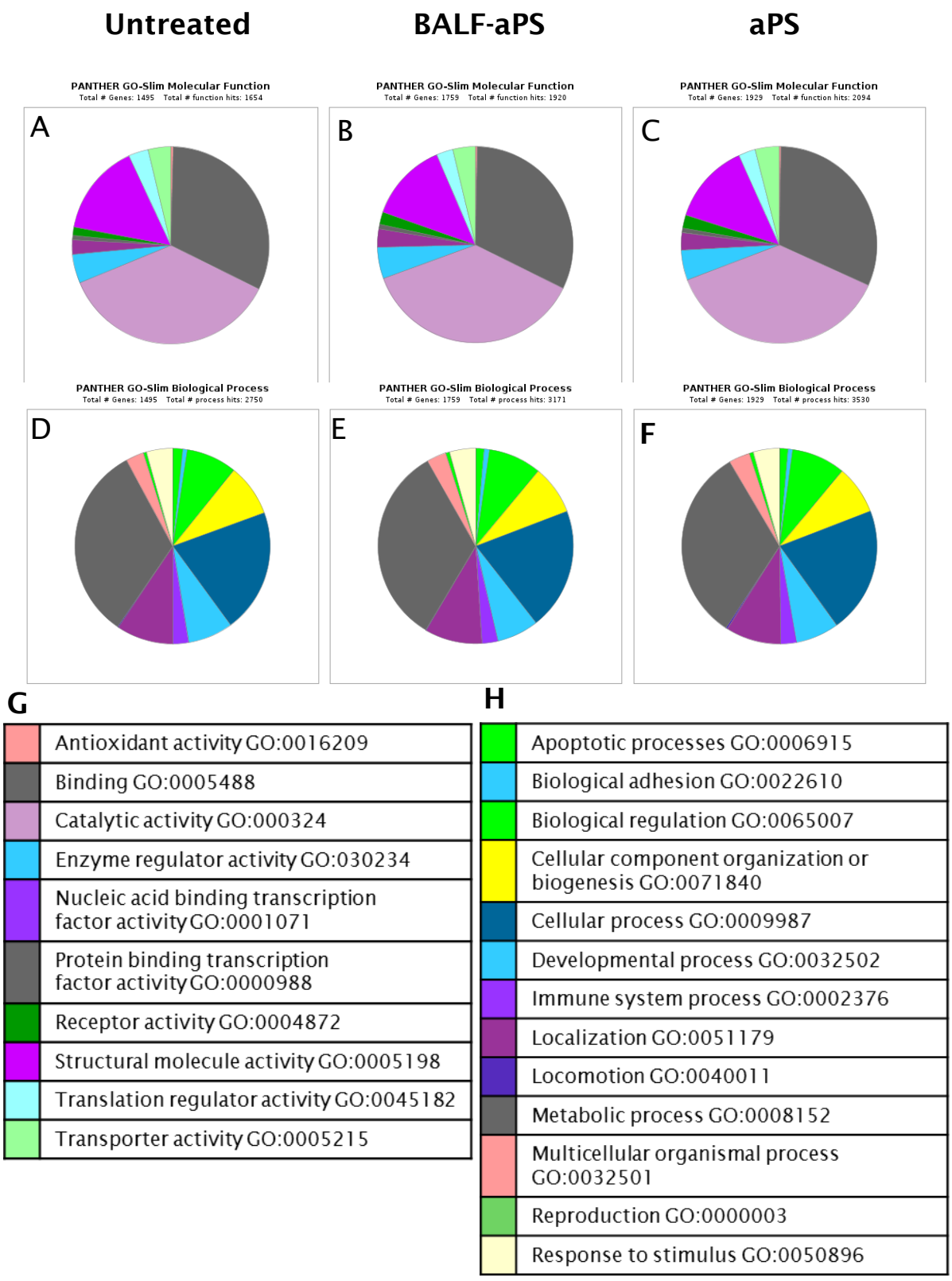

Figure 61: GO-term representations of all proteins detected in untreated cells (A, D), cells treated with BALF-Coated aPS (B, E) and cells treated with uncoated aPS (C, F) for 24 hours continuously. (A-C) GO Molecular function, (G) key. (D-F) GO Biological process, (H) key.

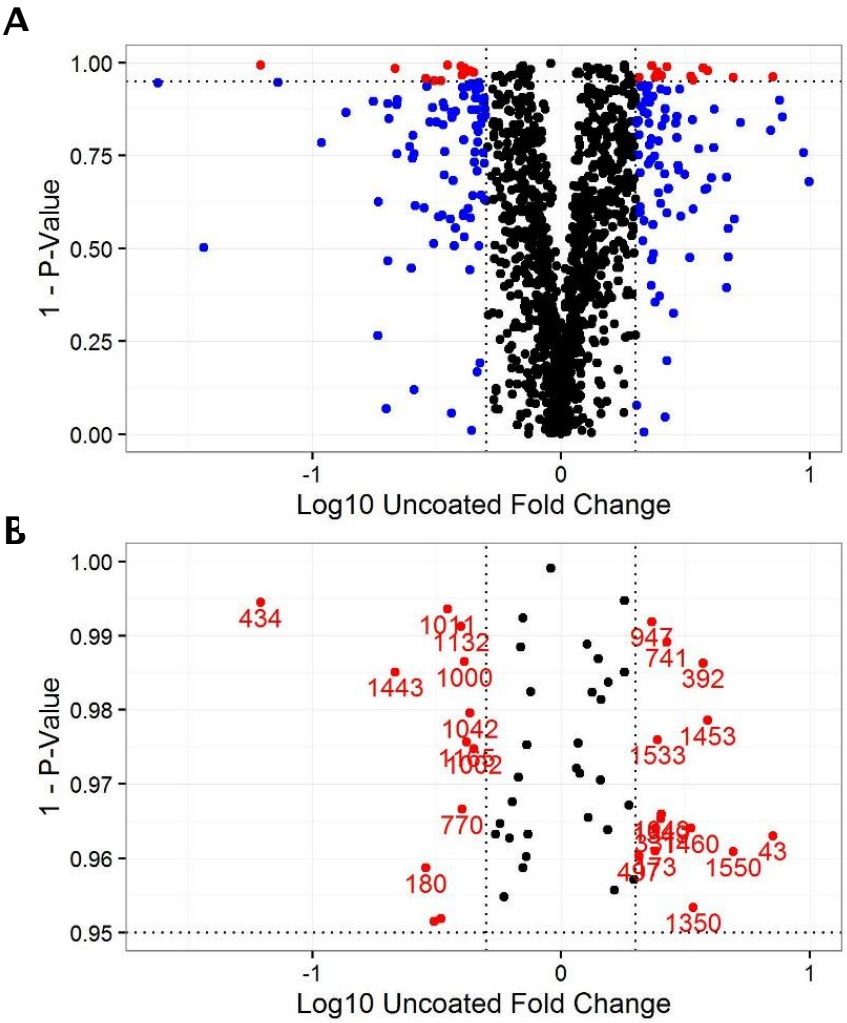

Figure 62: Volcano plot showing P-Value versus fold-change. (A) All proteins detected following incubation with uncoated aPS particles. (B) A zoomed plot, showing only the proteins with P<0.05 (>0.95 on plot). The numbers correspond to the protein 'key', see Table **??**. Red points are proteins with P<0.05 and >=2-fold change with respect to controls. Blue points are those with a fold change of at least 2.

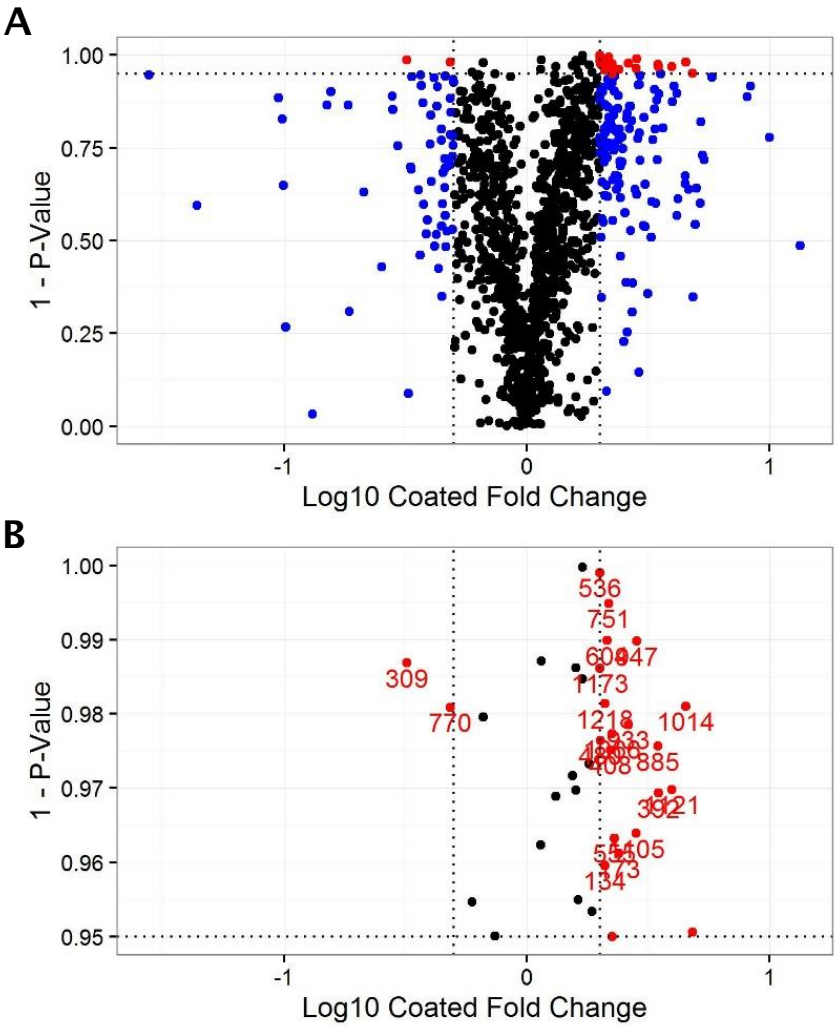

Figure 63: Volcano plot showing P-Value versus fold-change. (A) All proteins detected following incubation with coated aPS particles. (B) A zoomed plot, showing only the proteins with P<0.05 (>0.95 on plot). The numbers correspond to the protein 'key', see Table **??**. Red points are proteins with P<0.05 and >=2-fold change with respect to controls. Blue points are those with a fold change of at least 2.

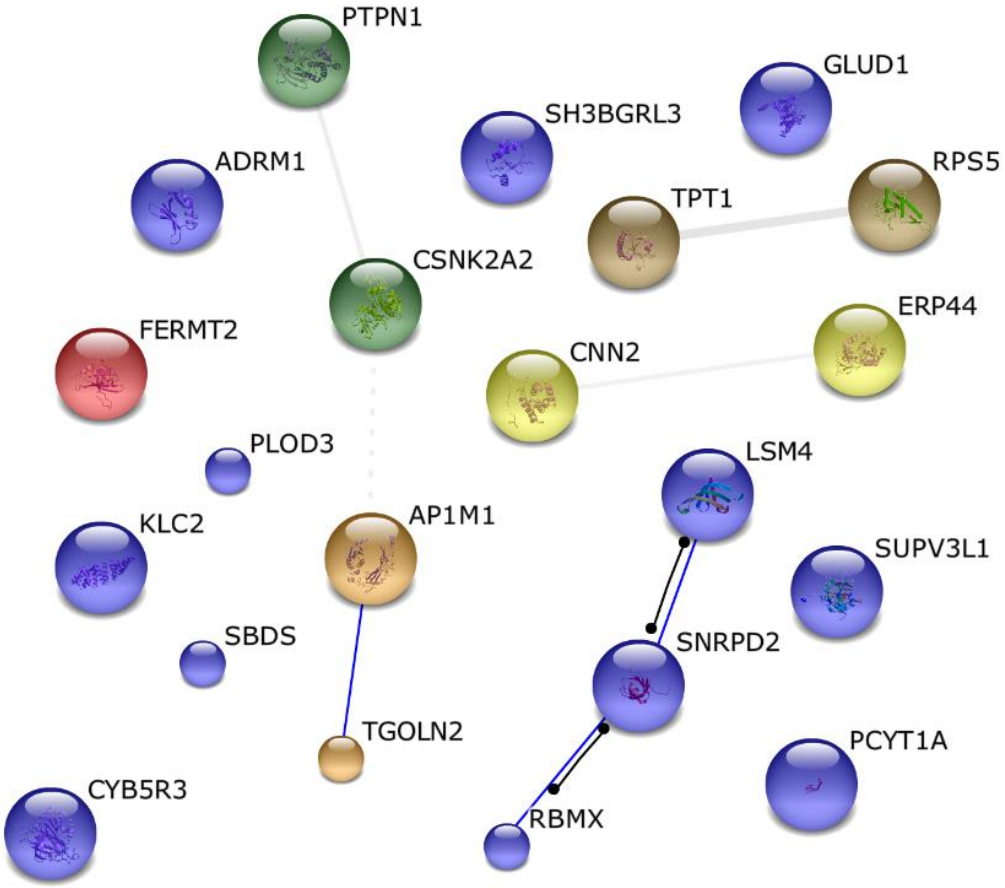

Figure 64: Protein-protein interactions from STRING$_{10}$ for proteins that had at least a 2-fold increase in expression with P<0.05 from cells exposed to BALF-coated aPS particles. Each protein is represented by a coloured spot and identified by the protein name. Linkages show the type interaction between the proteins. Blue lines indicate binding, black lines indicate a reaction and light grey indicates that the type of interaction is unknown. Colours of proteins represent k-mean clustering.

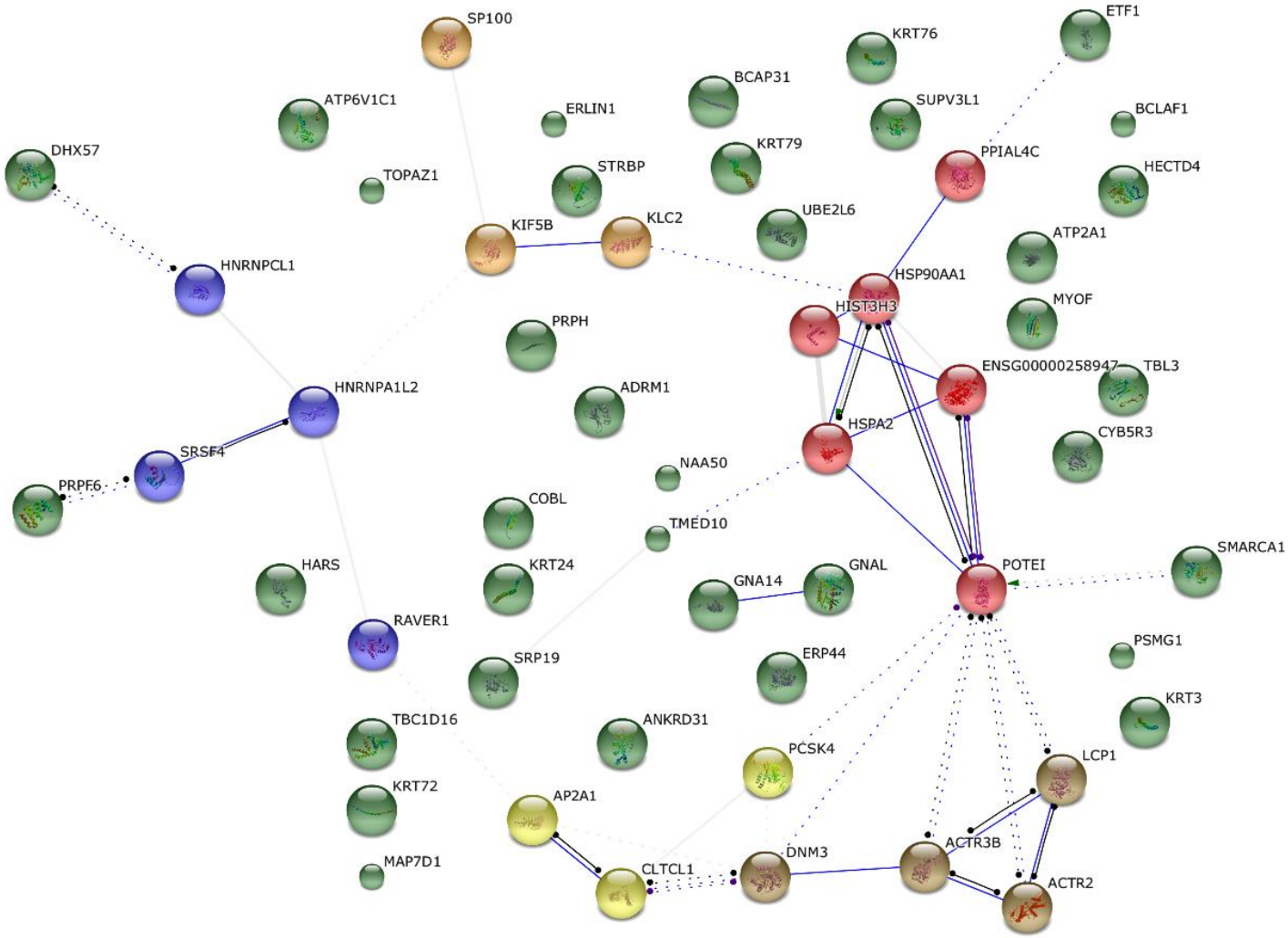

Figure 65: Protein-protein interactions from STRING$_{10}$ for proteins that had at least a 3-fold increase in expression from cells exposed to BALF-coated aPS particles. Each protein is represented by a coloured spot and identified by the protein name. Linkages show the type interaction between the proteins. Blue lines indicate binding, black lines indicate a reaction and light grey indicates that the type of interaction is unknown. Colours of proteins represent k-mean clustering and a dashed line shows interaction between clustered groups

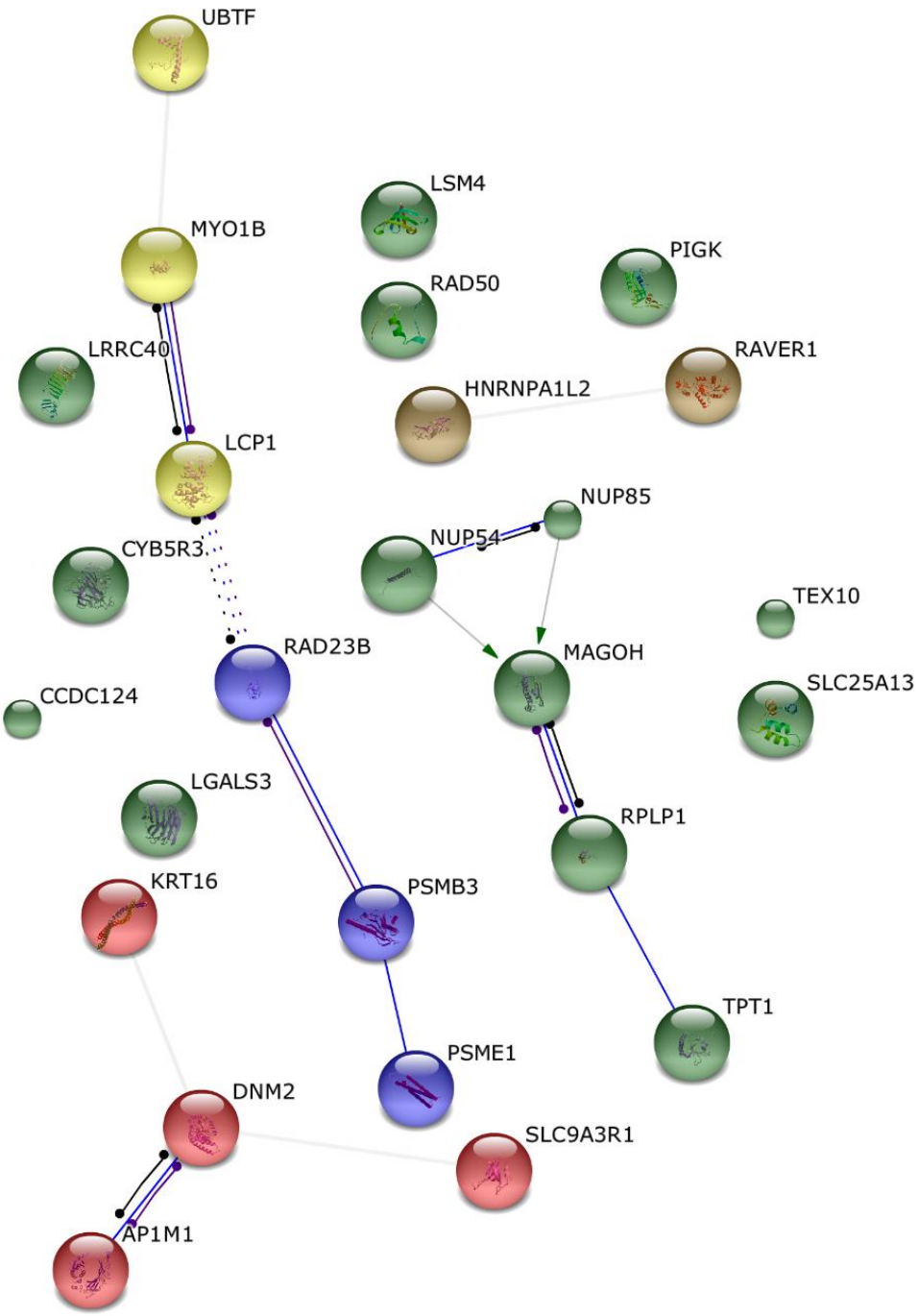

Figure 66: Protein-protein interactions from STRING$_{10}$ for proteins that had at least a 2-fold increase in expression and P-value<0.05 from cells exposed to uncoated aPS particles. Each protein is represented by a coloured spot and identified by the protein name. Linkages show the type interaction between the proteins. Blue lines indicate binding, black lines indicate a reaction, purple lines indicate catalysis and light grey indicates that the type of interaction is unknown. Colours of proteins represent k-mean clustering and a dashed line shows interaction between clustered groups.

Over representation analysis of the proteins was performed in Panther using Panther-pathways, GO-Slim biological process and GO-slim cellular location databases. GO-slim is a concise edition of the GO database, containing fewer dependencies and therefore provides a more over-arching view of the protein's function. Over representation

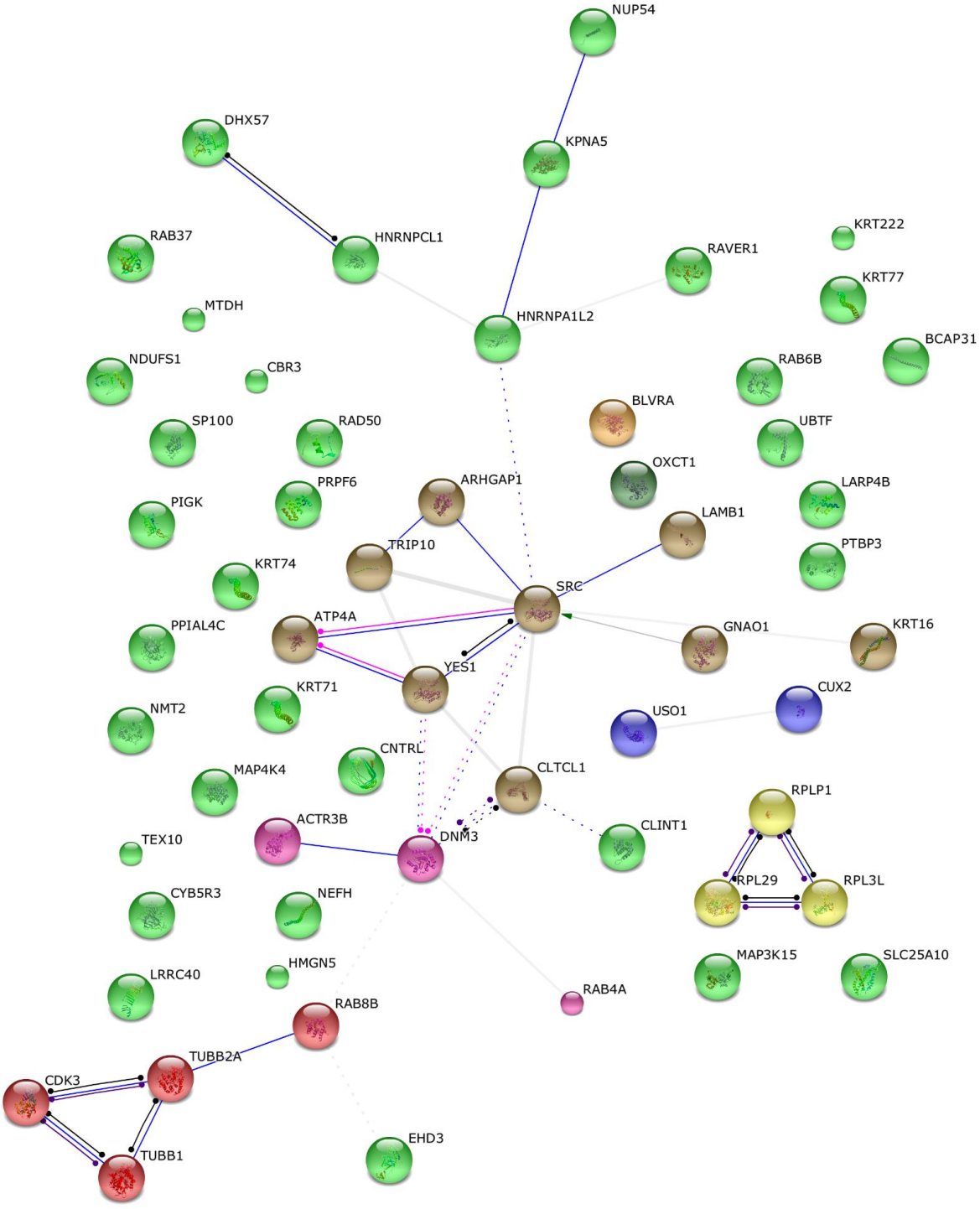

Figure 67: Protein-protein interactions from STRING$_{10}$ for proteins that had at least a 3-fold increase in expression from cells exposed to uncoated aPS particles. Each protein is represented by a coloured spot and identified by the protein name. Linkages show the type interaction between the proteins. Blue indicates binding, black indicates a reaction, pink indicates post translational modification and light grey indicates that the type of interaction is unknown. Colours of proteins represent k-mean clustering and a dashed line shows interaction between clustered groups.

was performed using the default settings and generated P-values based on the occurrence of the annotation term within the human genome compared with the submitted data set.

In response to coated particles, there was over representation in proteins localised to

microtubules (P=0.017) and the cytoskeleton (P<0.001) (Table **??**). There was also over representation for a number of biological process, including protein transport (P=0.01) and cellular component organization (P<0.001).

Proteins from cells exposed to uncoated particles displayed over representation for cytoskeletal localisation (P=0.048) and biological processes for cellular component morphogenesis (P= 0.017) and organisation (P=0.038) (Table **??**). No over representation was observed by this analysis for any pathway following either treatment.

Dataset	Databse	GO-Slim	P-Value
Coated aPS >3-fold change in expression	Biological Process	Cellular component morphgenesis GO:0032989	2.1×10^{-5}
		Anatomical structure morphogenesis GO:0009653	2.26×10^{-6}
		Cellular component organization or biogenesis GO: 0071840	2.99×10^{-6}
		Cellular component organization GO:0016043	2.55×10^{-5}
		Intracellular protein transport GO:0006886	7.4×10^{-3}
		Protein transport GO:005031	9.73×10^{-3}
Coated aPS >2-fold change in expression with P<0.05	Cellular Component	Microtubule GO:0005874	1.7×10^{-2}
Coated aPS >3-fold change in expression	Cellular Component	Intermediate filament cytoskeleton GO:0005856	3.64×10^{-6}
		Cytoskeleton GO: 0005856	3.96×10^{-8}
		Protein complex GO:0043234	1.52×10^{-5}
		Macromolecular complex GO:0032991	2.81×10^{-5}
		Organelle GO:0043226	3.43×10^{-6}
		Intracellular GO:0005622	1.86×10^{-5}
		Cell part GO:0044464	6.33×10^{-5}

Table 21: Over represented GO-Slim terms for proteins with altered expression following treatment with BALF-coated aPS.

A complementary analysis was performed in Cytoscape using protein subsets with a 3-fold change in expression. Protein-protein networks were exported from STRING_{10} and analysed using the BiNGO 'app' in Cytoscape for GO terms relating to cellular components using a hypergeometric test with Benjamini & Hochberh False Discovery Rate Correction.

Dataset	Database	GO-Slim	P-Value
Uncoated aPS >3-fold change in expression	Biological Process	Cellular component morphogenesis GO:0032989	1.7 x 10^{-2}
		Anatomical structure morphogenesis GO: 0009653	1.29 x 10^{-2}
		Cellular component organization GO: 0016043	3.82 x 10^{-2}
		Intermediate filament cytoskeleton	1.35 x 10-4
		Cytoskeleton	4.79 x 10-2
Uncoated aPS >3-fold change in expression	Cellular Component	Intracellular GO:0005622	3.13 x 10^{-4}
		Organelle GO: 0043226	1.53 x 10^{-2}
		Cell part GO:0044464	5.36 x 10^{-3}

Table 22: Over represented GO-Slim terms for proteins with altered expression following treatment with uncoated aPS.

In these figures, the size of the circle represents the relative number of proteins that contributed to that enrichment. Daughter ontology terms are linked by directional arrows. Yellow circles demonstrate that enrichment was observed for that GO term, whereas non-coloured were not enriched but are included as linking terms.

When performing complementary analysis, it was fund that proteins from cells exposed to coated particles showed enrichment for proteins relating to vesicle and clathrin-coated endocytosis as well as Golgi-related vesicular transport (Figure **??**). Proteins from cells exposed to uncoated particles did not show as specific enrichment, but localisations for microtubule and cytoskeletal components were observed (Figure **??**). A summary of proteins contributing to each highlighted zone is given in Table **??** and Table **??** for coated and uncoated particles respectively.

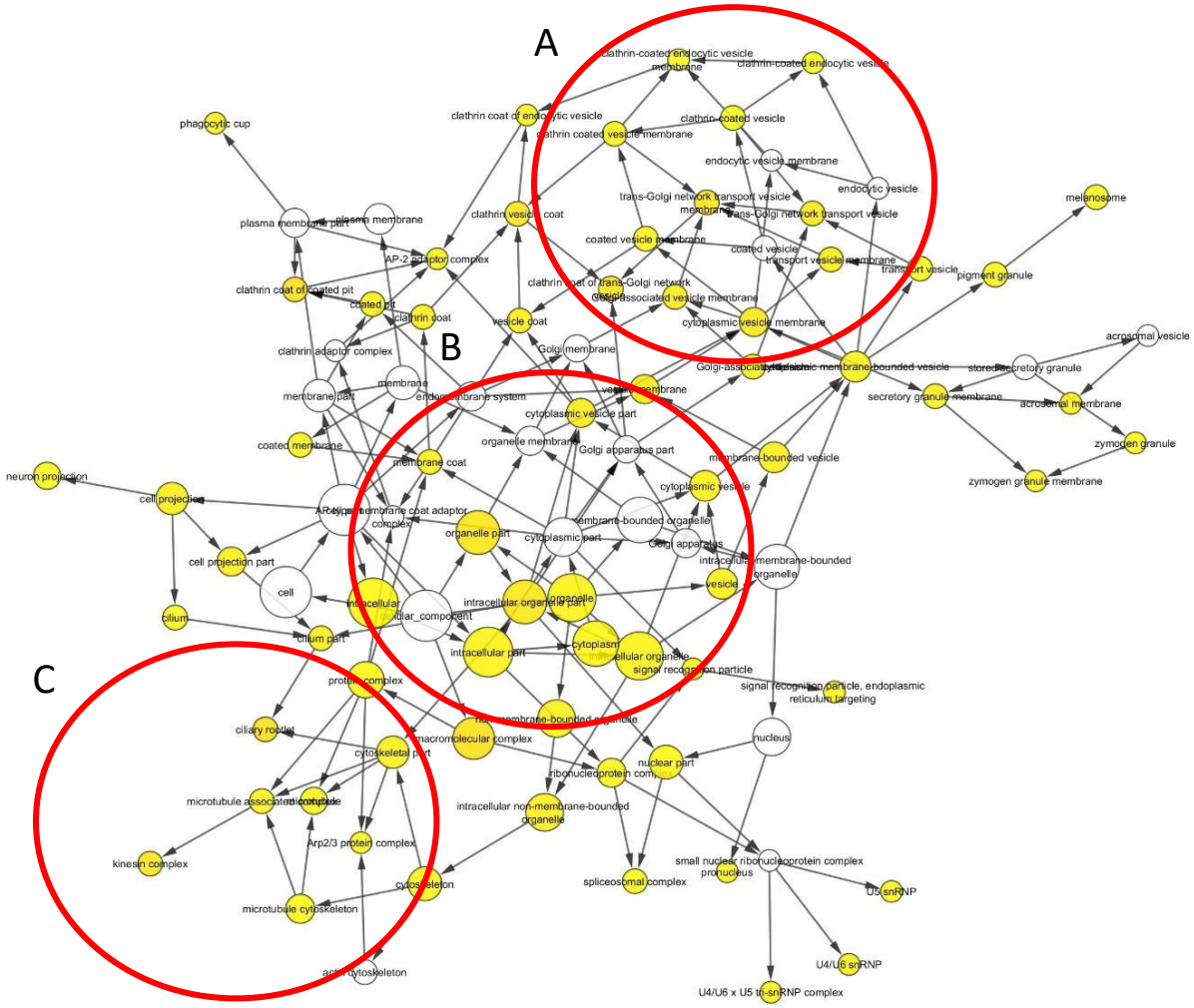

Figure 68: BiNGO analysis of proteins with at least 3-fold change in expression following exposure to BALF-coated aPS particles. Yellow indicates proteins were observed for that cellular location with a probability of over enrichment <0.05. Areas of interest are indicated by red circles; (A) Clatherin-coated vesiclular transport, (B) intracellular organelle localisation, (C) cytoskeletal and microtubule localisation.

Cellular-Localisation	Protein Accession	Protein Name	Protein Description	Fold-Change	P-Value
Clatherin-coated vesicular transport	Q6UW60	PCSK4	Proprotein convertase subtilisin/ kexin type 4	0.131	0.968
	P49755	TMED10	Transmembrane emp24 domain-containing protein 10	3.655	0.196
	P53675	CLTCL1	Clathrin heavy chain 2	0.151	0.134
	O95782	AP2A1	AP-2 complex subunit alpha-1	3.274	0.395
Intracellular organelle localisations	P49755	TMEDA	Transmembrane emp24 domain-containing protein 10	3.655	0.196
	Q9P1U1	ARP3B	Actin-related protein 3B	0.184	0.135
	O95782	AP2A1	AP-2 complex subunit alpha-1	3.274	0.395
	Q9UQ16	DYN3	Dynamin-3	3.456	0.281
	P62495	ERF1	Eukaryotic peptide chain release factor subunit 1	0.279	0.111
	O95837	GNA14	Guanine nucleotide-binding protein subunit alpha-14	0.333	0.301
	Q16695	H31T	Histone H3.1t	3.021	0.459
	O60812	HNRC1	Heterogeneous nuclear ribonucleoprotein C-like 1	0.102	0.734
	Q14568	HS902	Putative heat shock protein H90-alpha A2	0.044	0.406
	P54652	HSP72	Heat shock-related 70 kDa protein 2	0.028	0.054
	P33176	KINH	Kinesin-1 heavy chain	0.294	0.244
	Q9H0B6	KLC2	Kinesin light chain 2	4.530	0.019
	Q9Y536	PAL4A	Peptidyl-prolyl cis-trans isomerase A-like 4A/B/C	13.423	0.514
	P53675	CLH2	Clathrin heavy chain 2	0.151	0.134
	P13796	PLSL	Plastin-2	4.201	0.387
	O94906	PRP6	Pre-mRNA-processing factor 6	4.167	0.104
	Q8IY67	RAVR1	Ribonucleoprotein PTB-binding 1	4.849	0.652
	P28370	SMCA1	Probable global transcription activator SNF2L1	3.321	0.228
	P23497	SP100	Nuclear autoantigen Sp-100	4.499	0.347
	P09132	SRP19	Signal recognition particle 19 kDa protein	3.368	0.092
	Q08170	SRSF4	Serine/arginine-rich splicing factor 4	8.105	0.111
	Q6UW60	PCSK4	Proprotein convertase subtilisin/ kexin type 4	0.131	0.968
Cytoskeletal and microtubule location	Q9P1U1	ARP3B	Actin-related protein 3B	0.184	0.135
	O95782	AP2A1	AP-2 complex subunit alpha-1	3.274	0.395
	Q9UQ16	DYN3	Dynamin-3	3.456	0.281
	O95837	GNA14	Guanine nucleotide-binding protein subunit alpha-14	0.333	0.301
	P33176	KINH	Kinesin-1 heavy chain	0.294	0.244
	Q9H0B6	KLC2	Kinesin light chain 2	4.530	0.019
	P53675	CLH2	Clathrin heavy chain 2	0.151	0.134
	P13796	PLSL	Plastin-2	4.201	0.387
	P28370	SMCA1	Probable global transcription activator SNF2L1	3.321	0.228

Table 23: Proteins contributing to over representation observed for BALF-coated aPS exposed cells, as visualised in Figure **??**. Fold change and P-Values are compared to untreated cells. All proteins had at least 3-fold change in expression

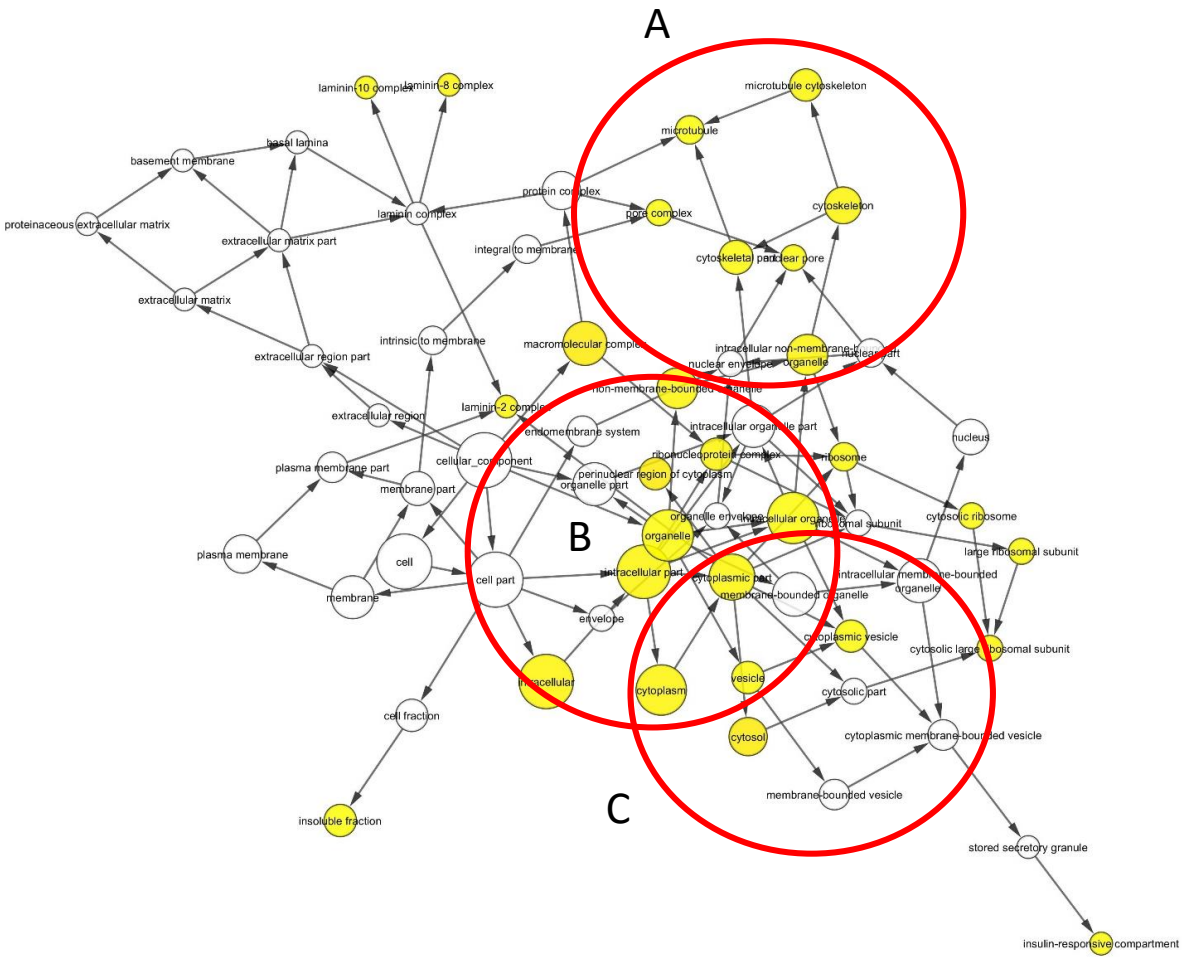

Figure 69: BiNGO analysis of proteins with at least 3-fold change in expression following exposure to uncoated aPS particles. Yellow indicates proteins were observed for that cellular location with a probability of over enrichment <0.05. Areas of interest are indicated by red circles; (A) Cytoskeletal and microtubule localisation, (B) intracellular organelle localisation, (C) cytoplasmic vesicle localisation

Table 24: (Below) Proteins contributing to over representation observed for uncoated aPS exposed cells, as visualised in Figure **??**. Fold change and P-Values are compared to untreated cells. All proteins had at least 3-fold change in expression.

Cellular Localisation	Protein Accession	Protein Name	Protein Description	Fold-Change	P-Value
Cytoskeletal and microtubule localisation	P08779	K1C16	Keratin_ type I cytoskeletal 16	0.062	0.006
	P53675	CLH2	Clathrin heavy chain 2	0.176	0.104
	P47914	RL29	60S ribosomal protein L29	0.201	0.110
	Q7Z3B4	NUP54	Nucleoporin p54	4.925	0.039
	Q9UQ16	DYN3	Dynamin-3	4.043	0.310
	Q9P1U1	ARP3B	Actin-related protein 3B	0.254	0.196
	O15131	IMA6	Importin subunit alpha-6	0.257	0.880
	Q15642	CIP4	Cdc42-interacting protein 4	3.784	0.341
	Q92901	RL3L	60S ribosomal protein L3-like	0.282	0.391
	P05386	RLA1	60S acidic ribosomal protein P1	0.287	0.041
	Q13885	TBB2A	Tubulin beta-2A chain	0.322	0.415
	Q07960	RHG01	Rho GTPase-activating protein 1	3.006	0.071
	Q9H4B7	TBB1	Tubulin beta-1 chain	0.333	0.410
Intracellular organelle localisation	P08779	K1C16	Keratin_ type I cytoskeletal 16	0.062	0.006
	P12931	SRC	Proto-oncogene tyrosine-protein kinase Src	7.582	0.100
	Q32P51	RA1L2	Heterogeneous nuclear ribonucleoprotein A1-like 2	7.122	0.037
	Q92930	RAB8B	Ras-related protein Rab-8B	6.992	0.181
	P53675	CLH2	Clathrin heavy chain 2	0.176	0.104
	Q9NZN3	EHD3	EH domain-containing protein 3	0.184	0.374
	O60812	HNRC1	Heterogeneous nuclear ribonucleoprotein C-like 1	0.199	0.932
	P47914	RL29	60S ribosomal protein L29	0.201	0.110
	Q7Z3B4	NUP54	Nucleoporin p54	4.925	0.039
	P07947	YES	Tyrosine-protein kinase Yes	4.645	0.606
	O14529	CUX2	Homeobox protein cut-like 2	4.629	0.307
	P20338	RAB4A	Ras-related protein Rab-4A	4.118	0.228
	Q9UQ16	DYN3	Dynamin-3	4.043	0.310
	Q9P1U1	ARP3B	Actin-related protein 3B	0.254	0.196
	O15131	IMA6	Importin subunit alpha-6	0.257	0.880

This table continues on the next page ...

	Q14677	EPN4	Clathrin interactor 1	0.257	0.245
	Q92901	RL3L	60S ribosomal protein L3-like	0.282	0.391
	P05386	RLA1	60S acidic ribosomal protein P1	0.287	0.041
	O60763	USO1	General vesicular transport factor p115	0.289	0.063
	Q8IY67	RAVR1	Ribonucleoprotein PTB-binding 1	3.405	0.047
	P07942	LAMB1	Laminin subunit beta-1	3.405	0.394
	Q13885	TBB2A	Tubulin beta-2A chain	0.322	0.415
	Q07960	RHG01	Rho GTPase-activating protein 1	3.006	0.071
	Q9H4B7	TBB1	Tubulin beta-1 chain	0.333	0.410
	P08779	K1C16	Keratin_ type I cytoskeletal 16	0.062	0.006
	P12931	SRC	Proto-oncogene tyrosine-protein kinase Src	7.582	0.100
	Q32P51	RA1L2	Heterogeneous nuclear ribonucleoprotein A1-like 2	7.122	0.037
	Q92930	RAB8B	Ras-related protein Rab-8B	6.992	0.181
	P53675	CLH2	Clathrin heavy chain 2	0.176	0.104
	Q9NZN3	EHD3	EH domain-containing protein 3	0.184	0.374
	O60812	HNRC1	Heterogeneous nuclear ribonucleoprotein C-like 1	0.199	0.932
Cytoplasmic vesicle	P47914	RL29	60S ribosomal protein L29	0.201	0.110
localisation	Q7Z3B4	NUP54	Nucleoporin p54	4.925	0.039
	P07947	YES	Tyrosine-protein kinase Yes	4.645	0.606
	O14529	CUX2	Homeobox protein cut-like 2	4.629	0.307
	P20338	RAB4A	Ras-related protein Rab-4A	4.118	0.228
	Q9UQ16	DYN3	Dynamin-3	4.043	0.310
	Q9P1U1	ARP3B	Actin-related protein 3B	0.254	0.196
	O15131	IMA6	Importin subunit alpha-6	0.257	0.880
	Q14677	EPN4	Clathrin interactor 1	0.257	0.245
	Q15642	CIP4	Cdc42-interacting protein 4	3.784	0.341
	Q92901	RL3L	60S ribosomal protein L3-like	0.282	0.391
	P05386	RLA1	60S acidic ribosomal protein P1	0.287	0.041
	O60763	USO1	General vesicular transport factor p115	0.289	0.063
	Q8IY67	RAVR1	Ribonucleoprotein PTB-binding 1	3.405	0.047
	P07942	LAMB1	Laminin subunit beta-1	3.405	0.394
	Q13885	TBB2A	Tubulin beta-2A chain	0.322	0.415
	Q07960	RHG01	Rho GTPase-activating protein 1	3.006	0.071
	Q9H4B7	TBB1	Tubulin beta-1 chain	0.333	0.410

6.4 Discussion

Cells were exposed to 1 cm^2/mL of aPS particles. This concentration was chosen as it did not reduce viability in TT1 cells but did elicit greater mitochondrial activity compared with other concentrations and therefore the cellular reaction may be evident as an altered proteome. Upon inhalation, NPs may reach the terminal alveolar (Section **??**) and, given that AEI cells account for 95% of alveolar surface area[124], it follows that these are the most likely to come into contact with inhaled particles. Maynard et al.[269] highlighted AEI cells as cells capable of taking up particles and hypothesised that increased rate of apoptosis within particle-laden AEI cells may assist in the overall clearance of particles from the alveolus.

Initial analysis of the identified proteins' biological and molecular function did not show any difference between control and treated cells (Figure **??**). This analysis is not weighted for protein abundance and therefore does not reflect the cellular dynamics of the proteins. The similarity is therefore expected since most of the proteins belonging to each data set are shared.

Network analysis of large scale proteomic data sets is capable of highlighting enriched or altered pathways and generating hypothesis for future investigation. The aim here is to identify proteins with altered expression between cells exposed to NPs and controls and further identify the pathways involved in the cellular changes. Since we observed a difference in reaction from cells exposed to BALF-coated or uncoated particles, the cells were exposed to coated or uncoated aPS particles. Polystyrene uptake of TT1 cells is immediate and the uptake rate increases over at least 4 hours.[270] To observe the effect of aPS particles over a longer term, cells were exposed for 24 hours, thus ensuring maximal particle uptake.

There was significantly more proteins yielding from cells that were not exposed to NPs compared to those that were (Figure **??**). There was no obvious difference in cells following microscopic examination prior to harvesting, so this may be due to a decreased rate of cell division in cells exposed to particles, however there was no statistical difference in the number of cells or cell-viability after treatment in any group (Figure **??**). Kim *et al.*[271] demonstrated that exposure to sub-toxic (25 µg/mL, approximately 13 cm^2/mL) doses of aPS particles, the proportion of A549 cells in s-phase of the cell cycle was less than cells exposed to carboxylated PS particles or no particles. The authors offer no mechanism for this observation but speculate that different particles may trigger different cellular pathways.

There were 2353 unique proteins identified in at least two repeats of any treatment, with nearly 2000 proteins in uncoated and coated aPS treatment groups (Figure ??). There were fewer proteins in the control group which means that it was not possible to obtain a ratio of control:treatment for a large number of proteins. However, there was still over 1,000 proteins common to both control and treatment samples.

There were relatively few proteins with significantly altered expression compared to controls (Figure ?? and Figure ??). The number of replicates was limited by available time on the mass spectrometer. With three repeats, 10 fractions, and 4 sample groups, this experiment took in excess of 2 weeks continual machine time, which in practice translated to nearly 1 month. Therefore the data set was expanded to include proteins that were increased by at least 3 fold. With the average coefficient of variation approximately 30% (Table ??), this is an appropriate level of discrimination between true changes in expression, however does not account for the spread of the data.

It would be useful here to analyse the entire set of proteins identified in the control cells for enriched pathways. However, this dataset is too large for free online resources and therefore this analysis was not possible. Therefore, only the proteins that displayed a difference were analysed, providing insight into the pathways that are altered by the presence of NPs.

Two pathway analyses were performed. The KEGG database is a manually curated database of known pathways upon which proteins can be mapped and analysed for enrichment (against a reference data set, e.g. the human proteome/genome). It was established as part of the Japanese Human Genome Program and currently holds 484 pathway maps.[272] Panther databases are similarly curated through manual updates and bioinformatic algorithms and currently has 177 pathways described in the database.[228] Since such databases require manual curation and depend on experimental/published evidence, searches are performed on the assumption that the proteins are described within the database. Since this is not always the case, or protein definitions may not be complete, I have searched two complimentary databases. Enrichment was only observed in the larger database, KEGG, for proteins that had at least a 3-fold change in expression after exposure to BALF-coated aPS particles (Table ??). These observations are supported by network analysis in STRING_{10}, where significant enrichment for protein-protein interactions was observed for the same dataset (Table ??).

The concentration of particles used was chosen to represent sub-toxic levels of aPS particles (Section ??). From pathway analysis and levels of detected caspases (Supplementary 4),

there was no evidence of the activation of apoptotic or necrotic pathways detected here.

6.4.1 Exposure to Uncoated aPS Particles

Proteins with vesicle-related functions were enriched in both data sets, either through analysis of cellular location or pathways and a number of proteins involved in vesicle trafficking were identified. In the uncoated data set, $STRING_{10}$ analysis identified 3 protein-protein interaction networks from proteins that were significantly different by at least 2-fold compared with controls (Figure **??**).

The longest 'string' of proteins, shows interactions between myosin 1b (MYO1B) to proteasome activator subunit 1 (PSME1). MYO1B was upregulated by 2.4 fold (P=0.024) (Table **??**), whilst the exact cellular functions of myosin-1s are unknown, there is experimental evidence that supports its role in calcium-regulated vesicle trafficking.[273, 274] The evidence that connects MYO1B to plastin-1 (LCP1), is based upon text mining of abstracts for co-reporting of MYO1B and LCP1, and lacks any experimental evidence. PSME1 and PSMB3 were both down regulated and are involved in protein degradation as part of the 20S proteasome complex.[275]

Both DNM2 and AP1M1 were down regulated and their interaction was identified by $STRING_{10}$ analysis. AP1M1 facilitates the budding of clathrin-coated vesicles from the Golgi membrane[276, 277] and it's down regulation, along with decreased expression of proteasomal proteins may suggest decreased protein synthesis, as observed from cell lysis yields (Figure **??**). Similar analysis of proteins with at least a 3-fold change showed a 3-5 fold change decrease in ribosomal proteins RL29, RL3L and RLA1 (P=0.04) (Figure **??**, and Supplementary 5), supporting an effect on protein synthesis.[278] Such observations are not supported by enrichment for protein-sythesis pathways here and therefore would require further investigation. Whilst a decrease in protein production in a neurite cell line (P12 cells) following exposure to 10 nm silver NPs has been reported in the literature[279], no explanation was suggested and to the best of the author's knowledge it has not been investigated for PS exposure.

6.4.2 Exposure to BALF-Coated aPS Particles

Analysis for pathway enrichment within KEGG identified synaptic vesicle cycle as being significantly enriched (P=0.006, Table **??**), and this finding is further supported by the significant enrichment for vesicular localisation of regulated proteins by BiNGO (Figure **??**).

The endocytosis of NPs is well reported in the literature[74, 80, 203, 243], however there is debate as to whether the uptake of 100 nm particles is possible via clathrin-mediated endocytosis. A recent publication by Maria Monti *et al.*[68] observed no co-localisation between fluorescently labelled clathrin and 44 nm PS particles. Similarly, Guarnieri *et al.*[270] have observed no co-localisation of 100 nm PS particles and clathrin in fibroblast, retinal endothelial or porcine aortic endothelial cells. Both argue that clathrin-coated vesicles have a size range of 50-150 nm[280] and therefore are too small to accommodate 100 nm particles. However, clathrin mediated endocytosis has been reported in particles up to 200 nm[83, 280] by co-localisation of fluorescent labels or drug inhibition.[203, 281]

Analysis of proteins by BiNGO, showed that there was enrichment for clathrin coated vesicle-association (Figure **??**). The proteins responsible for the enrichment included upregulated (TMED10, AP2A1) and down regulated (PCSK4, CLTCL1) proteins (Table **??**). Both transmembrane emp24 domain-containing protein 10 (TMED10) and AP-2 complex subunit alpha-1 are involved in trans-Golgi network vesicle trafficking, and there was less clathrin heavy chain (CLTCL1 and CLH2) observed from treated cells compared to untreated (approximately 6.7-fold reduction). Therefore the observations may reflect a reduction in Golgi-vesicle trafficking and not endocytosis.

A reduction in trans-Golgi vesicle activity would add credence to the reduction in protein synthesis discussed earlier. However altered protein levels does not necessarily equal altered protein function, as proteomic identification by this methodology cannot distinguish between activated/inactivated proteins etc. Furthermore, a reduction in detected protein may be due to altered peptide masses (i.e. post translational modification) and therefore does not necessarily translate to reduced protein-per cell or inform about protein activity. Further work to investigate this observation is required.

As discussed previously, an increase in mitochondrial activity was observed following exposure to low concentrations of particles. The increase in mitochondrial activity of TT1 cells exposed to 1 cm^2/mL of aPS particles was marginal and slightly greater for exposure to BALF-coated particles (Section **??**). The evidence here suggests that over all, protein production was decreased and therefore, enhanced mitochondrial activity must be due to other energy-dependant mechanisms.

Whilst evidence suggests that trans-Golgi activity may be decreased, there were potential increases observed for other vesicle-transport-related proteins. For instance Dynamin-3 (Table **??** and Table **??**), Rho GTPase activating protein 1 and Rab-4A (Table **??**) are

upregulated by at least 3 fold in response to coated (Dynamin-3 only) or uncoated (all) aPS particles and are involved in endosomal recycling.[282–284] Ruenraroengsak[93] has described membrane damage from aPS particles as 'holes' punctured through the membrane. A paper examining hypertonic stress in AEI cells through the induction of a similar injury (micro-puncture with a glass needle) observed that calveolar-mediated endocytosis was enhanced, whilst clathrin-mediated endocytosis was inhibited.[285] In relation to the data here, it is not possible to assign much weight to observations of individual proteins from such a large data due to over fitting, but, the data suggests there may be an increase in other forms of vesicular transport. It is possible that this is responsible for increased mitochondrial activity and provides an interesting hypothesis for future work.

6.4.3 Further Work

A number of interesting observations have come out of this study. It would be interesting to follow up on the effect of particles on protein synthesis as this could potentially have impact on long term effect of particle exposure *in vivo*.

Investigation into the enrichment for vesicle associated proteins may yield information regarding particulate uptake. Clathrin-related proteins were observed and enriched within the data set which may support evidence of clathrin-mediated endocytosis. This would be supported by uptake studies of particles in TT1 cells. Such experiments were prepared for analysis by CARS, but due to unforeseen circumstances could not be analysed.

The pathway analyses performed here are limited by the number of pathways described in the KEGG and Panther databases. More sophisticated searches of more comprehensive databases are available but require expensive licences (e.g. Metacore or Ingenuity), these may be capable of identifying more enriched pathways.

There were few statistically significant changes between proteins and this could be improved with further repeats.

These experiments were performed over a single time point of 24 hours and therefore lack information on protein dynamics during this time window. Repeat sampling of cells over time could provide interesting information regarding protein and pathway dynamics in response to particulate exposure.

There was no clear effect of the protein corona on the regulated cells here. Whilst there was

enrichment for vesicle cycle pathways following exposure to BALF-coated particles, overall the regulated proteins in both data sets compared with controls were similar. It is clear from the literature that the presence of a corona can slow particle uptake. However, once the particles have been taken up into the cells, degradation of the corona in lysosomes may negate the effect of the corona. Analysis of recovered particles would be an interesting experiment to perform, although recovering particles from cells whilst maintaining their surface corona would be technically challenging.

7 Primary Alvaolar Epithelial Cell Isolation

7.1 Introduction

The use of cell lines for the study of alveolar epithelium is widespread in the literature and there are a number of commonly used transformed or tumour-derived immortalised AEI and AEII cells. These lines have the advantage of being easy to culture and store allowing replicate experiments to be performed without the effect of patient to patient variation. Furthermore, they are generally very well characterised and common usage within a field allows for comparison of results between laboratories.

However, their similarities with endogenous cells can be poor, owing to loss of the cells' endogenous niche and increased mutagenesis inherent with continuous cell division. For example, A549 cells, a lung adenocarcinoma cell line,[101] are frequently used as a model for AEII cells. They were derived in 1972 by Giard *et al.*[101] from a 58 year old male and shown to possess multi-lamella bodies and produce phosphatidylcholines via the cytidine diphosphocholine pathway as in AEII cells.[190] They are easy to grow in cell culture and consequently have been used extensively for toxicity modelling and cytokine expression profiling. However, there are some important differences between A549 cells and AEII cells that should be considered. There is an absence of SP-A, SP-B or SP-C expression in these cells.[286] In particular, the expression of SP-C is a defining characteristic of AEII cells that differentiates them from similar Clara cells. Furthermore, whilst these cells had human male karyotype (i.e. 46 chromosomes, XY), current cell stocks held by the American Type Culture Collection (ATCC) have a modal chromosome count of 66 including duplication of sex chromosomes.[287] In 60% of cells, the Y-chromosome was missing entirely. For any immortalised cell line, there is an increased risk of accumulating mutations which may ultimately affect phenotype. Furthermore, given the culture environment, *in vitro* is different to the cells' *in vivo* niche. Natural selection may further aggravate the evolution of the cells away from a true *in vivo* phenotype.

A number of methods have been described[174, 175, 177] for isolation of AEI and AEII cells from rat lung. However, the enzymatic dissociation of cells from human lungs tends to be too abrasive towards human AEI cells which are fragile and lower in abundance than AEII cells. That said, degradation of the extra-cellular matrix (ECM) using collagenase or trypsin for the isolation of AEII cells is routine in many laboratories. After dissociation, the cells are purified through a number of rounds of cell adhesion/passage designed to

negatively select for AEI or AEII cells. However, this takes approximately 40 hours to get pure cells and the yields of AEI cells can be very low due to the digestion conditions. It has been proposed by Dobbs[178, 180] that elastase digestion of the ECM may be more gentle on AEI cells than other enzymes.

In culture, the capacity for AEII cells to produce surfactant associated proteins – a defining feature of their phenotype – rapidly decreases[288, 289] and they develop a more AEI-like phenotype, reminiscent of their function *in vivo* to repopulate surrounding cells following tissue damage.[127–129] Consequently, methods that take days to isolate them significantly reduce time available for experimentation.

Novel antibodies against human AEI and AEII-specific antigens HTI_{56}[178] and $HTII_{280}$[180] have been developed by Dobbs and Gonzalez *et al.* (see Table **??**). The same authors describe a method to isolate the cells from intact rat lungs or lobes by instilling them with elastase solution via distal airways and purifying by FACS.[176] However, whilst methods describe the isolation of rat AEI and AEII cells, the results published in Gonzalez *et al.* (2010)[180] for humans are limited to the isolation of AEII only. We aim to adapt these methods to the isolation of human AEI and AEII cells from smaller sections of lung acquired during bullectomy where no major airways are available. Using this method, it was hoped to substantially reduce the time needed to isolate the cells, helping to maintain high viability, in particular of AEI cells, and achieve high purity through cell sorting.

As mentioned above, AEII cells rapidly lose their phenotypic characteristics, such as expression of pro-SP-C, SP-A and aquaporin 3 (AQP-3) whilst gain AEI-like characteristics, such as the presence of AQP-3.[288, 290] Mao *et al.*[288]300 have shown that primary human AEII cells maintained their expression of SP-A, B, C, D and AQP-3 for 20 days when cultured in small airway epithelium growth medium (SAGM). They suggest that this is due to epinephrine, hydrocortisone and retinoic acid present in the media, that are important for preventing differentiation. Keratinocyte growth factor (KGF) has been shown to help maintain SP-A expression in rat primary AEII cells[291, 292] and epidermal growth factor, also present in SAGM[288], is able to induce proliferation in epithelial cells.[293]

Rat AEI cells, isolated from healthy animals, have been shown to divide from very low densities when cultured on bovine fibronectin in 20% FBS and to express aquaporin 5 (AQP-5), a phenotypic marker.[176] Consequently, it may be possible to expand small cultures of AEI cells, although phenotypic changes would have to be carefully monitored.

7.1.1 Aims

1. Assess the specificity of the monoclonal antibodies against HTI_{56} and $HTII_{280}$ to AEI and æaeii cells respectively.
2. Develop the methodology for isolation of AEI and AEII cells from human lung tissue by FACS.
3. Culture human AEI and AEII cells, assesing their viability and phenotype.

7.2 Methods

7.2.1 Dot Blot

Nitrocellulose membrane was first wetted in methanol before washing thoroughly in tris-buffered saline (TBS). The membrane was assembled into a Bio-Dot (Bio-Rad) and 150 µL TBS was passed through each well under a light vacuum to equilibrate. 50 µL of TBS was applied to each well followed by an equal volume of sample and drawn through the membrane under vacuum. Each spot was washed with 150 µL TBS, the membrane removed and stained with Panceuax. Excess stain was rinsed with TBS and the membrane placed in blocking buffer. The rest of the procedure is the same as described in Section **??**.

7.2.2 Cross-Reactivity Assay

2 µL of sample was pipetted onto nitrocellulose membrane. The membrane was blocked with 5% milk in TBST for 1 hour and probed with AlexaFlour 488-conjugated anti-mouse IgM (AF488) (1:2000) or AlexaFluor 633-conjugated anti-mouse IgG_1 (AF633) (1:1000) or TBST only (control) for 1 hour at room temperature. After washing, 3x with TBST, samples were probed with anti-goat.horse radish peroxidase (HRP) conjugate (1:5000 in TBST) for 1 hour before being re-washed and imaged on photographic film with TMA-6 chemiluminescent substrate. 0.5 µL of AF488 and AF633 were dotted onto the membrane as a positive control.

7.2.3 Antibody Titration

Primary antibodies were supplied as culture supernatants from hybirdoma cells and as such their concentration unknown. The concentration was determined by dot blot, creating a standard curve using commercial antibodies of the same isotype (Table **??**). The primary

antibodies were analysed in triplicate at multiple dilutions and all antibodies adsorbed onto the membrane and blocked as described previously (Section **??**). Secondary antibodies against mouse IgG_1 or IgM, conjugated to HRP were diluted 1:5000 (10mL) and incubated for 20 minutes prior to washing 3x5 minutes with TBST. Dots were imaged and densitometry performed in a gel doc (Syngene) using Syngen Tools software. A standard curve was fitted and unknown concentrations determined in Prism (Graphpad).

7.2.4 Immunohistochemistry

Tissue was prepared based on the protocol from Gonzalez *et al.*.[180] Human lung tissue, acquired from bullectomy, lobectomy or wedge resection (Section **??**), was cut into approximately 5 mm^3 pieces and fixed in 4% paraformaldehyde (PFA) in PBS at room temperature overnight. Fixed tissue was cryoprotected in 30% sucrose (w/v) in TBS (10 mM Tris.HCl pH 7.4, 150 mM NaCl) overnight at 4°C before being coated in Optimal Cutting Temperature solution (OTC) and flash frozen in liquid nitrogen. If not used immediately, tissue was stored at -80°C.

For immunohistochemistry (IHC) of AEI and AEII cells, tissue was cut to 4 µm sections using a Leica CM1850 UV cryosectioner at -19°C. Sections were placed Poly-L Lysine coated slides and allowed to dry for 1 hour. Three sections were prepared per slide.

A square approximately 1 cm x 1 cm was drawn around each section with a PAP-pen which allowed 100 µL of liquid to be applied to each section and aspirated off as required. Sections were blocked with blocking solution (RPMI, 10% FBS (v/v), 1% pen/strep (v/v)) for 20 minutes before human IgG (50 µg/mL) was added to block endogenous Fc receptors for 20 minutes.

Anti-HTI_{56} (diluted 1:10) and Anti-$HTII_{280}$ (diluted 1:50) primary antibodies were applied simultaneously and left over night at 4°C. Sections were washed 3x with 100 µL TBS for 5 minutes before AF633 (diluted 1:1000) and/or AF488 (diluted 1:1000) were added for 30 minutes at room temperature in the dark (for more information, see Table **??**). Sections were washed 3 times for 5 minutes with TBS before being mounted using ProLong Gold antifade reagent with 4',6-diamidino-2-phenylidole (DAPI).

Slides were imaged using Leica TCS-SP5 laser scanning confocal microscope and analysed using Leica Application Suite Advanced Fluorescence 2.6.0 software.

7.2.5 Co-Immunoprecipitation

co-IP with protein-L conjugated magnetic beads (Pierce) was performed by an adaptation of the manufactures instructions. 300 µL of BALF was incubated with 300 µL of primary antibody (approx. 0.4 µg IgM) over night at 4°Cwith continual rotation. 25 µL of magnetic beads were washed with 175 µL of wash buffer (TBS, 0.05% Tween 20, 0.5 M NaCl) by rotating for 1 minute and removing the wash solution by immobilising the magnetic beads on the side of the tube with a magnet. The antibody-antigen solution was mixed with the beads for 2 hours with rotation at room temperature after which time the solution was removed and stored (flow through). The beads were washed with 500 µL of wash buffer three times and once with ddH_2O before eluting with 100 µL low pH-glycine (0.1M glycine, pH 2) by rotating for 10 minutes at room temperature. After neutralisation with 15 µL 1M Tris, the elute was kept for analysis. The beads were suspended in 100 µL ddH_2O and 10 µL was checked by Western blot. Controls were prepared by combining 300 µL of BALF or antibody with an equal amount of binding buffer (TBS, 0.05% Tween-20) and continuing the protocol as described.

7.2.6 Cell Dissociation

Lung tissue was used immediately upon receipt. Cells were dissociated from approximately 5g of lung tissue acquired from lung wedge resection or bullectomy. Tissue was dissociated by either elastase (methods based on Gonzalez *et al.*[180]) or trypsin (methods based on Thorley *et al.*[132]).

Cells were dissociated by elastase by first dicing the tissue to approximately 1mm^3 pieces and washing through 100 µm cell strainer with 50 mL RPMI. Tissue was then suspended in at least 1 mL elastase (Worthington Biomed. Corp. LS002294) (RPMI, 25 mM Hepes, 4.5 U/mL elastase), or enough to cover all the tissue for 1 hour at 37°C. DNase was added to a final concentration of 50 µg/mL and the solution rocked for 5 minutes at room temperature. The resulting solution was passed sequentially through 100, 70 and 40 µm cell strainers and the cell suspension centrifuged at 300 x g for 10 minutes. The pellet was finally suspended in RPMI/FBS (10% w/w).

For tryptic dissociation, tissue was first perfused with saline (150 mM NaCl) with a syringe at multiple injection sites until the draining solution appeared clear. Trypsin (sigma, T8003) solution (0.25% w/v in PBS) was injected at multiple sights and left for 15 minutes at 37°C. This was repeated a further two times for a total of 45 minutes and 45 mL of

trypsin solution per 7 g of tissue. Excess trypsin was removed and the tissue chopped finely in the presence of FBS (10% v/v in RPMI). The chopped tissue was rinsed in 50 mL DNase (250 µg/mL in PBS) by gently inverting a 50 mL falcon tube for 5 minutes. Tissue suspension was passed through a sterile 100 µm cell strainer, followed by a 40 µm cell strainer and the resulting cell suspension centrifuged at 290 x g for 10 minutes. Cells were suspended in 10 mL media (DCCM-1, 1% Pen/strep, 2 mM L-glutamine, 50 µg/mL DNase).

7.2.7 Fluorescence Activated Cell Sorting

Cells were suspended in 10 mL of RPMI-FBS with 50 µg/mL human IgG and left on ice for 10 minutes. Small aliquots (200 µL) were removed for controls (isotype and negative controls). To the remaining suspension anti-HTI_{56} and anti-$HTII_{280}$ were added to a final concentration of 0.08 and 0.11 µg/mL respectively (determined by antibody titration) and left for 5 minutes on ice. Following centrifugation (290 x g, 4°C) for 10 minutes, cells were suspended in 985 µL RPMI-FBS and 100 µL anti-CD45, 10 µL AF488 and 5 µL AF633 (Table **??**) were added and cells left for 10 minutes on ice, in the dark. Cells were centrifuged for 10 minutes and suspended in 5 mL RPMI-FBS for FACS. Cell sorting and analysis was performed on FACS-ARIA (BD Scientific), equipped with 405 nm, 488 nm and 635 nm lasers. Sorting was performed in yield or purity mode at low flow rates. For gating, see Figure **??**.

7.2.8 Cytospinning

Cells sorted by FACS were centrifuged at 150 x g for 10 minutes, suspended in 400 µL PBS and counted. 100,000 cells were adjusted to 150-200 µL in PBS and cytospun (Cytospin 3, ThermoShandon) at 500 rpm for 10 minutes onto poly L-lysine coated slides. Cover slips were mounted using ProLong Gold Antifade with DAPI (Life Technologies) and cells stored at 4°Cuntil imaged by confocal microscopy.

7.2.9 Transmission Electron Microscopy

Cells were fixed by combining 1:1 with fixative (3% glutaraldehyde, 4% formaldehyde in 0.1M PIPES buffer at pH 7.2) and left over night at 4°C. Fixed cells were embedded into 5% sodium alginate by adding a drop of resin to the bottom of the tube containing the cells and centrifuging at 1250 x g for approximately 5 minutes. Fixative was carefully removed from the top of the tube and the resin hardened with calcium chloride (0.05M in 0.1M

PIPES buffer) for 15 minutes. The hardened resin was removed from the tube and left to harden further at room temperature for 5 minutes. Sections were cut with glass knives to a thickness of approximately 100 nm and floated onto formvar-coated copper grids. Sections were stained with lead tartrate for 3 minutes and imaged on a Hitachi H7000 transmission electron microscope.

7.3 Results

7.3.1 Characterisation of Primary Antibodies and Antigen

The monoclonal antibodies Anti-HTI_{56} and Anti-$HTII_{280}$ were supplied as culture supernatants. Their concentration was determined by interpolation of a standard curve made from commercial antibody of the same isotype (mouse IgG1 and IgM respectively) (Figure **??**). HTI_{56} was determined to be at a concentration of 1.6 µg/mL and $HTII_{280}$ at a concentration of 2.2 µg/mL.

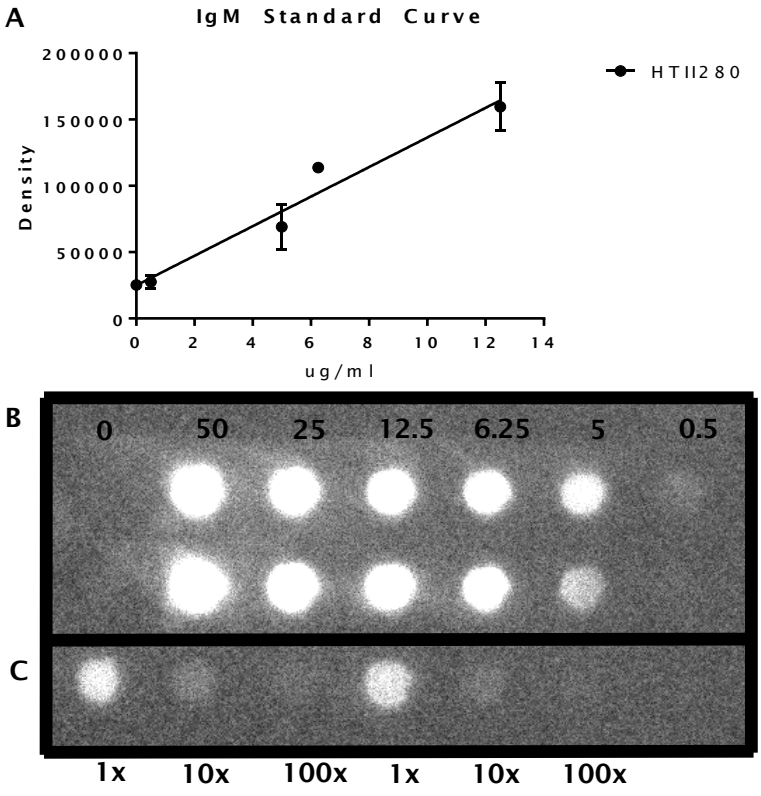

Figure 70: Antibody titration to determine the concentration of Anti-HTI_{56} and Anti-$HTII_{280}$, a standard curve (A) of matched isotype was generated by dot blot (B). Intensity of samples (C) was measured by densitometry and plotted against concentration. Linear regression was plotted to determine the concentration of primary antibodies. Representative examples are given, with error bars representing standard deviation.

To assess the antibodies' specificity, a human lung homogenate was analysed by Western

blotting for AEI and AEII cell antigens, HTI_{56} and $HTII_{280}$ respectively (Figure **??**). Under non-reducing conditions, anti-HTI_{56} identified a single band between 64 and 51 kDa, whilst under reducing conditions, Anti-$HTII_{280}$ bound to two proteins with molecular weights above 188 kDa. These results were as expected form published results by Dobbs and Gonzalez.[178, 180]

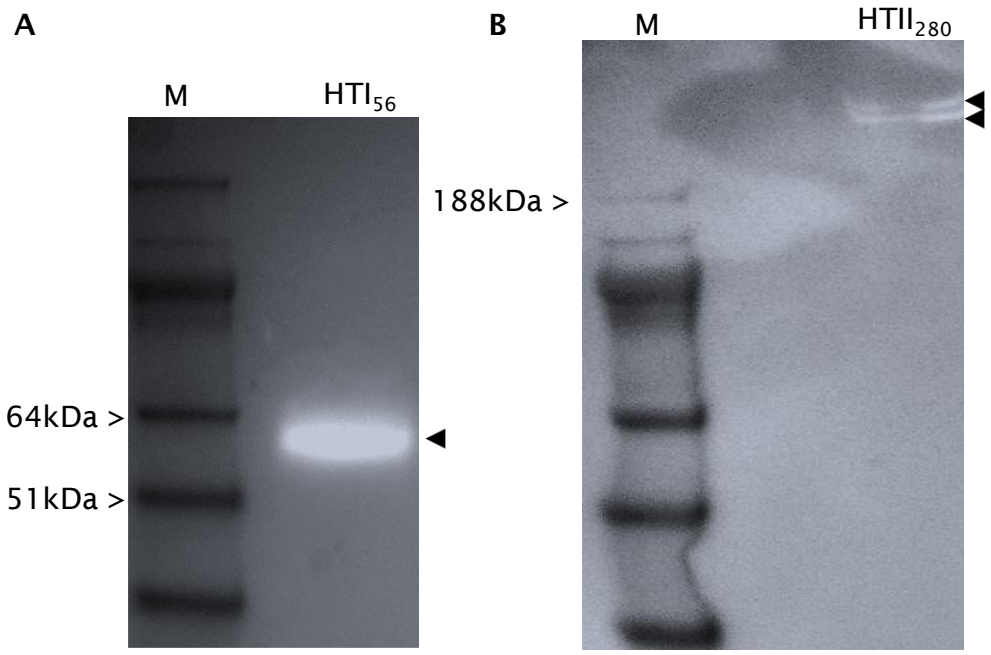

Figure 71: Western blot of HTI_{56} (A) and $HTII_{280}$ (B) antigen from human lung homogenate. Non-reduced HTI_{56} was detected at a molecular weight between 64 Kda and 51 kDa. $HTII_{280}$ was detected under reducing conditions and formed a dimer with a molecular weight greater than 188 kDa. Molecular marker (M) were imaged non-fluorescently and overlaid onto the Western blot image. Molecular weights are indicated (kDa).

In order to further assess their specificity for AEI and AEII cells and show the location of the antigens, lung tissue sections were stained with Anti-HTI_{56} and Anti-$HTII_{280}$ using secondary antibodies coupled to a fluorescent tag to label the cells. Potential cross reactivity of the secondary antibodies was assessed by dot blot (Figure **??**). Human lung sections were incubated with the two antibodies for staining against AEI and AEII cells, respectively. With both antibodies, staining was membrane localised with no overlap of staining to suggest co-localisation (Figure **??**). Anti-HTI_{56} labelled membranes of long, thin cells surrounding alveolar with $HTII_{280}$ localised to the 'corners' of the airspaces. There was no staining from within the airspaces to suggest cross-reactivity to macrophage.

Following damage, AEI cells are replenished by AEII cell plasticity. We wondered if the AEII cell-surface marker $HTII_{280}$ was lost after lung damage from LPS. LPS treated, inflation-fixed tissue was prepared by Dr Mark Griffiths (Royal Brompton, Imperial College) and probed with anti-HTI_{56} and anti-$HTII_{280}$ antibodies (Figure **??**). Following

LPS treatment, both HTI_{56} and $HTII_{280}$ were detected, however $HTII_{280}$ staining had moved away from the alveolar wall and into the airspace, suggesting AEII cell are trans-locating away from the alveolar lining. Nuclei were also seen with no surrounding HTI_{56} or $HTII_{280}$ staining suggesting the migration of immune cells into the alveolar space. The alveolar air-sacs appeared generally smaller and less rounded than untreated cells. The differences may be artefactual from the inflation-fix process, and I think further investigation into the movement of AEII cells in the airspace is warranted.

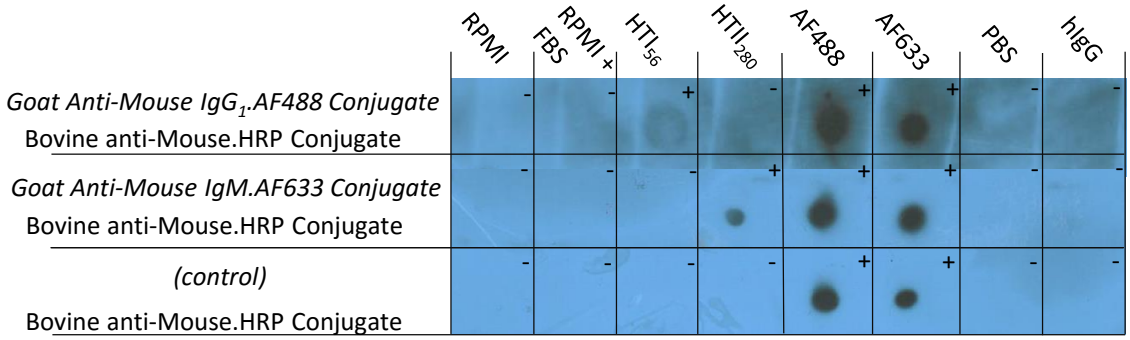

Figure 72: Dot bot showing no cross-reactivity of secondary antibody. Various solutions were dotted onto the membrane before incubation with the labelled antibodies. The expected results indicating working controls and no cross reactivity are given as a '+' or '-' in the top right hand corner of each square. AF488 and AF633 were dotted onto the membrane as positive controls. There was reactivity towards anti-HTI_{56} (mouse IgG1) and anti-$HTII_{280}$ (mouse IgM) with no cross-reactivity between isotypes or human IgG (hIgG).

7.3.2 Co-Immunoprecipitation

$HTII_{280}$ was immunocaptured on protein-L coupled magnetic beads before being incubated in BALF. Western blot of the unbound and eluted material showed that there was binding of anti-$HTII_{280}$ antibody to the beads and that these were able to capture $HTII_{280}$ antigen (Figure **??**). Capturing of the antigen was antibody specific as no antigen was captured when beads-only were incubated in BALF. $HTII_{280}$ did not elute in low pH-glycine buffer. However some antibody was recovered from the beads suggesting that there was an excess of anti-$HTII_{280}$ bound to the beads. This is further exemplified by the presence of $HTII_{280}$ antigen in the unbound material (flow through). After elution with low pH-glycine buffer, the material remaining on the beads was denatured in SDS PAGE loading buffer at 80°C. This eluted $HTII_{280}$ as well as bands at approximately 70 kDa and 40 kDa (IgM heavy chain and recombinant protein L respectively).

Following co-IP, proteins were eluted by SDS PAGE and the bands corresponding to $HTII_{280}$ antigen cut out for protein digestion and extraction. Proteins were identified by

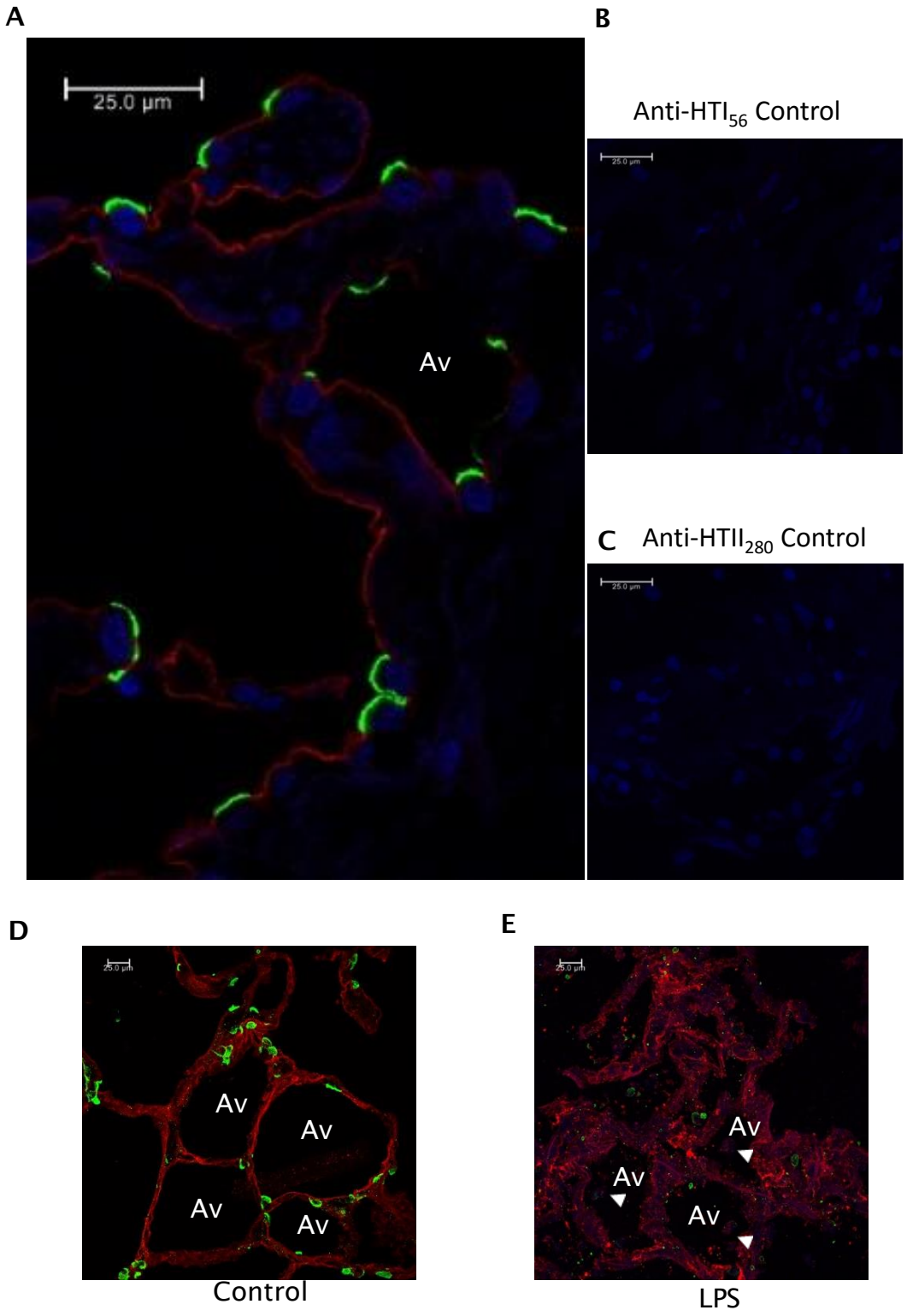

Figure 73: Immunohistochemistry of AEI (red) and AEII (green) distal lung sections. Sections were probed with both primary antibodies (anti-HTI_{56} and anti-$HTII_{280}$) (A) and secondary antibodies (AF633 and AF488), or primary antibodies with non-matching secondary antibody as controls (C, B). Lung ex-plant treated with (E) or without (D) LPS were inflation fixed and probed with all antibodies. Lung infiltrates (white arrow) were seen in the airways of LPS treated tissue (E) and the alveoli (Av) were smaller. Nuclei were stained blue with DAPI.

MS in a bottom up approach (Supplementary 6). Identified proteins were excluded if identification was from only 1 peptide and filtered by average mass to give a short list of

two proteins between 200 and 300 kDa (Table ??).

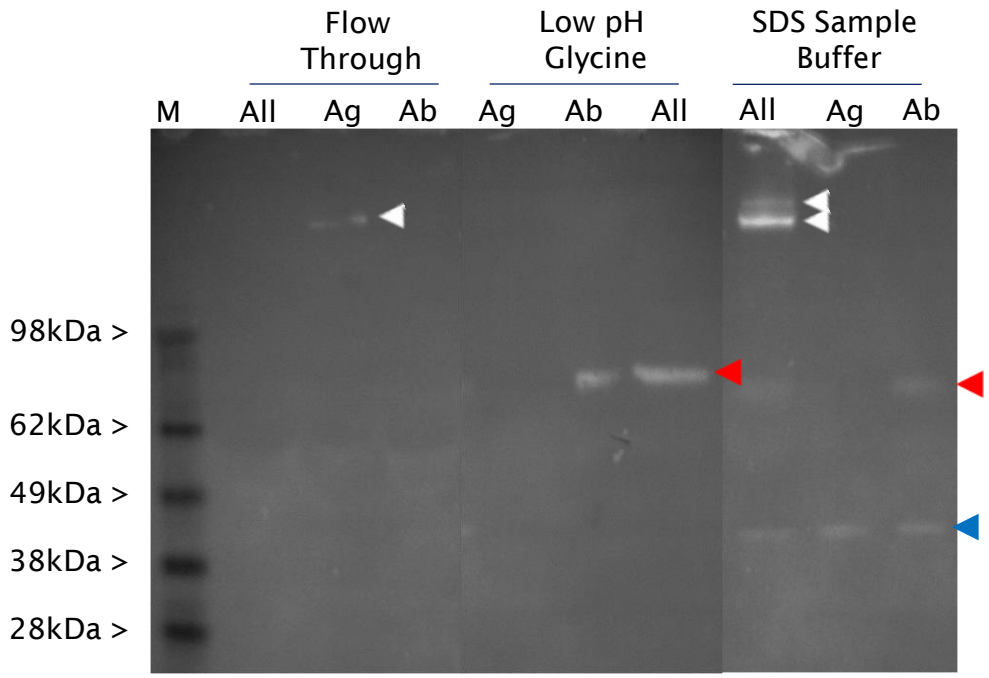

Figure 74: Western blot of Co-immunoprecipitation of $HTII_{280}$ in BALF. Protein L conjugated magnetic beads were incubated in antibody only (Ab), BALF only (Ag) or antibody and BALF (All). Unbound material (Flow Through), low pH eluted (Low pH Glycine) and proteins eluted in SDS loading buffer (SDS Loading Buffer) were analysed. $HTII_{280}$ (white arrow) was present in a small amount in unbound material. $HTII_{280}$ was retained on the beads during low pH elution but was eluted by SDS PAGE loading buffer. Small amounts of IgM were eluted (red arrow) by low pH glycine and SDS loading buffer. Recombinant protein L (blue arrow) was eluted by SDS PAGE loading buffer but not low pH-glycine.

UniProt Accession	Gene Name	Protein Name	Average Mass (Da)	Isoelectric Point
Q9UGM3	DMBT1	Deleted in malignant brain tumours 1 protein	268206	5.19
Q9Y490	TLN-1	Talin-1	271935	5.77

Table 25: Proteins recovered from $HTII_{280}$ co-IP and identified by MS. Proteins identified by only 1 peptide or that were smaller than 200 kDa were excluded. Theoretical average isoelectric point is given for the main chain of each protein (Compute pI/Mw tool, ExPASy[220]).

7.3.3 Cell Sorting

Anti-HTI_{56} and anti-$HTII_{280}$ antibodies were titrated using cells dissociated by elastase digestion. Cells were analysed by FACS and median fluorescent index (MFI) was recorded (Figure ??). Anti-HTI_{56} reached saturation with 0.05 µg/mL however, there also appeared to be some non-specific binding of the primary antibody as shown by isotype controls. Anti-$HTII_{280}$ did not reach saturation at the concentrations tested and there was no binding of isotype controls, indicating high specificity of the primary antibody.

Macrophage Fc receptors were blocked with human IgG_1; however, primary antibodies are

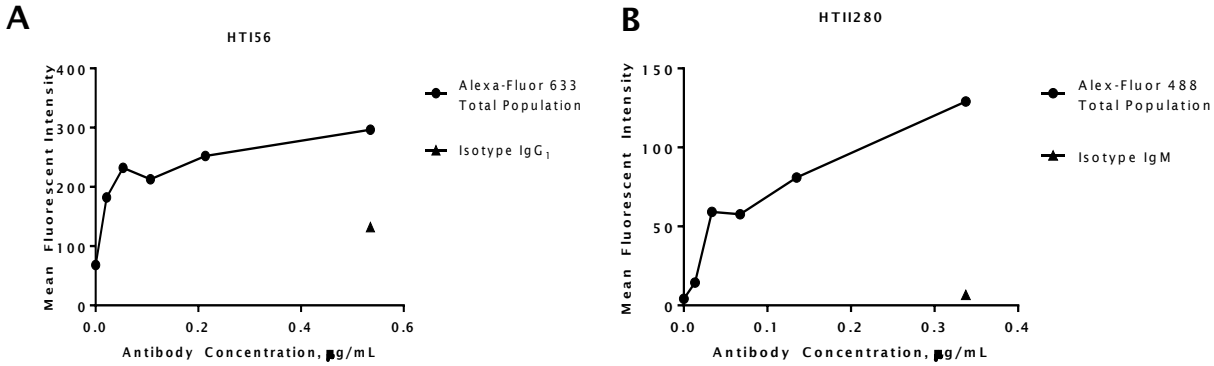

Figure 75: Titration of anti-HTI_{56} (A) and anti-$HTII_{280}$ (B). Cells were incubated with different concentrations of primary antibody, fluorescently labelled and analysed by FACS. An isotype control (triangle) was included at the highest concentration of primary antibody. Median fluorescent index of 10,000 cells was recorded.

mouse Ig. This could account for non-specific activity of mouse IgG_1 isotype control. To exclude macrophage from sorting, anti-human CD45 antibody conjugated to VioBlue was included in order to gate out all leukocytes (see Figure **??** for gating).

Cells were dissociated by either elastase or tryptic digestion of the extracellular matrix and CD45 negative cells sorted by FACS (Figure **??**).

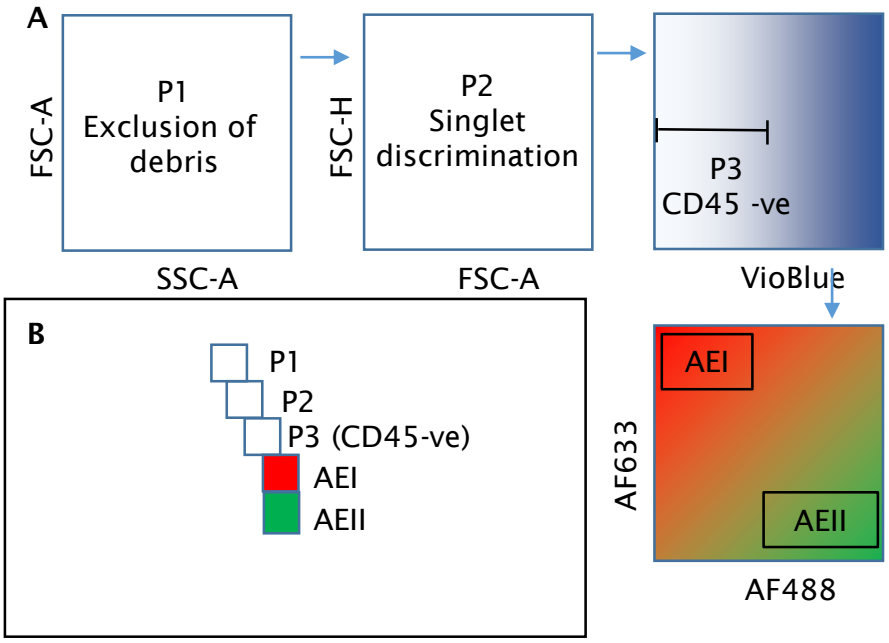

Figure 76: Gating strategy for sorting of AEI and AEII cells by FACS. Channels and plots used to define populations (A) are shown. Doublets and CD45 positive cells were excluded by gating. AEI and AEII cells were sorted by AF633 and AF488 fluorescence respectively. The gating hierarchy is shown (B). Labelled axis represent fluorescence intensity

Cells released by elastase digestion did not yield obvious populations of AF633 or AF488 (AEI and AEII) positive cells (Figure **??**). A population of cells weakly positive for AF633 was observed, confocal imaging showed these to have no-membrane localised staining and

lobed nuclei (Figure ??). Cells positive for AF488 did have membrane-localised staining although there was not enough sorted for further analysis.

Dissociation of cells using trypsin yielded a large population of AF488 that were sorted and an aliquot cytospun for confocal imaging (Figure ??) or fixed for TEM (Figure ??). From confocal analysis, these cells were estimated to be 93% AEII cells. Electron micrographs of the sorted cells showed that they contained lamella bodies indicative of AEII cells (Figure ??). Red blood cells were also visible by TEM. These would be removed during culture and therefore were not included in the yield approximation. There were very few AF633 positive cells and sorted cells all were spun onto glass slides for confocal microscopy showing no membrane localised staining. There was some leaking of DAPI into the cytoplasm suggesting these cells had lost integrity and DNA was leaking out of the nuclei. In these cases, red fluorescence was co-localised with cytoplasmic DAPI and may have been due to auto-fluorescence. The proportion of AEI and AEII cells sorted are given in Table ??.

Unsorted cells were also cytospun and observed by confocal microscopy (Figure ??). These showed an abundance of cells positive for AF488, and some were AF633 positive.

Elastase	Trypsin	
Events per 1000 AEI	7.5	0.006
Events per 1000 AEII	8.5	15.7

Table 26: Proportion of AEI and AEII cells yielded from two different enzymatic dissociations. Proportions are given as per 1000 of the total population of cells.

7.4 Discussion

7.4.1 Antibody Characterisation

Anti-HTI_{56} binds a single protein form lung homogenate, of approximately 56 kDa. Anti-$HTII_{280}$ bound a dimer of high molecular weight. The identity of the either target antigen is unknown, however, when detected by Western blot, $HTII_{280}$ bares striking similarity to glycoprotein 340 (GP-340 or deleted in malignant brain tumour-1, DMTB1)[294], which is known to be localised to the lung, amongst other epithelium.[294, 295]

To investigate further the identity of $HTII_{280}$, we used magnetic beads coupled to Protein-L to immunoprecipitate the target antigen with the aim of identifying it by MS. Western blotting (Figure ??) showed the capture of $HTII_{280}$ antigen was successful and was captured

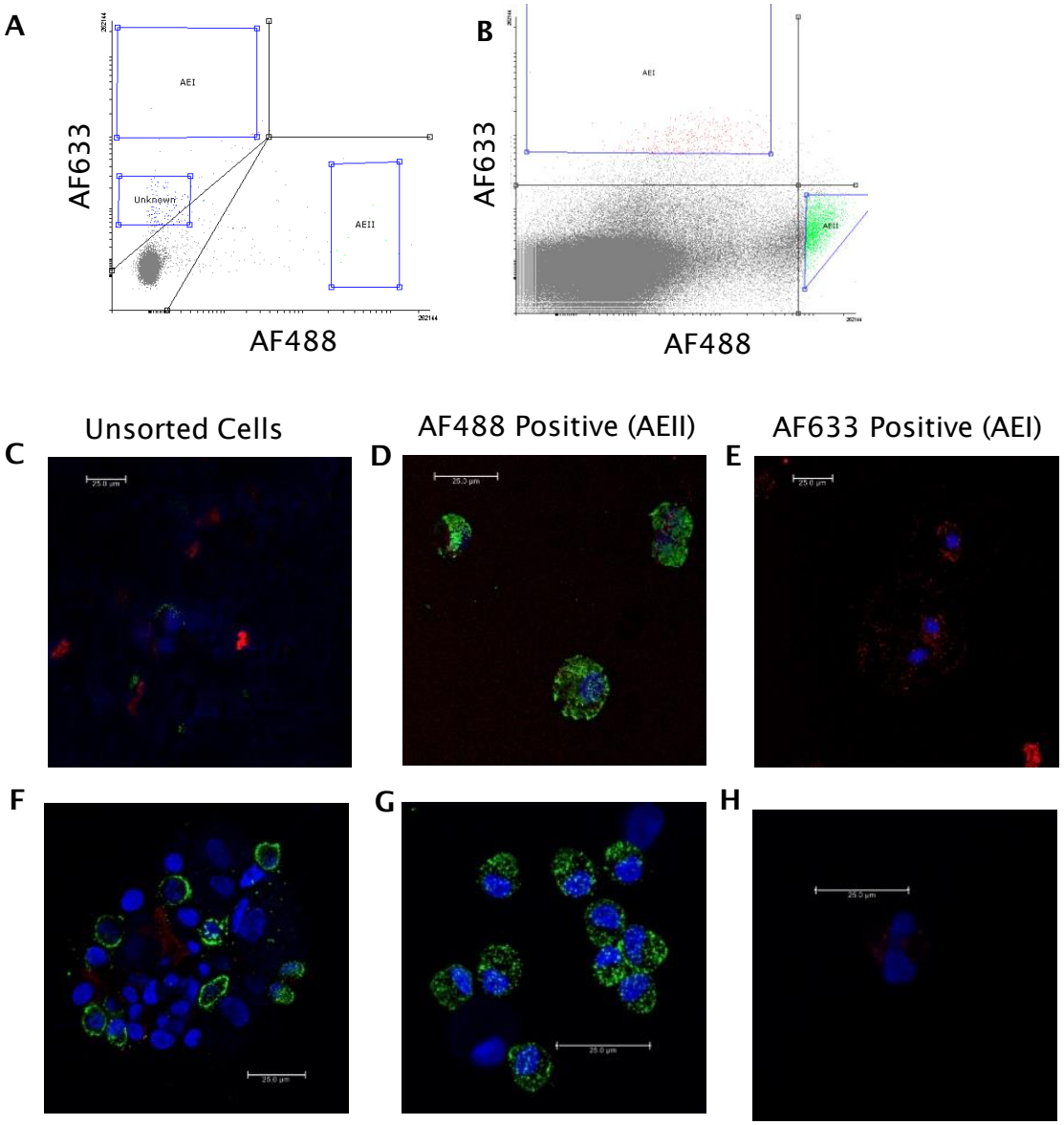

Figure 77: Cell sorting of AEI and AEII cells after elastase (A) or tryptic dissociation (B) are shown. Quadrats were set using isotype control and CD45+ cells were excluded. There was a small population of macrophage-like cells that separated following elastase digestion that were not present following trypsin protocol. Dissociation by trypsin produced a AF488 positive cell population (AEII) and a smear of AF633 positive cells (AEI) protruding from the main cluster. Unsorted (C, F) and sorted (D, E, G, H) cells from elastase (C-E) or trypsin (F-H) dissociation were imaged by confocal microscopy. Staining for both AEI and AEII cells were visible in unsorted cells (C, F). Both protocols produced AEI and AEII-like cells however the number of cells from trypsin digestion was much greater. AEI cells sorted by elastase (E) digestion had intact nuclei although the membrane was slightly disbanded – this is probably due to forces applied during cytospinning.

via antibody mediated binding. Low pH-glycine elution buffer was not sufficient to release $HTII_{280}$ from binding suggesting a high affinity between the antibody and the antigen, however under reducing and denaturing conditions, both the antibody and antigen were eluted from the beads. Mass spectrometry identified candidate proteins from SDS PAGE bands corresponding to $HTII_{280}$. After excluding proteins identified from only 1 peptide, MS yielded a total of 81 proteins (Supplementary 6) including albumin and SP-A which are

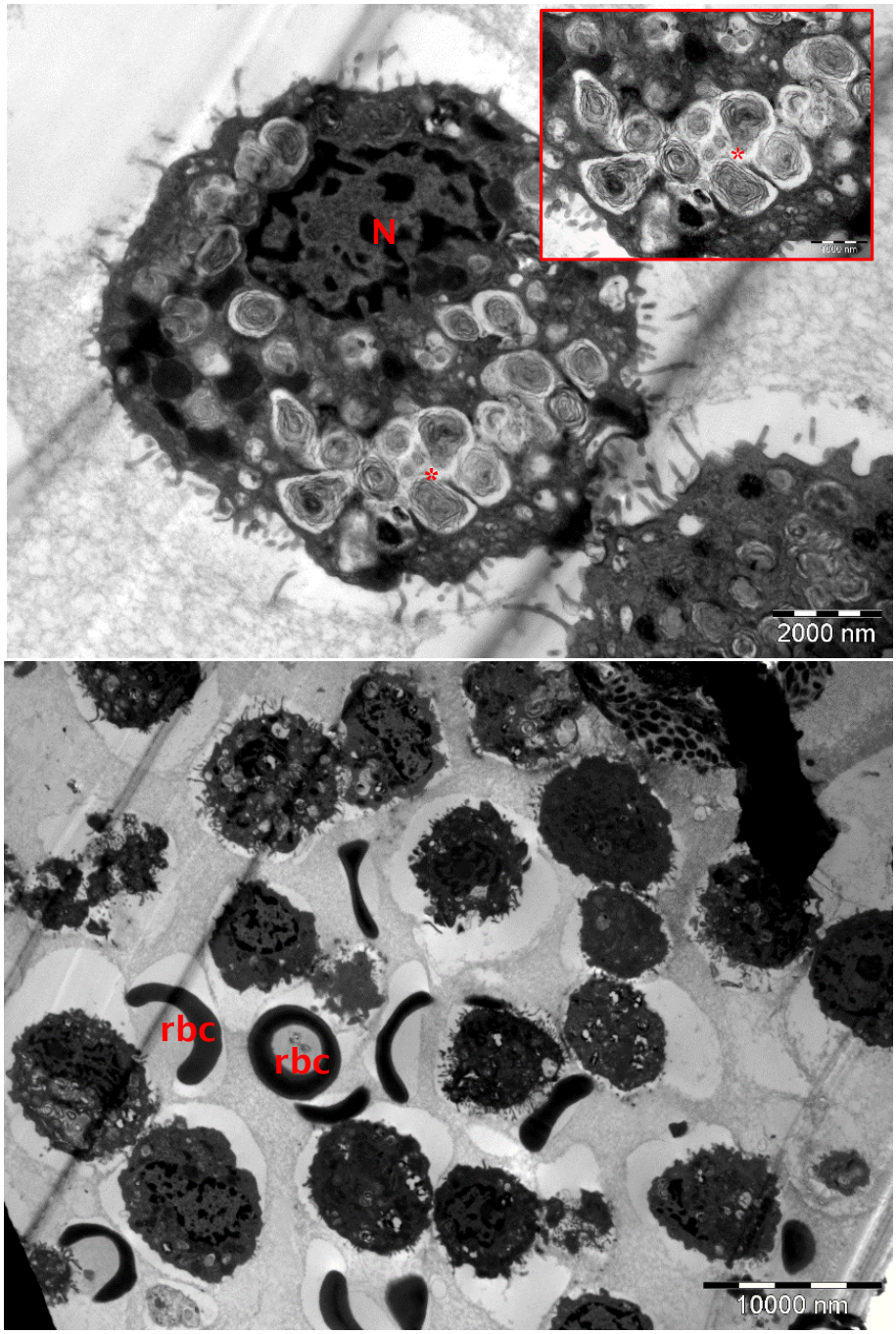

Figure 78: Transmission electron micrograph of AEII cells sorted by FACS. Cells had lamella bodies (A, marked with $*$) and microvilli (A, marked with). Red blood cells (rbc) were also co-sorted with AEII cells (B) however there were no other morphologically distinct cells present. Insert shows greater magnification.

most likely present through adsorption to the metallic bead surface. For that reason it is impossible to ascertain definite identification of the antigen through this method. Excluding proteins smaller than 200 kDa left two potential candidates: DMBT1 and Talin-1 of mass 268 kDa and 278 kDa respectively (Table **??**).

Talin-1 is involved in integrin-mediated cellular adhesion**??** and is expressed on the basal surface of pulmonary epithelial cells, as well as a range of tissue and cell types, including T-cells. Staining of AEII cells appears apically (Figure **??**) and therefore $HTII_{280}$ is unlikely

to be important for cellular adhesion. Furthermore, as Talin-1 is present on T-cells, which may be present in the lung following extravasation from the blood stream, it is unlikely to be specific to a single population of cells within the pulmonary system. Talin-1 may form a homo-dimer[296] which would not show as two distinct bands by Western blot as seen here (Figure **??**), however, it may be phosphorylated[297] at multiple sites and this could result in a similar banding by Western blot analysis.

DMBT-1 is a member of the scavenger receptor cysteine-rich superfamily of proteins whose function is related to innate immunity and epithelial cell differentiation[298] is known to bind SP-A[299] and D[300] and has both soluble and membrane-localised forms. DMBT1 has a theoretical isoelectric point (pI) of 5.19 which does differ from the value of 4.4 described by Gonzalez *et al.*[180] The antigen captured by anti-$HTII_{280}$ from BALF may be a soluble form of the protein, however it cannot be ruled out that it is there from small amounts of cellular tissue present in the BALF. DMBT1 has also been identified in BALF and shows a similar band-pattern by Western blot.[298] The similarity of molecular weight, dimerization and membrane or soluble localisation make DMBT1 a strong candidate for the identification of $HTII_{280}$. Whilst DMBT1 has been identified in number of tissues, unlike $HTII_{280}$, it can have a number of splice-varients,[298, 301] isoforms of which may be specific to epithelial membranes. Further investigation would be necessary to confirm this identification; IHC of lung tissue for DMBT1 may show localisation to $HTII_{280}$ or purification of $HTII_{280}$ and DMBT1 would permit *de novo* sequencing.

Anti-HTI_{56} and anti-$HTII_{280}$ antibodies have specificity towards AEI and AEII cells respectively. The reactivity of each antibody to cellular homogenate of a number of tissues has been assessed elsewhere and shown to be limited to the lung.[178, 180] Immunohistochemistry of lung tissue shows that the antibodies are specific to distinct cell types within the lung and we did not see specific cross-reactivity to other cell types (Figure **??**). Analysis of the antibody's affinity towards specific cell populations within the lung, such as macrophage and neutrophil which are highly abundant was not assessed however could be in the future by including a pan-leukocyte marker into the IHC fluorescent panel.

7.4.2 Isolation of AEI and AEII Cells

Two methods of dissociation were tried, a 'gentle' approach, using elastase to specifically target elastin fibres in underlying extracellular matrix and a 'rougher' approach with trypsin. Whilst a reduced yield was anticipated using elastase, it was hoped that the fragile

AEI cells may be preserved better. Both methods yielded AEI and AEII cells in unsorted samples (Figure **??**).

Titration of the anti-HTI_{56} and anti-$HTII_{280}$ was performed on cells dissociated from human lung tissue by elastase. MFI was recorded for the total population and isotype controls applied at the maximal concentration of primary antibody used. Anti-$HTII_{280}$ was not applied in excess at any of the concentrations tested as the MFI was still increasing at 0.3 µg/mL (Figure **??**). However, due to a limited amount of antibody available for this work, it was decided not to increase the concentration used. This provides room to improve the yield of AEII cells obtainable through this method through further optimisation. Isotype control for $HTII_{280}$ showed there was no non-specific binding of the primary antibody. Anti-HTI_{56} was assessed similarly (Figure **??**) and the MFI plateaued at approximately 0.2 µg/mL. Mouse IgG_1 was applied as an isotype control and showed a small amount of non-specific activity, which could be due to binding to endogenous Fc receptors. Human IgG was used as a blocking agent to minimise non-specific binding in this manner and to further moderate this, anti-CD45, a pan-leukocyte marker, was included to reduce the number of Fc receptors in the final sort.

Digestion by both methods resulted in cells stained for $HTII_{280}$ and HTI_{56} and isotype labelled samples were negative for HTI_{56} and $HTII_{280}$ by both FACS and confocal microscopy (Figure **??**). In particular with AEII cells, there was large increase in the proportion of cells yielded by trypsin dissociation compared with elastase digestion of the ECM – 0.1 % compared to 2.9%. AEI cells on the other hand fared better when dissociated by elastase, though the proportion of cells acquired were still very low (Table). Confocal imaging of AEI cells sorted by either method showed a 'splatter' of staining around a nucleus suggesting these cells had disintegrated – most likely due to the cytospinning. Gating for AEII were set very stringently to only allow sort the most positively stained cells and cells sorted on 'purity' mode – i.e. the number of cells was sacrificed over purity. Further work needs to be done to optimise this balance to achieve the highest yield with the least contamination. Regardless, enough AEII cells were acquired for analysis by TEM (Figure **??**) which showed a highly pure population of cells displaying multi-lamella bodies and micro-villi indicative of AEII cells.[302] As tissue was very limited, methods were continually developed, therefore there is only n of 1 for each enzymatic digestion.

Isolation of AEI and AEII cells by 'panning' (isolation of AEI and AEII cells by sequential selective adherence of cells to culture plates)[94] or gradient centrifugation[174] can yield both AEI and AEII cells. In the case of panning, the methodologies are very slow to yield

highly pure populations of AEII cells and, as with gradient centrifugation, yields and purity of AEI cells are poor (85% for gradient centrifugation).[174] Chen *et al.* have isolated AEI and AEII cells form rat lung by magnetic affinity cell sorting (MACS)[175], an analogous method using magnetic beads rather than fluorescence to sort cells. Here, a similar purity of AEII cells was achieved (93% vs 95%). MACS may offer a significant advantage over FACS for the isolation of AEI cells as cells are be immobilised in a magnetic field, rather than being exposed to high forces during centrifugation. Chen *et al.* were able to isolation 2.93 million AEI cells by this method using rat lung. However, the mass of tissue is much higher (250 g) compared with the amount used here – typically <5 g.

Optimisation of the dissociation is necessary to further improve the yield of AEI and AEII cells. The concentration of anti-HTI_{56} used was on the threshold of optimum as determined by titration (Figure **??**) and below optimum for anti-$HTII_{280}$. A balance between yield and selectivity of the enzymes may be achieved through a mixture of trypsin-elastase.[303] Yield may also be increased through sorting the cells in 'yield' which is not as stringent as 'purity' and could be used as an enrichment, prior sorting in 'purity.'

7.4.3 Conclusions and Future Work

HTI_{56} and $HTII_{280}$ appear to be highly specific to AEI and AEII cells in the lung. The identification of $HTII_{280}$ by co-IP and MS yielded two potential candidates, DMBT1 and Talin1. Further work is required to confirm its identity definitively. This may be difficult as the number of splice-variants of DMBT1 could leave to false negatives when analysing by Western blot with commercial antibodies. Purification of the target antigen by a higher through-put method, such as MACS, followed by de novo sequencing may be a good approach. This method could also be applied to identifying HTI_{56}.

FACS offers a relatively quick method for the isolation of human lung epithelial cells. It was possible to isolate AEII cells by this method, and with further optimisation, such as antibody concentration and digestion, it may be possible to further improve the yield. Factors such as age and the time since surgery may be important factors in isolating epithelia; analysis of this was not possible here given the low n numbers.

Cell culture and longitudinal analysis of their *in vitro* phenotype was not carried out owing to time, antibody and tissue availability. There are a number of papers discussing the culture of human AEII cells (Section **??**) and minimising their conversion towards an AEI phenotype. Given the poor acquisition of AEI cells, the study of AEI cells using

AEII-differentiated models may be an alternative.

8 Summary and Future Work

8.1 Summary and Future Work

8.1.1 Interactions of Nanoparticles with Epithelial Lining Fluid

The aim of this work was to investigate the effect of the protein corona on the immune function of human lung cells, in particular AEI and AEII cells. Throughout the course of this project, it became very apparent that the protein corona studies performed to date do not accurately reflect the interactions of particles with pulmonary fluids. Primarily, this is due to the presence of the highly lipidascious pulmonary surfactant layer, through which particles must pass prior to reaching the more aqueous environment and epithelial cell surface beneath. To fully characterise the NP surface and hence mechanisms behind their interaction with cells, it is important to consider their entire corona – both lipid and protein. Therefore, the research focus has shifted emphasis towards characterising the bio-corona formed around particles following their incubation in pulmonary epithelial lining fluid.

Initial studies into the protein corona from BALF-incubated particles showed that when considering only the uniquely bound proteins, compared to another particles, there were some differences in the average biophysical properties of the proteins. For instance, proteins uniquely bound to aPS particles contained a greater proportion of theoretical β-sheet regions compared to TiO_2 and cPS particles. However, when considering all the proteins, these differences were almost entirely negated.

When considering particles suspended in BALF over time, there was no difference between the biophysical properties of the corona at 15 minutes or 120 minutes on cPS or aPS particles, showing that proteins bind rapidly, and a stable corona forms almost immediately.

It is only a small number of proteins that contribute to an entire corona, with 20% of the bound proteins accounting for 50-60% of the total protein bound to a particle. These proteins are not necessarily the most abundant protein in BALF, suggesting that there is some property of the proteins that is driving the protein-particle interactions. Further work is needed to elucidate what drives these interactions. For example, circular dichroism can elucidate protein structures via the absorbance of polarised light at specific wave lengths. This was experimented with using diluted BALF to discover if there were changes, on average, to the protein structures upon binding to particles. However, with the resources available, this was not possible. The experiment would be interesting to perform, either with whole BALF, or with the most abundant proteins identified from this study.

The bound proteins included surfactant-associated proteins. In particular SP-A was bound in high abundance (top 10 on all particles) and this may have effects on pulmonary surfactant function *in vivo*. It would be interesting investigate the functional role these proteins may have on the cell's surface. For instance does the affinity of the particles towards the phospholipids change when coated in protein known to interact with phospholipids? It may be possible to examine such specific interactions with surface plasmon resonance (SPR) or force microscopy. This experiment would yield both information regarding the functionality of the proteins once they are absorbed on the particle surface, and potential interaction between particles and pulmonary surfactant or cell membranes.

The corona of aPS and cPS particles was measured over time. These particles were chosen since they represented very different surface chemistries. In solution, their stability differed; aPS particles were stabilised when incubated in BALF and cPS particles remained agglomerated. The inverse was true for PBS suspended particles. This suggests very different interactions with the solutes in each solution and therefore would give the largest difference in terms of the corona. However, upon analysing the coronas of these two particles over time, there was no change in either the composition of each, or the average surface properties. The corona therefore forms stably within the first 15 minutes of incubation and does not change in solution over time.

Upon inhalation, particles reaching the lung alveoli will first encounter pulmonary surfactant. We have observed that aPS and TiO_2 particles are capable of increasing the surface tension of this layer during compression-spreading cycles using a porcine-derived pulmonary surfactant, Curosurf^{TM}. Furthermore, it was demonstrated by density-gradient centrifugation that there are strong interactions between the particles and the lipid component of Curosurf^{TM}. The interactions were further confirmed by electron microscopy, showing that particles were agglomerated with lipids and the formation of structures that were not present in surfactant on its own.

Analysis of the lipid composition of Curosurf^{TM} and the lipids that interact with particles showed that there was more phosphocholine (PC) species bound to the particles compared to phosphoglycerol (PG) species. However, in relation to Curosurf^{TM}, there was enrichment for the charged lipid species, PG, on all PS particles, with aPS having significantly lower PC:PG ratio (therefore proportionally a greater amount of PG) compared to cPS or uPS particles.

Since aPS particles are more likely to carry a positive charge than cPS or uPS particles, it is possible that this is due to charge-mediated interactions between the negatively charged head group of PG and the aPS particles. Further work to confirm this hypothesis using high or low pH values was carried out to shift the equilibrium of $[DPPC]H^+$ and $[DPPC]^- + H^+$, and the amount of particle-bound DPPC was detected by MS. These experiments were inconclusive because changes in detected DPPC were found in both sample and controls, which may be due to efficiency of lipid-extraction or transfer efficiency into the MS. With further optimisation, this experiment may yield valid results. It may be better to use a sample of only DPPC, rather than Curosurf^{TM} that contains many different components and, after washing, neutralisation of the solutions prior to lipid extraction may negate differences in extraction/transfer efficiency. The binding affinity could also be studied using biophysical techniques such as SPR to investigate binding under different pH values.

Interactions of TiO_2 particles with Curosurf^{TM} showed no enrichment for PG as observed with PS particles. Therefore the mechanisms for interrupting pulmonary surfactant are potentially different to disruption from aPS particles. The differences here may be explained by the size (14 nm versus 100 nm diameter for PS particles), surface chemistry or shape. The effect of particle shape on the interactions can be studied using nanofabricated polyethyleneglycol hydrogel particles that can be produced in various shapes from the same material.[3]

All particles caused a small increase in mitochondrial activity at low concentrations in TT1 and A549 cells to some extent, either as bare particles or BALF-coated. This is interesting, particularly as there was little increase in ROS or pro-inflammatory cytokines detected and, in TT1 cells, less protein was yielded following exposure to aPS particulates. A reduced rate of cell division is reported in the literature following exposure to aPS particles and this suggests the cells are stressed in some manner by the particles. This could explain the reduced yield of protein since fewer cells may be harvested following particle exposure, however there was no difference between the number of cells after treatment in samples or controls and nor it does explain the increased mitochondrial activity. One hypothesis is that it is due to increased endocytosis and vesicle transport. The uptake of particles was to be investigated here in a number of cell types by CARS. Unfortunately, whilst the samples were prepared, they could not be analysed. This experiment is an important next step in this investigation and would help explore this hypothesis further by looking for correlation between particle uptake and mitochondrial activity.

Experiments investigating the expression of proteins from whole cell lysate go some way in

supporting this hypothesis as there was enrichment for changes in proteins relating to vesicle transport. Although a more detailed pathways analysis of these proteins was not possible, this may help to elucidate more specific reactions of the cells.

Ideally, the analysis of whole cell lysate from TT1 cells exposed to aPS particles would have been better performed at the beginning of this investigation rather than the end. With a greater number of treatments and repeats the experiments would have provided a platform to generate testable hypotheses. As performed, the experiment provided some very valuable information. There was no evidence of apoptosis within the cells from pathway analysis and no increase in caspases was observed between aPS-treated and non-treated cells, which is in alignment with MTT assays at the same concentration. It was evident that the cellular response from exposed TT1 cells was actually relatively narrow with very few pathways found to be altered. Overall, there was very little difference between the cells' response to BALF-coated or uncoated aPS particles. For BALF-coated, the enrichments were slightly more significant. Pathway enrichment was only observed for BALF-coated aPS particles, with vesicle cycling being highly statistically significant. Pathways for mRNA processing was also statistically enriched for down regulated proteins within these samples and this supports observations of decreased protein production, since enriched protein were down regulated.

In vivo, alveolar epithelial cells are beneath a layer of pulmonary surfactant and therefore particles need to translocate through this layer prior to reaching the underlying cells. A limitation in this experiment is the absence of this layer. As demonstrated earlier, the particles very rapidly acquire a 'lipid-corona' when incubated in Curosurf^{TM}, therefore we would expect this to occur *in vivo* prior to the particles reaching the underlying epithelium. The experiments performed here in BALF may help to mimic this to some degree as it contained both proteins and surfactant lipids. However, as judged by the protein and lipid quantification assays used here, the concentration of protein vastly exceeds the lipid component. Two questions arise from this. Firstly what is the effect of lipids on the formation of a protein corona? Secondly what is the effect of the presence of pulmonary surfactant on the cellular effect of NPs?

An experiment to examine particle uptake in TT1, A549 and THP-1 cells was prepared for examination by coherent anti-Stokes Raman scattering (CARS). As mentioned earlier, due to unfoseen circumstances, these samples could not be analysed. The experiment was designed to examin the effect the effect of both the protein and lipid corona on NP uptake. Both AEII cells and alveolar macrophage actively internalised pulmonary surfactant, the

strong interaction between particles and pulmonary surfactant observed here may further the uptake of the particles into these cell types.

As discussed, the ubiquitous protein corona on the particles is largely identical and therefore independent of the particle core or surface modification. It can therefore be considered a constant between all particles. However, NPs entering the alveolus with firstly have to pass through pulmonary surfactant and therefore may have a lipid corona prior to interactions with proteins. It has not been investigated here if the protein corona can displace lipids already adsorbed to the particle surface. This would be technically challenging using the methods developed for this investigation. Indeed a preparatory experiment was performed whereby NPs were isolated from Curosurf^{TM} and adsorbed lipids measured before and after incubation in BALF however the experimental set up was not sensitive enough to measure any changes (data not shown). Uptake of NPs by CARS could investigate this at a cellular level. Samples were prepared, where particles were incubated in Curosurf^{TM} followed by increasing concentrations of BALF before cellular exposure. Uptake was to be measured after multiple time points. It is a shame this experiment could not be analysed. However, it could be an exciting experiment for future work.

8.1.2 Isolation of Primary AEI and AEII Cells

The isolation of human AEI and AEII cells from primary tissue is difficult. The yield of AEII cells is often very low and AEI cells do not survive following the digestion of extra-cellular matrix. The time taken to isolate the cells using conventional methods can be days to get a pure population. Furthermore, de-differentiation of AEII cells occurs within a few days and therefore the window of opportunity for experimentation is limited. The lag time between surgery and cell isolation can vary and meaningful results can be difficult to reproduce. Therefore, I aimed to improve upon this, by applying antibodies specifically against human AEI or AEII cells and sorting the cells by FACS with fluorescence labels against the cell-targeted antibodies.

This approach has been used similarly in rats with equivalent antibodies against rat AEI and AEII cells.[176] The same group raised the antibodies against human AEI and AEII cells and have shown that human AEII cells can be isolated using this methodology with FACS.[180] However, there are no published results for the isolation of human AEI and AEII cells simultaneously from human tissue.

By using this method, the isolation of AEII cells was possible, yielding a population of AEII

cells at least 93% pure. With further optimisation of the digestion protocol, I am confident this could be increased. Whilst there were FACS events recorded for AEI cell positive staining, no intact cells were detected by cytospinning. The use of elastase rather than trypsin generated a greater number of hits for AEI antibody-stained cells, however it was not possible to visualise these cells microscopically since they did not survive cytospinning. Therefore it is not clear if the AEI cells survive the isolation or not. If a good yield of AEI-type cells could be acquired, then it would be possible to allow these cells to adhere to cell culture flasks and image them by fluorescence microscopy.

The procedure suffered from poor yields of AEII cells in comparison to other methods that use a stronger cocktail of enzymes, however these methods are not aimed at getting both AEI and AEII cells simultaneously. A two-step digestion could be the solution, firstly using elastase to target AEI cells, followed by further isolation of cells with trypsin to yield more AEII cells.

The surface antigen for the antibodies used here is unknown. I investigated the antigen for the AEII specific antibody $HTII_{280}$ by co-immunoprecipitation and MS analysis. The results showed that DMBT1 was a likely candidate, and this was further supported by the similarity between western blots stained with $HTII_{280}$ and DMBT1 antibody. DMBT1 has multiple splice variants and therefore careful validation is required; this may be possible by western blot, using DMBT1 antibody to inhibit the binding of AEII and *vice-versa*. A further validation can be performed from the use of purified DMBT1 protein for cross reactivity with $HTII_{280}$, but care has to be taken that the correct splice variant of DMBT1 is used.

8.2 Conclusions

8.2.1 Research Aim: Isolate AEI and AEII Cells from Human Lung Tissue and Develop Primary Cell Culture

I was able to isolate both AEI and AEII cells, although only AEII cells maintained cellular integrity. This was achieved via a novel and simplified approach to their isolation that greatly reduced the time needed to isolate such cells into a pure population. Further optimisation is required to generate higher yielding isolates and no primary cell culture of these cells was developed.

The primary antibody directed against AEII cells, $HTII_{280}$ may be directed against

DMBT1 or Talin 1 on the cell surface.

8.2.2 Research Aim: Determine and Characterise the Protein Corona when Particles are Incubated with Human Lung Lavage

All particles used were characterised fully by a number of complementary techniques. All particles were observed to agglomerate in BALF, except for aPS particles which despite forming large agglomerates initially, stabilised over time. Size changes of particles incubated in BALF are consistent with agglomeration and protein-binding. Particle agglomeration was with weak association as they collapsed during atomic force microscopy.

A full characterisation of the proteins bound to particles was performed. There was little difference between the average physiochemical properties of the bound proteins between any particles. The protein corona formed stably after only 15 minutes with little change in the physiochemical or protein-identity of the bound component over time. Some protein abundances changed over time, but no link between the protein dynamic and the physio-chemical properties of the proteins was determined.

The proteins bound to BALF-incubated particles were not necessarily the most abundant proteins, suggesting there is a property of the protein, be it function or physiochemical property that was not picked up here. This may be due to nature of such analysis which looks at the average of a large population of proteins.

A large proportion of the corona was made up of the same proteins and these were common across all particles investigated, suggesting that there is a subset of proteins with high affinity and these may have a more significant role in defining the particle-cell interactions than others. A number of surfactant-associated proteins were bound to the particles; in particular surfactant protein-A was bound in high concentration. This suggests there could be a physiological effect of the particles due to the sequestration of surfactant proteins that have essential roles in both pulmonary surfactant recycling and spreading and innate immunity.

This aim was expanded to include the lipid-interactions of the particles. The major phospholipid components of pulmonary surfactant (Curosurf^{TM}) were observed to bind to all NPs tested. With polystyrene particles, this interaction could, in part be charge mediated via surface groups on the nanoparticles and charged head groups of phospholipids and by hydrophobicity between the lipid-tail and particle surface.

Both TiO_2 and aPS particles have a detrimental effect on the spreading of pulmonary surfactant and limit its ability to reduce surface tension *in vitro*. Since they bind different proportions of surfactant components, this is likely via different mechanisms.

8.2.3 Research Aim: Determine the Effect of the Protein Corona on AEI and AEII Cells from the Perspective of their Pro-Inflammatory Response

Cationic particles are toxic to A549 and TT1 cells, model cells lines for AEII and AEI cells respectively. No toxicity was observed for cPS, uPS or TiO_2. However, at low concentrations, all particles induce increased mitochondrial activity in both cell lines. The degree of reaction is dependent upon the surface corona with bare uPS and cPS particles causing a greater response when uncoated and TiO_2 causing a greater response when the particles are prior incubated in BALF.

The cause of this increase was not determined. There was no statistically significant change in IL-6 or IL-8 in A549 cells exposed to PS nanoparticles. Whilst there was a slight increase in IL-6 and IL-8 following exposure to low concentrations of uncoated aPS or uPS particles, this is unlikely to be biologically significant. Similarly, there was no significant increase in TNFR1, however there were slight increases following exposure to uncoated aPS particles. This is worth investigating further since it may represent the potential for these cells to react to inflammatory responses.

TiO_2 and cPS particles may be capable of inducing ROS in alveolar macrophages (THP-1 cell line). No changes in intracellular ROS was observed in THP-1 cells following exposure to uPS particles, and a decrease was observed for aPS particles. High variation in the experimental procedure make these results difficult to interpret and further replicates are required to draw firm conclusions.

Whilst aPS particles were observed to reduce mictochondrial activity, they do not directly lyse red blood cells, which act as a model for cell lysis. On the other hand, cPS and uPS particles are capable of causing red blood cell lysis although were not observed to be toxic to A549 or TT1 cells. Cell lysis was prevented by pre-incubating the particles in BALF. Therefore, the rapid formation of a protein corona *in vivo* would protect against such mechanical toxicity.

Proteomic changes were investigated for TT1 cells exposed to subtoxic (1 cm^2/mL) aPS particles. At this concentration of aPS particles, there was an increase in mitochondrial activity when exposed to coated particles compared to non-coated particles. Protein with

altered abundance from cells exposed to BALF-coated particles were significantly enriched for pathways for vesicular transportation, calcium reabsorption and splicesome. There was no significant enrichment for pathways from cells exposed to uncoated aPS particles. There was similar enrichment for both treatments for cellular location, with proteins known to localise to vesicles enriched in both treatment groups.

Protein production is reduced in TT1 cells exposed to sub-toxic concentrations of aPS particles. This further correlates with decrease in abundance of proteins relating to translation.

8.2.4 Final Remarks and Key Finding

Airborne nano-particulates have been linked, through epidemiological studies, to a range of diseases. In a recent study chaired by Professor Stephen Holgate, University of Southampton[40], the risk to health has been highlighted, and particles generated from many types of combustion both within the home and in urban streets have been implicated. Despite this, many airborne particles do not induce cell death or oxidative pathways *in vitro* and therefore the mechanism through which they are harmful to health is largely unknown.

Here, we have shown that two types of particles, aminated polystyrene and the common industrially produced particle TiO_2, are capable of inhibiting pulmonary surfactant, through both reduction in its ability to reduce surface tension and by binding to key surfactant constituents. Thus effects of particles to health may be indirect, via their effects on pulmonary surfactant rather than their direct effect on cells. Interactions between proteins and nanoparticles occurs independently of surface modifications for particles, whereas lipids may interact with specific surface groups to oppositly charged phospholipids on their surface.

Appendicies

For supplementary data, please see the List of Accompanying Materials (page **??**) attached CD-ROM or contact the author for an online version of the supplementary data.

References

1. Commission, E. Commission Recommendation of 18 October 2011 on the definition of nanomaterial. *Official Journal of the European Union* **54,** 38–40 (2011).
2. Lundqvist, M. *et al.* Nanoparticle size and surface properties determine the protein corona with possible implications for biological impacts. *Proceedings of the National Academy of Sciences of the United States of America* **105,** 14265–70. ISSN: 1091-6490 (Sept. 2008).
3. Gratton, S. E. a. *et al.* The effect of particle design on cellular internalization pathways. *Proceedings of the National Academy of Sciences of the United States of America* **105,** 11613–8. ISSN: 1091-6490 (Aug. 2008).
4. Albanese, A., Tang, P. S. & Chan, W. C. W. The Effect of Nanoparticle Size, Shape, and Surface Chemistry on Biological Systems. *Annual review of biomedical engineering* **14,** 1–16. ISSN: 1545-4274 (Apr. 2012).
5. McCarthy, H. O. *et al.* Development and characterization of self-assembling nanoparticles using a bio-inspired amphipathic peptide for gene delivery. *Journal of controlled release : official journal of the Controlled Release Society* **189,** 141–9. ISSN: 1873-4995 (Sept. 2014).
6. Mahon, E., Salvati, A., Baldelli Bombelli, F., Lynch, I. & Dawson, K. a. Designing the nanoparticle-biomolecule interface for "targeting and therapeutic delivery". *Journal of controlled release : official journal of the Controlled Release Society* **161,** 164–74. ISSN: 1873-4995 (July 2012).
7. Almeida, J. P. M., Chen, A. L., Foster, A. & Drezek, R. In vivo biodistribution of nanoparticles. *Nanomedicine (London, England)* **6,** 815–35. ISSN: 1748-6963 (July 2011).
8. Buzea, C., Pacheco, I. I. & Robbie, K. Nanomaterials and nanoparticles: sources and toxicity. *Biointerphases* **2,** MR17–71. ISSN: 1559-4106 (Dec. 2007).
9. Waychunas, G. A. *et al.* Natural Nanoparticle Structure, Properties and Reactivity From X-Ray Studies. *JCPDS-International Centre for Diffraction Data,* 41–49 (2009).
10. Wang, P. *et al.* Highly Efficient Visual Detection of Trace Copper(II) and Protein by the Quantum Photoelectric Effect. *Analytical chemistry* **85,** 8735–40. ISSN: 1520-6882 (Sept. 2013).
11. Courty, S. & Dahan, M. Tracking Individual Membrane Proteins Using Quantum Dots. *Cold Spring Harbor protocols* **2013.** ISSN: 1559-6095. doi:10.1101/pdb.prot078196. <http://www.ncbi.nlm.nih.gov/pubmed/24086060> (Jan. 2013).
12. Ahmed, S. R. *et al.* Quantum dots incorporated magnetic nanoparticles for imaging colon carcinoma cells. *Journal of nanobiotechnology* **11,** 28. ISSN: 1477-3155 (Aug. 2013).
13. Zhang, Y. *et al.* Highly luminescent, fluorinated semiconducting polymer dots for cellular imaging and analysis. *Chemical communications (Cambridge, England)* **49,** 8256–8. ISSN: 1364-548X (Aug. 2013).
14. Dames, P. *et al.* Targeted delivery of magnetic aerosol droplets to the lung. *Nature nanotechnology* **2,** 495–9. ISSN: 1748-3395 (Aug. 2007).
15. Rytting, E., Nguyen, J., Wang, X. & Kissel, T. Biodegradable polymeric nanocarriers for pulmonary drug delivery. *Expert opinion on drug delivery* **5,** 629–39. ISSN: 1742-5247 (June 2008).
16. Kurmi, B. D., Kayat, J., Gajbhiye, V., Tekade, R. K. & Jain, N. K. Micro- and nanocarrier-mediated lung targeting. *Expert opinion on drug delivery* **7,** 781–94. ISSN: 1744-7593 (July 2010).

17. Irngartinger, M., Camuglia, V., Damm, M., Goede, J. & Frijlink, H. W. Pulmonary delivery of therapeutic peptides via dry powder inhalation: effects of micronisation and manufacturing. *European journal of pharmaceutics and biopharmaceutics : official journal of Arbeitsgemeinschaft für Pharmazeutische Verfahrenstechnik e.V* **58,** 7–14. ISSN: 0939-6411 (July 2004).

18. Jensen, D. K. *et al.* Design of an inhalable dry powder formulation of DOTAP-modified PLGA nanoparticles loaded with siRNA. *Journal of controlled release : official journal of the Controlled Release Society* **157,** 141–8. ISSN: 1873-4995 (Jan. 2012).

19. Hickey, A. J., Misra, A. & Fourie, P. B. Dry powder antibiotic aerosol product development: inhaled therapy for tuberculosis. *Journal of pharmaceutical sciences* **102,** 3900–7. ISSN: 1520-6017 (Nov. 2013).

20. Tsuzuki, T. Commercial scale production of inorganic nanoparticles. en. *International Journal of Nanotechnology* **6,** 567. ISSN: 1475-7435 (2009).

21. Oberdörster, G., Oberdörster, E. & Oberdörster, J. Nanotoxicology: An Emerging Discipline Evolving from Studies of Ultrafine Particles. *Environmental Health Perspectives* **113,** 823–839. ISSN: 0091-6765 (Mar. 2005).

22. *Understanding Particle Pollution* 2015. <https://www3.epa.gov/airtrends/aqtrnd04/pmreport03/pmunderstand%7B%5C_%7D2405.pdf> (visited on 03/09/2016).

23. Kittelson, D. *Recent Measurements of Nanoparticle Emissions from Engines* in *Current Research on Diesel Exhaust Particles Japan Association of Aerosol Science and Technology* (Tokyo, 2001). <http://www.me.umn.edu/centers/mel/reports/JAASTpaper.pdf>.

24. Evelyn, A., Mannick, S. & Sermon, P. A. Unusual Carbon-Based Nanofibers and Chains among Diesel-Emitted Particles. *Nano Letters* **3,** 63–64. ISSN: 1530-6984 (Jan. 2003).

25. Samet, J. M., Dominici, F., Curriero, F. C., Coursac, I. & Zeger, S. L. Fine particulate air pollution and mortality in 20 U.S. cities, 1987-1994. *The New England journal of medicine* **343,** 1742–9. ISSN: 0028-4793 (Dec. 2000).

26. Pope, C. A. *et al.* Cardiovascular mortality and long-term exposure to particulate air pollution: epidemiological evidence of general pathophysiological pathways of disease. *Circulation* **109,** 71–7. ISSN: 1524-4539 (Jan. 2004).

27. Jedrychowski, W. A. *et al.* Effect of prenatal exposure to fine particulate matter on ventilatory lung function of preschool children of non-smoking mothers. *Paediatric and perinatal epidemiology* **24,** 492–501. ISSN: 1365-3016 (Sept. 2010).

28. Laden, F., Neas, L. M., Dockery, D. W. & Schwartz, J. Association of fine particulate matter from different sources with daily mortality in six U.S. cities. *Environmental health perspectives* **108,** 941–7. ISSN: 0091-6765 (Oct. 2000).

29. Raaschou-Nielsen, O. *et al.* Air pollution and lung cancer incidence in 17 European cohorts: prospective analyses from the European Study of Cohorts for Air Pollution Effects (ESCAPE). *The Lancet. Oncology* **14,** 813–22. ISSN: 1474-5488 (Aug. 2013).

30. Powers, C. M., Yen, J., Linney, E. A., Seidler, F. J. & Slotkin, T. A. Silver exposure in developing zebrafish (Danio rerio): Persistent effects on larval behavior and survival. *Neurotoxicology and Teratology* **32,** 391–397. ISSN: 08920362 (May 2010).

31. De Nicola, F. *et al.* A multi-approach monitoring of particulate matter, metals and PAHs in an urban street canyon. *Environmental science and pollution research international* **20,** 4969–79. ISSN: 1614-7499 (July 2013).

32. Laden, F., Schwartz, J., Speizer, F. E. & Dockery, D. W. Reduction in fine particulate air pollution and mortality: Extended follow-up of the Harvard Six Cities study. *American journal of respiratory and critical care medicine* **173,** 667–72. ISSN: 1073-449X (Mar. 2006).

33. *Air Quality Standards* <http://ec.europa.eu/environment/air/quality/standards.htm> (visited on 06/17/2015).

34. Sioutas, C., Delfino, R. J. & Singh, M. Exposure assessment for atmospheric ultrafine particles (UFPs) and implications in epidemiologic research. *Environmental health perspectives* **113,** 947–55. ISSN: 0091-6765 (Aug. 2005).

35. Shi, J. P., Evans, D. E., Khan, A. & Harrison, R. M. Sources and concentration of nanoparticles (¡10nm diameter) in the urban atmosphere. *Atmospheric Environment* **35,** 1193–1202. ISSN: 13522310 (Jan. 2001).

36. Woo, K. S., Chen, D. R., Pui, D. Y. H. & McMurry, P. H. Measurement of Atlanta Aerosol Size Distributions: Observations of Ultrafine Particle Events. en. *Aerosol Science & Technology.* <http://www.tandfonline.com/doi/abs/10.1080/02786820120056%7B%5C#%7D.VynN3%7B%5C_%7DkrLIU> (Nov. 2010).

37. Wick, P. *et al.* Barrier capacity of human placenta for nanosized materials. *Environmental health perspectives* **118,** 432–6. ISSN: 1552-9924 (Mar. 2010).

38. Johnston, B. D. *et al.* Bioavailability of nanoscale metal oxides TiO(2), CeO(2), and ZnO to fish. *Environmental science & technology* **44,** 1144–51. ISSN: 0013-936X (Feb. 2010).

39. Glinianaia, S. V., Rankin, J., Bell, R., Pless-Mulloli, T. & Howel, D. Particulate air pollution and fetal health: a systematic review of the epidemiologic evidence. *Epidemiology (Cambridge, Mass.)* **15,** 36–45. ISSN: 1044-3983 (Jan. 2004).

40. Holgate, S. *et al. Every breath we take: the lifelong impact of air pollution* tech. rep. (Royal College of Physicians, 2016). <file:///C:/Users/Harry/Downloads/Air%7B%5C_%7Dpollution%7B%5C_%7Dmain%20report%7B%5C_%7DWEB%7B%5C_%7D1%7B%5C_%7D0.pdf>.

41. Yoo-Iam, M., Chaichana, R. & Satapanajaru, T. Toxicity, bioaccumulation and biomagnification of silver nanoparticles in green algae (¡I¿Chlorella¡/I¿ sp.), water flea (¡I¿Moina macrocopa¡/I¿), blood worm (¡I¿Chironomus¡/I¿ spp.) and silver barb (¡I¿Barbonymus gonionotus¡/I¿). *Chemical Speciation and Bioavailability* **26,** 257–265. ISSN: 09542299 (Nov. 2014).

42. Lee, J. H. *et al.* Biopersistence of silver nanoparticles in tissues from Sprague-Dawley rats. *Particle and fibre toxicology* **10,** 36. ISSN: 1743-8977 (Jan. 2013).

43. Karakoti, A. S. *et al.* Nanoceria as Antioxidant: Synthesis and Biomedical Applications. *JOM (Warrendale, Pa. : 1989)* **60,** 33–37. ISSN: 1047-4838 (Mar. 2008).

44. Chen, J., Patil, S., Seal, S. & McGinnis, J. F. Rare earth nanoparticles prevent retinal degeneration induced by intracellular peroxides. *Nature nanotechnology* **1,** 142–50. ISSN: 1748-3395 (Nov. 2006).

45. Bachler, G. *et al.* Translocation of gold nanoparticles across the lung epithelial tissue barrier: Combining in vitro and in silico methods to substitute in vivo experiments. En. *Particle and fibre toxicology* **12,** 18. ISSN: 1743-8977 (Jan. 2015).

46. Choi, H. S. *et al.* Rapid translocation of nanoparticles from the lung airspaces to the body. en. *Nature biotechnology* **28,** 1300–3. ISSN: 1546-1696 (Dec. 2010).

47. Oyabu, T. *et al.* Biopersistence of inhaled nickel oxide nanoparticles in rat lung. *Inhalation toxicology* **19 Suppl 1,** 55–8. ISSN: 1091-7691 (Jan. 2007).

48. Lammers, T., Wohlfart, S., Gelperina, S. & Kreuter, J. Transport of drugs across the blood–brain barrier by nanoparticles. *Journal of Controlled Release* **161,** 264–273 (2012).

49. Kreyling, W. G., Hirn, S. & Schleh, C. Nanoparticles in the lung. *Nature biotechnology* **28,** 1275–6. ISSN: 1546-1696 (Dec. 2010).

50. Lundqvist, M. *et al.* The evolution of the protein corona around nanoparticles: a test study. *ACS nano* **5,** 7503–9. ISSN: 1936-086X (Sept. 2011).

51. Cedervall, T. *et al.* Understanding the nanoparticle-protein corona using methods to quantify exchange rates and affinities of proteins for nanoparticles. *Proceedings of the National Academy of Sciences of the United States of America* **104,** 2050–5. ISSN: 0027-8424 (Feb. 2007).

52. Walczyk, D., Bombelli, F. B., Monopoli, M. P., Lynch, I. & Dawson, K. a. What the cell "sees" in bionanoscience. *Journal of the American Chemical Society* **132,** 5761–8. ISSN: 1520-5126 (Apr. 2010).

53. Becker, S., Mundandhara, S., Devlin, R. B. & Madden, M. Regulation of cytokine production in human alveolar macrophages and airway epithelial cells in response to ambient air pollution particles: further mechanistic studies. *Toxicology and applied pharmacology* **207,** 269–75. ISSN: 1096-0333 (Sept. 2005).

54. Lynch, I. & Dawson, K. A. Protein-nanoparticle interactions. *Nano Today* **3,** 40–47. ISSN: 17480132 (Feb. 2008).

55. Arai, T. & Norde, W. The behavior of some model proteins at solid—liquid interfaces 2. Sequential and competitive adsorption. *Colloids and Surfaces* **51,** 17–28. ISSN: 01666622 (Jan. 1990).

56. Lindman, S. *et al.* Systematic investigation of the thermodynamics of HSA adsorption to N-iso-propylacrylamide/N-tert-butylacrylamide copolymer nanoparticles. Effects of particle size and hydrophobicity. en. *Nano letters* **7,** 914–20. ISSN: 1530-6984 (Apr. 2007).

57. Deng, Z. J., Liang, M., Monteiro, M., Toth, I. & Minchin, R. F. Nanoparticle-induced unfolding of fibrinogen promotes Mac-1 receptor activation and inflammation. *Nature nanotechnology* **6,** 39–44. ISSN: 1748-3395 (Jan. 2011).

58. Vroman, L. & Adams, A. Findings with the recording ellipsometer suggesting rapid exchange of specific plasma proteins at liquid/solid interfaces. *Surface Science* **16,** 438–446 (1969).

59. Jung, S.-Y. *et al.* The Vroman effect: a molecular level description of fibrinogen displacement. *Journal of the American Chemical Society* **125,** 12782–6. ISSN: 0002-7863 (Oct. 2003).

60. Barrán-Berdón, A. L. *et al.* Time Evolution of Nanoparticle-Protein Corona in Human Plasma: Relevance for Targeted Drug Delivery. *Langmuir : the ACS journal of surfaces and colloids.* ISSN: 1520-5827. doi:10.1021/la401192x. <http://www.ncbi.nlm.nih.gov/pubmed/23631648> (May 2013).

61. Liu, W. *et al.* Protein corona formation for nanomaterials and proteins of a similar size: hard or soft corona? *Nanoscale* **5,** 1658–68. ISSN: 2040-3372 (Jan. 2013).

62. Zhang, H. *et al.* Quantitative proteomics analysis of adsorbed plasma proteins classifies nanoparticles with different surface properties and size. *Proteomics* **11,** 4569–77. ISSN: 1615-9861 (Dec. 2011).

63. Tenzer, S. *et al.* Rapid formation of plasma protein corona critically affects nanoparticle pathophysiology. *Nature Nanotechnology* **8,** 772–781. ISSN: 1748-3387 (Sept. 2013).

64. Milani, S., Bombelli, F. B., Pitek, A. S., Dawson, K. a. & Rädler, J. Reversible versus irreversible binding of transferrin to polystyrene nanoparticles: soft and hard corona. *ACS nano* **6,** 2532–41. ISSN: 1936-086X (Mar. 2012).

65. Harford, C. G., Hamlin, A. & Parker, E. Electron microscopy of HeLa cells after the ingestion of colloidal gold. *The Journal of biophysical and biochemical cytology* **3,** 749–56. ISSN: 0095-9901 (Sept. 1957).

66. Iversen, T.-G., Skotland, T. & Sandvig, K. Endocytosis and intracellular transport of nanoparticles: Present knowledge and need for future studies. *Nano Today* **6,** 176–185. ISSN: 17480132 (Apr. 2011).

67. Treuel, L., Jiang, X. & Nienhaus, G. U. New views on cellular uptake and trafficking of manufactured nanoparticles. *Journal of the Royal Society, Interface / the Royal Society* **10,** 20120939. ISSN: 1742-5662 (May 2013).

68. Monti, D. M. *et al.* Biocompatibility, uptake and endocytosis pathways of polystyrene nanoparticles in primary human renal epithelial cells. *Journal of biotechnology* **193,** 3–10. ISSN: 1873-4863 (Jan. 2015).

69. Verma, A. *et al.* Surface-structure-regulated cell-membrane penetration by monolayer-protected nanoparticles. *Nature materials* **7,** 588–95. ISSN: 1476-1122 (July 2008).

70. Geiser, M. *et al.* Ultrafine particles cross cellular membranes by nonphagocytic mechanisms in lungs and in cultured cells. *Environmental health perspectives* **113,** 1555–60. ISSN: 0091-6765 (Nov. 2005).

71. Fujimoto, L. M., Roth, R., Heuser, J. E. & Schmid, S. L. Actin assembly plays a variable, but not obligatory role in receptor-mediated endocytosis in mammalian cells. *Traffic (Copenhagen, Denmark)* **1,** 161–71. ISSN: 1398-9219 (Feb. 2000).

72. Boulant, S., Kural, C., Zeeh, J.-C., Ubelmann, F. & Kirchhausen, T. Actin dynamics counteract membrane tension during clathrin-mediated endocytosis. *Nature cell biology* **13,** 1124–31. ISSN: 1476-4679 (Sept. 2011).

73. Banerji, S. K. & Hayes, M. A. Examination of nonendocytotic bulk transport of nanoparticles across phospholipid membranes. *Langmuir : the ACS journal of surfaces and colloids* **23,** 3305–13. ISSN: 0743-7463 (Mar. 2007).

74. Ruenraroengsak, P. & Tetley, T. D. Differential bioreactivity of neutral, cationic and anionic polystyrene nanoparticles with cells from the human alveolar compartment: robust response of alveolar type 1 epithelial cells. En. *Particle and fibre toxicology* **12,** 19. ISSN: 1743-8977 (Jan. 2015).

75. Lin, J. & Alexander-Katz, A. Cell membranes open "doors" for cationic nanoparticles/biomolecules: insights into uptake kinetics. *ACS nano* **7,** 10799–808. ISSN: 1936-086X (Dec. 2013).

76. Lesniak, A. *et al.* Nanoparticle adhesion to the cell membrane and its effect on nanoparticle uptake efficiency. *Journal of the American Chemical Society* **135,** 1438–44. ISSN: 1520-5126 (Jan. 2013).

77. Treuel, L. *et al.* Impact of Protein Modification on the Protein Corona on Nanoparticles and Nanoparticle-Cell Interactions. *ACS nano*. ISSN: 1936-086X. doi:10.1021/nn405019v. <http://www.ncbi.nlm.nih.gov/pubmed/24377255> (Dec. 2013).

78. Tedja, R., Lim, M., Amal, R. & Marquis, C. Effects of serum adsorption on cellular uptake profile and consequent impact of titanium dioxide nanoparticles on human lung cell lines. *ACS nano* **6,** 4083–93. ISSN: 1936-086X (May 2012).

79. Zhang, S., Gao, H. & Bao, G. Physical Principles of Nanoparticle Cellular Endocytosis. *ACS nano* **9,** 8655–71. ISSN: 1936-086X (Sept. 2015).

80. Shan, Y. *et al.* Size-dependent endocytosis of single gold nanoparticles. *Chemical communications (Cambridge, England)* **47,** 8091–3. ISSN: 1364-548X (July 2011).

81. Kim, J. A., Åberg, C., Salvati, A. & Dawson, K. A. Role of cell cycle on the cellular uptake and dilution of nanoparticles in a cell population. *Nature nanotechnology* **7,** 62–8. ISSN: 1748-3395 (Jan. 2012).

82. Jiang, X. *et al.* Specific effects of surface carboxyl groups on anionic polystyrene particles in their interactions with mesenchymal stem cells. *Nanoscale* **3,** 2028–35. ISSN: 2040-3372 (May 2011).

83. Rejman, J., Oberle, V., Zuhorn, I. S. & Hoekstra, D. Size-dependent internalization of particles via the pathways of clathrin- and caveolae-mediated endocytosis. *The Biochemical journal* **377,** 159–69. ISSN: 1470-8728 (Jan. 2004).

84. Gehr, P., Blank, F. & Rothen-Rutishauser, B. M. Fate of inhaled particles after interaction with the lung surface. *Paediatric respiratory reviews* **7 Suppl 1,** S73–5. ISSN: 1526-0542 (Jan. 2006).

85. McKenzie, Z. *et al.* Surfactant protein A (SP-A) inhibits agglomeration and macrophage uptake of toxic amine modified nanoparticles. *Nanotoxicology* **5390,** 1–11. ISSN: 1743-5390 (2015).

86. Ruge, C. a. *et al.* Uptake of nanoparticles by alveolar macrophages is triggered by surfactant protein A. *Nanomedicine : nanotechnology, biology, and medicine* **7,** 690–3. ISSN: 1549-9642 (Dec. 2011).

87. Ruge, C. a. *et al.* The interplay of lung surfactant proteins and lipids assimilates the macrophage clearance of nanoparticles. *PloS one* **7,** e40775. ISSN: 1932-6203 (Jan. 2012).

88. Kendall, M. *et al.* Surfactant protein D (SP-D) alters cellular uptake of particles and nanoparticles. EN. *Nanotoxicology.* ISSN: 1743-5404. doi:10.3109/17435390.2012.689880. <http://informahealthcare.com/doi/abs/10.3109/17435390.2012.689880> (July 2012).

89. Wang, F., Yu, L., Salvati, A. & Dawson, K. A. The biomolecular corona is retained during nanoparticle uptake and protects the cells from the damage induced by cationic nanoparticles until degraded in the lysosomes. *Nanomedicine : nanotechnology, biology, and medicine* **null.** ISSN: 1549-9642. doi:10.1016/j.nano.2013.04.010. <http://dx.doi.org/10.1016/j.nano.2013.04.010> (May 2013).

90. Bexiga, M. G. *et al.* Cationic nanoparticles induce caspase 3-, 7- and 9-mediated cytotoxicity in a human astrocytoma cell line. *Nanotoxicology* **5,** 557–67. ISSN: 1743-5404 (Dec. 2011).

91. Wang, F. *et al.* Time resolved study of cell death mechanisms induced by amine-modified polystyrene nanoparticles. en. *Nanoscale* **5,** 10868–10876. ISSN: 2040-3372 (Oct. 2013).

92. Xia, T., Kovochich, M., Liong, M., Zink, J. I. & Nel, A. E. Cationic polystyrene nanosphere toxicity depends on cell-specific endocytic and mitochondrial injury pathways. *ACS nano* **2,** 85–96. ISSN: 1936-086X (Jan. 2008).

93. Ruenraroengsak, P. *et al.* Respiratory epithelial cytotoxicity and membrane damage (holes) caused by amine-modified nanoparticles. *Nanotoxicology* **6,** 94–108. ISSN: 1743-5404 (Feb. 2012).

94. Kemp, S. J. *et al.* Immortalization of human alveolar epithelial cells to investigate nanoparticle uptake. *American journal of respiratory cell and molecular biology* **39,** 591–7. ISSN: 1535-4989 (Nov. 2008).

95. Van Lehn, R. C. *et al.* Effect of particle diameter and surface composition on the spontaneous fusion of monolayer-protected gold nanoparticles with lipid bilayers. *Nano letters* **13,** 4060–7. ISSN: 1530-6992 (Sept. 2013).

96. Aoyama, Y. *et al.* Artificial viruses and their application to gene delivery. Size-controlled gene coating with glycocluster nanoparticles. *Journal of the American Chemical Society* **125,** 3455–7. ISSN: 0002-7863 (Mar. 2003).

97. Reddy, S. T. *et al.* Exploiting lymphatic transport and complement activation in nanoparticle vaccines. *Nature biotechnology* **25,** 1159–64. ISSN: 1087-0156 (Oct. 2007).

98. Doorley, G. W. & Payne, C. K. Nanoparticles act as protein carriers during cellular internalization. *Chemical communications (Cambridge, England)* **48,** 2961–3. ISSN: 1364-548X (Mar. 2012).

99. Müller, L. *et al.* Oxidative stress and inflammation response after nanoparticle exposure: differences between human lung cell monocultures and an advanced three-dimensional model of the human epithelial airways. *Journal of the Royal Society, Interface / the Royal Society* **7 Suppl 1,** S27–40. ISSN: 1742-5662 (Feb. 2010).

100. Xia, T. *et al.* Comparison of the abilities of ambient and manufactured nanoparticles to induce cellular toxicity according to an oxidative stress paradigm. *Nano letters* **6,** 1794–807. ISSN: 1530-6984 (Aug. 2006).

101. Giard, D. J. *et al.* In vitro cultivation of human tumors: establishment of cell lines derived from a series of solid tumors. *Journal of the National Cancer Institute* **51,** 1417–23. ISSN: 0027-8874 (Nov. 1973).

102. Thach, C. T. & Finkelstein, J. N. Cationic nanoparticles disrupt cellular signaling in a cholesterol dependent manner. *Toxicology in vitro : an international journal published in association with BIBRA* **27,** 1277–86. ISSN: 1879-3177 (June 2013).

103. Card, J. W., Zeldin, D. C., Bonner, J. C. & Nestmann, E. R. Pulmonary applications and toxicity of engineered nanoparticles. *American journal of physiology. Lung cellular and molecular physiology* **295,** L400–11. ISSN: 1040-0605 (Sept. 2008).

104. Pastva, A. M., Wright, J. R. & Williams, K. L. Immunomodulatory roles of surfactant proteins A and D: implications in lung disease. *Proceedings of the American Thoracic Society* **4,** 252–7. ISSN: 1546-3222 (July 2007).

105. Thawer, S. *et al.* Surfactant Protein-D Is Essential for Immunity to Helminth Infection. *PLoS pathogens* **12,** e1005461. ISSN: 1553-7374 (Feb. 2016).

106. McKenzie, Z. *et al.* Nanoparticles modulate surfactant protein A and D mediated protection against influenza A infection in vitro. *Philosophical transactions of the Royal Society of London. Series B, Biological sciences* **370,** 20140049. ISSN: 1471-2970 (Feb. 2015).

107. Mackay, R.-M. A. *et al.* Airway surfactant protein D (SP-D) deficiency in adults with severe asthma. *Chest.* ISSN: 1931-3543. doi:10.1016/j.chest.2015.11.012. <http://www.ncbi.nlm.nih.gov/pubmed/26836907> (Jan. 2016).

108. Kendall, M., Hodges, N. J., Whitwell, H., Tyrrell, J. & Cangul, H. Nanoparticle growth and surface chemistry changes in cell-conditioned culture medium. *Philosophical transactions of the Royal Society of London. Series B, Biological sciences* **370.** ISSN: 1471-2970. doi:10.1098/rstb.2014.0100. <http://www.ncbi.nlm.nih.gov/pubmed/25533102> (Feb. 2015).

109. Maiorano, G. *et al.* Effects of cell culture media on the dynamic formation of protein-nanoparticle complexes and influence on the cellular response. *ACS nano* **4,** 7481–91. ISSN: 1936-086X (Dec. 2010).

110. Card, J. W., Zeldin, D. C., Bonner, J. C. & Nestmann, E. R. Pulmonary applications and toxicity of engineered nanoparticles. *American journal of physiology. Lung cellular and molecular physiology* **295,** L400–11. ISSN: 1040-0605 (Sept. 2008).

111. *Dynamic Light Scattering: An Introduction in 30 Minutes* tech. rep. (Malvern Instruments, 2014). <http://www.malvern.com/en/pdf/secure/TN101104DynamicLightScatteringIntroduction.pdf>.

112. Mortensen, N. P. *et al.* Dynamic development of the protein corona on silica nanoparticles: composition and role in toxicity. en. *Nanoscale* **5,** 6372–80. ISSN: 2040-3372 (July 2013).

113. Casals, E., Pfaller, T., Duschl, A., Oostingh, G. J. & Puntes, V. Time evolution of the nanoparticle protein corona. *ACS nano* **4,** 3623–32. ISSN: 1936-086X (July 2010).

114. Baldelli Bombelli, F. *et al.* High-resolution isolation of protein corona nanoparticles from complex physiological fluids. en. *Nanoscale.* ISSN: 2040-3364. doi:10.1039/C5NR02618K. <http://pubs.rsc.org/en/content/articlehtml/2015/nr/c5nr02618k> (June 2015).

115. Dwivedi, M. V., Harishchandra, R. K., Koshkina, O., Maskos, M. & Galla, H.-J. Size influences the effect of hydrophobic nanoparticles on lung surfactant model systems. *Biophysical journal* **106,** 289–98. ISSN: 1542-0086 (Jan. 2014).

116. Den Engelsman, J. *et al.* Strategies for the assessment of protein aggregates in pharmaceutical biotech product development. *Pharmaceutical research* **28,** 920–33. ISSN: 1573-904X (Apr. 2011).

117. Schäffler, M. *et al.* Serum protein identification and quantification of the corona of 5, 15 and 80 nm gold nanoparticles. *Nanotechnology* **24,** 265103. ISSN: 1361-6528 (June 2013).

118. Lundqvist, M. *et al.* Nanoparticle size and surface properties determine the protein corona with possible implications for biological impacts. *Proceedings of the National Academy of Sciences of the United States of America* **105,** 14265–70. ISSN: 1091-6490 (Sept. 2008).

119. Cai, X. *et al. Characterization of carbon nanotube protein corona by using quantitative proteomics.* ISBN: 8523442634. doi:10.1016/j.nano.2012.09.004. <http://www.ncbi.nlm.nih.gov/pubmed/23117048> (Elsevier B.V., Oct. 2012).

120. Simberg, D. *et al.* Differential proteomics analysis of the surface heterogeneity of dextran iron oxide nanoparticles and the implications for their in vivo clearance. *Biomaterials* **30,** 3926–33. ISSN: 1878-5905 (Aug. 2009).

121. Cedervall, T. *et al.* Detailed identification of plasma proteins adsorbed on copolymer nanoparticles. *Angewandte Chemie (International ed. in English)* **46,** 5754–6. ISSN: 1433-7851 (Jan. 2007).

122. Walkey, C. D. & Chan, W. C. W. Understanding and controlling the interaction of nanomaterials with proteins in a physiological environment. *Chemical Society reviews* **41,** 2780–99. ISSN: 1460-4744 (Apr. 2012).

123. Ashby, J., Schachermeyer, S., Pan, S. & Zhong, W. Dissociation-Based Screening of Nanoparticle-Protein Interaction via Flow Field-Flow Fractionation. *Analytical chemistry* **85,** 7494–501. ISSN: 1520-6882 (Aug. 2013).

124. Stone, K. C., Mercer, R. R., Gehr, P., Stockstill, B. & Crapo, J. D. Allometric relationships of cell numbers and size in the mammalian lung. *American journal of respiratory cell and molecular biology* **6,** 235–43. ISSN: 1044-1549 (Feb. 1992).

125. Gehr, P., Bachofen, M. & Weilbel, E. R. The Normal Human Lung: Ultrastructure and Morphometric Estimation of Diffusion Capacity. *Respiratory Physiology* **32,** 121–140 (1978).

126. Dobbs, L. G. *et al.* Highly water-permeable type I alveolar epithelial cells confer high water permeability between the airspace and vasculature in rat lung. *Proceedings of the National Academy of Sciences of the United States of America* **95,** 2991–6. ISSN: 0027-8424 (Mar. 1998).

127. Evans, M. J., Cabral, L. J., Stephens, R. J. & Freeman, G. Transformation of alveolar type 2 cells to type 1 cells following exposure to NO2. *Experimental and molecular pathology* **22,** 142–50. ISSN: 0014-4800 (Feb. 1975).

128. Evans, M. J., Cabral, L. J., Stephens, R. J. & Freeman, G. Renewal of alveolar epithelium in the rat following exposure to NO2. *The American journal of pathology* **70,** 175–98. ISSN: 0002-9440 (Feb. 1973).

129. Adamson, I. Y. & Bowden, D. H. Derivation of type 1 epithelium from type 2 cells in the developing rat lung. *Laboratory investigation; a journal of technical methods and pathology* **32,** 736–45. ISSN: 0023-6837 (June 1975).

130. Zissel, G. *et al.* Human alveolar epithelial cells type II are capable of regulating T-cell activity. *Journal of investigative medicine : the official publication of the American Federation for Clinical Research* **48,** 66–75. ISSN: 1081-5589 (Jan. 2000).

131. Chan, M. C. W. *et al.* Proinflammatory cytokine responses induced by influenza A (H5N1) viruses in primary human alveolar and bronchial epithelial cells. *Respiratory research* **6,** 135. ISSN: 1465-993X (Jan. 2005).

132. Thorley, A. J. *et al.* Differential regulation of cytokine release and leukocyte migration by lipopolysaccharide-stimulated primary human lung alveolar type II epithelial cells and macrophages. *Journal of immunology (Baltimore, Md. : 1950)* **178,** 463–73. ISSN: 0022-1767 (Jan. 2007).

133. Chuquimia, O. D. *et al.* The role of alveolar epithelial cells in initiating and shaping pulmonary immune responses: communication between innate and adaptive immune systems. *PloS one* **7,** e32125. ISSN: 1932-6203 (Jan. 2012).

134. Lin, Y., Zhang, M. & Barnes, P. F. Chemokine production by a human alveolar epithelial cell line in response to Mycobacterium tuberculosis. *Infection and immunity* **66,** 1121–6. ISSN: 0019-9567 (Mar. 1998).

135. Espinoza, L. A. *et al.* Expression of JP-8-induced inflammatory genes in AEII cells is mediated by NF-kappaB and PARP-1. en. *American journal of respiratory cell and molecular biology* **35,** 479–87. ISSN: 1044-1549 (Oct. 2006).

136. Veldhuizen, E. J. & Haagsman, H. P. Role of pulmonary surfactant components in surface film formation and dynamics. *Biochimica et Biophysica Acta (BBA) - Biomembranes* **1467,** 255–270. ISSN: 00052736 (Aug. 2000).

137. Pérez-Gil, J. Structure of pulmonary surfactant membranes and films: the role of proteins and lipid-protein interactions. *Biochimica et biophysica acta* **1778,** 1676–95. ISSN: 0006-3002 (Jan. 2008).

138. Jobe, A. H. Pulmonary Surfactant Therapy. *The New England Journal of Medicine,* 861–868 (1993).

139. Soll, R. F. & Blanco, F. Natural surfactant extract versus synthetic surfactant for neonatal respiratory distress syndrome. *The Cochrane database of systematic reviews,* CD000144. ISSN: 1469-493X (Jan. 2001).

140. Clark, H. W. Untapped therapeutic potential of surfactant proteins: is there a case for recombinant SP-D supplementation in neonatal lung disease? *Neonatology* **97,** 380–7. ISSN: 1661-7819 (June 2010).

141. Schürch, S. Surface tension at low lung volumes: dependence on time and alveolar size. *Respiration physiology* **48,** 339–55. ISSN: 0034-5687 (June 1982).

142. Zuo, Y. Y. & Possmayer, F. How does pulmonary surfactant reduce surface tension to very low values? *Journal of applied physiology (Bethesda, Md. : 1985)* **102,** 1733–4. ISSN: 8750-7587 (May 2007).

143. Meban, C. Effect of lipids and other substances on the adsorption of dipalmitoyl phosphatidylcholine. *Pediatric research* **15,** 1029–31. ISSN: 0031-3998 (July 1981).

144. Tokieda, K. *et al.* Pulmonary dysfunction in neonatal SP-B-deficient mice. *The American journal of physiology* **273,** L875–82. ISSN: 0002-9513 (Oct. 1997).

145. Klein, J. M. *et al.* Transient surfactant protein B deficiency in a term infant with severe respiratory failure. *The Journal of Pediatrics* **132,** 244–248. ISSN: 00223476 (Feb. 1998).

146. Wright, J. R. & Dobbs, L. G. Regulation of pulmonary surfactant secretion and clearance. *Annual review of physiology* **53,** 395–414. ISSN: 0066-4278 (Jan. 1991).

147. Kishore, U. *et al.* Surfactant proteins SP-A and SP-D: Structure, function and receptors. *Molecular Immunology* **43,** 1293–1315 (2006).

148. McKenzie, Z. *Nanotoxicology: Nanoparticle Interactions with Surfactant Proteins A and D* PhD thesis (2013), 214–218.

149. Madsen, J. *et al.* Surfactant Protein D Modulates HIV Infection of Both T-Cells and Dendritic Cells. *PloS one* **8,** e59047. ISSN: 1932-6203 (Jan. 2013).

150. Brown-Augsburger, P. *et al.* Site-directed mutagenesis of Cys-15 and Cys-20 of pulmonary surfactant protein D. Expression of a trimeric protein with altered anti-viral properties. *The Journal of biological chemistry* **271,** 13724–30. ISSN: 0021-9258 (June 1996).

151. McCormack, F. X., Damodarasamy, M. & Elhalwagi, B. M. Deletion mapping of N-terminal domains of surfactant protein A. The N-terminal segment is required for phospholipid aggregation and specific inhibition of surfactant secretion. *The Journal of biological chemistry* **274,** 3173–81. ISSN: 0021-9258 (Jan. 1999).

152. Zhang, P. *et al.* The amino-terminal heptad repeats of the coiled-coil neck domain of pulmonary surfactant protein d are necessary for the assembly of trimeric subunits and dodecamers. *The Journal of biological chemistry* **276,** 19862–70. ISSN: 0021-9258 (June 2001).

153. Head, J. F., Mealy, T. R., McCormack, F. X. & Seaton, B. A. Crystal structure of trimeric carbohydrate recognition and neck domains of surfactant protein A. *The Journal of biological chemistry* **278,** 43254–60. ISSN: 0021-9258 (Oct. 2003).

154. Clark, H. W. *et al.* Crystal structure of a complex of Surfactant Protein D and Haemophilus influenzae lipopolysaccharide reveals shielding of core structures in SP-D resistant strains. *Infection and immunity.* ISSN: 1098-5522. doi:10.1128/IAI.01239-15. <http://www.ncbi.nlm.nih.gov/pubmed/26953329> (Mar. 2016).

155. Crouch, E., Persson, A., Chang, D. & Heuser, J. Molecular structure of pulmonary surfactant protein D (SP-D). *The Journal of biological chemistry* **269,** 17311–9. ISSN: 0021-9258 (June 1994).

156. Sorensen, G. L. *et al.* Multimeric and trimeric subunit SP-D are interconvertible structures with distinct ligand interaction. *Molecular immunology* **46,** 3060–9. ISSN: 1872-9142 (Sept. 2009).

157. Seymour, J. F. & Presneill, J. J. Pulmonary alveolar proteinosis: progress in the first 44 years. en. *American journal of respiratory and critical care medicine* **166,** 215–35. ISSN: 1073-449X (July 2002).

158. Shah, P. L. Rare diseases bullet 6: Pulmonary alveolar proteinosis: clinical aspects and current concepts on pathogenesis. *Thorax* **55,** 67–77. ISSN: 00406376 (Jan. 2000).

159. Honda, Y. *et al.* Pulmonary surfactant protein D in sera and bronchoalveolar lavage fluids. *American journal of respiratory and critical care medicine* **152,** 1860–6. ISSN: 1073-449X (Dec. 1995).

160. Honda, Y. Surfactant protein-A concentration in bronchoalveolar lavage fluids of patients with pulmonary alveolar proteinosis. *CHEST Journal* **103,** 496. ISSN: 0012-3692 (Feb. 1993).

161. Bakshi, M. S., Zhao, L., Smith, R., Possmayer, F. & Petersen, N. O. Metal nanoparticle pollutants interfere with pulmonary surfactant function in vitro. *Biophysical journal* **94,** 855–68. ISSN: 1542-0086 (Feb. 2008).

162. Hu, G. *et al.* Physicochemical properties of nanoparticles regulate translocation across pulmonary surfactant monolayer and formation of lipoprotein corona. *ACS nano* **7,** 10525–33. ISSN: 1936-086X (Dec. 2013).

163. Kendall, M. Fine airborne urban particles (PM2.5) sequester lung surfactant and amino acids from human lung lavage. *American journal of physiology. Lung cellular and molecular physiology* **293,** L1053–8. ISSN: 1040-0605 (Oct. 2007).

164. Kendall, M. *et al.* Lung lining liquid modifies PM2.5 in favor of particle aggregation: a protective mechanism. *Am J Physiol Lung Cell Mol Physiol* **282,** L109–114 (Jan. 2002).

165. Gonzalez, F. G., Vilchez, M. A. C. & Hidalgo-Alvarez, R. Adsorption of anionic surfactants on positively charged polystyrene particles II. *Colloid & Polymer Science* **269,** 406–411. ISSN: 0303-402X (Apr. 1991).

166. GEHR, P., SCHÜRCH, S., BERTHIAUME, Y., HOF, V. I. & GEISER, M. Particle Retention in Airways by Surfactant. EN. <http://online.liebertpub.com/doi/abs/10.1089/jam.1990.3.27> (Mar. 2009).

167. Geiser, M., Schurch, S. & Gehr, P. Influence of surface chemistry and topography of particles on their immersion into the lung's surface-lining layer. *Journal of applied physiology (Bethesda, Md. : 1985)* **94,** 1793–801. ISSN: 8750-7587 (May 2003).

168. Harishchandra, R. K., Saleem, M. & Galla, H.-J. Nanoparticle interaction with model lung surfactant monolayers. *Journal of the Royal Society, Interface / the Royal Society* **7 Suppl 1,** S15–26. ISSN: 1742-5662 (Feb. 2010).

169. Fan, Q., Wang, Y. E., Zhao, X., Loo, J. S. C. & Zuo, Y. Y. Adverse biophysical effects of hydroxyapatite nanoparticles on natural pulmonary surfactant. *ACS nano* **5,** 6410–6. ISSN: 1936-086X (Aug. 2011).

170. George, I. *et al.* Metallic oxide nanoparticle translocation across the human bronchial epithelial barrier. en. *Nanoscale* **7,** 4529–44. ISSN: 2040-3372 (Feb. 2015).

171. Beck-Broichsitter, M. *et al.* Biophysical investigation of pulmonary surfactant surface properties upon contact with polymeric nanoparticles in vitro. *Nanomedicine : nanotechnology, biology, and medicine* **7,** 341–50. ISSN: 1549-9642 (June 2011).

172. Schleh, C. *et al.* The effect of titanium dioxide nanoparticles on pulmonary surfactant function and ultrastructure. *Respiratory research* **10,** 90. ISSN: 1465-993X (Jan. 2009).

173. Botas, C. *et al.* Altered surfactant homeostasis and alveolar type II cell morphology in mice lacking surfactant protein D. *Proceedings of the National Academy of Sciences of the United States of America* **95,** 11869–74. ISSN: 0027-8424 (Sept. 1998).

174. Weller, N. K. & Karnovsky, M. J. Isolation of pulmonary alveolar type I cells from adult rats. *The American journal of pathology* **124,** 448–56. ISSN: 0002-9440 (Sept. 1986).

175. Chen, J., Chen, Z., Narasaraju, T., Jin, N. & Liu, L. Isolation of highly pure alveolar epithelial type I and type II cells from rat lungs. *Laboratory investigation; a journal of technical methods and pathology* **84,** 727–35. ISSN: 0023-6837 (June 2004).

176. Gonzalez, R. F., Allen, L. & Dobbs, L. G. Rat alveolar type I cells proliferate, express OCT-4, and exhibit phenotypic plasticity in vitro. *American journal of physiology. Lung cellular and molecular physiology* **297,** L1045–55. ISSN: 1522-1504 (Dec. 2009).

177. R.F, G. & Dobbs, L. in *Epithelial Cell Culture Protocols* 2nd ed., 145–159 (2012). <http://link.springer.com/content/pdf/10.1007/978-1-62703-125-7%7B%5C_%7D10>.

178. Dobbs, L. G., Gonzalez, R. F., Allen, L. & Froh, D. K. HTI56, an Integral Membrane Protein Specific to Human Alveolar Type I Cells. *Journal of Histochemistry & Cytochemistry* **47,** 129–137. ISSN: 0022-1554 (Feb. 1999).

179. Newman, V., Gonzalez, R. F., Matthay, M. A. & Dobbs, L. G. A novel alveolar type I cell-specific biochemical marker of human acute lung injury. en. *American journal of respiratory and critical care medicine* **161,** 990–5. ISSN: 1073-449X (Mar. 2000).

180. Gonzalez, R. F., Allen, L., Gonzales, L., Ballard, P. L. & Dobbs, L. G. HTII-280, a biomarker specific to the apical plasma membrane of human lung alveolar type II cells. *The journal of histochemistry and cytochemistry : official journal of the Histochemistry Society* **58,** 891–901. ISSN: 1551-5044 (Oct. 2010).

181. El-Aneed, A., Cohen, A. & Banoub, J. Mass Spectrometry, Review of the Basics: Electrospray, MALDI, and Commonly Used Mass Analyzers. *Applied Spectroscopy Reviews* **44,** 210–230. ISSN: 0570-4928 (Apr. 2009).

182. Glish, G. L. & Burinsky, D. J. Hybrid mass spectrometers for tandem mass spectrometry. *Journal of the American Society for Mass Spectrometry* **19,** 161–72. ISSN: 1044-0305 (Feb. 2008).

183. Aebersold, R. & Mann, M. Mass spectrometry-based proteomics. *Nature* **422,** 198–207. ISSN: 0028-0836 (Mar. 2003).

184. Michalski, A., Cox, J. & Mann, M. More than 100,000 detectable peptide species elute in single shotgun proteomics runs but the majority is inaccessible to data-dependent LC-MS/MS. *Journal of proteome research* **10,** 1785–93. ISSN: 1535-3907 (Apr. 2011).

185. Cheng, F.-y., Blackburn, K., Lin, Y.-m., Goshe, M. B. & Williamsom, J. D. Absolute Protein Quantification by LC/MSe for Global Analysis of Salicylic Acid-Induced Plant Protein Secretion Responses. *Journal of proteome research* **8,** 82–93 (2009).

186. Silva, J. C., Gorenstein, M. V., Li, G.-Z., Vissers, J. P. C. & Geromanos, S. J. Absolute quantification of proteins by LCMSE: a virtue of parallel MS acquisition. *Molecular & cellular proteomics : MCP* **5,** 144–56. ISSN: 1535-9476 (Jan. 2006).

187. Arike, L. *et al.* Comparison and applications of label-free absolute proteome quantification methods on Escherichia coli. *Journal of proteomics* **75,** 5437–48. ISSN: 1876-7737 (Sept. 2012).

188. Wilhelm, M. *et al.* Mass-spectrometry-based draft of the human proteome. *Nature* **509,** 582–7. ISSN: 1476-4687 (May 2014).

189. Fabre, B. *et al.* Comparison of label-free quantification methods for the determination of protein complexes subunits stoichiometry. *EuPA Open Proteomics* **4,** 82–86. ISSN: 22129685 (Sept. 2014).

190. Lieber, M., Smith, B., Szakal, A., Nelson-Rees, W. & Todaro, G. A continuous tumor-cell line from a human lung carcinoma with properties of type II alveolar epithelial cells. *International journal of cancer. Journal international du cancer* **17,** 62–70. ISSN: 0020-7136 (Jan. 1976).

191. Raschke, W., Baird, S., Ralph, P. & Nakoinz, I. Functional macrophage cell lines transformed by abelson leukemia virus. *Cell* **15,** 261–267. ISSN: 00928674 (Sept. 1978).

192. Tsuchiya, S. *et al.* Establishment and characterization of a human acute monocytic leukemia cell line (THP-1). *International journal of cancer. Journal international du cancer* **26,** 171–6. ISSN: 0020-7136 (Aug. 1980).

193. Smith, P. K. *et al.* Measurement of protein using bicinchoninic acid. *Analytical biochemistry* **150,** 76–85. ISSN: 0003-2697 (Oct. 1985).

194. Elbir, T., Kara, M., Bayram, A., Altiok, H. & Dumanoglu, Y. Comparison of predicted and observed PM10 concentrations in several urban street canyons. *Air Quality, Atmosphere & Health* **4,** 121–131. ISSN: 1873-9318 (July 2010).

195. Lee, W.-H., Loo, C.-Y., Traini, D. & Young, P. M. Inhalation of nanoparticles-based drug for lung cancer treatment: advantages and challenges. *Asian Journal of Pharmaceutical Sciences* **10,** 481–489. ISSN: 18180876 (Sept. 2015).

196. Fireman, E., Bliznuk, D., Schwarz, Y., Soferman, R. & Kivity, S. Biological monitoring of particulate matter accumulated in the lungs of urban asthmatic children in the Tel-Aviv area. *International archives of occupational and environmental health* **88,** 443–53. ISSN: 1432-1246 (May 2015).

197. Sayes, C. M. *et al.* Correlating nanoscale titania structure with toxicity: a cytotoxicity and inflammatory response study with human dermal fibroblasts and human lung epithelial cells. *Toxicological sciences : an official journal of the Society of Toxicology* **92,** 174–85. ISSN: 1096-6080 (July 2006).

198. McGuinnes, C. *et al.* Surface derivatization state of polystyrene latex nanoparticles determines both their potency and their mechanism of causing human platelet aggregation in vitro. *Toxicological sciences : an official journal of the Society of Toxicology* **119,** 359–68. ISSN: 1096-0929 (Feb. 2011).

199. Elmore, S. Apoptosis: a review of programmed cell death. *Toxicologic pathology* **35,** 495–516. ISSN: 0192-6233 (June 2007).

200. Wang, F. *et al.* Time resolved study of cell death mechanisms induced by amine-modified polystyrene nanoparticles. *Nanoscale* **5,** 10868–76. ISSN: 2040-3372 (Nov. 2013).

201. Dobrovolskaia, M. A. *et al.* Method for analysis of nanoparticle hemolytic properties in vitro. *Nano letters* **8,** 2180–7. ISSN: 1530-6984 (Aug. 2008).

202. Dobrovolskaia, M. A. *et al.* Protein corona composition does not accurately predict hematocompatibility of colloidal gold nanoparticles. *Nanomedicine : nanotechnology, biology, and medicine* **10,** 1453–63. ISSN: 1549-9642 (Oct. 2014).

203. Xia, T., Kovochich, M., Liong, M., Zink, J. I. & Nel, A. E. Cationic polystyrene nanosphere toxicity depends on cell-specific endocytic and mitochondrial injury pathways. *ACS nano* **2,** 85–96. ISSN: 1936-086X (Jan. 2008).

204. Forman, H. J. & Torres, M. Reactive oxygen species and cell signaling: respiratory burst in macrophage signaling. *American journal of respiratory and critical care medicine* **166,** S4–8. ISSN: 1073-449X (Dec. 2002).

205. Ryan, S. F., Ghassibi, Y. & Liau, D. F. Effects of activated polymorphonuclear leukocytes upon pulmonary surfactant in vitro. *American journal of respiratory cell and molecular biology* **4,** 33–41. ISSN: 1044-1549 (Jan. 1991).

206. Rodríguez-Capote, K., Manzanares, D., Haines, T. & Possmayer, F. Reactive Oxygen Species Inactivation of Surfactant Involves Structural and Functional Alterations to Surfactant Proteins SP-B and SP-C. *Biophysical Journal* **90,** 2808–2821. ISSN: 00063495 (Apr. 2006).

207. Gil, H.-W. *et al.* Relationship between pulmonary surfactant protein and lipid peroxidation in lung injury due to paraquat intoxication in rats. *The Korean journal of internal medicine* **22,** 67–72. ISSN: 1226-3303 (June 2007).

208. Putman, E., van Golde, L. M. & Haagsman, H. P. Toxic oxidant species and their impact on the pulmonary surfactant system. *Lung* **175,** 75–103. ISSN: 0341-2040 (Jan. 1997).

209. Maurer-Jones, M. A., Christenson, J. R. & Haynes, C. L. TiO2 nanoparticle-induced ROS correlates with modulated immune cell function. *Journal of Nanoparticle Research* **14,** 1291. ISSN: 1388-0764 (Nov. 2012).

210. Johann, A. M., von Knethen, A., Lindemann, D. & Brüne, B. Recognition of apoptotic cells by macrophages activates the peroxisome proliferator-activated receptor-gamma and attenuates the oxidative burst. *Cell death and differentiation* **13,** 1533–40. ISSN: 1350-9047 (Sept. 2006).

211. Manke, A., Wang, L. & Rojanasakul, Y. Mechanisms of nanoparticle-induced oxidative stress and toxicity. en. *BioMed research international* **2013,** 942916. ISSN: 2314-6141 (Jan. 2013).

212. Gogniat, G. & Dukan, S. TiO2 photocatalysis causes DNA damage via fenton reaction-generated hydroxyl radicals during the recovery period. *Applied and environmental microbiology* **73,** 7740–3. ISSN: 1098-5336 (Dec. 2007).

213. Jin, C. *et al.* Cellular toxicity of TiO2 nanoparticles in anatase and rutile crystal phase. *Biological trace element research* **141,** 3–15. ISSN: 1559-0720 (June 2011).

214. Slowing, I. I., Wu, C.-W., Vivero-Escoto, J. L. & Lin, V. S.-Y. Mesoporous silica nanoparticles for reducing hemolytic activity towards mammalian red blood cells. *Small (Weinheim an der Bergstrasse, Germany)* **5,** 57–62. ISSN: 1613-6829 (Jan. 2009).

215. Murashov, V., Harper, M. & Demchuk, E. Impact of silanol surface density on the toxicity of silica aerosols measured by erythrocyte haemolysis. *Journal of occupational and environmental hygiene* **3,** 718–23. ISSN: 1545-9624 (Dec. 2006).

216. Walkey, C. D. *et al.* Protein Corona Fingerprinting Predicts the Cell Association of Gold Nanoparticles. *ACS nano.* ISSN: 1936-086X. doi:10.1021/nn406018q. <http://dx.doi.org/10.1021/nn406018q> (Feb. 2014).

217. Strong, P. *et al.* A novel method of purifying lung surfactant proteins A and D from the lung lavage of alveolar proteinosis patients and from pooled amniotic fluid. *Journal of immunological methods* **220,** 139–49. ISSN: 0022-1759 (Nov. 1998).

218. Silva, J. C. *et al.* Quantitative proteomic analysis by accurate mass retention time pairs. *Analytical chemistry* **77,** 2187–200. ISSN: 0003-2700 (Apr. 2005).

219. Shevchenko, a., Wilm, M., Vorm, O. & Mann, M. Mass spectrometric sequencing of proteins silver-stained polyacrylamide gels. *Analytical chemistry* **68,** 850–8. ISSN: 0003-2700 (Mar. 1996).

220. Gasteiger, E. *et al.* in *The Proteomics Protocols Handbook* (ed Walker, J. M.) 571–607 (Humana Press, 2005). doi:10.1385/1-59259-890-0:571. <http://dx.doi.org/10.1385/1-59259-890-0:571>.

221. Rigbolt, K. T. G., Vanselow, J. T. & Blagoev, B. GProX, a user-friendly platform for bioinformatics analysis and visualization of quantitative proteomics data. *Molecular & cellular proteomics : MCP* **10,** O110.007450. ISSN: 1535-9484 (Aug. 2011).

222. Gatto, L. & Lilley, K. S. MSnbase-an R/Bioconductor package for isobaric tagged mass spectrometry data visualization, processing and quantitation. *Bioinformatics (Oxford, England)* **28,** 288–9. ISSN: 1367-4811 (Jan. 2012).

223. Gatto, L., Breckels, L. M., Wieczorek, S., Burger, T. & Lilley, K. S. Mass-spectrometry-based spatial proteomics data analysis using pRoloc and pRolocdata. *Bioinformatics (Oxford, England)* **30,** 1322–4. ISSN: 1367-4811 (May 2014).

224. Kyte, J. & Doolittle, R. F. A simple method for displaying the hydropathic character of a protein. *Journal of molecular biology* **157,** 105–32. ISSN: 0022-2836 (May 1982).

225. Ikai, A. Thermostability and aliphatic index of globular proteins. *Journal of biochemistry* **88,** 1895–8. ISSN: 0021-924X (Dec. 1980).

226. Docter, D. *et al.* Quantitative profiling of the protein coronas that form around nanoparticles. *Nature protocols* **9,** 2030–2044. ISSN: 1750-2799 (Sept. 2014).

227. Keller, B. O., Sui, J., Young, A. B. & Whittal, R. M. Interferences and contaminants encountered in modern mass spectrometry. *Analytica chimica acta* **627,** 71–81. ISSN: 1873-4324 (Oct. 2008).

228. Mi, H., Muruganujan, A. & Thomas, P. D. PANTHER in 2013: modeling the evolution of gene function, and other gene attributes, in the context of phylogenetic trees. *Nucleic acids research* **41,** D377–86. ISSN: 1362-4962 (Jan. 2013).

229. Fleischer, C. & Payne, C. K. Secondary Structure of Corona Proteins Determines the Cell Surface Receptors Used by Nanoparticles. *The journal of physical chemistry. B.* ISSN: 1520-5207. doi:10.1021/jp502624n. <http://dx.doi.org/10.1021/jp502624n> (Apr. 2014).

230. Schäffler, M. *et al.* Serum protein identification and quantification of the corona of 5, 15 and 80 nm gold nanoparticles. *Nanotechnology* **24,** 265103. ISSN: 1361-6528 (July 2013).

231. Patil, S., Sandberg, A., Heckert, E., Self, W. & Seal, S. Protein adsoprtion and cellular uptake of cerium oxide nanoparticles as a function of zeta potential. *Biomaterials* **28,** 4600–4607 (2007).

232. Goerke, J. Pulmonary surfactant: functions and molecular composition. *Biochimica et Biophysica Acta (BBA) - Molecular Basis of Disease* **1408,** 79–89 (1998).

233. Schürch, D., Ospina, O. L., Cruz, A. & Pérez-Gil, J. Combined and independent action of proteins SP-B and SP-C in the surface behavior and mechanical stability of pulmonary surfactant films. *Biophysical journal* **99,** 3290–9. ISSN: 1542-0086 (Nov. 2010).

234. Suzuki, Y., Fujita, Y. & Kogishi, K. Reconstitution of tubular myelin from synthetic lipids and proteins associated with pig pulmonary surfactant. *The American review of respiratory disease* **140,** 75–81. ISSN: 0003-0805 (July 1989).

235. Kendall, M. & Holgate, S. Health impact and toxicological effects of nanomaterials in the lung. *Respirology (Carlton, Vic.)* **17,** 743–58. ISSN: 1440-1843 (July 2012).

236. Korfhagen, T. R. *et al.* Surfactant protein-D regulates surfactant phospholipid homeostasis in vivo. *The Journal of biological chemistry* **273,** 28438–43. ISSN: 0021-9258 (Oct. 1998).

237. Korfhagen, T. R. *et al.* Altered surfactant function and structure in SP-A gene targeted mice. *Proceedings of the National Academy of Sciences of the United States of America* **93,** 9594–9. ISSN: 0027-8424 (Sept. 1996).

238. Wang, J. Y., Kishore, U., Lim, B. L., Strong, P. & Reid, K. B. Interaction of human lung surfactant proteins A and D with mite (Dermatophagoides pteronyssinus) allergens. *Clinical and experimental immunology* **106,** 367–73. ISSN: 0009-9104 (Nov. 1996).

239. Choi, H. S. *et al.* Rapid translocation of nanoparticles from the lung airspaces to the body. *Nature biotechnology* **28,** 1300–3. ISSN: 1546-1696 (Dec. 2010).

240. Schleh, C., Kreyling, W. G. & Lehr, C.-M. Pulmonary surfactant is indispensable in order to simulate the in vivo situation. *Particle and fibre toxicology* **10,** 6. ISSN: 1743-8977 (Jan. 2013).

241. Beck-Broichsitter, M. *et al.* Biophysical investigation of pulmonary surfactant surface properties upon contact with polymeric nanoparticles in vitro. *Nanomedicine : nanotechnology, biology, and medicine* **7,** 341–50. ISSN: 1549-9642 (June 2011).

242. Lin, X., Bai, T., Zuo, Y. Y. & Gu, N. Promote potential applications of nanoparticles as respiratory drug carrier: insights from molecular dynamics simulations. en. *Nanoscale* **6,** 2759–67. ISSN: 2040-3372 (Mar. 2014).

243. Bannunah, A. M., Vllasaliu, D., Lord, J. & Stolnik, S. Mechanisms of Nanoparticle Internalization and Transport Across an Intestinal Epithelial Cell Model: Effect of Size and Surface Charge. *Molecular Pharmaceutics* **11,** 4363–4373. ISSN: 1543-8384 (Dec. 2014).

244. Veldhuizen, R., Nag, K., Orgeig, S. & Possmayer, F. The role of lipids in pulmonary surfactant. *Biochimica et Biophysica Acta (BBA) - Molecular Basis of Disease* **1408,** 90–108. ISSN: 09254439 (Nov. 1998).

245. Possmayer, F., Yu, S. H., Weber, J. M. & Harding, P. G. Pulmonary surfactant. *Canadian journal of biochemistry and cell biology = Revue canadienne de biochimie et biologie cellulaire* **62,** 1121–33. ISSN: 0714-7511 (Nov. 1984).

246. Brügger, B., Erben, G., Sandhoff, R., Wieland, F. T. & Lehmann, W. D. Quantitative analysis of biological membrane lipids at the low picomole level by nano-electrospray ionization tandem mass spectrometry. *Proceedings of the National Academy of Sciences of the United States of America* **94,** 2339–44. ISSN: 0027-8424 (Mar. 1997).

247. Shelley, S. a., Paciga, J. E. & Balis, J. U. Purification of surfactant from lung washings and washings contaminated with blood constituents. *Lipids* **12,** 505–10. ISSN: 0024-4201 (June 1977).

248. Löfgren, L. *et al.* The BUME method: a novel automated chloroform-free 96-well total lipid extraction method for blood plasma. *Journal of lipid research* **53,** 1690–700. ISSN: 0022-2275 (Aug. 2012).

249. Kuroki, Y. & Akino, T. Pulmonary surfactant protein A (SP-A) specifically binds dipalmitoylphosphatidylcholine. *The Journal of biological chemistry* **266,** 3068–73. ISSN: 0021-9258 (Feb. 1991).

250. Akino, T., Okano, G. & Ohno, K. Alveolar phospholipids in pulmonary alveolar proteinosis. *The Tohoku journal of experimental medicine* **126,** 51–62. ISSN: 0040-8727 (Sept. 1978).

251. Goerke, J. & Gonzales, J. Temperature dependence of dipalmitoyl phosphatidylcholine monolayer stability. *Journal of Applied Physiology Respiratory Environmental and Exercise Physiology* **51,** 1108–1114. ISSN: 01617567 (1981).

252. Honda, Y. *et al.* Alterations of acidic phospholipids in bronchoalveolar lavage fluids of patients with pulmonary alveolar proteinosis. *Clinica chimica acta; international journal of clinical chemistry* **181,** 11–8. ISSN: 0009-8981 (Apr. 1989).

253. Sahu, S., DiAugustine, R. P. & Lynn, W. S. Lipids found in pulmonary lavage of patients with alveolar proteinosis and in rabbit lung lamellar organelles. *The American review of respiratory disease* **114,** 177–85. ISSN: 0003-0805 (July 1976).

254. Dunkley, T. P. J., Watson, R., Griffin, J. L., Dupree, P. & Lilley, K. S. Localization of Organelle Proteins by Isotope Tagging (LOPIT). *Molecular & Cellular Proteomics* **3,** 1128–1134. ISSN: 1535-9476 (July 2004).

255. Jacobsen, P. B., Blindheim, L. & Skotland, T. Bioanalytical methods for iodixanol and their application to studies on metabolism and protein binding. *Acta radiologica. Supplementum* **399,** 61–6 (Jan. 1995).

256. Johnson, W. H. *et al.* Iodixanol pharmacokinetics in children. *Pediatric cardiology* **22,** 223–7. ISSN: 0172-0643.

257. Choe, S., Chang, R., Jeon, J. & Violi, A. Molecular dynamics simulation study of a pulmonary surfactant film interacting with a carbonaceous nanoparticle. *Biophysical journal* **95,** 4102–14. ISSN: 1542-0086 (Nov. 2008).

258. Bernhard, W. *et al.* Developmental changes in rat surfactant lipidomics in the context of species variability. *Pediatric pulmonology* **42,** 794–804. ISSN: 8755-6863 (Sept. 2007).

259. Kurashima, K., Fujimura, M., Matsuda, T. & Kobayashi, T. Surface activity of sputum from acute asthmatic patients. *American journal of respiratory and critical care medicine* **155,** 1254–9. ISSN: 1073-449X (Apr. 1997).

260. Schürch, S., Goerke, J. & Clements, J. A. Direct determination of surface tension in the lung. *Proceedings of the National Academy of Sciences of the United States of America* **73,** 4698–702. ISSN: 0027-8424 (Dec. 1976).

261. Cass, G. R. *et al.* The chemical composition of atmospheric ultrafine particles. *Philosophical Transactions of the Royal Society A: Mathematical, Physical and Engineering Sciences* **358,** 2581–2592. ISSN: 1364-503X (Oct. 2000).

262. Mulvey, C. M. *et al.* Dynamic Proteomic Profiling of Extra-Embryonic Endoderm Differentiation in Mouse Embryonic Stem Cells. *Stem cells (Dayton, Ohio)* **33,** 2712–25. ISSN: 1549-4918 (Sept. 2015).

263. Ternette, N., Wright, C., Kramer, H. B., Altun, M. & Kessler, B. M. Label-free quantitative proteomics reveals regulation of interferon-induced protein with tetratricopeptide repeats 3 (IFIT3) and 5'-3'-exoribonuclease 2 (XRN2) during respiratory syncytial virus infection. *Virology journal* **8,** 442. ISSN: 1743-422X (Jan. 2011).

264. Wu, X., Hasan, M. A. & Chen, J. Y. Pathway and network analysis in proteomics. *Journal of theoretical biology* **362,** 44–52. ISSN: 1095-8541 (Dec. 2014).

265. Wessel, D. & Flügge, U. I. A method for the quantitative recovery of protein in dilute solution in the presence of detergents and lipids. *Analytical biochemistry* **138,** 141–3. ISSN: 0003-2697 (Apr. 1984).

266. Szklarczyk, D. *et al.* STRING v10: protein-protein interaction networks, integrated over the tree of life. *Nucleic acids research* **43,** D447–52. ISSN: 1362-4962 (Jan. 2015).

267. Maere, S., Heymans, K. & Kuiper, M. BiNGO: a Cytoscape plugin to assess overrepresentation of gene ontology categories in biological networks. *Bioinformatics (Oxford, England)* **21,** 3448–9. ISSN: 1367-4803 (Aug. 2005).

268. Thomas, P. D. *et al.* PANTHER: a library of protein families and subfamilies indexed by function. *Genome research* **13,** 2129–41. ISSN: 1088-9051 (Sept. 2003).

269. Maynard, R. L., Donaldson, K. & Tetley, T. D. Type 1 pulmonary epithelial cells: a new compartment involved in the slow phase of particle clearance from alveoli. *Nanotoxicology,* 1–2. ISSN: 1743-5404 (Jan. 2012).

270. Guarnieri, D., Guaccio, A., Fusco, S. & Netti, P. A. Effect of serum proteins on polystyrene nanoparticle uptake and intracellular trafficking in endothelial cells. *Journal of Nanoparticle Research* **13,** 4295–4309. ISSN: 1388-0764 (Apr. 2011).

271. Kim, J. A. *et al.* Low dose of amino-modified nanoparticles induces cell cycle arrest. *ACS nano* **7,** 7483–94. ISSN: 1936-086X (Sept. 2013).

272. Kanehisa, M., Sato, Y., Kawashima, M., Furumichi, M. & Tanabe, M. KEGG as a reference resource for gene and protein annotation. *Nucleic acids research* **44,** D457–62. ISSN: 1362-4962 (Oct. 2015).

273. Hartman, M. A., Finan, D., Sivaramakrishnan, S. & Spudich, J. A. Principles of unconventional myosin function and targeting. *Annual review of cell and developmental biology* **27,** 133–55. ISSN: 1530-8995 (Jan. 2011).

274. Lin, T., Tang, N. & Ostap, E. M. Biochemical and motile properties of Myo1b splice isoforms. *The Journal of biological chemistry* **280,** 41562–7. ISSN: 0021-9258 (Dec. 2005).

275. Coux, O., Tanaka, K. & Goldberg, A. L. Structure and functions of the 20S and 26S proteasomes. en. *Annual review of biochemistry* **65,** 801–47. ISSN: 0066-4154 (Jan. 1996).

276. Medigeshi, G. R. *et al.* AP-1 membrane-cytoplasm recycling regulated by mu1A-adaptin. *Traffic (Copenhagen, Denmark)* **9,** 121–32. ISSN: 1398-9219 (Jan. 2008).

277. Wu, X. *et al.* Adaptor and clathrin exchange at the plasma membrane and trans-Golgi network. *Molecular biology of the cell* **14,** 516–28. ISSN: 1059-1524 (Feb. 2003).

278. Martinez-Azorin, F., Remacha, M. & Ballesta, J. P. G. Functional characterization of ribosomal P1/P2 proteins in human cells. *The Biochemical journal* **413,** 527–34. ISSN: 1470-8728 (Aug. 2008).

279. Powers, C. M., Badireddy, A. R., Ryde, I. T., Seidler, F. J. & Slotkin, T. A. Silver nanoparticles compromise neurodevelopment in PC12 cells: critical contributions of silver ion, particle size, coating, and composition. *Environmental health perspectives* **119,** 37–44. ISSN: 1552-9924 (Jan. 2011).

280. Hillaireau, H. & Couvreur, P. Nanocarriers' entry into the cell: relevance to drug delivery. *Cellular and molecular life sciences : CMLS* **66,** 2873–96. ISSN: 1420-9071 (Sept. 2009).

281. Lai, S. K. *et al.* Privileged delivery of polymer nanoparticles to the perinuclear region of live cells via a non-clathrin, non-degradative pathway. *Biomaterials* **28,** 2876–84. ISSN: 0142-9612 (June 2007).

282. Sönnichsen, B., De Renzis, S., Nielsen, E., Rietdorf, J. & Zerial, M. Distinct membrane domains on endosomes in the recycling pathway visualized by multicolor imaging of Rab4, Rab5, and Rab11. *The Journal of cell biology* **149,** 901–14. ISSN: 0021-9525 (May 2000).

283. Van der Sluijs, P. *et al.* The small GTP-binding protein rab4 controls an early sorting event on the endocytic pathway. *Cell* **70,** 729–740. ISSN: 00928674 (Sept. 1992).

284. Ferguson, S. M. & De Camilli, P. Dynamin, a membrane-remodelling GTPase. *Nature reviews. Molecular cell biology* **13,** 75–88. ISSN: 1471-0080 (Feb. 2012).

285. Wang, S., Singh, R. D., Godin, L., Pagano, R. E. & Hubmayr, R. D. Endocytic response of type I alveolar epithelial cells to hypertonic stress. *American journal of physiology. Lung cellular and molecular physiology* **300,** L560–8. ISSN: 1522-1504 (Apr. 2011).

286. Gazdar, A. F. *et al.* Peripheral airway cell differentiation in human lung cancer cell lines. *Cancer research* **50,** 5481–7. ISSN: 0008-5472 (Sept. 1990).

287. ATCC. *A549 (ATCC CCL-185)* 2014. <http://www.lgcstandards-atcc.org/products/all/CCL-185.aspx?geo%7B%5C_%7Dcountry=gb%7B%5C#%7Dcharacteristics> (visited on 03/18/2016).

288. Mao, P. *et al.* Human alveolar epithelial type II cells in primary culture. *Physiological reports* **3.** ISSN: 2051-817X. doi:10.14814/phy2.12288. <http://www.pubmedcentral.nih.gov/articlerender.fcgi?artid=4393197%7B%5C&%7Dtool=pmcentrez%7B%5C&%7Drendertype=abstract> (Feb. 2015).

289. Fuchs, S. *et al.* Differentiation of human alveolar epithelial cells in primary culture: morphological characterization and synthesis of caveolin-1 and surfactant protein-C. *Cell and tissue research* **311,** 31–45. ISSN: 0302-766X (Jan. 2003).

290. Bove, P. F. *et al.* Human alveolar type II cells secrete and absorb liquid in response to local nucleotide signaling. *The Journal of biological chemistry* **285,** 34939–49. ISSN: 1083-351X (Nov. 2010).

291. Borok, Z. *et al.* Keratinocyte Growth Factor Modulates Alveolar Epithelial Cell Phenotype In Vitro: Exprtession of Aquaporin 5. *American Journal of Respiratory Cell Molecular Biology* **18,** 554–561 (1998).

292. Sugahara, K., Rubin, J. S., Mason, R. J., Aronsen, E. L. & Shannon, J. M. Keratinocyte growth factor increases mRNAs for SP-A and SP-B in adult rat alveolar type II cells in culture. *The American journal of physiology* **269,** L344–50. ISSN: 0002-9513 (Sept. 1995).

293. Worster, D. T. *et al.* Akt and ERK control the proliferative response of mammary epithelial cells to the growth factors IGF-1 and EGF through the cell cycle inhibitor p57Kip2. *Science signaling* **5,** ra19. ISSN: 1937-9145 (Mar. 2012).

294. Mollenhauer, J. *et al.* DMBT1, a new member of the SRCR superfamily, on chromosome 10q25.3-26.1 is deleted in malignant brain tumours. *Nature genetics* **17,** 32–9. ISSN: 1061-4036 (Sept. 1997).

295. Critchley, D. Cytoskeletal proteins talin and vinculin in integrin-mediated adhesion. en. <http://www.biochemsoctrans.org/bst/032/0831/bst0320831.htm%7B%5C#%7DREF37> (Oct. 2004).

296. Muguruma, M., Nishimuta, S., Tomisaka, Y., Ito, T. & Matsumura, S. Organization of the functional domains in membrane cytoskeletal protein talin. *Journal of biochemistry* **117,** 1036–42. ISSN: 0021-924X (May 1995).

297. Ratnikov, B. *et al.* Talin phosphorylation sites mapped by mass spectrometry. *Journal of cell science* **118,** 4921–3. ISSN: 0021-9533 (Nov. 2005).

298. Mollenhauer, J. *et al.* DMBT1 Encodes a Protein Involved in the Immune Defense and in Epithelial Differentiation and Is Highly Unstable in Cancer. *Cancer Res.* **60,** 1704–1710 (Mar. 2000).

299. Tino, M. J. & Wright, J. R. Glycoprotein-340 binds surfactant protein-A (SP-A) and stimulates alveolar macrophage migration in an SP-A-independent manner. *American journal of respiratory cell and molecular biology* **20,** 759–68. ISSN: 1044-1549 (Apr. 1999).

300. Holmskov, U. *et al.* Isolation and characterization of a new member of the scavenger receptor superfamily, glycoprotein-340 (gp-340), as a lung surfactant protein-D binding molecule. *The Journal of biological chemistry* **272,** 13743–9. ISSN: 0021-9258 (May 1997).

301. Mollenhauer, J. *et al.* The genomic structure of the DMBT1 gene: evidence for a region with susceptibility to genomic instability. *Oncogene* **18,** 6233–40. ISSN: 0950-9232 (Nov. 1999).

302. Fehrenbach, H. Alveolar epithelial type II cell : defender of the alveolus revisited (2001).

303. Picot, J. *Human Cell Culture Protocols* ISBN: 1-59259-861-7. doi:10.1385/1592598617. <http://link.springer.com/10.1385/1592598617%20http://www.humanapress.com/Product.pasp?txtCatalog=HumanaBooks%7B%5C&%7DtxtProductID=1-59259-861-7%7B%5C&%7DisVariant=0> (Humana Press, New Jersey, Nov. 2004).